

Description of Radio-Frequency (RF) pulses in Quadrupolar nuclei

A Thesis

submitted

by

Venkata SubbaRao R

for the partial fulfillment of the degree

of

Doctor of Philosophy



Department of Chemical Sciences,
Indian Institute of Science Education and Research (IISER) Mohali,
Sector 81, Mohali-140306, Punjab, INDIA

March 2016

Dedicated to my loving parents
&
My late grandfather Sri. Chandu SitaKamaiah

Declaration

The work presented in this thesis entitled “Description of Radio-Frequency (RF) pulses in Quadrupolar nuclei” has been carried out by me under the supervision of Dr. Ramesh Ramachandran at the Indian Institute of Science Education and Research (IISER) Mohali.

This work has not been submitted in part or full for a degree, a diploma, or a fellowship to any university or institute. Whenever contributions of others are involved, every effort is made to indicate this clearly, with due acknowledgement of collaborative research and discussions. This thesis is a bona fide record of original work done by me and all sources listed within have been detailed in the references.

Date:

Venkata SubbaRao R

Place:

(Candidate)

In my capacity as the supervisor of the candidate’s thesis work, I certify that the above statements by the candidate are true to the best of my knowledge.

Date:

Dr. Ramesh Ramachandran

Place:

(Supervisor)

Acknowledgements

I take immense pleasure in thanking my supervisor **Dr. Ramesh Ramachandran** for giving me an opportunity to work with him and guide me in spite of being familiar with the fact that I have very little background of Physical Chemistry in my masters. I thank him for his utmost support from the beginning of my Phd till date, the care he has taken, efforts he has put through in making me a good researcher. I am deeply indebted to his patience, perseverance, encouragement and motivation. I would also like to thank him for sharing his personal office space by compromising his privacy and for many memorable events with him throughout my stay in IIT Roorkee and IISER Mohali. I also wish to thank him for being an inspiration with his passion towards teaching and science. He is very honest, straight forward, simple and awesome person I have ever met, I always feel lucky and proud for being associated with such person during on important phase of my life.

I would like to thank my doctoral committee members Prof. K. S. Viswanathan and Dr. P. Balanarayan for their valuable comments and suggestions. I express my gratitude towards Prof. K. S. Viswanathan (HoD, Chemistry) for the constant support and motivation during the course of my PhD.

I am thankful to IISER Mohali in particular the founding director, Prof. N. Sathyamurthy for providing me the Fellowship, all kinds of facilities and the support required for my PhD work.

I would like to thank all the faculty members of IISER Mohali for building up a healthy atmosphere for teaching and research. I also wish to thank Prof. Sanjay Mandal in particular for his concern about my thesis status and constant encouragement. I would also like to thank Dr. Samrat Ghosh for making the tough times light by providing different flavors of chocolates and cookies.

My special thanks goes to Prof. Mangala Sunder Krishnan for the helpful discussion and kind of affection he showed during his visit to IISER Mohali. I am grateful to Dr. Manoj Kumar Pandey for many sweet memories in my stay with him, continuous encouragement and kind of support he has given throughout my PhD program.

Many thanks to all my group members Ms. Zeba Qadri, Mr. SivaRanjan Uppala, Mr. Vinay

Ganapathy, Mr. Shivam Rai, Mr. Dharmendra K.Singh, Mr. Deepansh Srivastava, Ms. Manpreet Kaler, Mr. Rajat Garg, Ms. Bharti kumari, Ms. Lakshmi Bhai, Mr. Justin K. Thomas for stimulating discussions which motivated me in improving my technical skills and comprehensive understanding of many concepts. I express my deepest gratitude to all of them in maintaining friendly work environment and getting along with me for all these years.

I am grateful to Dr. P. Bapaiah (Registrar) and Dr. Visakhi (Deputy Librarian) for not only being great support towards my research activities but also for providing help, affection, motivation, personal care and for being as local guardians to me. I would especially mention the fun and memorable time, we had during festive celebrations at their home. I want to extend my thanks to all Telugu friends at IISER Mohali for many memorable events and for their support.

This long journey of my doctorate work would not have been accomplished without the support and love of my friends Dr. A. Venkat, Dr. B. Prasad, S. Kamesh, R. Chandra Sekhar, G. Srinivas, Dr. Venkat Babu, Dr. D. Anjaneyulu, Dr. Satya prakash, Y. Srinu, P. Purna, Siva Rajyamma, Ch. Venkata Rambabu, B. Gangadhar, Ch. Satyannarayana, G. Sambasivarao, K. Yedukondalu, MS 07 & 08 Batch students of IISER Mohali, Dr. Sukdeep, Nidhi, Dr. Kusum, Ameet, Dr. Sadhika, Hostel friends-Naveen and gang.

I believe that without the love and support of my family members, aunt, uncle and all cousins my success would not have been possible. I would like to thank all my relatives and well wishers for their constant support.

I also wish to express my sincere gratitude to all my teachers who have put their indispensable efforts in shaping up my career.

Contents

1	Introduction	1
1.1	Background	1
1.2	Methodology	5
1.2.1	Concept of effective Hamiltonians	9
1.3	Organization of the thesis	15
	Appendices	16
1.A	The van Vleck and Contact transformation	16
	References	26
2	Conventions and Notations for generalized representation of spin interactions	27
2.1	Background	27
2.2	Nuclear spin Hamiltonians and their representations	28
2.2.1	External Hamiltonians	29
2.2.1.1	Zeeman interaction	29
2.2.1.2	RF interaction	30
2.2.2	Internal Hamiltonians	30
2.2.2.1	Chemical Shift interaction	31
2.2.2.2	J-Coupling interaction	32
2.2.2.3	Dipolar Coupling interaction	34
2.2.2.4	Quadrupolar interaction	35
2.2.2.5	Spin-Rotation interaction	37
2.2.3	Transformation of spin Hamiltonians	38
2.3	Effective Hamiltonians for spin $I = 1/2$ system under MAS	40
	Appendices	45
2.A	Irreducible spherical tensors	45
2.B	Essential relations of tensor operators	49
2.B.1	Explicit form of $T^{(k)q}(I)$ operators up to the rank $k=7$	49
2.B.2	General relation of $T^{(k)q}(I)$ operator with product operators	51
2.B.3	Explicit form of $T^{(k)q}(\bar{\alpha})$ operators in multiple spin basis	52

2.B.4	Relation with level shift operators	52
2.B.5	Relation with unnormalized or non-unit tensors	52
2.B.6	Commutator relation between tensor operators $T^{(k)q}(\bar{I})$'s	53
2.C	Transformation properties	53
2.C.1	Passive rotation	55
2.C.2	Active rotation	56
2.D	Floquet theory	57
2.E	Normalization factors	59
	References	63
3	Concept of effective Hamiltonians for Single Quantum (SQ) transitions	65
3.1	Background	65
3.2	Methodology	66
3.3	Theory and Discussion	69
3.3.1	Effective Hamiltonians for $I=1$	69
3.3.1.1	Static (Single-crystal)	69
3.3.1.2	Magic Angle Spinning (Powder-sample)	76
3.3.2	Effective Hamiltonians for $I=3/2$	82
3.3.2.1	Static (Single-crystal)	82
3.3.2.2	Magic Angle Spinning (Powder-sample)	86
3.3.3	Effective Hamiltonians for $I=5/2$	91
3.3.3.1	Static (Single-crystal)	91
3.3.3.2	Magic Angle Spinning (Powder-sample)	95
3.4	Conclusions and Perspectives	101
	References	105
4	Theory of Multi-Quantum (MQ) excitation in multi-level systems	107
4.1	Background	107
4.2	Theory and Discussion	108
4.2.1	Description for $I=1$ system	109
4.2.1.1	Static (Single-crystal)	109
4.2.1.2	Magic Angle Spinning (Powder-sample)	113
4.2.2	Description for $I=3/2$ system	117
4.2.2.1	Static (Single-crystal)	117
4.2.2.2	Magic Angle Spinning (Powder-sample)	119
4.2.3	Description for $I=5/2$ system	122
4.2.3.1	Static (Single-crystal)	122
4.2.3.2	Magic Angle Spinning (Powder-sample)	124
4.3	Conclusions and Perspectives	128

References	131
5 Conclusions and Perspectives	133
5.1 Concept of effective RF Hamiltonians	134
5.2 Excitation of satellite transitions in MAS experiments	135
5.3 Excitation of MQ transitions in MAS experiments	137
Research Publications	141
Doctoral Committee	142
Curriculum Vitae	143

List of Figures

1.1	Energy level diagram for spin $I = 1/2$ system in the presence of chemical shift off-set along with simple single pulse sequence.	9
1.2	Simulations depicting the the role of off-sets ($\Delta\nu = 0$ to 40 kHz) on the NMR line shapes.	11
1.3	The figure depicts the tilted rotating frame transformation about $-\theta$ along y-axis.	13
2.1	Relationship between cartesian coordinates x, y, z and the polar coordinates r, θ, ϕ	34
2.2	The figure depicts the set of transformations which are required to transform MAS Hamiltonian from PAS to LAS for a single molecule in the powdered sample.	39
2.3	Simulations depicting the effects of spinning frequency on line shapes and intensities in spin $I = 1/2$	43
2.4	Representation of Euler angles (α, β, γ) rotation	54
2.5	A passive rotation of coordinate axes by $-\alpha$ or rotation of vector by α about z-axis.	55
2.6	Right hand rule: The right thumb denotes the axis of rotation, the remaining curled fingers depicts the direction of the rotation of tensor.	55
2.7	An active rotation of a vector with negative rotation by $-\alpha$ about z-axis	56
2.8	Left hand rule: The left thumb denotes the axis of rotation, the remaining curled fingers depicts the direction of the rotation of tensor.	57
3.1	Energy level diagram for spin $I=1$ system in the presence of first-order quadrupolar interactions.	69
3.2	Simulations depicting the FT-spectrum of ${}^6\text{Li}$ ($I = 1$) system corresponding to non-selective and selective excitation in a single crystal.	73
3.3	Simulations depicting the selective excitation using a $\frac{\pi}{2}$ -pulse ($\nu_1 = 20$ kHz, $t_p = 12.5 \mu\text{s}$) in a powder sample corresponding to $I=1$ system.	74
3.4	Simulations depicting the role of the flip angle in the selective excitation in a powder sample corresponding to $I=1$ system.	74
3.5	Simulations depicting the selective excitation ($\nu = \nu_0 + \frac{\nu_Q}{4}(\frac{\nu_Q}{4} = 75$ kHz)) in $I=1$ system corresponding to $C_Q = 200$ kHz, $\nu_Q = 300$ kHz, $\eta=0$	75
3.6	Simulations depicting the role of t_p on the efficiency of excitation.	76

3.7	Simulations depicting the role of spinning frequency ($\nu_r = 10$ & 11 kHz) on the excitation efficiency of SQ transitions in spin $I = 1$, (excitation frequency, $\nu = \nu_0 + \frac{\nu_Q}{4}$ or $\nu = \nu_0 + 90$ kHz).	79
3.8	Simulations depicting the role of spinning frequency ($\nu_r = 18$ & 19 kHz) on the excitation efficiency of SQ transitions in spin $I = 1$, (excitation frequency, $\nu = \nu_0 + \frac{\nu_Q}{4}$ or $\nu = \nu_0 + 90$ kHz).	80
3.9	Simulations depicting the role of spinning frequency ($\nu_r = 30$ & 31 kHz) on the excitation efficiency of SQ transitions in spin $I = 1$, (excitation frequency, $\nu = \nu_0 + \frac{\nu_Q}{4}$ or $\nu = \nu_0 + 90$ kHz).	81
3.10	Energy level diagram for spin $I=3/2$ system in the presence of first-order quadrupolar interactions.	83
3.11	Simulations depicting the FT-spectrum of ${}^7\text{Li}$ ($I = 3/2$) system corresponding to non-selective and selective excitation in a single crystal.	85
3.12	Simulations depicting selective excitations ($\nu = \nu_0 + \frac{\nu_Q}{2}$ ($\frac{\nu_Q}{2} = 300$ kHz) in figures D1, D2) and ($\nu = \nu_0$ in figures D3, D4) in $I=3/2$, system corresponding to $C_Q = 1.2$ MHz, $\nu_Q = 600$ kHz, $\eta = 0$.	86
3.13	Simulations depicting the role of spinning frequency ($\nu_r = 10$ & 11 kHz) on the excitation efficiency of SQ transitions in spin $I = 3/2$, (excitation frequency, $\nu = \nu_0 + \frac{\nu_Q}{2}$ or $\nu = \nu_0 + 270$ kHz).	88
3.14	Simulations depicting the role of spinning frequency ($\nu_r = 18$ & 19 kHz) on the excitation efficiency of SQ transitions in spin $I = 3/2$, (excitation frequency, $\nu = \nu_0 + \frac{\nu_Q}{2}$ or $\nu = \nu_0 + 270$ kHz).	89
3.15	Simulations depicting the role of spinning frequency ($\nu_r = 30$ & 31 kHz) on the excitation efficiency of SQ transitions in spin $I = 3/2$, (excitation frequency, $\nu = \nu_0 + \frac{\nu_Q}{2}$ or $\nu = \nu_0 + 270$ kHz).	90
3.16	Energy level diagram for spin $I=5/2$ system in the presence of first-order quadrupolar interactions.	92
3.17	Simulations depicting the FT-spectrum of ${}^{27}\text{Al}$ ($I = 5/2$) system corresponding to non-selective and selective excitation in a single crystal.	95
3.18	Simulations depicting selective excitations ($\nu = \nu_0 + \frac{\nu_Q}{2}$ ($\frac{\nu_Q}{2} = 120$ kHz) in figures E1, E2), ($\nu = \nu_0 + \nu_Q$ ($\nu_Q = 240$ kHz) in figures E3, E4 and $\nu = \nu_0$ in E5, E6) in $I=5/2$, system corresponding to $C_Q = 1.6$ MHz, $\nu_Q = 240$ kHz, $\eta = 0$.	96
3.19	Simulations depicting the role of spinning frequency ($\nu_r = 10$ & 11 kHz) on the excitation efficiency of SQ transitions (ST1) in spin $I = 5/2$, (excitation frequency, $\nu = \nu_0 + \frac{\nu_Q}{2}$ or $\nu = \nu_0 + 150$ kHz).	97
3.20	Simulations depicting the role of spinning frequency ($\nu_r = 30$ & 31 kHz) on the excitation efficiency of SQ transitions (ST1) in spin $I = 5/2$, (excitation frequency, $\nu = \nu_0 + \frac{\nu_Q}{2}$ or $\nu = \nu_0 + 150$ kHz).	98

3.21	Simulations depicting the role of spinning frequency ($\nu_r = 10$ & 11 kHz) on the excitation efficiency of SQ transitions (ST2) in spin $I = 5/2$, (excitation frequency, $\nu = \nu_0 + \frac{\nu_Q}{2}$ or $\nu = \nu_0 + 300$ kHz).	99
3.22	Simulations depicting the role of spinning frequency ($\nu_r = 30$ & 31 kHz) on the excitation efficiency of SQ transitions (ST2) in spin $I = 5/2$, (excitation frequency, $\nu = \nu_0 + \frac{\nu_Q}{2}$ or $\nu = \nu_0 + 300$ kHz).	100
4.1	Simulations depicting the role of RF amplitude and quadrupolar coupling strength on excitation efficiency of double-quantum (DQ) transitions in single-crystal spin $I = 1$.	112
4.2	Simulations depicting the role of RF amplitude and quadrupolar coupling strength on excitation efficiency of double-quantum (DQ) transitions in spin $I = 1$ at spinning frequency $\nu_r = 10$ kHz.	114
4.3	Simulations depicting the role of RF amplitude and quadrupolar coupling strength on excitation efficiency of double-quantum (DQ) transitions in spin $I = 1$ at spinning frequency $\nu_r = 30$ kHz.	115
4.4	Simulations depicting the role of RF amplitude and quadrupolar coupling strength on excitation efficiency of triple-quantum (TQ) transitions in single-crystal spin $I = 3/2$.	118
4.5	Simulations depicting the role of RF amplitude and quadrupolar coupling strength on excitation efficiency of triple-quantum (TQ) transitions in spin $I = 3/2$ at spinning frequency $\nu_r = 10$ kHz.	120
4.6	Simulations depicting the role of RF amplitude and quadrupolar coupling strength on excitation efficiency of triple-quantum (TQ) transitions in spin $I = 3/2$ at spinning frequency $\nu_r = 30$ kHz.	121
4.7	Simulations depicting the role of RF amplitude on excitation efficiency of triple-quantum (TQ) transition in panels (A1 & A2) and five-quantum (5Q) transition in panels (B1 & B2) in single-crystal spin $I = 5/2$.	123
4.8	Simulations depicting the role of RF amplitude on excitation efficiency of triple-quantum (TQ) transition in panels (A1 & A2) and five-quantum (5Q) transition in panels (B1 & B2) in spin $I = 5/2$ at spinning frequency $\nu_r = 10$ kHz.	125
4.9	Simulations depicting the role of RF amplitude on excitation efficiency of triple-quantum (TQ) transition in panels (A1 & A2) and five-quantum (5Q) transition in panels (B1 & B2) in spin $I = 5/2$ at spinning frequency $\nu_r = 30$ kHz.	127
5.1	Simulations depicting in panel (A) the role of excitation frequency using a $\frac{\pi}{2}$ -pulse ($\nu_1 = 20$ kHz, $t_p = 12.5$ μ s) and in panel (B) the role of the flip angle in the selective excitation of a powder sample corresponding to $I=1$ system.	135
5.2	Simulations depicting the FT-spectrum of ${}^6\text{Li}$ ($I = 1$) system corresponding to non-selective and selective excitation in a single crystal.	135

5.3	Numerical simulations depicting the role of spinning frequency on the excitation efficiency of SQ transitions in spin $I = 3/2$, (excitation frequency, $\nu = \nu_0 + \frac{\nu_Q}{2}$ or $\nu = \nu_0 + 270$ kHz).	136
5.4	Simulations depicting the role of RF amplitude and quadrupolar coupling strength on excitation efficiency of triple-quantum (TQ) transitions in spin $I = 3/2$ at spinning frequency $\nu_r = 10$ kHz.	138

List of Tables

2.1	Chemical shift Hamiltonian in tensorial representation.	32
2.2	J-coupling Hamiltonian in tensorial representation	33
2.3	Dipolar coupling Hamiltonian in tensorial representation	35
2.4	Quadrupolar coupling Hamiltonian in tensorial representation	37
2.5	Spin-rotation Hamiltonian in tensorial representation	38
2.6	Explicit form of the normalization constant	47
2.7	The spherical basis $e^{(k)q}$ and the corresponding spherical components of cartesian tensor of rank $k = 1$	48
2.8	The spherical basis $e^{(k)q}$ and the corresponding spherical components of cartesian tensor of rank $k = 2$	48
2.9	Explicit form of $T^{(k)q}(I)$ operators up to the rank $k=7$	51
2.10	The rotation operators corresponding to passive and active rotations.	54
2.11	The normalization factors corresponding to different detection operators for typical sin- gle X, Y-Pulses.	59
3.1	Summary of intensities and flip angles for selective excitations in integral and half- integral quadrupolar systems.	103

Acronyms and Abbreviations

5Q	Five-quantum
AHT	Average Hamiltonian theory
BCH	Baker-Campbell-Hausdorff
CSA	Chemical shift anisotropy
CP	Cross-polarization
CT	Central transition
DAS	Dynamic angle spinning
DQ	Double-quantum
DOR	Double Rotation
EFG	Electric field gradient
EM	Electromagnetic
LAS	Lab axes system
MAS	Magic angle spinning
MolAS	Molecular axes system
MQ	Multi-quantum (or) Multiple-quantum
MQMAS	Multi-quantum (MQ) MAS
NMR	Nuclear Magnetic Resonance
PAS	Principal axes system
QM	Quantum mechanics
RF	Radio-frequency
RAS	Rotor axes system
ST	Satellite transitions
S/N	Signal-to-noise ratio
SQ	Single quantum
ssNMR	solid-state NMR
TQ	Triple-quantum
VAS	Variable angle spinning
Z-Q	Zeeman-quadupolar

Glossary of Symbols and Notations

$(\alpha\beta\gamma)$	Euler angles
B_0	Strength of static magnetic field
B_1	Strength of oscillating magnetic field
\mathcal{B}	Thermodynamic beta or the inverse temperature
$C(k)$	Normalization constant corresponding to $T^{(k)q}$ operator
$D_{q'q}^{(k)}(\alpha\beta\gamma)$	Wigner functions (or) elements of Wigner rotation matrix $D^{(k)}(\alpha\beta\gamma)$
$d_{q'q}^{(k)}(\beta)$	Wigner formula (or) element of reduced Wigner rotation matrix $d^{(k)}(\beta)$
δ	Anisotropy
η	Asymmetry parameter
F_m	Fourier off-diagonal operator
F_I	Fourier diagonal operator
γ	Gyromagnetic ratio
H	Hamiltonian
H_λ	Interaction Hamiltonian
H_{eff}	Effective Hamiltonian
H_F	Floquet Hamiltonian
H_n^k	n^{th} order Hamiltonian after k^{th} transformation
i	Iota
k	Rank of the tensor
k_B	Boltzmann constant
h	Planck's constant (or) Universal constant
\hbar	Reduced Planck's constant (or) Dirac constant
I_F	Floquet diagonal operator
$I_{z,m}, T_m^{(k)q}$	Floquet off-diagonal operators
I	Spin quantum number
$ Im\rangle$	Ket eigen state
I^+, I_-	Ladder operators
I_x, I_y, I_z	Spin angular momentum operators
J	Total angular momentum
μ	Magnetic moment
m	Fourier label

$\langle o \rangle$	Expectation Value
ω_0 (ν_0)	Larmor frequency
ω_z (ν_z)	Chemically shifted Larmor frequency
ω (ν)	excitation frequency or carrier frequency
$\Delta\omega$ ($\Delta\nu$)	off-set frequency
ω_1 (ν_1)	Amplitude of RF pulse
ω_r (ν_r)	spinning frequency
ψ	State function
q	Component of the tensor
$\rho(0) = I_z$	Initial density operator
$R^{(k)q}, G^{(k)q}$	Spatial tensor
$\rho(t)$	Density operator at time 't'
S_k	k^{th} Transformation function
t_p	Duration of pulse
$T^{(k)q}$	Spin tensor operator
$T^{(k)q}(s)$	Symmetric tensor operator ($T^{(k)q} + T^{(k)-q}$)
$T^{(k)q}(a)$	Antisymmetric tensor operator ($T^{(k)q} - T^{(k)-q}$)
T	Wick-Dyson time ordering operator
Tr	Quantum trace
U	Unitary operator

Abstract

With the development of technology and improved understanding of nuclear spin-spin interactions and their behavior in static/oscillating magnetic fields, NMR spectroscopy has emerged as a powerful tool for characterizing molecular structure in wide range of systems of chemical, physical and biological relevance. Here in this thesis, employing the concept of effective Hamiltonians, an analytic theory is introduced to describe transitions in a multi-level system in nuclear magnetic resonance (NMR) spectroscopy. Specifically, the discussion is centered towards the treatment of selective and non-selective excitations in static single-crystal and magic angle spinning (MAS) powder sample in quadrupolar spin ($I > 1/2$) systems. Employing the spherical tensor formalism, effective radio-frequency (RF) Hamiltonians are proposed for describing transitions in $I=1, 3/2$ and $5/2$. The optimum conditions desired for selective excitation in a multi-level system are derived pedagogically from first principles and presented through analytic expressions. As an extension of this approach, multi-quantum (MQ) excitation in quadrupolar systems is discussed. Since MQ NMR spectroscopy of quadrupolar nuclei forms the basis for structural characterization of inorganic solids and clusters, we believe that the analytic theory presented herein would be beneficial both in the understanding and design of MQ NMR experiments.

Chapter 1

Introduction

1.1 Background

Recent technological advancements and innovations in methodology have established nuclear magnetic resonance¹⁻⁴ (NMR) as one of the most reliable spectroscopic tools available for determining molecular structure⁵ both in ordered and intrinsically disordered systems.⁶⁻¹⁴ In comparison to other forms of spectroscopy, the phenomenon of NMR¹⁵⁻¹⁹ results from an intrinsic quantum mechanical property, commonly referred to as ‘spin’²⁰⁻²⁵ and characterized through $2I + 1$ spin states (I represents the nuclear spin quantum number). To induce appreciable transitions, presence of an external magnetic field²⁶ is necessary to lift the degeneracy of the nuclear spin states. Subsequently, transitions between nuclear spin states are induced by employing oscillating magnetic fields¹⁷⁻¹⁹ with frequencies in the radio-frequency (RF) region of the electromagnetic (EM) spectrum. Nevertheless, the smaller energy gap between the nuclear spin states renders NMR spectroscopy, a less sensitive tool in comparison to other available spectroscopic techniques. In spite of this inherent limitation, the versatility (and uniqueness) of NMR spectroscopy lies in the flexibility that it provides in the design of experiments through careful control and manipulation²⁷ of the spin interactions at the atomic level. In particular, the nuclear spin interactions play an important role in defining the utility of NMR as a molecular probe. The information characterizing the chemical surroundings of the desired nuclei under investigation, depends on the availability of high-resolution spectrum.²⁸ In general, the resolution of the NMR spectrum depends on the state of the sample²⁹⁻³⁵ in addition to the spin quantum number of the nucleus under investigation. For example, in the case of a liquid sample, the inherent molecular motion renders the spin interactions isotropic and results in sharp, narrow spectra. On the contrary, the restricted mobility in the solid state renders the spin interactions anisotropic and results in broad spectra.

Depending on the magnitude of the spin quantum number of a particular nucleus, the

nature of the spin interactions vary. For spin-1/2 nuclei, the spin interactions mainly comprise of the dipole-dipole interaction between spins, chemical shift anisotropy (CSA), indirect spin-spin interaction (J -coupling), etc. Due to rapid molecular tumbling motion, the dipolar interactions in the liquid state are averaged to zero. With the advent of Magic angle spinning^{36,37} (MAS) and other sophisticated double resonance and multiple-pulse experiments such as cross-polarization^{38,39} (CP) and hetero-nuclear decoupling⁴⁰⁻⁴⁶ methods, the differences between solution and solid-state NMR (ssNMR) of spin 1/2 nuclei have narrowed down in recent years.⁴⁷⁻⁵¹ These developments, together with the continuing advances in NMR hardware and software, have facilitated molecular level structure determination of materials (of both chemical and biological relevance) in the solid-state.⁶⁻¹⁴

In spite of this tremendous success, the advancement of NMR methodology in quadrupolar nuclei (nuclei with $I > 1/2$) is only marginal. Since, 70% of the nuclei in the periodic table possess spin quantum numbers greater than 1/2, the NMR study of such nuclei become relevant. In contrast to their spin 1/2 counterparts, nuclei with spin $I > 1/2$ possess a non-spherical distribution of charge around the nucleus leading to an intrinsic property, commonly referred to as the "quadrupole moment".⁵² The interaction between this non-symmetrical charge distribution around the nucleus with the electric field gradients (EFG) resulting from the local charge distribution in a molecule (created by surrounding electrons) is referred to as the "quadrupolar interaction".^{47,52-57} In contrast to other internal spin interactions, the quadrupolar interactions are stronger and are primarily responsible for the observed line broadening. Interestingly, the rapid molecular tumbling motion present in liquids diminishes the impact of the quadrupolar interactions in solution NMR. Nevertheless, quadrupolar interactions do have a prominent role on the T_1 and T_2 relaxation times of nuclei in the solution state.²⁸ In the past, de novo structure determination (biological systems in particular) was primarily centered around studies involving spin 1/2 nuclei.^{6-14,58} The dipolar interactions in particular, have remained the main source for providing molecular constraints such as intramolecular distances ($^{13}\text{C} - ^{13}\text{C}$, $^{13}\text{C} - ^{15}\text{N}$) and molecular torsion angles.^{59-62,62-65} In a typical multidimensional solid-state NMR (ssNMR) experiment involving spin 1/2 nuclei, the spatial averaging effect of MAS is partially compensated through multiple-pulse schemes during selected periods of time (or dipolar mixing time), resulting in the reintroduction of dipolar interactions without compromising the spectral resolution afforded by MAS.⁶⁶⁻⁶⁸ Depending on the nature of the experiment, the dipolar interactions are reintroduced in a controlled fashion.⁶⁹⁻⁷⁴ A detailed account of such experiments is well documented in the literature⁶⁹⁻⁷⁴ and would not be elaborated upon any further in this thesis.

Alternatively, we shall confine our discussion to the quadrupolar interactions encountered in the study of quadrupolar nuclei. Many interesting systems (such as biological

molecules, catalysts, glasses, metals, semiconductors, superconductors and other advanced materials) of importance containing quadrupolar nuclei are insoluble in typical solvents and/or lose their structure on dissolution. In cases where these materials are soluble in liquids, rapid molecular tumbling averages the nuclear quadrupolar interactions resulting in broad, uninformative NMR peaks. Hence, their characterization in the solid state is mandatory. Furthermore, ssNMR spectra of quadrupolar nuclei (in contrast to their spin 1/2 counterparts) are extremely sensitive to the inherent dynamical changes in the molecular structure. Very often, the dynamical changes taking place in the structure are monitored through the changes in the NMR line shapes and the chemical shifts of the participating nuclei. In the case of spin 1/2 nuclei, the observable dynamical time scale is limited to the milli-seconds regime (often decided by the dominant interaction present in the system), while dynamical processes occurring at faster time scales (in the range of few micro-seconds) could well be studied using quadrupolar nuclei as molecular probes.

To realize these objectives and beyond, it is important to quantify the line-shapes of quadrupolar nuclei.^{47,75,76} This in turn, requires spectral resolution, which in the case of quadrupolar nuclei is obscured by the presence of the dominant quadrupolar interactions. To this end, special techniques such as Variable Angle Spinning^{77,78} (VAS), Double Rotation⁷⁹ (DOR) and Dynamic Angle Spinning⁸⁰⁻⁸² (DAS) were introduced in the past to improve the spectral resolution of quadrupolar nuclei. Due to technical limitations and the degree of sophistication required, such techniques could never be implemented with the available NMR hardware. To overcome this limitation, Frydman and co-workers proposed the multi-quantum (MQ) MAS (MQMAS) experiments^{83,84} for acquiring isotropic spectra of quadrupolar nuclei with traditional NMR hardware. The MQMAS technique⁸⁵⁻⁸⁷ is essentially a two-dimensional experiment, that provides a correlation between the second-order quadrupolar shifted isotropic chemical shifts in the indirect dimension (or MQ dimension) with that of the second-order quadrupolar powder pattern in the direct dimension. The local structural information contained in the electric field gradients (EFG's) of the individual sites is deduced from the resolution obtained in the MQ dimension. Although, such an approach seems very viable, the poor excitation^{85,88-97} efficiency of the MQ coherences and its reconversion^{87,88,93,94,98-101} to detectable single-quantum (SQ) coherence, seems to be the major limiting factor. The multi-quantum (MQ) coherences are quite important not only for MQMAS experiments of half-integer quadrupolar nuclei, but also for X-¹⁴N HMQC type of experiments.¹⁰²⁻¹⁰⁴ Since measurements in NMR are carried out on bulk samples, the efficiency of excitation depends on contributions from the individual crystallites present in a polycrystalline sample. In a typical powder sample, the presence of anisotropic interactions such as CSA, dipolar and quadrupolar interactions results in a distribution of resonance frequencies leading to the so-called "powder spectrum". In such cases, the excitation profile and the overall excitation efficiency of a

particular transition depends on several parameters that includes the type of anisotropic interaction, its magnitude relative to the amplitude of the RF fields, the pulse duration besides the sample rotor period in MAS experiments.

In cases where the amplitude of the RF fields employed in the excitation pulse exceeds the magnitudes of the internal interactions present in the system, uniform excitation similar to those obtained in the solution state is possible, at least in principle. Such idealized conditions are less practical in the NMR studies involving quadrupolar nuclei. Additionally, the presence of multiple levels in the quadrupolar spin system, only adds on to the complexities involved in the excitation process. For example, in the case of half-integral quadrupolar spin systems, the line broadening effects arising from the first-order quadrupolar interactions are avoided when the excitation is confined either to the central or the symmetric MQ transition (of highest order) present in the system. However, both the central and MQ transitions are influenced by second-order quadrupolar interactions and the information about the local environment contained in the EFG tensors are obtained by quantifying the second-order quadrupolar interactions manifested in such transitions. Despite its success in improving the resolution in the MQ dimension, the utility of MQMAS experiments depends on the extraction of the quadrupolar coupling constant and asymmetry parameters from the experimental data. This in turn, requires a formal understanding of the response of the system (say quadrupolar nuclei) under an RF pulse.

In the past, several theoretical approaches based on fictitious spin operators^{29,105–108} and spherical tensor operator formalisms^{109–124} were proposed to address this issue. In particular, fictitious spin operator formalism has been employed extensively for describing selective excitations¹⁰⁸ in a wide range of quadrupolar systems.^{106,107,125–130} However, a rigorous description of the spin dynamics under MAS conditions has not yet been reported in the literature. This has been the main motivation behind this thesis. As an alternative, a solution in the form of effective Hamiltonians is proposed in this thesis for describing the evolution of the system under RF pulses under different experimental conditions. The differences in the excitation conditions in single crystals and polycrystalline sample are investigated and optimum excitation conditions are derived both in spinning and non-spinning regimes. A brief outline of the thesis is presented in the following sections.

2. Objectives and Motivation

To quantify the experimental data in NMR experiments involving quadrupolar nuclei, systematic investigation of the quantum evolution of the system during the pulse and free evolution under MAS conditions is mandatory. To realize this objective, a formal theoretical framework based on spherical tensor formalism is presented in this thesis.

To explicate the inconsistencies in the notations and conventions, the spherical tensor formalism is revisited and a consistent framework for the representation of the spatial and spin tensor operators is presented. Employing the spherical tensor formalism, effective radio-frequency (RF) Hamiltonians are proposed to describe both single-quantum (SQ) and multi-quantum (MQ) transitions in quadrupolar systems under static and MAS conditions. Below, we give a brief outline of the general methodology adopted in this thesis.

1.2 Methodology

In quantum mechanics (QM), depending on the state of a system the response of a system is studied using either the Schrödinger equation or through the Quantum-Liouville equation.¹³¹ When the state of a quantum mechanical system (comprising of single or collection of identical systems) is represented through a single wave-function, the time-evolution of the system is described through a simple linear differential equation proposed by Schrödinger:

$$i\hbar \frac{d|\psi(t)\rangle}{dt} = H(t) |\psi(t)\rangle \quad (1.1)$$

In the above equation $|\psi(t)\rangle$ represents the state of the system after time ‘t’ and $H(t)$ is the Hamiltonian of the system. The solution to the above differential equation is given by,

$$|\psi(t)\rangle = U(t, t_0) |\psi(t_0)\rangle \quad (1.2)$$

where $|\psi(t_0)\rangle$ is the initial state of the system at time $t = t_0$ and $U(t, t_0)$ is the evolution operator,

$$U(t, t_0) = T \exp\left(-\frac{i}{\hbar} \int_{t_0}^t H(t') dt'\right) \quad (1.3)$$

In Eq. (1.3) ‘ T ’ represents the Wick-Dyson time ordering operator,^{132,133} and orders the Hamiltonian $H(t)$ at different times such that only products $\dots H(t_3)H(t_2)H(t_1)$ with $t_3 > t_2 > t_1$ are allowed. Since, the state of a quantum mechanical system is not defined (prior to measurement), the state function $|\psi(t)\rangle$ is often expanded in terms of a complete orthonormal basis $|\varphi_j\rangle$ as given below,

$$|\psi(t)\rangle = \sum_j^n c_j(t) |\varphi_j\rangle \quad (1.4)$$

Subsequently, the expectation value of any observable at time ‘t’ is calculated using the standard expression

$$\langle o \rangle = \frac{\langle \psi(t) | o | \psi(t) \rangle}{\langle \psi(t) | \psi(t) \rangle} \quad (1.5)$$

Since measurements in NMR spectroscopy are made on bulk sample, a single state function does not suffice to provide a complete description. Often, the state of such a system (comprising of a collection of identical quantum mechanical systems) is said to be in a mixed state. From a theoretical standpoint, it would be impractical to calculate a macroscopic property (such as spin polarization) by handling the state function of each spin individually and summing the results over the entire ensemble. In such cases, the density operator formalism is employed in quantum mechanics (and in particular in NMR spectroscopy) to study the evolution of a system.^{134–136} To present a reasonable depiction of the system, the idea of describing the states of individual spins is abandoned in favor of a description for the entire ensemble. Operationally, the state of the entire ensemble is described (through $\rho(t)$) by defining an average over the entire ensemble as given below,

$$\rho(t) = \overline{|\psi^s(t)\rangle \langle \psi^s(t)|} = \sum_s^N p_s |\psi^s(t)\rangle \langle \psi^s(t)| \quad (1.6)$$

Employing a suitable basis (the choice of which is dependent on the problem of interest), the density operator for a system is constructed as described below,

$$\begin{aligned} \rho(t) &= \sum_s^N p_s \sum_j^n \sum_l^n c_j^s(t) c_l^{s*}(t) |\varphi_j\rangle \langle \varphi_l| \\ &= \sum_j^n \sum_l^n \overline{c_j(t) c_l^*(t)} |\varphi_j\rangle \langle \varphi_l| \\ &= \sum_j^n \sum_l^n \rho_{jl}(t) |\varphi_j\rangle \langle \varphi_l| \end{aligned} \quad (1.7)$$

In Eq. (1.7), $\rho_{jl}(t) = \overline{c_j(t) c_l^*(t)}$ represents the elements of the density matrix. The diagonal elements $\rho_{jj}(t) = \overline{|c_j(t)|^2}$ of the density matrix are the populations of the corresponding states, while the off-diagonal elements $\rho_{jl}(t) = \overline{c_j(t) c_l^*(t)}$ are known as coherences.^{28,29,52} When the off-diagonal elements are non-zero, the states $|\varphi_j\rangle$ and $|\varphi_l\rangle$ are statistically correlated. The coherence order between spin states $|\varphi_j\rangle$ and $|\varphi_l\rangle$ is given by the difference of corresponding magnetic quantum numbers(m) as given below,

$$M_{jl} = m_j - m_l \quad (1.8)$$

When an external magnetic field is applied to an ensemble of spins at a temperature ‘T’, the coherence between states with differing energies are absent and the populations define the probability of finding the system in a given energy eigenstate. Subsequently, employing the Boltzmann distribution, the equilibrium density operator for a system at a given temperature ‘T’ is defined by,

$$\begin{aligned}\rho_{eq}(t) &= A \exp(-H/k_B T) \\ &= A \exp(-\mathcal{B}H)\end{aligned}\tag{1.9}$$

where $A = \frac{1}{\text{Tr}\{\exp(-\mathcal{B}H)\}}$ and $\mathcal{B} = 1/k_B T$ is called the thermodynamic beta or the inverse temperature ($k_B = 1.3807 \times 10^{-23} JK^{-1}$ is the Boltzmann constant). Under the high-temperature approximation (generally fulfilled at room temperature), expanding and neglecting the higher order terms in \mathcal{B} , a truncated form of the above equation is employed as indicated below,

$$\rho^{eq}(t) \simeq A(I - \mathcal{B}H)\tag{1.10}$$

In the high temperature limit, the value of A is equal to,

$$A = \frac{1}{\text{Tr}\{I\}} = \frac{1}{n}\tag{1.11}$$

with ‘n’ denoting the dimension of the system. Since the Zeeman interaction (Hamiltonian) is dominant (proportional to I_z), the density operator at thermal equilibrium (neglecting the Identity operator) is usually represented by,

$$\rho^{eq}(t) \simeq I_z\tag{1.12}$$

Employing Eq. (1.6) in Eq. (1.1) the evolution of the quantum mechanical system is described by,

$$i\hbar \frac{d\rho(t)}{dt} = [H(t), \rho(t)]\tag{1.13}$$

This differential equation is commonly referred to as Liouville- von Neumann equation¹³¹ or more simply density operator equation and is of central importance for calculating the dynamics of quantum mechanical systems.^{47,131,137-140}

Analogous to Eq. (1.3) the formal solution to the Liouville equation is represented by,

$$\begin{aligned}\rho(t) &= U(t, t_0)\rho(t_0)U^{-1}(t, t_0) \\ &= T \exp\left(-\frac{i}{\hbar} \int_{t_0}^t H(t')dt'\right)\rho(t_0) \exp\left(\frac{i}{\hbar} \int_{t_0}^t H(t')dt'\right)\end{aligned}\quad (1.14)$$

In cases where the Hamiltonian is time-independent, the solution reduces to a much simpler form as illustrated below,

$$\rho(t) = \exp\left[-\frac{i}{\hbar}H(t - t_0)\right]\rho(t_0) \exp\left[\frac{i}{\hbar}H(t - t_0)\right] \quad (1.15)$$

In contrast to Eq. (1.5), the expectation value of an observable is calculated employing the following equation,

$$\langle o \rangle = Tr[\rho(t).o] \quad (1.16)$$

When the Hamiltonian is explicitly time-dependent (refer to Eq. (1.14)), analytic description of the time evolution becomes complicated. In such cases, the standard approach involves a description based on numerical methods. In the numerical approach, the evolution under a time-dependent Hamiltonian is approximated through a description that involves a series of time-independent Hamiltonians defined at shorter time-scales. Accordingly, the total evolution of the system is expressed as a product of the evolution at shorter times through the solution described in Eq. (1.15). Although, such methods yield accurate results, they are of less utility in the design and optimization of experiments.

To this end, development of analytical methods has remained a major pursuit for several decades.^{111,141–146} In the analytic based methods, the time-evolution of the system is described through a time-averaged Hamiltonian under certain approximations. In NMR spectroscopy, analytical methods are based on (1) Average Hamiltonian theory (AHT)^{147–149} (2) Floquet theory.¹⁵⁰ In the AHT framework proposed by Waugh and Haeberlen, the evolution of a system under time-dependent Hamiltonians is described through a time-averaged Hamiltonian that is derived based on the Magnus expansion^{147,151–153} formula for time-dependent equations. By contrast, in Floquet theory, the time-evolution is described in terms of time-independent Hamiltonians defined in an infinite dimensional vector space. Employing the contact transformation^{143,154–159} procedure, the dimensionality of the problem in the Floquet calculations are alleviated through the concept of effective Hamiltonians.^{143,160–162} Here in this thesis, we confine our discussion to Floquet based methods for describing the dynamics of quadrupolar nuclei under RF fields. In the following Section 1.2.1, we list the analytic methods employed for studying the time evolution of a system (1/2) under different experimental conditions.

1.2.1 Concept of effective Hamiltonians

To, illustrate the effective Hamiltonian approach, a pedagogical description of the ‘spin dynamics’ is presented with an isolated spin $I = 1/2$ nuclei as an example. The Hamiltonian for an isolated spin ($I = 1/2$) system is represented by,

$$\begin{aligned} H &= \underbrace{\hbar\omega_0 I_z}_{H_Z} + \underbrace{\hbar\omega_0 \sigma_{iso} I_z}_{H_{C,iso}} + \underbrace{2\hbar\omega_1 \cos \omega t I_x}_{H_{RF}} \\ &= \underbrace{\hbar\omega_z I_z}_{H_{Z,C}} + \underbrace{2\hbar\omega_1 \cos \omega t I_x}_{H_{RF}} \end{aligned} \quad (1.17)$$

with H_Z denoting the Zeeman interaction, $H_{C,iso}$ the isotropic chemical shift and H_{RF} the interaction of the oscillating RF field with the spin system.

In the above equation $\omega_0 = -\gamma B_0$ represents the Larmor frequency, ω_z the chemically shifted Larmor frequency, $\omega_{iso} = -\sigma_{iso}\gamma B_0$ the isotropic chemical shift, ω the carrier frequency and ω_1 the amplitude of the oscillating field. To describe the effects of the oscillating field, the Hamiltonian is transformed into a rotating frame,

$$\tilde{H} = U H U^{-1} \quad (1.18)$$

where $U = \exp(iI_z \omega t)$. When $\omega = \omega_0$ the rotating frame Hamiltonian has both a longitudinal as well as transverse component.

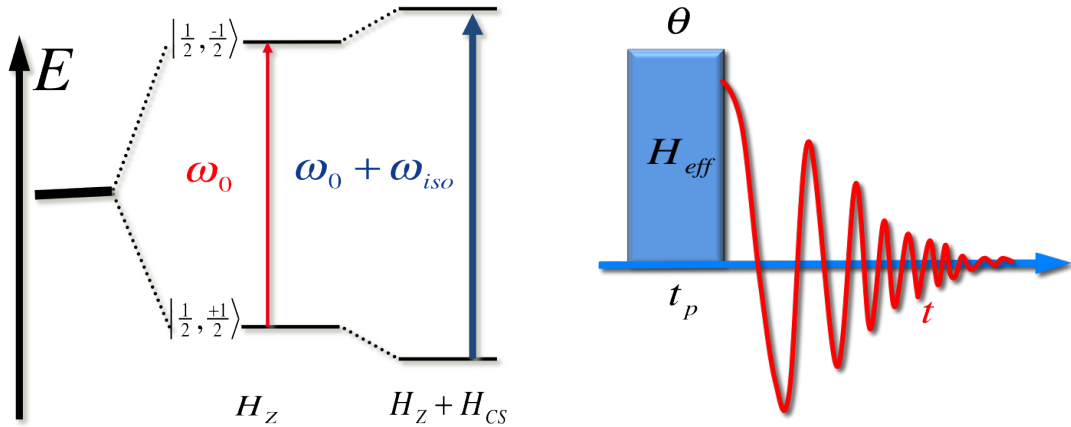


Figure 1.1: Energy level diagram for spin $I = 1/2$ system in the presence of chemical shift off-set along with simple single pulse sequence.

$$\tilde{H} = \hbar\Delta\omega I_z + \hbar\omega_1 I_x \quad (1.19)$$

where $\Delta\omega$ is the off-set frequency (i.e $\Delta\omega = \omega_z - \omega$). Depending on the magnitudes of these interactions, different theoretical frameworks^{34,38,107,112,163–165} have emerged in the past to

describe the evolution of the system under time-dependent fields. For illustrative purposes, some of the general procedures employed in this thesis are summarized below.

Case I: $\omega_1 \gg \Delta\omega$

When the amplitude of the oscillating field exceeds the magnitude of the chemical-shift offset term, the off-set contributions ($\Delta\omega$) are ignored during the pulse. Subsequently, the effective Hamiltonian during the pulse is represented by,

$$\tilde{H}_{eff} = \hbar\omega_1 I_x \quad (1.20)$$

To have a consistent description, the initial density operator is also transformed into the rotating frame (i.e. $U = \exp(iI_z\omega t)$). Since, $[I_z, \rho(0)] = 0$, the equilibrium density operator remains invariant. Subsequently, the density operator after the pulse is evaluated and is represented below.

$$\tilde{\rho}(t_p) = I_z \cos(\omega_1 t_p) - I_y \sin(\omega_1 t_p) \quad (1.21)$$

As depicted in Eq. (1.21), the maximum signal in the transverse plane is obtained when $\omega_1 t_p = \frac{\pi}{2}$. Subsequently, the density operator after the pulse is represented by,

$$\tilde{\rho}(t_p) = -I_y \quad (1.22)$$

The density operator after the pulse evolves under the chemical shift Hamiltonian and is represented below,

$$\tilde{\rho}(t_p + t) = -I_y \cos(\Delta\omega t) + I_x \sin(\Delta\omega t) \quad (1.23)$$

To have a consistent description, the detection operator ' I^+ ' is also transformed ($\tilde{I}^+ = UI^+U^- = \tilde{I}^+(t) = I^+ \exp(i\omega t)$). Employing Eq. (1.16), the optimized time domain signal is evaluated.

$$\begin{aligned} \langle I^+(t) \rangle &= Tr[\rho(t_p + t)\tilde{I}^+] \\ &= C(1)^2 \cdot \frac{1}{2} \exp(i\omega_0 + \Delta\omega t) \end{aligned} \quad (1.24)$$

Case I: $\omega_1 \approx \Delta\omega$

Method I: Brute force approach

When the magnitude of the chemical shift offset term is comparable to that of the ampli-

tude of the RF field, a more rigorous description is required. In the brute force approach, the evolution of the system during the pulse is evaluated using the Baker-Campbell-Hausdorff (BCH) [166-171,171,172](#) expansion as given below,

$$\tilde{\rho}(t_p) = \left[\frac{\Delta\omega^2}{\omega_{eff}^2} + \frac{\omega_1^2}{\omega_{eff}^2} \cos(\omega_{eff}t_p) \right] I_z + \left[\frac{\Delta\omega\omega_1}{\omega_{eff}^2} - \frac{\Delta\omega\omega_1}{\omega_{eff}^2} \cos(\omega_{eff}t_p) \right] I_x - \frac{\omega_1}{\omega_{eff}} \sin(\omega_{eff}t_p) I_y \quad (1.25)$$

with $\omega_{eff} = \sqrt{\omega_1^2 + \Delta\omega^2}$. As illustrated in Eq. (1.25), maximum signal in the transverse plane is obtained when $\omega_{eff}t_p = \frac{\pi}{2}$. Subsequently, the density operator after the pulse is evaluated and is represented by,

$$\tilde{\rho}(t_p) = \frac{\Delta\omega^2}{\omega_{eff}^2} I_z + \frac{\Delta\omega\omega_1}{\omega_{eff}^2} I_x - \frac{\omega_1}{\omega_{eff}} I_y \quad (1.26)$$

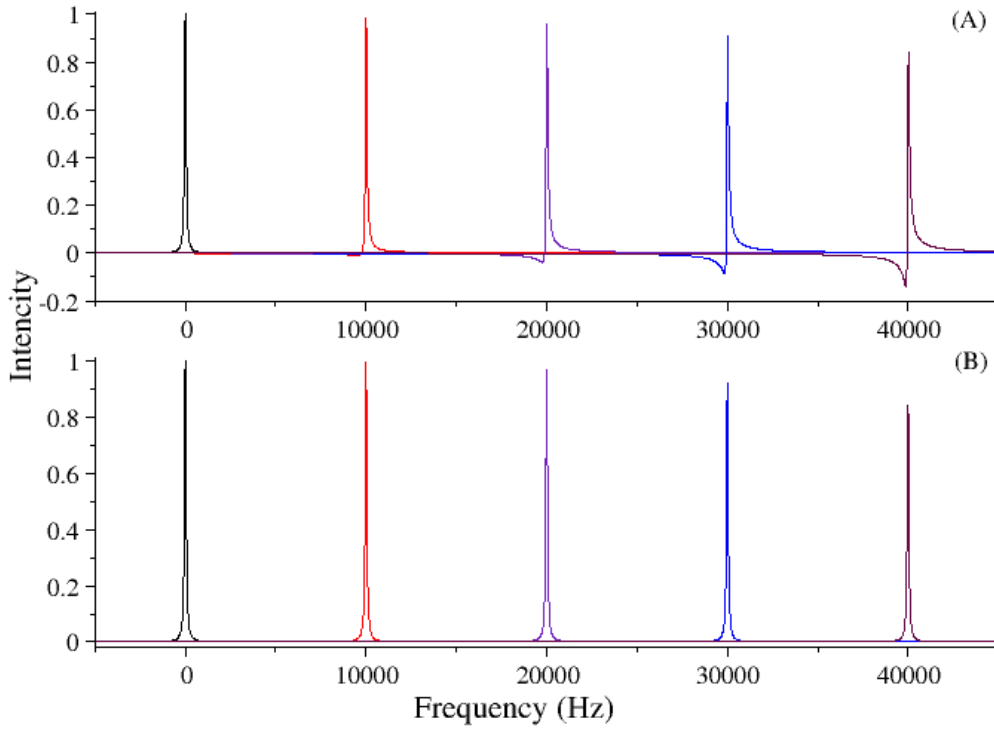


Figure 1.2: Simulations depicting the the role of off-sets ($\Delta\nu = 0$ to 40 kHz) on the NMR line shapes. In panel A, the the off-sets were ignored in the optimization process ($\omega_1 t = \pi/2$). In panel B, off-set frequencies were included in the optimization process i.e $\omega_{eff} t = \pi/2$ along with intensity correction (see Eqs. (1.25) and (1.28)).

Following our earlier description, the density operator under free evolution is represented

by,

$$\begin{aligned}\tilde{\rho}(t_p + t) = & \frac{\Delta\omega^2}{\omega_{eff}^2} I_z - I_y \left[\frac{\omega_1}{\omega_{eff}} \cos(\Delta\omega t) - \frac{\Delta\omega\omega_1}{\omega_{eff}^2} \sin(\Delta\omega t) \right] \\ & + I_x \left[\frac{\Delta\omega\omega_1}{\omega_{eff}^2} \cos(\Delta\omega t) + \frac{\omega_1}{\omega_{eff}} \sin(\Delta\omega t) \right]\end{aligned}\quad (1.27)$$

Accordingly, the optimized time-domain signal is evaluated and is represented by,

$$\langle I^+(t) \rangle = C(1)^2 \cdot \frac{1}{2} \left(\frac{\omega_1}{\omega_{eff}} + \frac{i\Delta\omega\omega_1}{\omega_{eff}^2} \right) \exp(i\omega t) \quad (1.28)$$

In Fig. 1.2, the effects of finite off-sets on the NMR line-shapes is depicted through a set of simulations employing different offsets. In systems with finite off-sets, the flip angle depends on both the RF amplitude as well as the chemical shift off-set. When the chemical shift off-set terms are incorporated in the optimization of the flip angles along with intensities, the distortions observed in the line shapes are removed completely from the spectrum.

Method II: Tilted rotating frame method

As an alternative to the brute force approach, the Hamiltonian in the rotating frame is transformed into a tilted frame^{34,164,165} such that the effective field experienced by the spin is quantized along the z-axis. Mathematically, this is accomplished by the transformation function,

$$U = \exp(i\theta I_y) \quad (1.29)$$

where $\tan\theta = \frac{\omega_1}{\Delta\omega}$. The effective Hamiltonian in the tilted rotating frame during the pulse is represent by,

$$\tilde{H}_{eff} = U H U^{-1} = \hbar\omega_{eff} I_z \quad (1.30)$$

Accordingly, the initial density operator is transformed and is represented in the tilted rotating frame by,

$$\tilde{\rho}(0) = I_z \cos\theta - I_x \sin\theta \quad (1.31)$$

Employing the effective Hamiltonian (Eq. (1.30)), the density operator after the pulse (under the Eq. (1.30)) is evaluated and represented by,

$$\tilde{\rho}(t_p) = I_z \cos\theta - I_x \sin\theta \cos(\omega_{eff} t_p) - I_y \sin\theta \sin(\omega_{eff} t_p) \quad (1.32)$$

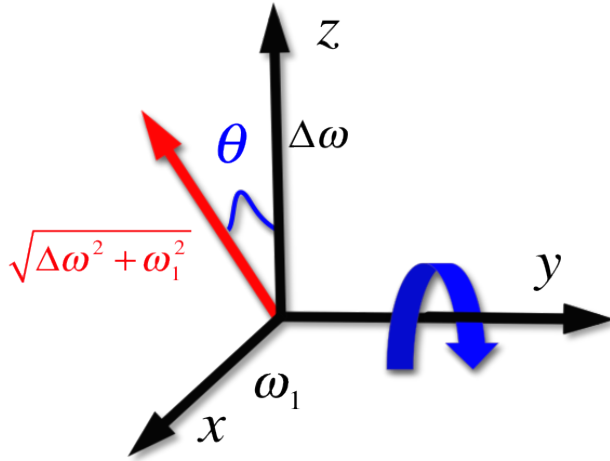


Figure 1.3: The figure depicts the tilted rotating frame transformation about $-\theta$ along y-axis.

As depicted in Eq. (1.32), the maximum signal in the transverse plane is obtained when $\omega_{eff}t_p = \frac{\pi}{2}$. Following this procedure, the density operator in the titled rotating frame is transformed into the rotating frame by the following reverse transformation:

$$\tilde{\rho}(t_p) = U^{-1} \tilde{\tilde{\rho}}(t_p) U = \cos^2\theta I_z + \sin\theta \cos\theta I_x - \sin\theta I_y \quad (1.33)$$

The evolution of the density operator under the chemical shift Hamiltonian in the rotating frame is represented by,

$$\begin{aligned} \tilde{\rho}(t_p + t) = & \cos^2\theta I_z - I_y [\sin\theta \cos(\Delta\omega t) - \cos\theta \sin\theta \sin(\Delta\omega t)] \\ & + I_x [\cos\theta \sin\theta \cos(\Delta\omega t) + \sin\theta \sin(\Delta\omega t)] \end{aligned} \quad (1.34)$$

The optimized time-domain signal is evaluated accordingly and is represented by,

$$\langle I^+(t) \rangle = C(1)^2 \cdot \frac{1}{2} (\sin\theta + i \sin\theta \cos\theta) \exp(i\omega_z t) \quad (1.35)$$

On substitution ($\sin\theta = \frac{\omega_1}{\omega_{eff}}$, $\cos\theta = \frac{\Delta\omega}{\omega_{eff}}$), the above Eq. (1.35) reduces to the familiar form depicted in Eq. (1.28)

Method III: Contact Transformation Method

To illustrate the utility of the contact transformation^{143,154–159} procedure in the derivation of effective Hamiltonians, an alternate description based on perturbation theory is presented in this section. Since the amplitude of the RF field often exceeds the magnitude of the chemical-shift off-set, the RF Hamiltonian defined in the rotating frame is quantized along the z-axis through a $\pi/2$ rotation along y-axis using the transformation function $U = \exp(i\frac{\pi}{2}I_y)$. As is the case with perturbation techniques, the Hamiltonian in the tilted

rotating frame is divided into zero-order and first-order term as given below.

$$\tilde{H} = \underbrace{\hbar\omega_1 I_z}_{H_0} - \underbrace{\hbar\Delta\omega I_x}_{H_1} \quad (1.36)$$

Following the procedure described in the appendix Section 1.A, the off-diagonal contributions in the original Hamiltonian are folded through a unitary transformation, defined by the transformation function,

$$S_1 = -\frac{\Delta\omega}{\omega_1} I_y \quad (1.37)$$

The operators (along with their coefficients) present in the transformation function are chosen such that the off-diagonal contributions resulting from H_1 are removed to first order. Following the procedure, the second order corrections are evaluated.

$$\begin{aligned} H_2^{(1)} &= i[S_1, H_1] - \frac{1}{2}[S_1, [S_1, H_0]] \\ &= \frac{i}{2}[S_1, H_1] \\ &= \frac{\hbar\Delta\omega^2}{2\omega_1} I_z \end{aligned} \quad (1.38)$$

The effective Hamiltonian during the pulse (to second order) is represented by,

$$H_{eff} = \hbar\omega_1 I_z + \frac{\hbar\Delta\omega^2}{2\omega_1} I_z \quad (1.39)$$

In a similar vein, the initial density operator is transformed using the transformation functions, as illustrated below.

$$\tilde{\tilde{\rho}}(0) = -I_x \cos\left(\frac{\Delta\omega}{\omega_1}\right) + I_z \sin\left(\frac{\Delta\omega}{\omega_1}\right) \quad (1.40)$$

Subsequently, employing the effective Hamiltonian, the evolution of the density operator under the pulse is calculated as represented below,

$$\begin{aligned} \tilde{\tilde{\rho}}(t_p) &= I_z \sin\left(\frac{\Delta\omega}{\omega_1}\right) - I_x \cos\left(\frac{\Delta\omega}{\omega_1}\right) \cos\left(\left(\omega_1 + \frac{\Delta\omega^2}{2\omega_1}\right)t_p\right) \\ &\quad - I_y \cos\left(\frac{\Delta\omega}{\omega_1}\right) \sin\left(\left(\omega_1 + \frac{\Delta\omega^2}{2\omega_1}\right)t_p\right) \end{aligned} \quad (1.41)$$

From Eq. (1.41), the maximum signal in the transverse plane is obtained when $(\omega_1 + \frac{\Delta\omega^2}{2\omega_1})t_p = \frac{\pi}{2}$. As described earlier, the density operator after the pulse is transformed back into the standard rotating frame through the reverse transformations as illustrated below.

$$\tilde{\rho}(t_p) = U^- e^{-is_1} \tilde{\tilde{\rho}}(t_p) e^{is_1} U = \sin^2\left(\frac{\Delta\omega}{\omega_1}\right) I_z + \sin\left(\frac{\Delta\omega}{\omega_1}\right) \cos\left(\frac{\Delta\omega}{\omega_1}\right) I_x - \cos\left(\frac{\Delta\omega}{\omega_1}\right) I_y \quad (1.42)$$

The free evolution of the density operator under the chemical shift Hamiltonian in the rotating frame is calculated and the time-domain signal is evaluated.

$$\begin{aligned} \tilde{\rho}(t_p + t) = & \sin^2\left(\frac{\Delta\omega}{\omega_1}\right)I_z - I_y \left[\cos\left(\frac{\Delta\omega}{\omega_1}\right) \cos(\Delta\omega t) - \sin\left(\frac{\Delta\omega}{\omega_1}\right) \cos\left(\frac{\Delta\omega}{\omega_1}\right) \sin(\Delta\omega t) \right] \\ & + I_x \left[\cos\left(\frac{\Delta\omega}{\omega_1}\right) \sin\left(\frac{\Delta\omega}{\omega_1}\right) \cos(\Delta\omega t) + \cos\left(\frac{\Delta\omega}{\omega_1}\right) \sin(\Delta\omega t) \right] \end{aligned} \quad (1.43)$$

$$\langle I^+(t) \rangle = C(1)^2 \cdot \frac{1}{2} \left[\cos\left(\frac{\Delta\omega}{\omega_1}\right) + i \sin\left(\frac{\Delta\omega}{\omega_1}\right) \cos\left(\frac{\Delta\omega}{\omega_1}\right) \right] \exp(i\omega_z t) \quad (1.44)$$

It is important to realize here that, when the magnitudes of the perturbing Hamiltonians are comparable to the zero order Hamiltonian, there could be significant deviations observed in the results emerging from the contact transformation procedure with those derived from other methods. Moreover, the extension of the methods proposed in this section to the study of the quadrupolar spin is less straightforward and forms the main motivation behind this thesis.

1.3 Organization of the thesis

In this thesis, an analytic framework based on the concept of effective Hamiltonians is proposed to describe the effects of RF pulses on quadrupolar nuclei. The description presented is well suited for describing the excitation in both static and spinning samples. To present a pedagogical description, the conventions employed in the description of spin Hamiltonians in the solid-state based on spherical tensor formalism is revisited in chapter-2. Although, several descriptions do exist in the literature,^{30,56,75,87,173-179} the motivation for this pursuit has been to develop a consistent notation for the description of both spatial and spin tensor operators and develop a framework for extending its utility in the description of coupled spin systems. Accordingly, the normalization constants and phase factors employed in the description of spatial and spin tensor operators is re-derived. Employing the spherical tensor formalism, effective Hamiltonians are derived to explain the excitation of quadrupolar nuclei in the third chapter. To understand the effects of the spatial anisotropy, excitations in single crystals and powder samples is described both in the static and spinning conditions. The optimum conditions required for excitation are derived for both selective and non-selective excitation conditions. Employing the method of contact transformation, the excitation of quadrupolar nuclei is described in terms of effective RF Hamiltonians. In the fourth chapter, excitation of MQ transitions is described. The role of sample spinning frequency, RF amplitudes, duration of the pulse and the magnitude of the quadrupolar coupling constant in the excitation process is analyzed in detail. In the past, such descriptions existed only for static single crystals.¹⁰⁵⁻¹⁰⁷ The validity of the secular approximation in the MQ excitation process is discussed thoroughly through analytic expressions and simulations. Finally, a brief summary of the proposed effective Hamiltonian approach is presented in chapter-5 along with possible extensions.

Appendix

1.A The van Vleck and Contact transformation

In NMR spectroscopy, the magnitude of the internal Hamiltonians differ significantly from one another. Since the eigenvalues encode the frequencies observed in the spectrum, accurate determination of them play an important role in the spectral interpretation. To this end, analytical methods such as the Rayleigh-Schrödinger perturbation theory have found extensive utility in the determination of eigenvalues. In the Rayleigh-Schrödinger method, corrections to the zero-order (dominant term) eigen values are obtained in terms of matrix elements. As an alternative to this exercise, derivation of effective Hamiltonians has long been known and practiced in molecular spectroscopy.^{156,159,180} In this section, we describe two such methods (van Vleck^{154,155} and contact transformation^{143,156–159,181}) for deriving effective Hamiltonians. In contrast to the Rayleigh-Schrödinger approach, the perturbation corrections are obtained in terms of operators resulting in the concept of effective Hamiltonians.

Analogous to the standard perturbation theory, the interaction Hamiltonians are arranged in the decreasing order of their magnitude as follows,

$$H = H_0 + \lambda H_1 + \lambda^2 H_2 + \dots \quad (1.45)$$

where λ is perturbation or bookkeeping parameter, H_0 is the zero-order Hamiltonian and H_1, H_2 , etc. are the perturbation Hamiltonians. Employing series of unitary transformations, the original Hamiltonian is transformed.

$$\tilde{H} = H^{(n)} = U H U^{-1} \quad (1.46)$$

The series of unitary transformations are represented by,

$$U = U_n U_{n-1} \dots U_2 U_1 \quad (1.47)$$

with

$$U_n = e^{i\lambda^n S_n} \quad (1.48)$$

The transformation functions S_1, S_2, S_3, \dots are chosen to remove the effects of off-diagonal operators in H to order $\lambda, \lambda^2, \lambda^3, \dots$ respectively. Each of the successive transformations produced by the development of U is known as a contact transformation, while the first transformation ($H^{(1)} = U_1 H U_1^{-1} = e^{iS_1} H e^{-iS_1}$) is what is usually referred to as the van Vleck transformation.

Now we can expand the Hamiltonian after the first transformation (van Vleck transformation) as given below,

$$H^{(1)} = U_1 H U_1^{-1} = H_0^{(1)} + \lambda H_1^{(1)} + \lambda^2 H_2^{(1)} + \dots \quad (1.49)$$

The transformed Hamiltonian $H^{(1)}$ obtained after first transformation is given by,

$$H^{(1)} = U_1 H U_1^{-1} = H + \sum_{n=1}^{\infty} \frac{i^n \lambda^n}{n!} \underbrace{[S_1, [S_1, \dots, [S_1, H] \dots]]}_n \quad (1.50)$$

with unitary transformation:

$$U_1 = e^{i\lambda S_1} = 1 + i\lambda S_1 - \lambda^2 S_1^2 \dots \quad (1.51)$$

Equating like powers in Eqs. (1.49) and (1.50), the perturbation corrections to orders are obtained.

$$\begin{aligned} H_0^{(1)} &= H_0, \\ H_1^{(1)} &= H_1 + i[S_1, H_0], \\ H_2^{(1)} &= H_2 + i[S_1, H_1] - \frac{1}{2}[S_1, [S_1, H_0]], \\ H_3^{(1)} &= H_3 + i[S_1, H_2] - \frac{1}{2}[S_1, [S_1, H_1]] - \frac{i}{6}[S_1, [S_1, [S_1, H_0]]], \\ &\vdots \\ &\vdots \end{aligned} \quad (1.52)$$

In general, the n^{th} -order correction (resulting from the first transformation) is represented by,

$$H_n^{(1)} = H_n + \sum_{m=0}^{n-1} \frac{i^{n-m}}{(n-m)!} \underbrace{[S_1, [S_1, \dots, [S_1, H_m] \dots]]}_{n-m} \quad (1.53)$$

The crux of the contact transformation procedure lies in the determination/choice of trans-

formation function.^{143,156} For e.g, the transformation function S_1 is chosen to compensate the off-diagonal term in H_1 .

$$H_1^{(1)} = H_1 + i[S_1, H_0] \quad (1.54)$$

In general, H_1 may contain both diagonal and off-diagonal terms. The operator S_1 is chosen such that the transformed Hamiltonian $H_1^{(1)}$ does not contain any off-diagonal terms to order λ^1 (commutator $[S_1, H_0]$ compensates the off-diagonal terms present in H_1).

The above procedure can be repeated to perform a second contact transformation. The Hamiltonian obtained by van Vleck transformation can be subjected to successive contact transformations using transformation function S_2 such that $H_0 + \lambda H_1^{(1)} + H_2^{(2)}$ would be diagonal.

$$H^{(2)} = e^{i\lambda^2 S_2} H^{(1)} e^{-i\lambda^2 S_2} = H_0^{(2)} + \lambda H_1^{(2)} + \lambda^2 H_2^{(2)} + \dots \quad (1.55)$$

Equating like powers in Eq. (1.55) we get,

$$\begin{aligned} H_0^{(2)} &= H_0, \\ H_1^{(2)} &= H_1^{(1)}, \\ H_2^{(2)} &= H_2^{(1)} + i[S_2, H_0], \\ H_3^{(2)} &= H_3^{(1)} + i[S_2, H_1^{(1)}], \\ H_4^{(2)} &= H_4^{(1)} + i[S_2, H_2^{(1)}] - \frac{1}{2}[S_2, [S_2, H_0]], \\ H_5^{(2)} &= H_5^{(1)} + i[S_2, H_3^{(1)}] - \frac{1}{2}[S_2, [S_2, H_1^{(1)}]], \end{aligned} \quad (1.56)$$

The above procedure is repeated until eigenvalues of the transformed Hamiltonian are closer to the exact eigenvalues of the untransformed Hamiltonian.

In general, the effective Hamiltonian after k^{th} transformation is given by,

$$H_n^{(k)} = H_n^{(k-1)} + \sum_{m=0}^{n-k} \frac{i^{\binom{n-m}{k}}}{\binom{n-m}{k}!} \underbrace{[S_k, [S_k, \dots, [S_k, H_m^{(k-1)}] \dots]}_{\frac{n-m}{k}} \quad \forall \frac{n-m}{k}, +\text{integers} \quad (1.57)$$

References

- [1] E. M. Purcell, H. C. Torrey and R. V. Pound, *Phys. Rev.*, 1946, **69**, 37.
- [2] F. Bloch, W. W. Hansen and M. Packard, *Phys. Rev.*, 1946, **69**, 127.
- [3] F. Bloch, *Phys. Rev.*, 1946, **70**, 460.
- [4] F. Bloch, W. W. Hansen and M. Packard, *Phys. Rev.*, 1946, **70**, 474.
- [5] J. T. Arnold, S. S. Dharmatti and M. E. Packard, *J. Chem. Phys.*, 1951, **19**, 507.
- [6] C. Rienstra, L. Tucker-Kellogg, C. Jaroniec, M. Hohwy, B. Reif, M. T. McMahon, B. Tidor, T. Lozano-Perez and R. Griffin, *Proc. Nat. Acad. Sci. USA*, 2002, **99**, 10260.
- [7] F. Castellani, B. van Rossum, A. Diehl, M. Schubert, K. Rehbein and H. Oschkinat, *Nature*, 2002, **420**, 98.
- [8] U. Heinemann, G. Illing and H. Oschkinat, *Curr. Opin. Biotechnol.*, 2001, **12**, 348.
- [9] J. Pauli, M. Baldus, B. van Rossum, H. de Groot and H. Oschkinat, *ChemBioChem*, 2001, **2**, 272.
- [10] R. Tycko, *Annu. Rev. Phys. Chem.*, 2001, **52**, 575.
- [11] R. Tycko, *Curr. Opin. Chem. Biol.*, 2000, **4**, 500.
- [12] C. P. Jaroniec, C. E. MacPhee, N. S. Astrof, C. M. Dobson and R. G. Griffin, *Proc. Nat. Acad. Sci.*, 2002, **99**, 16748.
- [13] R. Tycko, *J. Biomol. NMR*, 1996, **8**, 239.
- [14] C. P. Jaroniec, C. E. MacPhee, V. S. Bajaj, M. T. MacMahon, C. M. Dobson and R. G. Griffin, *Proc. Nat. Acad. Sci. USA*, 2004, **101**, 711.
- [15] C. J. Gorter, *Physica*, 1936, **3**, 503.
- [16] C. J. Gorter, *Physica*, 1936, **3**, 995.
- [17] I. I. Rabi, *Phys. Rev.*, 1937, **51**, 652.
- [18] I. I. Rabi, J. R. Zacharias, S. Millman and P. Kusch, *Phys. Rev.*, 1938, **53**, 318.
- [19] I. I. Rabi, S. Millman, P. Kusch and J. R. Zacharias, *Phys. Rev.*, 1939, **55**, 526.
- [20] W. Gerlach and O. Stern, *Zeitschrift für Physik A Hadrons and Nuclei*, 1922, **9**, 349.

- [21] G. E. Uhlenbeck and S. Goudsmit, *Naturwissenschaften*, 1925, **13**, 953.
- [22] W. Pauli, *Zeitschrift für Physik A Hadrons and Nuclei*, 1925, **31**, 765.
- [23] W. Heisenberg, *Z. Phys.*, 1928, **49**, 619.
- [24] P. A. M. Dirac, *Proc. R. Soc. London.*, 1928, p. 351.
- [25] W. Pauli, *Phys. Rev.*, 1940, **58**, 716.
- [26] P. Zeeman, *Versl. Kon. Ak. Wet.*, 1896, **5**, 181.
- [27] E. L. Hahn, *Phys. Rev.*, 1950, **80**, 580.
- [28] R. R. Ernst, G. Bodenhausen and A. Wokaun, *Principles of nuclear magnetic resonance in one and two dimensions*, Clarendon Press Oxford, 1987.
- [29] A. Abragam, *The principles of nuclear magnetism*, Oxford university press, 1961.
- [30] M. Mehring, *Principles of high resolution NMR in solids*, Springer Springer Science & Business Media, 2012.
- [31] M. J. Duer, *Solid state NMR spectroscopy: principles and applications*, John Wiley & Sons, 2008.
- [32] K. Schmidt-Rohr and H. W. Spiess, *Multidimensional solid-state NMR and polymers*, 1994.
- [33] J. H. Baltisberger, S. L. Gann, P. J. Grandinetti and A. Pines, *Mol. Phys.*, 1994, **81**, 1109.
- [34] M. Baldus, A. T. Petkova, J. Herzfeld and R. G. Griffin, *Mol. Phys.*, 1998, **95**, 1197.
- [35] M. H. Levitt, D. Suter and R. R. Ernst, *J. Chem. Phys.*, 1986, **84**, 4243.
- [36] E. R. Andrew, A. Bradbury and R. G. Eades, *Nature*, 1958, **182**, 1659.
- [37] I. J. Lowe, *Phys. Rev. Lett.*, 1959, **2**, 285.
- [38] S. R. Hartmann and E. L. Hahn, *Phys. Rev.*, 1962, **128**, 2042.
- [39] A. Pines, M. G. Gibby and J. S. Waugh, *J. Chem. Phys.*, 1973, **59**, 569.
- [40] A. L. Bloom and J. N. Shoolery, *Phys. Rev.*, 1955, **97**, 1261.
- [41] Z. Gan and R. R. Ernst, *Solid State Nucl. Magn. Reson.*, 1997, **8**, 153.
- [42] A. E. Bennett, C. M. Rienstra, M. Auger, K. V. Lakshmi and R. G. Griffin, *J. Chem. Phys.*, 1995, **103**, 6951.
- [43] A. Detken, E. H. Hardy, M. Ernst and B. H. Meier, *Chem. Phys. Lett.*, 2002, **356**, 298.
- [44] P. Tekely, P. Palmas and D. Canet, *J. Magn. Reson., Ser. A*, 1994, **107**, 129.
- [45] B. M. Fung, A. K. Khitrin and K. Ermolaev, *J. Magn. Reson.*, 2000, **142**, 97.
- [46] R. S. Thakur, N. D. Kurur and P. K. Madhu, *Chem. Phys. Lett.*, 2006, **426**, 459.

- [47] R. E. Wasylshen, S. E. Ashbrook and S. Wimperis, *NMR of Quadrupolar Nuclei in Solid Materials*, John Wiley & Sons, 2012.
- [48] C. H. Wu, A. Ramamoorthy and S. J. Opella, *J. Magn. Reson., Ser. A*, 1994, **109**, 270.
- [49] G. Wu, D. Rovnyank, B. Sun and R. G. Griffin, *Chem. Phys. Lett.*, 1996, **249**, 210.
- [50] L. Frydman and J. S. Harwood, *J. Am Chem. Soc.*, 1995, **117**, 5367.
- [51] T. Gullion and J. Schaefer, *J. Magn. Reson.*, 1989, **81**, 196.
- [52] C. P. Slichter, *Principles of magnetic resonance*, Springer Springer Science & Business Media, 2013.
- [53] R. V. Pound, *Phys. Rev.*, 1950, **79**, 685.
- [54] A. J. Vega, in *Quadrupolar Nuclei in Solids*, John Wiley & Sons, Ltd, 2007.
- [55] M. H. Cohen, F. Reif, F. Seitz and D. Turnbull, *Solid state physics*, 1957, p. 38.
- [56] P. P. Man, in *Quadrupolar Interactions*, John Wiley & Sons, Ltd, 2007.
- [57] M. G. Colombo, B. H. Meier and R. R. Ernst, *Chem. Phys. Lett.*, 1988, **146**, 189.
- [58] K. Nomura, K. Takegoshi, T. Terao, K. Uchida and M. Kainosho, *J. Am. Chem. Soc.*, 1999, **121**, 4064.
- [59] Y. Ishii, T. Terao and M. Kainosho, *Chem. Phys. Lett.*, 1996, **256**, 133.
- [60] N. Tjandra and A. Bax, *Science*, 1997, **278**, 1111.
- [61] Y. Ishii, K. Hirao, T. Terao, T. Terauchi, M. Oba, K. Nishiyama and M. Kainosho, *Solid State Nucl. Magn. Reson.*, 1998, **11**, 169.
- [62] I. Sack, Y. Balazs, S. Rahimipour and S. Vega, *J. Am. Chem. Soc.*, 2000, **122**, 12263.
- [63] M. Hohwy, C. P. Jaroniec, B. Reif, C. M. Rienstra and R. G. Griffin, *J. Am. Chem. Soc.*, 2000, **122**, 3218.
- [64] V. Ladizhansky, C. P. Jaroniec, A. Diehl, H. Oschkinat and R. G. Griffin, *J. Am. Chem. Soc.*, 2003, **125**, 6827.
- [65] K. Schmidt-Rohr, *J. Am. Chem. Soc.*, 1996, **118**, 7601.
- [66] C. P. Jaroniec, B. A. Tounge, J. Herzfeld and R. G. Griffin, *J. Am. Chem. Soc.*, 2001, **123**, 3507.
- [67] A. Bennett, R. Griffin and S. Vega, in *Recoupling of homo- and heteronuclear dipolar interactions in rotating solids*, ed. B. Blumich, Springer-Verlag, Berlin, 1994.
- [68] C. P. Jaroniec, C. Filip and R. G. Griffin, *J. Am. Chem. Soc.*, 2002, **124**, 10728.
- [69] T. Gullion and J. Schaefer, *J. Magn. Reson.*, 1989, **81**, 196.
- [70] A. E. Bennett, R. G. Griffin, J. H. Ok and S. Vega, *J. Chem. Phys.*, 1992, **96**, 8624.
- [71] N. C. Nielsen, H. Bildso, H. J. Jakobsen and M. H. Levitt, *J. Chem. Phys.*, 1994, **101**, 1805.

- [72] N. C. Nielsen, H. Bildso, H. J. Jakobsen and M. H. Levitt, *J. Chem. Phys.*, 1994, **101**, 1805.
- [73] Y. K. Lee, N. D. Kurur, M. Helmle, O. G. Johannessen, N. C. Nielsen and M. H. Levitt, *Chem. Phys. Lett.*, 1995, **242**, 304.
- [74] M. Hohwy, H. J. Jakobsen, M. Eden, M. H. Levitt and N. C. Nielsen, *J. Chem. Phys.*, 1998, **108**, 2686.
- [75] A. Jerschow, *Prog. Nucl. Magn. Reson. Spectrosc.*, 2005, **46**, 63.
- [76] P. P. Man, E. Duprey, J. Fraissard, P. Tougne and J.-B. d’Espinose, *Solid State Nucl. Magn. Reson.*, 1995, **5**, 181.
- [77] S. Ganapathy, S. Schramm and E. Oldfield, *J. Chem. Phys.*, 1982, **77**, 4360.
- [78] E. Oldfield and R. J. Kirkpatrick, *Science*, 1985, **227**, 1537.
- [79] A. Samoson, E. Lippmaa and A. Pines, *Mol. Phys.*, 1988, **65**, 1013.
- [80] A. Llor and J. Virlet, *Chem. Phys. Lett.*, 1988, **152**, 248.
- [81] B. F. Chmelka, K. T. Mueller, A. Pines, J. Stebbins, Y. Wu and J. W. Swanziger, *Nature*, 1989, **339**, 42.
- [82] P. J. Grandinetti, J. H. Baltisberger, I. Farnan, J. F. Stebbins, U. Werner and A. Pines, *J. Phys. Chem.*, 1995, **99**, 12341.
- [83] L. Frydman and J. S. Harwood, *J. Am. Chem. Soc.*, 1995, **117**, 5367.
- [84] A. Medek, J. S. Harwood and L. Frydman, *J. Am. Chem. Soc.*, 1995, **117**, 12779.
- [85] L. Frydman, in *Multiple-Quantum Magic-Angle Spinning Experiments on Half-Integer Nuclei: Fundamentals*, John Wiley & Sons, Ltd, 2007.
- [86] M. E. Smith and E. R. H. van Eck, *Prog. Nucl. Magn. Reson. Spectrosc.*, 1999, **34**, 159.
- [87] A. Goldbourt and P. K. Madhu, *Annu. Rep. NMR. Spectrosc.*, 2004, **54**, 81.
- [88] P. K. Madhu, A. Goldbourt, L. Frydman and S. Vega, *Chem. Phys. Lett.*, 1999, **307**, 41.
- [89] P. K. Madhu, A. Goldbourt, L. Frydman and S. Vega, *J. Chem. Phys.*, 2000, **112**, 2377.
- [90] J. P. Amoureux and M. Pruski, *Advances in MQMAS NMR*, Ames laboratory (ames), ames, ia report, 2001.
- [91] J.-P. Amoureux, C. Fernandez and L. Frydman, *Chem. Phys. Lett.*, 1996, **259**, 347.
- [92] L. Marinelli and L. Frydman, *Chem. Phys. Lett.*, 1997, **275**, 188.
- [93] G. Wu, D. Rovnyank, B. Sun and R. G. Griffin, *Chem. Phys. Lett.*, 1996, **249**, 210.
- [94] G. Wu, D. Rovnyak and R. G. Griffin, *J. Am. Chem. Soc.*, 1996, **118**, 9326.
- [95] J. P. Amoureux, M. Pruski, D. P. Lang and C. Fernandez, *J. Magn. Reson.*, 1998, **131**, 170.

- [96] S. Ding and C. A. McDowell, *Chem. Phys. Lett.*, 1997, **270**, 81.
- [97] S. Ding and C. A. McDowell, *J. Magn. Reson.*, 1998, **135**, 61.
- [98] A. P. M. Kentgens and R. Verhagen, *Chem. Phys. Lett.*, 1999, **300**, 435.
- [99] T. Bräuniger, K. J. Pike, R. K. Harris and P. K. Madhu, *J. Magn. Reson.*, 2003, **163**, 64.
- [100] T. Bräuniger, G. Hempel and P. K. Madhu, *J. Magn. Reson.*, 2006, **181**, 68.
- [101] T. Bräuniger, P. K. Madhu, A. Pampel and D. Reichert, *Solid State Nucl. Magn. Reson.*, 2004, **26**, 114.
- [102] S. Cavadini, A. Lupulescu, S. Antonijevic and G. Bodenhausen, *J. Am. Chem. Soc.*, 2006, **128**, 7706.
- [103] Z. Gan, *J. Am. Chem. Soc.*, 2006, **128**, 6040.
- [104] U. Akbey, H. Oschkinat and B.-J. van Rossum, *J. Am. Chem. Soc.*, 2009, **131**, 17054.
- [105] S. Vega and A. Pines, *J. Chem. Phys.*, 1977, **66**, 5624.
- [106] A. Wokaun and R. R. Ernst, *J. Chem. Phys.*, 1977, **67**, 1752.
- [107] S. Vega and Y. Naor, *J. Chem. Phys.*, 1981, **75**, 75.
- [108] S. Vega, *J. Chem. Phys.*, 1978, **68**, 5518.
- [109] B. C. Sanctuary, *J. Chem. Phys.*, 1976, **64**, 4352.
- [110] D. A. Varshalovich, A. N. Moskalev and V. K. Khersonskii, *Quantum theory of angular momentum*, World Scientific, 1988.
- [111] B. C. Sanctuary and T. K. Halstead, in *Multipole NMR*, ed. S. W. Warren, Academic Press, 1990, vol. 15, p. 79.
- [112] G. J. Bowden, J. Khachan and J. P. D. Martin, *J. Magn. Reson.*, 1989, **83**, 79.
- [113] G. J. Bowden and W. D. Hutchison, *J. Magn. Reson.*, 1986, **67**, 403.
- [114] G. J. Bowden, W. D. Hutchison and J. Khachan, *J. Magn. Reson.*, 1986, **67**, 415.
- [115] H. A. Buckmaster and R. Chatterjee, *Phys. Status Solidi (b)*, 1998, **209**, 433.
- [116] H. A. Buckmaster, R. Chatterjee and Y. H. Shing, *Phys. Status Solidi (a)*, 1972, **13**, 9.
- [117] B. L. Silver, *Irreducible tensor methods: an introduction for chemists*, Academic Press, 2013, vol. 36.
- [118] A. R. Edmonds, *Angular momentum in quantum mechanics*, Princeton University Press, 1996.
- [119] A. Ramamoorthy and P. T. Narasimhan, *Pramana*, 1991, **36**, 399.
- [120] A. Ramamoorthy and P. T. Narasimhan, *Mol. Phys.*, 1991, **73**, 207.
- [121] A. K. Dubey, A. Ramamoorthy and P. Raghunathan, *Chem. Phys. Lett.*, 1990, **168**, 401.

- [122] T. T. Nakashima, K. J. Harris and R. E. Wasylshen, *J. Magn. Reson.*, 2010, **202**, 162.
- [123] L. Pandey, S. Towta and D. G. Hughes, *J. Chem. Phys.*, 1986, **85**, 6923.
- [124] L. Pandey, M. Kotecha and D. G. Hughes, *Solid State Nucl. Magn. Reson.*, 2000, **16**, 261.
- [125] P. P. Man, *Chem. Phys. Lett.*, 1990, **168**, 227.
- [126] P. P. Man, *Mol. Phys.*, 1992, **76**, 1119.
- [127] P. P. Man, J. Klinowski, A. Trokiner, H. Zanni and P. Papon, *Chem. Phys. Lett.*, 1988, **151**, 143.
- [128] P. P. Man, *J. Magn. Reson., Ser. A*, 1995, **114**, 59.
- [129] P. P. Man, *Mol. Phys.*, 1993, **78**, 307.
- [130] P. P. Man and P. Tougne, *Mol. Phys.*, 1994, **83**, 997.
- [131] N. John Von, *Mathematical foundations of quantum mechanics*, Princeton university press, 1955.
- [132] F. J. Dyson, *Phys. Rev.*, 1949, **75**, 1736.
- [133] R. P. Feynman, *Phys. Rev.*, 1951, **84**, 108.
- [134] K. Blum, *Density matrix theory and applications*, Springer Science & Business Media, 2012, vol. 64.
- [135] G. D. Mateescu and A. Valeriu, *2D NMR: density matrix and product operator treatment*, Prentice Hall, 1993.
- [136] W. H. Louisell, *Quantum statistical properties of radiation*, 1973.
- [137] P. A. M. Dirac, *Proc. R. Soc. London.*, 1929, p. 714.
- [138] N. Zettili, *Quantum mechanics: concepts and applications*, John Wiley & Sons, 2009.
- [139] A. Messiah, *Quantum Mechanics. I.*, 1958.
- [140] A. Messiah, *Quantum mechanics, 2 vols*, 1962.
- [141] C. N. Banwell and H. Primas, *Mol. Phys.*, 1963, **6**, 225.
- [142] P.-K. Wang and C. P. Slichter, *Bull. Magn. Reson.*, 1986, **8**, 3.
- [143] R. Ramesh and M. S. Krishnan, *J. Chem. Phys.*, 2001, **114**, 5967.
- [144] M. M. Maricq and J. S. Waugh, *J. Chem. Phys.*, 1979, **70**, 3300.
- [145] E. Vinogradov, P. K. Madhu and S. Vega, *J. Chem. Phys.*, 2001, **115**, 8983.
- [146] O. W. Sørensen, G. W. Eich, M. H. Levitt, G. Bodenhausen and R. R. Ernst, *Prog. Nucl. Magn. Reson. Spectrosc.*, 1984, **16**, 163.
- [147] U. Haeblerlen and J. S. Waugh, *Phys. Rev.*, 1968, **175**, 453.
- [148] J. S. Waugh, in *Average Hamiltonian Theory*, John Wiley & Sons, Ltd, 2007.

- [149] J. S. Waugh, *J. Magn. Reson.*, 1982, **50**, 30.
- [150] J. H. Shirley, *Phys. Rev.*, 1965, **138**, B979.
- [151] W. Magnus, *Commun. Pure Appl. Math.*, 1954, **7**, 649.
- [152] R. M. Wilcox, *J. Math. Phys.*, 1967, **8**, 962.
- [153] N. Chandrakumar and S. Subramanian, *Modern techniques in high-resolution FT-NMR*, Springer Science & Business Media, 2012.
- [154] J. H. Van Vleck, *Phys. Rev.*, 1929, **33**, 467.
- [155] E. C. Kemble, *The Fundamental Principles of Quantum Physics*, 1958.
- [156] D. Papousek and M. R. Aliev, *Molecular vibrational-rotational spectra*, 1982.
- [157] M. Born, W. Heisenberg and P. Jordan, *Z. Phys.*, 1926, **35**, 557.
- [158] L. H. Thomas, *J. Chem. Phys.*, 1942, **10**, 538.
- [159] M. R. Aliev, J. K. G. Watson and K. N. Rao, *Molecular spectroscopy: modern research*, Academic, New York, 1985, vol. III.
- [160] D. J. Griffiths, *Introduction to quantum mechanics*, Pearson Education India, 2005.
- [161] R. Venkata SubbaRao, D. Srivastava and R. Ramachandran, *PCCP*, 2013, **15**, 2081.
- [162] R. Ramachandran and R. G. Griffin, *J. Chem. Phys.*, 2005, **122**, 164502.
- [163] J. Keeler, *Understanding NMR spectroscopy*, John Wiley & Sons, 2011.
- [164] K. Takegoshi, K. Nomura and T. Terao, *Chem. Phys. Lett.*, 1995, **232**, 424.
- [165] K. Takegoshi, K. Nomura and T. Terao, *J. Magn. Reson.*, 1997, **127**, 206.
- [166] H. F. Baker, *Proc. London Math. Soc.*, 1905, **2**, 24.
- [167] H. F. Baker, *Proc. London Math. Soc.*, 1901, **1**, 347.
- [168] H. F. Baker, *Proc. London Math. Soc.*, 1902, **1**, 333.
- [169] J. E. Campbell, *Proc. London Math. Soc.*, 1897, **1**, 14.
- [170] J. E. Campbell, *Proc. London Math. Soc.*, 1896, **1**, 381.
- [171] F. Hausdorff, *Ber. Verh. Kgl. Sächsis. Ges. Wiss. Leipzig., Math. phys. Kl.*, 1906, **58**, 19.
- [172] K. Kumar, *J. Math. Phys.*, 1965, **6**, 1928.
- [173] B. C. Gerstein and C. R. Dybowski, *Transient Techniques in NMR of Solids*, Academic Press, Orlando, 1985.
- [174] U. Haeberlen, *High Resolution NMR in Solids Selective Averaging: Supplement 1 Advances in Magnetic Resonance*, Elsevier, 2012, vol. 1.

- [175] R. L. Cook and F. C. De Lucia, *Am. J. Phys.*, 1971, **39**, 1433.
- [176] M. Mehring, in *Internal Spin Interactions and Rotations in Solids*, John Wiley & Sons, Ltd, 2007.
- [177] M. Bak, J. T. Rasmussen and N. C. Nielsen, *J. Magn. Reson.*, 2000, **147**, 296.
- [178] M. Veshtort and R. G. Griffin, *J. Magn. Reson.*, 2006, **178**, 248.
- [179] M. Edén, *Concepts Magn. Reson. Part A*, 2003, **17**, 117.
- [180] J. K. G. Watson, *Mol. Phys.*, 2005, **103**, 3283.
- [181] H. Lefebvre-Brion and R. W. Field, *Perturbations in the spectra of diatomic molecules*, 1986.

Chapter 2

Conventions and Notations for generalized representation of spin interactions

2.1 Background

The versatility of NMR spectroscopy¹⁻⁴ lies in the interactions of the nuclear spins among themselves in addition to external sources such as static and oscillating magnetic field strengths.⁵⁻¹⁰ The controlled manipulation of nuclear spin interactions through radio-frequency (RF) pulses^{11,12} has led to many exciting developments in the field of NMR spectroscopy and remains an active area of research. To maximize the information content derived from NMR experiments, understanding of the nuclear spin interactions^{5-10,13-15} is quintessential both in the design of new experiments as well as in the interpretation of experimental data. Since the phenomenon of magnetic resonance¹⁶⁻²⁰ emerges from a quantum mechanical property, quantum mechanics²¹⁻²⁷ seems to be the theory of choice for any formal description of the spin physics. From a theoretical perspective, a semiclassical approach has always been employed to describe the interaction of radiation (both electric or magnetic field) with matter.^{5,7,28} The classical potential describing the interaction of EM radiation with matter is recast into a Hamiltonian form and the dynamical changes in the system are monitored within the Hamiltonian framework. Although, several excellent treatise on NMR theory do exist in the literature,^{14,15,29-36} the notations and conventions employed in the description of the spin interactions seem to differ. In particular, understanding the convention/notations employed in the description of nuclear spin interactions in terms of spherical tensor operator formalism³⁵⁻⁵¹ remains a daunting task for a beginner or any serious experimentalist. This has been the main motivation behind the inclusion of this chapter in this thesis. Since analytic formulation of the nuclear spin

dynamics involving quadrupolar nuclei^{5,14,52-56} is facilitated through the tensor operator formalism, a formal understanding of the notations seem mandatory. Furthermore, since tensorial representation of the spatial and spin components is convenient for theoretical studies in MAS experiments,^{32,57,58} the transformation properties^{23,35,38,43,44,51,59-65} of the tensor operators under rotations is essential. Below, we summarize the conventions and notations that would be closely followed in the thesis to describe the spin dynamics involving quadrupolar nuclei.

2.2 Nuclear spin Hamiltonians and their representations

Just like charge, mass etc, spin is also a fundamental property of matter and is exhibited by all subatomic particles. In addition to the spin property, each nucleus in turn comprises of fundamental particles (that possess electric charge) that are coupled together. The presence of moving charged particles within the nucleus results in an intrinsic total angular momentum J and a total magnetic moment, μ . When these two vectors are aligned in parallel, they are related through a simple expression illustrated below.

$$\mu = \gamma J \quad (2.1)$$

(where ‘ γ ’ represents the gyromagnetic ratio and is characteristic of a particular nucleus) The total angular momentum (J) is related to a dimensionless angular momentum operator through the equation illustrated below.

$$J = \hbar I \quad (2.2)$$

The individual components of the angular momentum operator (say I_x , I_y , I_z) commute with I^2 and are non-commuting among themselves. Employing commuting set of observables (I_z and I^2), the basis set ($|Im\rangle$) for a given spin system is constructed.

$$\begin{aligned} I^2 |Im\rangle &= I(I+1) |Im\rangle \\ I_z |Im\rangle &= m |Im\rangle \end{aligned} \quad (2.3)$$

The changes observed (due to rotation) in the magnetic moment and the electric charge within a nucleus, results in an interaction energy and is quantum mechanically studied through the corresponding interaction Hamiltonians (or internal Hamiltonians). In general, the nuclear spin Hamiltonian has two contributions, an electric spin Hamiltonian, which describes the way the nuclear electric energy changes (as the nucleus rotates) and a

magnetic spin Hamiltonian, which describes the way the nuclear magnetic energy changes as the nucleus rotates. Accordingly, the spin Hamiltonian operator for a nucleus may therefore be written as

$$H = H_{elec} + H_{mag} \quad (2.4)$$

In NMR, all spin interaction Hamiltonians are magnetic spin Hamiltonians, with quadrupolar interaction being the one exception. In addition to the internal interactions, the interaction of the nuclear spin with the external magnetic fields (both static and oscillating) is often referred to as external interaction.

$$H = H_{Ext} + H_{Int} \quad (2.5)$$

To have a consistent notation, a brief quantum mechanical description of the interactions is illustrated in the following sections.

2.2.1 External Hamiltonians

The external Hamiltonian comprises of the interactions between the nuclear spin magnetic moment with the static and oscillating magnetic fields.

$$H_{Ext} = H_Z + H_{RF} \quad (2.6)$$

2.2.1.1 Zeeman interaction

The direct magnetic interaction of the nuclear spin with the static external magnetic field is called Zeeman interaction. In spin $I = 1/2$ nuclei, Zeeman interaction dominates all other internal spin interactions. In the absence of static external magnetic field, all the 2^n energy levels corresponding to 'n' spin $I = 1/2$ nuclei are degenerate. By contrast, the electric quadrupolar interaction (only found in nucleus with $I > 1/2$), dominates all other internal spin interactions and in some cases has magnitudes comparable to the Zeeman interaction. In the absence of the static magnetic field, the $(2I+1)$ states in a quadrupolar nuclei are doubly degenerate and are studied through NQR spectroscopy.

The application of a static magnetic field (of strength B) results in an interaction energy in the nucleus and is quantum mechanically represented by,

$$H = - \sum_{j=1} \mu_j \cdot B \quad (2.7)$$

where the negative sign is indicative of the fact that the interaction energy is minimum, when the magnetic moment of the nucleus is parallel to the applied field. When the static

external magnetic field is applied along the z-direction, the Eq. (2.7) reduces to a simpler form,

$$\begin{aligned} H_Z &= -\hbar \sum_j \gamma_j B_0 I_{jz} \\ &= \hbar \sum_j \omega_{j0} I_{jz} \end{aligned} \quad (2.8)$$

with $\omega_{j0} = -\gamma_j B_0$ representing the Larmor frequency of the j^{th} nucleus. Following the description presented in the Appendix, the above Hamiltonian is reexpressed in terms of irreducible spherical tensor operators.

$$H_Z = \hbar \sum \omega_{j0} \left[\frac{-i}{C(0..1_j0..)} T^{(1)0}(0..1_j0..) \right] \quad (2.9)$$

In Eq. (2.9), the constant ‘C’ differs depending on the number of spins presented in the system and is deduced from the Table 2.6.

2.2.1.2 RF interaction

The interaction of the nuclear spin with the oscillating external field is commonly referred to as RF interaction. When the oscillating field (with amplitude B_1) is applied along x-direction, the Hamiltonian is represented by,

$$\begin{aligned} H_{RF} &= -2\hbar \sum_j \gamma_j B_{j,1} \cos(\omega_j t + \phi_j) I_{jx} \\ &= 2\hbar \sum_j \omega_{j,1} \cos(\omega_j t + \phi_j) I_{jx} \end{aligned} \quad (2.10)$$

where $\omega_{j,1} = -\gamma_j B_{j,1}$ is the nutation frequency, ω_j is carrier frequency and ϕ_j is the phase of the RF pulse for the j^{th} nucleus. The corresponding Hamiltonian in terms of tensor operators is represented below,

$$H_{RF} = 2\hbar \sum_j \omega_{j,1} \cos(\omega_j t + \phi) \left[\frac{i}{\sqrt{2}C(0..1_j0..)} T^{(1)1}(0..1_j0..) - \frac{i}{\sqrt{2}C(0..1_j0..)} T^{(1)-1}(0..1_j0..) \right] \quad (2.11)$$

2.2.2 Internal Hamiltonians

The internal Hamiltonian represents the sum contribution of all the interactions present within the system.

$$H_{Int} = H_C + H_J + H_D + H_Q + H_S \quad (2.12)$$

2.2.2.1 Chemical Shift interaction

The indirect magnetic interaction of the nuclear spins with the static external magnetic field mediated through the surrounding electronic clouds in a molecule is often termed as the chemical shift interaction. The magnetic fields induced by the surrounding electronic clouds differ at different nuclear sites aid in the identification of different nuclear sites within a molecule. The local field at a site 'j' has contributions from the static field as well as that induced by the surrounding electron cloud.

$$B_{j,local} = B_0 + B_{j,Induced} \quad (2.13)$$

where $B_{j,Induced} = \sigma^j \cdot B_0$. In general, the chemical shift Hamiltonian is represented through a product between vectors (I & B) and a second rank tensor ' σ '.

$$\begin{aligned} H_C &= -\hbar \sum_j \gamma_j (I_j \cdot \sigma^j \cdot B) \\ &= -\hbar \sum_j \gamma_j I_{jz} \sigma_{zz}^j B_0 \end{aligned} \quad (2.14)$$

In Eq. (2.14), σ^j represents the orientation dependent chemical shift tensor and in the principal axis frame (PAS) is represented by,

$$\sigma^j = \begin{pmatrix} \sigma_{xx}^j & 0 & 0 \\ 0 & \sigma_{yy}^j & 0 \\ 0 & 0 & \sigma_{zz}^j \end{pmatrix} \quad (2.15)$$

Due to rapid molecular motion, the chemical shift interaction is isotropic in the solution state and is represented by,

$$\begin{aligned} H_C &= -\hbar \sum_j \gamma_j \sigma_{iso}^j I_{jz} B_0 \\ &= \hbar \sum_j \sigma_{iso}^j \omega_{j0} I_{jz} \end{aligned} \quad (2.16)$$

where σ_{iso}^j represents the isotropic value of chemical shift tensor.

$$\sigma_{iso}^j = \frac{1}{3}(\sigma_{xx}^j + \sigma_{yy}^j + \sigma_{zz}^j) \quad (2.17)$$

Along with the isotropic chemical shift, the chemical shift interaction is defined in terms of chemical shift anisotropy δ_j^C and asymmetry parameter η_j^C .

$$\delta_j^C = \sigma_{zz}^j - \frac{1}{3}(\sigma_{xx}^j + \sigma_{yy}^j + \sigma_{zz}^j) = \sigma_{zz}^j - \sigma_{iso}^j \quad (2.18)$$

$$\eta_j^C = \frac{\sigma_{xx}^j - \sigma_{yy}^j}{\delta_j^C} \quad (2.19)$$

Employing these definitions and the relations described in Tables 2.7 and 2.8, the chemical shift interaction is represented in terms of spherical tensors. The spatial and spin irreducible tensors (operators) depicting the chemical shift interactions are listed in Table 2.1.

Spatial components	Spin components
$R_{C,P}^{(0)0} = \frac{-i\sqrt{3}}{C(0..1_j0..)}\sigma_{iso}^j$	$Y^{(0)0} = \frac{iC(0..1_j0..)}{\sqrt{3}}I_{jz}B_0 = \frac{B_0}{\sqrt{3}}T^{(1)0}(0..1_j0..)$
$R_{C,P}^{(1)0} = 0$	$Y^{(1)0} = 0$
$R_{C,P}^{(1)\pm 1} = 0$	$Y^{(1)\pm 1} = \frac{iC(0..1_j0..)}{2}I_j^\pm B_0 = \frac{-B_0}{\sqrt{2}}T^{(1)\pm 1}(0..1_j0..)$
$R_{C,P}^{(2)0} = \frac{i}{C(0..1_j0..)}(\sqrt{\frac{3}{2}}\delta_j^C)$	$Y^{(2)0} = \frac{-i2C(0..1_j0..)}{\sqrt{6}}I_{jz}B_0 = \frac{-2B_0}{\sqrt{6}}T^{(1)0}(0..1_j0..)$
$R_{C,P}^{(2)\pm 1} = 0$	$Y^{(2)\pm 1} = \frac{\pm iC(0..1_j0..)}{2}I_j^\pm B_0 = \frac{\mp B_0}{\sqrt{2}}T^{(1)\pm 1}(0..1_j0..)$
$R_{C,P}^{(2)\pm 2} = \frac{i}{2C(0..1_j0..)}(\delta_j^C\eta_j^C)$	$Y^{(2)\pm 2} = 0$
$H_C = \hbar \sum_j C_j^C \sum_{k=0}^2 \sum_{q=k}^{-k} (-1)^{k-q} R_{C,P}^{(k)-q} Y^{(k)q}(I)$ where $C_j^C = -\gamma_j$	

Table 2.1: Chemical shift Hamiltonian in tensorial representation.

2.2.2.2 J-Coupling interaction

The indirect magnetic interaction of the nuclear spins with each other mediated through bonded electrons is commonly referred to as J-coupling or spin-spin coupling interaction.

$$H_J = \hbar \sum_{j<l} I_j \cdot J^{jl} \cdot I_l \quad (2.20)$$

The term J^{jl} represents the orientation dependent J-coupling interaction tensor between j^{th} and l^{th} nucleus and is represented by (in the PAS),

$$J^{jl} = \begin{pmatrix} J_{XX}^{jl} & 0 & 0 \\ 0 & J_{YY}^{jl} & 0 \\ 0 & 0 & J_{ZZ}^{jl} \end{pmatrix} \quad (2.21)$$

Similar to the chemical shift interaction, the J-coupling interaction tensor in the solution state is averaged out to isotropic form due to rapid tumbling motion. Accordingly, the isotropic form of J-coupling or scalar coupling Hamiltonian represented by,

$$H_J = \hbar J^{jl} \sum_{j<l} I_j \cdot I_l \quad (2.22)$$

with J^{jl} representing the isotropic J-coupling or scalar coupling constant.

$$J_{iso}^{jl} = \frac{1}{3}(J_{xx}^{jl} + J_{yy}^{jl} + J_{zz}^{jl}) \quad (2.23)$$

In addition to the isotropic constant, the J-interaction is characterized through the J-coupling anisotropy δ_{jl}^J and asymmetry parameter η_{jl}^J .

$$\begin{aligned} \delta_{jl}^J &= J_{zz}^{jl} - \frac{1}{3}(J_{xx}^{jl} + J_{yy}^{jl} + J_{zz}^{jl}) = J_{zz}^{jl} - J_{iso}^{jl} \\ \eta_{jl}^J &= \frac{J_{xx}^{jl} - J_{yy}^{jl}}{\delta_{jl}^J} \end{aligned} \quad (2.24)$$

The spatial and spin components of the tensors are represented in Table 2.2.

Spatial components	Spin components
$R_{J,P}^{(0)0} = \frac{\sqrt{3}}{C(0..1_j0..1_l0..)}(J_{iso}^{jl})$	$T^{(0)0}(0..1_j0..1_l0..) = \frac{C(0..1_j0..1_l0..)}{\sqrt{3}} I_j \cdot I_l$
$R_{J,P}^{(1)0} = 0$	$T^{(1)0}(0..1_j0..1_l0..) = \frac{C(0..1_j0..1_l0..)}{2\sqrt{2}} [I_j^+ I_l^- - I_j^- I_l^+]$
$R_{J,P}^{(1)\pm 1} = 0$	$T^{(1)\pm 1}(0..1_j0..1_l0..) = \frac{C(0..1_j0..1_l0..)}{2} [I_j^\pm I_{lz} - I_{jz} I_l^\pm]$
$R_{J,P}^{(2)0} = \frac{-1}{C(0..1_j0..1_l0..)}(\sqrt{\frac{3}{2}}\delta_{jl}^J)$	$T^{(2)0}(0..1_j0..1_l0..) = \frac{-C(0..1_j0..1_l0..)}{\sqrt{6}} [3I_{jz}I_{lz} - I_j \cdot I_l]$
$R_{J,P}^{(2)\pm 1} = 0$	$T^{(2)\pm 1}(0..1_j0..1_l0..) = \pm \frac{C(0..1_j0..1_l0..)}{2} [I_j^\pm I_{lz} + I_{jz} I_l^\pm]$
$R_{J,P}^{(2)\pm 2} = \frac{-1}{2C(0..1_j0..1_l0..)}(\delta_{jl}^J \eta_{jl}^J)$	$T^{(2)\pm 2}(0..1_j0..1_l0..) = \frac{-C(0..1_j0..1_l0..)}{2} I_j^\pm I_l^\pm$
$H_J = \hbar \sum_{j<l} C_{jl}^J \sum_{k=0}^2 \sum_{q=k}^{-k} (-1)^{k-q} R_{J,P}^{(k)-q} T^{(k)q}(II)$ where $C_{jl}^J = 1$	

Table 2.2: J-coupling Hamiltonian in tensorial representation

2.2.2.3 Dipolar Coupling interaction

The direct magnetic interaction of the nuclear spins with each other (through space) is referred to as the dipolar interaction. In the spherical polar coordinates, the dipolar Hamiltonian is represented by,

$$H_D = \frac{\mu_0}{4\pi} \sum_{j<l} \left[\frac{\mu_j \cdot \mu_l}{|r_{jl}|^3} - \frac{3(\mu_j \cdot r_{jl})(\mu_l \cdot r_{jl})}{|r_{jl}|^5} \right] \quad (2.25)$$

$$H_D = -\hbar \sum_{j<l} b_{jl} (A_{jl} + B_{jl} + C_{jl} + D_{jl} + E_{jl} + F_{jl}) \quad (2.26)$$

with $b_{jl} = -\frac{\mu_0 \hbar \gamma_j \gamma_l}{4\pi |r_{jl}|^3}$ denoting the dipolar constant and $\mu_0 = 4\pi \times 10^{-7} \text{Hm}^{-1}$ the magnetic constant or permeability of free space. The dipolar alphabets⁵ in Eq. (2.26) are represented below,

$$\begin{aligned} A_{jl} &= I_{jz} I_{lz} (1 - 3\cos^2\theta_{jl}) & D_{jl} &= -\frac{3}{2} (I_j^- I_{lz} + I_{jz} I_l^-) \sin\theta_{jl} \cos\theta_{jl} e^{i\phi_{jl}} \\ B_{jl} &= -\frac{1}{4} (I_j^+ I_l^- + I_j^- I_l^+) (1 - 3\cos^2\theta_{jl}) & E_{jl} &= -\frac{3}{4} I_j^+ I_l^+ \sin^2\theta_{jl} e^{-2i\phi_{jl}} \\ C_{jl} &= -\frac{3}{2} (I_j^+ I_{lz} + I_{jz} I_l^+) \sin\theta_{jl} \cos\theta_{jl} e^{-i\phi_{jl}} & F_{jl} &= -\frac{3}{4} I_j^- I_l^- \sin^2\theta_{jl} e^{2i\phi_{jl}} \end{aligned} \quad (2.27)$$

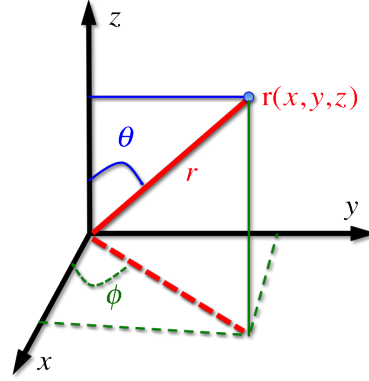


Figure 2.1: Relationship between cartecian coordinates x, y, z (describing the position of nucleus j relative to nucleus l) and the polar coordinates r, θ, ϕ

Analogous to the scalar interaction (see Eq. (2.20)), the dipolar Hamiltonian is reexpressed in terms of the dipolar tensor, D^{jl}

$$H_D = \hbar \sum_{j<l} \frac{\hbar \mu_0 \gamma_j \gamma_l}{4\pi} I_j \cdot D^{jl} \cdot I_l \quad (2.28)$$

For illustrative purpose, the explicit form of the components in the dipolar tensor is represented below,

$$D_{\alpha\beta}^{jl} = \frac{1}{|r_{jl}|^3} (\delta_{\alpha\beta} - 3e_\alpha e_\beta) \quad \text{with } (\alpha, \beta) = x, y, z \quad (2.29)$$

$$\begin{aligned}
D_{xx}^{jl} &= \frac{1}{|r_{jl}|^3} (1 - 3\sin^2\theta_{jl}\cos^2\phi_{jl}) & D_{xy}^{jl} &= D_{yx}^{jl} = -\frac{1}{|r_{jl}|^3} (3\sin^2\theta_{jl}\cos\phi_{jl}\sin\phi_{jl}) \\
D_{yy}^{jl} &= \frac{1}{|r_{jl}|^3} (1 - 3\sin^2\theta_{jl}\sin^2\phi_{jl}) & D_{xz}^{jl} &= D_{zx}^{jl} = -\frac{1}{|r_{jl}|^3} (3\sin\theta_{jl}\cos\theta_{jl}\cos\phi_{jl}) \\
D_{zz}^{jl} &= \frac{1}{|r_{jl}|^3} (1 - 3\cos^2\theta_{jl}) & D_{yz}^{jl} &= D_{zy}^{jl} = -\frac{1}{|r_{jl}|^3} (3\sin\theta_{jl}\cos\theta_{jl}\sin\phi_{jl})
\end{aligned} \tag{2.30}$$

In the PAS ($\theta_{jl} = 0$ and $\phi_{jl} = 0$), the dipolar tensor has a simpler form.

$$D^{jl} = \begin{pmatrix} D_{xx}^{jl} & 0 & 0 \\ 0 & D_{yy}^{jl} & 0 \\ 0 & 0 & D_{zz}^{jl} \end{pmatrix} = \begin{pmatrix} \frac{1}{|r_{jl}|^3} & 0 & 0 \\ 0 & \frac{1}{|r_{jl}|^3} & 0 \\ 0 & 0 & -\frac{2}{|r_{jl}|^3} \end{pmatrix} \tag{2.31}$$

Based on the relations listed in Tables 2.7 and 2.8, the spatial and spin tensors for the dipolar interaction are listed in Table 2.3.

Spatial components	Spin components
$R_{D,P}^{(0)0} = 0$	$T^{(0)0}(0..1_j0..1_l0..) = \frac{C(0..1_j0..1_l0..)}{\sqrt{3}} I_j \cdot I_j$
$R_{D,P}^{(1)0} = 0$	$T^{(1)0}(0..1_j0..1_l0..) = \frac{C(0..1_j0..1_l0..)}{2\sqrt{2}} [I_j^+ I_j^- - I_j^- I_j^+]$
$R_{D,P}^{(1)\pm 1} = 0$	$T^{(1)\pm 1}(0..1_j0..1_l0..) = \frac{C(0..1_j0..1_l0..)}{2} [I_j^\pm I_{jz} - I_{jz} I_j^\pm]$
$R_{D,P}^{(2)0} = \frac{\sqrt{6}}{C(0..1_j0..1_l0..) r_{jl} ^3}$	$T^{(2)0}(0..1_j0..1_l0..) = \frac{-C(0..1_j0..1_l0..)}{\sqrt{6}} [3I_{jz} I_{lz} - I_j \cdot I_j]$
$R_{D,P}^{(2)\pm 1} = 0$	$T^{(2)\pm 1}(0..1_j0..1_l0..) = \pm \frac{C(0..1_j0..1_l0..)}{2} [I_j^\pm I_{jz} + I_{jz} I_j^\pm]$
$R_{D,P}^{(2)\pm 2} = 0$	$T^{(2)\pm 2}(0..1_j0..1_l0..) = \frac{-C(0..1_j0..1_l0..)}{2} I_j^\pm I_j^\pm$
$H_D = \hbar \sum_{j<l} C_{jl}^D \sum_{k=0}^2 \sum_{q=k}^{-k} (-1)^{k-q} R_{D,P}^{(k)-q} T^{(k)q}(II) \text{ where } C_{jl}^D = \frac{\hbar\mu_0\gamma_j\gamma_l}{4\pi}$	

Table 2.3: Dipolar coupling Hamiltonian in tensorial representation

2.2.2.4 Quadrupolar interaction

The interaction of the quadrupole moment (observed in spin $I > 1/2$) with the surrounding electric field gradient (generated by molecular electronic clouds) is termed the

quadrupolar interaction.

$$\begin{aligned}
H_Q &= \sum_j \sum_{\alpha, \beta=x, y, z} \frac{eQ_j}{6I_j(2I_j-1)} \left\{ V_{\alpha\beta}^j \left[\frac{3}{2}(I_{j\alpha}I_{j\beta} + I_{j\beta}I_{j\alpha}) - \delta_{\alpha\beta}I_j(I_j+1) \right] \right\} \\
&= \sum_j \frac{eQ_j}{4I_j(2I_j-1)} [V_{zz}^j(3I_{jz}^2 - I_j^2) + (V_{xx}^j - V_{yy}^j)(I_{jx}^2 - I_{jy}^2)]
\end{aligned} \tag{2.32}$$

The term Q_j represents the quadrupolar moment of the j^{th} nucleus and ‘e’ the elementary charge. The components of the electric field gradient tensor $V_{\alpha\beta}^j$ are conveniently expressed.

$$\begin{aligned}
\eta_j^Q &= \frac{V_{xx}^j - V_{yy}^j}{V_{zz}^j} \\
eq_j &= V_{zz}^j
\end{aligned} \tag{2.33}$$

The asymmetry parameter η_j is in the range ($0 \leq \eta_j \leq 1$) with the convention $V_{zz}^j \geq V_{yy}^j \geq V_{xx}^j$. Employing these relations, the above Eq. (2.32) reduces to,

$$\begin{aligned}
H_Q &= \sum_j \frac{e^2q_jQ_j}{4I_j(2I_j-1)} [3I_{jz}^2 - I_j(I_j+1) + \eta_j(I_{jx}^2 - I_{jy}^2)] \\
&= -\hbar \sum_j \frac{\omega_{Q_j}^{PAS}}{6} [3I_{jz}^2 - I_j(I_j+1) + \frac{\eta_j}{2}(I_j^{+2} + I_j^{-2})]
\end{aligned} \tag{2.34}$$

where $\omega_{Q_j}^{PAS} = \frac{-3e^2q_jQ_j}{2I_j(2I_j-1)\hbar} = \frac{-3\pi C_{Q_j}}{I_j(2I_j-1)}$, the quadrupolar splitting parameter and $C_{Q_j} = \frac{e^2q_jQ_j}{h}$ is quadrupolar coupling constant for the j^{th} nucleus. In terms of the electric field gradient tensor V^j , the quadrupolar Hamiltonian is often represented by,

$$H_Q = \hbar \sum_j \frac{eQ_j}{2I_j(2I_j-1)\hbar} I_j \cdot V^j \cdot I_j \tag{2.35}$$

The form of the electric field gradient tensor in the PAS is represented below,

$$V^j = \begin{pmatrix} V_{xx}^j & 0 & 0 \\ 0 & V_{yy}^j & 0 \\ 0 & 0 & V_{zz}^j \end{pmatrix} \tag{2.36}$$

Following the procedure described in the previous sections, the spatial and spin tensor operators are derived and listed in Table 2.4.

Spatial components	Spin components
$R_{Q,P}^{(0)0} = 0$	$T^{(0)0}(I) = C(0..0j..0)I$
$R_{Q,P}^{(1)0} = 0$	$T^{(1)0}(I) = C(0..1j..0)iI_z$
$R_{Q,P}^{(1)\pm 1} = 0$	$T^{(0..1j..0)\pm 1}(I) = \mp \frac{C(0..1j..0)i}{\sqrt{2}} I_{\pm}$
$R_{Q,P}^{(2)0} = -\frac{1}{C(0..2j..0)}(\sqrt{\frac{3}{2}}eq_j)$	$T^{(2)0}(I) = \frac{-C(0..2j..0)}{\sqrt{6}}[3I_z^2 - I(I+1)]$
$R_{Q,P}^{(2)\pm 1} = 0$	$T^{(2)\pm 1}(I) = \pm \frac{C(0..2j..0)}{2}(I_z I_{\pm} + I_{\pm} I_z)$
$R_{Q,P}^{(2)\pm 2} = -\frac{1}{2C(0..2j..0)}(\eta_j^Q eq_j)$	$T^{(2)\pm 2}(I) = -\frac{C(0..2j..0)}{2}I_{\pm}I_{\pm}$
$H_Q = \hbar \sum_j C_j^Q \sum_{k=0}^2 \sum_{q=k}^{-k} (-1)^{k-q} R_{Q,P}^{(k)-q} T^{(k)q}(I)$ where $C_j^Q = \frac{eQ_j}{2I_j(2I_j-1)\hbar}$	

Table 2.4: Quadrupolar coupling Hamiltonian in tensorial representation

2.2.2.5 Spin-Rotation interaction

Interaction of the nuclear spins (nuclear spin magnetic moment) with the magnetic moment produced by the angular momentum of the molecule due to rotational motion is defined as spin-rotation interaction. Even though spin-rotation interaction in solids is unimportant (due to restricted mobility of molecule), a brief description is presented to complete the description of spin interactions in NMR.

$$H_S = \hbar \sum_j I_j \cdot S^j \cdot J \quad (2.37)$$

In Eq. (2.37) S^j denotes the spin-rotation interaction tensor. The isotopic form of the spin-rotation interaction (in liquids) is represented by,

$$H_S = \hbar \sum_j S_{iso}^j I_j \cdot J \quad (2.38)$$

with S_{iso}^j denoting the isotopic spin-rotation coupling constant.

$$S_{iso}^j = \frac{1}{3}(S_{xx}^j + S_{yy}^j + S_{zz}^j) \quad (2.39)$$

In similar vein, the anisotropic part of the interaction is represented through spin-rotation anisotropy δ_j^S and asymmetry parameter η_j^S .

$$\begin{aligned}\delta_j^S &= S_{zz}^j - \frac{1}{3}(S_{xx}^j + S_{yy}^j + S_{zz}^j) = S_{zz}^j - S_{iso}^j \\ \eta_j^S &= \frac{S_{xx}^j - S_{yy}^j}{\delta_j^S}\end{aligned}\quad (2.40)$$

The normalized tensor operators for the spin-rotation interaction is represented in Table 2.5,

Spatial components	Spin components
$R_{S,P}^{(0)0} = \frac{\sqrt{3}}{C(0..1_j0..1_l)}(S_{iso}^j)$	$T^{(0)0}(0..1_j0..1_l) = \frac{C(0..1_j0..1_l)}{\sqrt{3}}I_j \cdot J$
$R_{S,P}^{(1)0} = 0$	$T^{(1)0}(0..1_j0..1_l) = \frac{C(0..1_j0..1_l)}{2\sqrt{2}} [I_j^+ J^- - I_j^- J^+]$
$R_{S,P}^{(1)\pm 1} = 0$	$T^{(1)\pm 1}(0..1_j0..1_l) = \frac{C(0..1_j0..1_l)}{2} [I_j^\pm J_z - I_{jz} J^\pm]$
$R_{S,P}^{(2)0} = \frac{-1}{C(0..1_j0..1_l)}(\sqrt{\frac{3}{2}}\delta_j^S)$	$T^{(2)0}(0..1_j0..1_l) = \frac{-C(0..1_j0..1_l)}{\sqrt{6}} [3I_{jz} J_z - I_j \cdot J]$
$R_{S,P}^{(2)\pm 1} = 0$	$T^{(2)\pm 1}(0..1_j0..1_l) = \pm \frac{C(0..1_j0..1_l)}{2} [I_j^\pm J_z + I_{jz} J^\pm]$
$R_{S,P}^{(2)\pm 2} = \frac{-1}{2C(0..1_j0..1_l)}(\delta_j^S \eta_j^S)$	$T^{(2)\pm 2}(0..1_j0..1_l) = \frac{-C(0..1_j0..1_l)}{2} I_j^\pm J^\pm$
$H_S = \hbar \sum_j C_j^S \sum_{k=0}^2 \sum_{q=k}^{-k} (-1)^{k-q} R_{S,P}^{(k)-q} T^{(k)q}(IJ)$ where $C_j^S = 1$	

Table 2.5: Spin-rotation Hamiltonian in tensorial representation

2.2.3 Transformation of spin Hamiltonians

As illustrated in the previous sections, the spatial tensors ($R^{(k)q}$) are defined in the PAS of the respective interactions. A detailed description of the rotational transformations and conventions employed are briefly discussed in the Appendix. Employing Wigner rotation matrices, the spatial tensors defined in the PAS are transformed in the LAB frame.

In the case of MAS experiments involving powder samples, three sets of transformations are required to transform the spatial tensors from the PAS to the LAB frame (see Fig. 2.2).

$$\text{PAS} \xrightarrow{D(\Omega_{FM})} \text{MolAS} \xrightarrow{D(\Omega_{MR})} \text{RAS} \xrightarrow{D(\Omega_{RL})} \text{LAS} \quad (2.41)$$

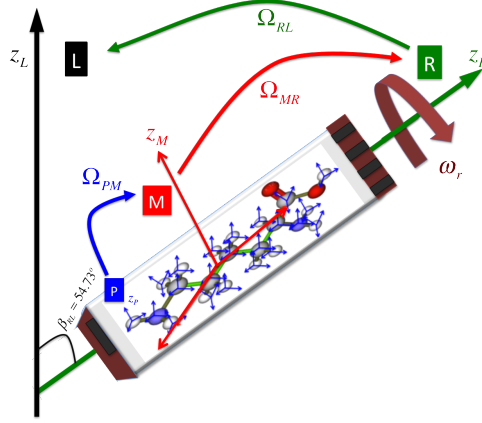


Figure 2.2: The figure depicts the set of transformations which are required to transform MAS Hamiltonian from PAS to LAS for a single molecule in the powdered sample. The coordinate axes frames shown in blue, red, green and black are corresponding to PAS, MolAS, RAS and LAS respectively.

Based on the relations expressed in Tables 2.1 to 2.5 the spin Hamiltonian can be expressed as a product of the spatial and spin tensor operators.

$$H_\lambda = \hbar C^\lambda \sum_{k=0}^2 \sum_{q=-k}^k (-1)^{k-q} R_{\lambda,L}^{(k)-q} T_\lambda^{(k)q} \quad (2.42)$$

In Eq. (2.42), ‘ λ ’ represents the spin interactions (such as chemical shift, J-coupling, dipolar coupling, quadrupolar coupling, spin-rotation coupling). The term $R_{\lambda,L}^{(0)0}$ corresponding $k = 0$ is isotropic part and is invariant under rotational transformations. The tensors $R_{\lambda,L}^{(1)q}$ corresponding to $k = 1$ are traceless antisymmetric parts have no importance in NMR (more over from above Tables 2.1 to 2.5 the contribution of these parts are zero). The tensors $R_{\lambda,L}^{(2)q}$ corresponding to $k = 2$ are traceless symmetric parts and contribute to the spectrum in MAS experiments.

$$H_\lambda = \hbar C^\lambda R_{\lambda,L}^{(0)0} T_\lambda^{(0)0} + \hbar C^\lambda \sum_{q=-2}^2 (-1)^{2-q} R_{\lambda,L}^{(2)-q} T_\lambda^{(2)q} \quad (2.43)$$

At higher external magnetic field strengths, the contributions from the terms that are non-commuting with the Zeeman interaction (i.e $[I_z, T^{(k)q}] \neq 0$ for $q \neq 0$) are ignored.

The transformed spatial part of the Hamiltonian $R_{\lambda,L}^{(2)q}$ is represented by,

$$\begin{aligned} R_{\lambda,L}^{(2)q} &= \sum_{q_1, q_2, q_3=-2}^2 R_{\lambda,P}^{(2)q_3} D_{q_3 q_2}^{(2)}(\Omega_{PM}) D_{q_2 q_1}^{(2)}(\Omega_{MR}) D_{q_1 q}^{(2)}(\Omega_{RL}) \\ &= \sum_{q_1, q_2, q_3=-2}^2 R_{\lambda,P}^{(2)q_3} D_{q_3 q_2}^{(2)}(\Omega_{PM}) D_{q_2 q_1}^{(2)}(\Omega_{MR}) D_{q_1 q}^{(2)}(-\omega_r t, \beta_{RL}, 0) \end{aligned} \quad (2.44)$$

Employing the spatial components and the properties of the Wigner-rotation matri-

ces, ^{23,38,43,44,63} the Hamiltonians is reexpressed in a compact form. The secular ($q = 0$) spatial part of the Hamiltonian ⁹ is represented by,

$$C^\lambda R_{\lambda,L}^{(2)0} = \sum_{\substack{m=-2 \\ m \neq 0}}^2 G_{\lambda,m}^{(2)0} e^{im\omega_r t} \quad (2.45)$$

with

$$G_{\lambda,m}^{(2)0} = C^\lambda \sum_{q_2, q_3 = -2}^2 R_{\lambda,P}^{(2)q_3} D_{q_3 q_2}^{(2)}(\Omega_{PM}) D_{q_2 m}^{(2)}(\Omega_{MR}) d_{m0}^{(2)}(\beta_{RL}) \quad (2.46)$$

The non-secular ($q \neq 0$) spatial part of the Hamiltonian (relevant only in the case of quadrupolar interaction) is represented by,

$$C^\lambda (-1)^{2-q} R_{Q,L}^{(2)-q} = \sum_{\substack{m=-2 \\ m \neq 0}}^2 G_{Q,m}^{(2)q} e^{im\omega_r t} \quad (2.47)$$

with

$$G_{Q,m}^{(2)-q} = C^Q \sum_{q_2, q_3 = -2}^2 R_{Q,P}^{(2)q_3} D_{q_3 q_2}^{(2)}(\Omega_{PM}) D_{q_2 m}^{(2)}(\Omega_{MR}) d_{mq}^{(2)}(\beta_{RL}) \quad (2.48)$$

Employing these relations, the Hamiltonian under MAS is represented by,

$$H = H_Z + H_{RF} + \underbrace{\hbar C^\lambda R_{\lambda,L}^{(0)0} T_\lambda^{(0)0}}_{\text{Isotropic}(\lambda=C,J,S)} + \underbrace{\hbar \sum_{\substack{m=-2 \\ m \neq 0}}^2 G_{\lambda,m}^{(2)0} e^{im\omega_r t} T_\lambda^{(2)0}}_{\text{Secular}(\lambda=C,J,D,Q,S)} + \underbrace{\hbar \sum_{\substack{q=-2 \\ q \neq 0}}^2 \sum_{\substack{m=-2 \\ m \neq 0}}^2 G_{Q,m}^{(2)q} e^{im\omega_r t} T_Q^{(2)q}}_{\text{Non-secular}} \quad (2.49)$$

2.3 Effective Hamiltonians for spin $I = 1/2$ system under MAS

The Hamiltonian for an isolated spin ($I = 1/2$) system under MAS in rotating frame is represented by,

$$\tilde{H} = \hbar\omega_1 I_x + \hbar \sum_{\substack{m \neq 0 \\ m=2}}^{-2} \omega_C^{(m)} I_z e^{im\omega_r t} \quad (2.50)$$

with $\omega_C^{(m)} = -iC(1)\sqrt{\frac{2}{3}}B_0 G_m^{(2)0}$, Since the magnitude of the RF field exceeds the CSA interaction ($\omega_C^{(m)}$), the RF Hamiltonian is quantized along the z-axis using unitary trans-

formation, $U = e^{i\frac{\pi}{2}I_y}$

$$\tilde{H} = \hbar\omega_1 I_z - \hbar \sum_{\substack{m \neq 0 \\ m=2}}^{-2} \omega_C^{(m)} I_x e^{im\omega_r t} \quad (2.51)$$

Employing the Floquet framework (see Appendix Section 2.D) the time-dependent MAS Hamiltonian is transformed into time-independent Floquet Hamiltonian.⁶⁶ The Floquet Hamiltonian corresponding to equation Eq. (2.50) is written as follows

$$\tilde{H}_F = \hbar\omega_r I_F + \hbar\omega_1 I_{z,0} - \hbar \sum_{\substack{m \neq 0 \\ m=2}}^{-2} \omega_C^{(m)} I_{x,m} \quad (2.52)$$

The index ‘m’ denotes the off-diagonality in the Fourier space and is folded using the contact transformation procedure.^{31,33,67-72} To facilitate the process, the Hamiltonian is expressed as a sum of zero-order and perturbation Hamiltonian.

$$\tilde{H}_0 = \hbar\omega_r I_F + \hbar\omega_1 I_{z,0} \quad (2.53)$$

$$\tilde{H}_1 = -\hbar \sum_{\substack{m \neq 0 \\ m=2}}^{-2} \omega_C^{(m)} I_{x,m} = -\hbar \sum_{\substack{m \neq 0 \\ m=2}}^{-2} \frac{\omega_C^{(m)}}{2} (I_m^+ + I_m^-) \quad (2.54)$$

The effective Hamiltonian is obtained by transforming the Floquet Hamiltonian using a unitary transformation.

$$H_{eff} = e^{iS_1} H_F e^{-iS_1} \quad (2.55)$$

The transformation function³¹ $S_1 = i \sum_{\substack{m \neq 0 \\ m=2}}^{-2} (C_{1,m} I_m^+ + C_{2,m} I_m^-)$ is chosen to compensate the off-diagonality due to H_1 (i.e $H_1^{(1)} = H_1 + i[S_1, H_0]$) with the constants $C_{1,m} = \frac{\omega_C^{(m)}}{2(m\omega_r + \omega_1)}$, $C_{2,m} = \frac{\omega_C^{(m)}}{2(m\omega_r - \omega_1)}$. The diagonal corrections to the zero order Hamiltonian are obtained by evaluating the expression given below,

$$\begin{aligned} H_2^{(1)} &= \frac{i}{2} [S_1, H_1] \\ &= \hbar \sum_{\substack{m \neq 0 \\ m=2}}^{-2} (\omega_C^{(-m)} C_{1,m} - \omega_C^{(-m)} C_{2,m}) I_z \end{aligned} \quad (2.56)$$

To second-order, the effective Floquet Hamiltonian during the pulse is represented by,

$$H_{eff} = H_0 + H_2^{(1)} \quad (2.57)$$

Since $[I_z, \rho(0)] = 0$, the thermal equilibrium density operator ($\rho(0)$) remains invariant in the rotating frame i.e. $\tilde{\rho}(0) = \rho(0)$. The density operator after second transformation is represented by $\tilde{\tilde{\rho}}(0) = -I_x$. Subsequently, in the Floquet frame, the density operator gets reduced to,

$$\tilde{\tilde{\rho}}(0) = -I_x \cos a_1 + \sum_{\substack{m \neq 0 \\ m=2}}^{-2} \frac{(C_{1,m} - C_{2,m}) \sin a_1}{a_1} I_{z,m} \quad (2.58)$$

The density operator after the pulse is denoted and represented by,

$$\begin{aligned} \tilde{\tilde{\rho}}(t_p) = & -\cos a_1 I_x \cos \left(\left[\omega_1 + \sum_{\substack{m \neq 0 \\ m=2}}^{-2} (\omega_C^{(-m)} C_{1,m} - \omega_C^{(-m)} C_{2,m}) \right] t_p \right) \\ & - \cos a_1 I_y \sin \left(\left[\omega_1 + \sum_{\substack{m \neq 0 \\ m=2}}^{-2} (\omega_C^{(-m)} C_{1,m} - \omega_C^{(-m)} C_{2,m}) \right] t_p \right) \end{aligned} \quad (2.59)$$

where $a_1 = \sqrt{(C_{1,m} - C_{2,m})(C_{1,-m} - C_{2,-m})}$. As depicted in Eq. (2.59), the maximum signal in the transverse plane is obtained when $[\omega_1 + \sum_{\substack{m \neq 0 \\ m=2}}^{-2} (\omega_C^{(-m)} C_{1,m} - \omega_C^{(-m)} C_{2,m})] t_p = \frac{\pi}{2}$.

The density operator corresponding to maximum signal after the pulse is given by,

$$\tilde{\rho}(t_p) = U^- e^{-is_1} \tilde{\tilde{\rho}}(t_p) e^{is_1} U = -\cos a_1 \cos a_2 I_y \quad (2.60)$$

with $a_2 = \sqrt{(C_{1,m} + C_{2,m})(C_{1,-m} + C_{2,-m})}$. Subsequently, the system evolves under the evolution Hamiltonian. In the Floquet framework, the evolution Hamiltonian is represented by,

$$\tilde{H}_F = \underbrace{\hbar \omega_r I_F}_{H_0} + \hbar \underbrace{\sum_{\substack{m \neq 0 \\ m=2}}^{-2} \omega_C^{(m)} I_{z,m}}_{H_1} \quad (2.61)$$

Employing the contact transformation procedure, the effective Hamiltonian during the evolution period is obtained by the transformation function $S_1 = -i \sum_{\substack{m \neq 0 \\ m=2}}^{-2} \frac{\omega_C^{(m)}}{m \omega_r} I_{z,m}$,

$$H_{evol} = H_0 = \hbar \omega_r I_F \quad (2.62)$$

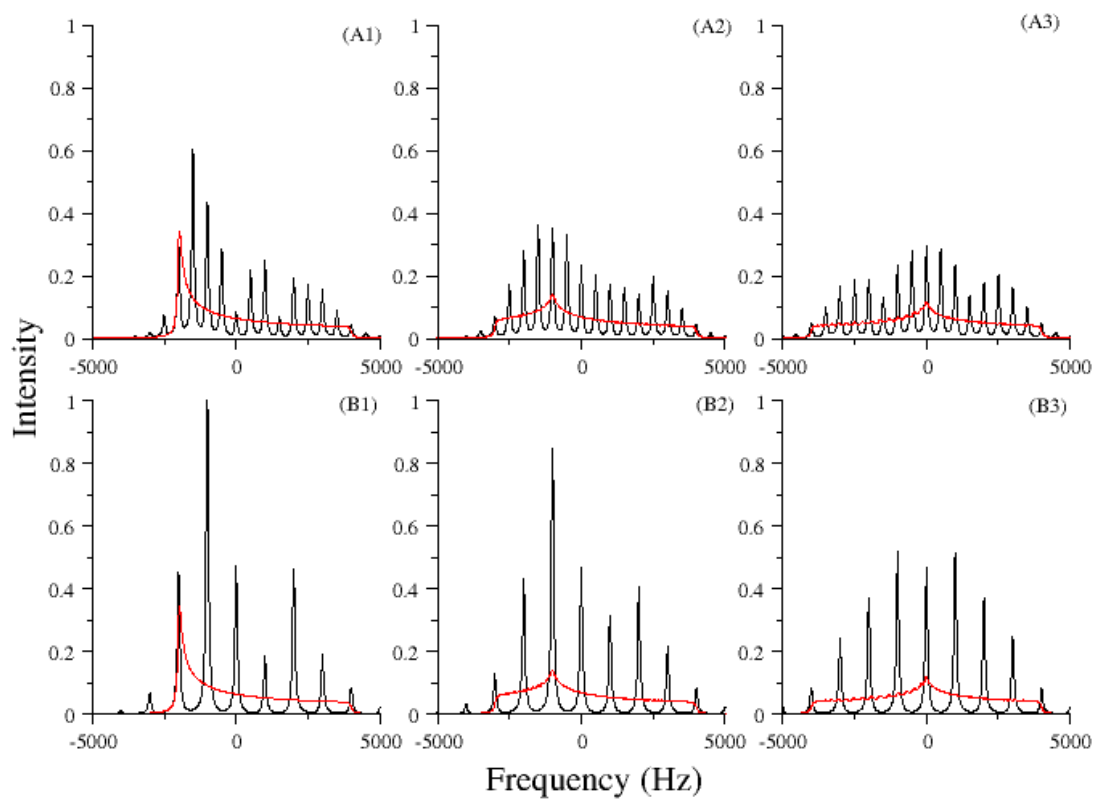


Figure 2.3: Simulations depicting the effects of spinning frequency on line shapes and intensities employing in panel (A) red line for static and black lines with spinning frequency $\nu_r = 5$ kHz, (B) red line for static and black lines with spinning frequency $\nu_r = 10$ kHz at different asymmetry parameters $\eta = 0.0, 0.5, 1.0$ for panels 1, 2, 3 respectively. All other parameters like chemical shift anisotropy $\delta^C = 4$ kHz, $\nu_1 = 50$ kHz kept constant.

Accordingly, the density operator after the pulse is derived and represented by,

$$\tilde{\rho}(t_p) = -\cos a_1 \cos a_2 \left[I_y - \sum_{\substack{m \neq 0 \\ m=2}}^{-2} \frac{i\omega_C^{(m)}}{m\omega_r} I_{x,m} + \sum_{\substack{m_1, m_2 \neq 0 \\ m_1, m_2=2}}^{-2} \frac{\omega_C^{(m_1)} \omega_C^{(m_2)}}{m_1 m_2 \omega_r^2} \frac{I_{y, m_1+m_2}}{2!} + \dots \right] \quad (2.63)$$

The density operator after the evolution for the time 't' is given by,

$$\tilde{\rho}(t_p + t) = -\cos a_1 \cos a_2 \left[I_y - \sum_{\substack{m \neq 0 \\ m=2}}^{-2} \frac{i\omega_C^{(m)}}{m\omega_r} I_{x,m} e^{-im\omega_r t} + \sum_{\substack{m_1, m_2 \neq 0 \\ m_1, m_2=2}}^{-2} \frac{\omega_C^{(m_1)} \omega_C^{(m_2)}}{m_1 m_2 \omega_r^2} \frac{I_{y, m_1+m_2}}{2!} e^{-i(m_1+m_2)\omega_r t} + \dots \right] \quad (2.64)$$

$$\begin{aligned} \tilde{\rho}(t_p + t) &= e^{-is_1} \tilde{\rho}(t_p + t) e^{is_1} \\ &= -\cos a_1 \cos a_2 \left[I_y - \frac{iI_x}{2!} \sum_{\substack{m_1, m_2, m_3 \neq 0 \\ m_1, m_2, m_3=2 \\ m_1+m_2+m_3=0}}^{-2} \frac{\omega_C^{(m_1)} \omega_C^{(m_2)} \omega_C^{(m_3)}}{m_1 m_2 m_3 \omega_r^3} (e^{-im_1\omega_r t} - e^{-i(m_1+m_2)\omega_r t}) \right. \\ &\quad \left. - I_y \sum_{\substack{m_1, m_2 \neq 0 \\ m_1, m_2=2 \\ m_1+m_2=0}}^{-2} \frac{\omega_C^{(m_1)} \omega_C^{(m_2)}}{m_1 m_2 \omega_r^2} e^{-im_1\omega_r t} + \frac{I_y}{2!2!} \sum_{\substack{m_1, m_2, m_3, m_4 \neq 0 \\ m_1, m_2, m_3, m_4=2 \\ m_1+m_2+m_3+m_4=0}}^{-2} \frac{\omega_C^{(m_1)} \omega_C^{(m_2)} \omega_C^{(m_3)} \omega_C^{(m_4)}}{m_1 m_2 m_3 m_4 \omega_r^4} e^{-i(m_1+m_2)\omega_r t} \dots \right] \quad (2.65) \end{aligned}$$

Employing Eq. (1.16), the time-domain signal is evaluated accordingly and is represented by,

$$\begin{aligned} \langle I^+(t) \rangle &= \frac{\cos a_1 \cos a_2 C(1)^2}{2} \left[e^{-i\omega_0 t} - \sum_{\substack{m_1, m_2, m_3 \neq 0 \\ m_1, m_2, m_3=2 \\ m_1+m_2+m_3=0}}^{-2} \frac{\omega_C^{(m_1)} \omega_C^{(m_2)} \omega_C^{(m_3)}}{2! m_1 m_2 m_3 \omega_r^3} (e^{-i(m_1\omega_r + \omega_0)t} - e^{-i[(m_1+m_2)\omega_r + \omega_0]t}) \right. \\ &\quad \left. - \sum_{\substack{m_1, m_2 \neq 0 \\ m_1, m_2=2 \\ m_1+m_2=0}}^{-2} \frac{\omega_C^{(m_1)} \omega_C^{(m_2)}}{m_1 m_2 \omega_r^2} e^{-i(m_1\omega_r + \omega_0)t} + \sum_{\substack{m_1, m_2, m_3, m_4 \neq 0 \\ m_1, m_2, m_3, m_4=2 \\ m_1+m_2+m_3+m_4=0}}^{-2} \frac{\omega_C^{(m_1)} \omega_C^{(m_2)} \omega_C^{(m_3)} \omega_C^{(m_4)}}{2!2! m_1 m_2 m_3 m_4 \omega_r^4} e^{-i[(m_1+m_2)\omega_r + \omega_0]t} \dots \right] \quad (2.66) \end{aligned}$$

In the Floquet framework, the time-domain signal comprises of the center band and a series of side bands. The simulations depicted in Fig. 2.3, substantiate the analytic results presented in this section.

Appendix

2.A Irreducible spherical tensors³⁷

Tensors: Tensors are geometric objects with arrays of numbers or functions that describe linear relations between scalars, vectors and other tensors.

$$Y = \begin{pmatrix} Y_{xx} & Y_{xy} & Y_{xz} \\ Y_{yx} & Y_{yy} & Y_{yz} \\ Y_{zx} & Y_{zy} & Y_{zz} \end{pmatrix} \quad (2.67)$$

Cartesian tensor

The more familiar cartesian tensors are not suitable because they usually appear in reducible form. Thus, from direct product of cartesian tensors, one can form sets of linear combination of components of a cartesian tensor which transform differently. Transformation laws are much simpler for the tensors with spherical components since they are proportional to the spherical Harmonics, Y_l^m

Irreducible spherical tensor: An irreducible tensor operator of rank ‘ k ’ is defined as a set of $2k + 1$ functions $T^{(k)q}$, which transform under the $2k + 1$ dimensional representation of the rotation group as⁶³

$$D(\alpha\beta\gamma)T^{(k)q}D^{-1}(\alpha\beta\gamma) = \sum_{q'=k}^{-k} D_{q'q}^{(k)}(\alpha\beta\gamma)T^{(k)q'} \quad (2.68)$$

(or)

The set $T^{(k)q}$ constitutes an irreducible tensor if the following commutator relationships with angular momentum operators are fulfilled⁶⁵

$$\begin{aligned} [I_z, T^{(k)q}] &= qT^{(k)q} \\ [I^\pm, T^{(k)q}] &= \sqrt{k(k+1) - q(q \pm 1)}T^{(k)q} \end{aligned} \quad (2.69)$$

Employing the theory of addition of angular momentum, a general representation of irreducible spherical tensors^{35,37,73} for a coupled spin system is represented by,

$$T_{(K_1 K_2 K_3 \dots K_{N-2})}^{(k)q} (k_1 k_2 k_3 \dots k_N) \quad (2.70)$$

where N is the number of spins, k is the overall rank, q the component which takes values from $-k$ to k , K_{N-2} the intermediate angular momentum vector and k_N the rank of individual spins and it takes the values from 0 to $2I_N$.

These tensor operators are irreducible and symmetric traceless⁷⁴⁻⁷⁶ and are denoted by $[I]^{(k)}$. The normalized form^{77,78} of these operators are given by,

$$T^{(k)}(I) = \sqrt{\frac{2k+1}{2I+1}} \frac{[I]^{(k)}}{\sqrt{[I]^{(k)} \odot^k [I]^{(k)}}} \quad (2.71)$$

$$Tr[T^{(k)}(I) \odot^k T^{(k)}(I)] = 2k + 1 \quad (2.72)$$

The factor in denominator in Eq. (2.71) is evaluated by the equation given below,

$$[I]^{(k)} \odot^k [I]^{(k)} = \frac{(k!)^2 (2I+k+1)!}{2^k (2I+1) (2k)! (2I-k)!} \quad (2.73)$$

Based (Eq. (2.73)), The normalization constant $C(k)$ is defined.

$$C(k) = \sqrt{\frac{(2k+1)2^k (2k)! (2I-k)!}{(k!)^2 (2I+k+1)!}} \quad (2.74)$$

$$T^{(k)}(I) = C(k)[I]^{(k)} \quad (2.75)$$

The $2k + 1$ spherical components of above tensor $T^{(k)}(I)$ can be written with respect to covariant^I spherical basis⁷⁴⁻⁷⁶ $e^{(k)q}$ which is given in Tables 2.7 and 2.8. The complex conjugate of $e^{(k)q}$ is

$$e^{(k)q*} = (-1)^{k-q} e^{(k)-q} = e_q^{(k)} \quad (2.76)$$

Accordingly, the spherical components in this basis is expressed by,

$$T^{(k)q}(I) = T^{(k)}(I) \odot^k e^{(k)q} \quad (2.77)$$

^IIn literature we find covariant representation as component q in superscript $e_q^{(k)}$ and for contravariant representation as component q in subscript $e^{(k)q}$ but we are following opposite convention just for better representation of spin and other label in covariant tensors.

k	$C(k)$
0	$\sqrt{\frac{(2I)!}{(2I+1)!}} = \sqrt{\frac{1}{(2I+1)}}$
1	$2\sqrt{3}\sqrt{\frac{(2I-1)!}{(2I+2)!}} = \sqrt{\frac{3}{(2I+1)I(I+1)}}$
2	$2\sqrt{30}\sqrt{\frac{(2I-2)!}{(2I+3)!}} = \sqrt{\frac{30}{(2I+1)I(I+1)(2I+3)(2I-1)}}$
3	$4\sqrt{70}\sqrt{\frac{(2I-3)!}{(2I+4)!}}$
4	$12\sqrt{70}\sqrt{\frac{(2I-4)!}{(2I+5)!}}$
5	$24\sqrt{124}\sqrt{\frac{(2I-5)!}{(2I+6)!}}$
6	$16\sqrt{3003}\sqrt{\frac{(2I-6)!}{(2I+7)!}}$
7	$96\sqrt{715}\sqrt{\frac{(2I-7)!}{(2I+8)!}}$
$C(k_1 k_2 \dots k_N) = C(k_1)C(k_2) \dots C(k_N)$	

Table 2.6: Explicit form of the normalization constant for single spin operators up to rank $k = 7$ and multiple spin operator in N spin basis

with the complex conjugate of $T^{(k)q}$ defined by,

$$T^{(k)q}(I)^\dagger = (-1)^{k-q} T^{(k)-q}(I) = T_q^{(k)} \quad (2.78)$$

The normalization condition for the tensor operators is defined by taking the quantum trace.

$$Tr[T^{(k)q}(I)^\dagger T^{(k')q'}(I)] = \delta_{kk'} \delta_{qq'} \quad (2.79)$$

The quantum trace of any individual tensor operator defined by,

$$Tr[T^{(k)q}(I)] = \frac{1}{C(0)} Tr[T^{(k)q}(I) T^{(0)0}(I)] = \frac{\delta_{k0} \delta_{q0}}{C(0)} \quad (2.80)$$

with $T^{(0)0}$ is the tensor with rank zero. In usual terms we call it as a scalar.

$$T^{(0)0}(I) = C(0)I \quad (2.81)$$

where I is the Identity operator. The spherical basis $e^{(k)q}$ and the corresponding components of cartesian tensors with different ranks are given in Tables 2.7 and 2.8. The

explicit form of tensors up to rank 1 in the basis $e^{(1)q}$ of Table 2.7 are given by,

$$\begin{aligned} T^{(1)0}(I) &= C(1)iI_z \\ T^{(1)\pm 1}(I) &= \mp \frac{C(1)i}{\sqrt{2}}I_{\pm} \end{aligned} \quad (2.82)$$

Spherical coordinates	Spherical components
$e^{(1)0} = i\hat{z}$	$Y^{(1)0} = iY_z$
$e^{(1)1} = -\frac{i}{\sqrt{2}}(\hat{x} + i\hat{y})$	$Y^{(1)1} = -\frac{i}{\sqrt{2}}(Y_x + iY_y)$
$e^{(1)-1} = \frac{i}{\sqrt{2}}(\hat{x} - i\hat{y})$	$Y^{(1)-1} = \frac{i}{\sqrt{2}}(Y_x - iY_y)$
$Y = \sum_{q=-1}^{-1} (-1)^{1-q} Y^{(1)q} e^{(1)-q}$	

Table 2.7: The spherical basis $e^{(k)q}$ and the corresponding spherical components of cartesian tensor of rank $k = 1$

Spherical coordinates	Spherical components
$e^{(0)0} = \frac{1}{\sqrt{3}}(xx + yy + zz)$	$Y^{(0)0} = \frac{1}{\sqrt{3}}(Y_{xx} + Y_{yy} + Y_{zz})$
$e^{(1)0} = -\frac{i}{\sqrt{2}}(xy - yx)$	$Y^{(1)0} = -\frac{i}{\sqrt{2}}(Y_{xy} - Y_{yx})$
$e^{(1)\pm 1} = -\frac{1}{2}[zx - xz \pm i(zy - yz)]$	$Y^{(1)\pm 1} = -\frac{1}{2}[Y_{zx} - Y_{xz} \pm i(Y_{zy} - Y_{yz})]$ $= -\frac{1}{2}[Y_{zx} \pm iY_{zy} - (Y_{xz} \pm iY_{yz})]$
$e^{(2)0} = \frac{-1}{\sqrt{6}}[3zz - (xx + yy + zz)]$	$Y^{(2)0} = \frac{-1}{\sqrt{6}}[3Y_{zz} - (Y_{xx} + Y_{yy} + Y_{zz})]$
$e^{(2)\pm 1} = \pm \frac{1}{2}[xz + zx \pm i(yz + zy)]$	$Y^{(2)\pm 1} = \pm \frac{1}{2}[Y_{xz} + Y_{zx} \pm i(Y_{yz} + Y_{zy})]$ $= \pm \frac{1}{2}[Y_{xz} \pm iY_{yz} + Y_{zx} \pm iY_{zy}]$
$e^{(2)\pm 2} = \frac{-1}{2}[xx - yy \pm i(xy + yx)]$	$Y^{(2)\pm 2} = \frac{-1}{2}[Y_{xx} - Y_{yy} \pm i(Y_{xy} + Y_{yx})]$
$Y = \sum_{k=0}^2 \sum_{q=k}^{-k} (-1)^{k-q} Y^{(k)q} e^{(k)-q}$	

Table 2.8: The spherical basis $e^{(k)q}$ and the corresponding spherical components of cartesian tensor of rank $k = 2$

The higher rank tensors are constructed by coupling of lower rank tensors as illustrated in Eq. (2.83). Explicit forms of tensor operators corresponding to single spin up to rank

$k = 7$ is given in Table 2.9. The general relation of $T^{(k)q}(I)$ operator with product operators is given in Appendix Section 2.B.2.

$$T^{(k)q} = \sum_{q_1, q_2} \sqrt{(2k+1)(-1)^{(k-q)}} \begin{pmatrix} k_1 & k_2 & k \\ q_1 & q_2 & -q \end{pmatrix} T^{(k_1)q_1} T^{(k_2)q_2} \quad (2.83)$$

Extending this algebra, tensor operators corresponding to multiple spins derived by coupling of individual spin operators as given in Eq. (2.84). The essential tensor operators in multiple spin basis is given in Appendix Section 2.B.3.

$$T_{\{\bar{K}_{N-2}\}}^{(k)q}(k_1 k_2 \dots k_N) = \sum_{\substack{q_1, q_2, \dots, q_N \\ \bar{q}_1, \bar{q}_2, \dots, \bar{q}_{N-2}}} \sqrt{(2\bar{K}_1+1)(2\bar{K}_2+1)\dots(2\bar{K}_{N-2}+1)(2k+1)} \\ (-1)^{(\bar{K}_1+\bar{K}_2+\dots+\bar{K}_{N-2})} (-1)^{(k_1+k_2+k_3+\dots+k_N+k)} (-1)^{(\bar{q}_1+\bar{q}_2+\dots+\bar{q}_{N-2})} (-1)^{(k-q)} \begin{pmatrix} k_1 & k_2 & \bar{K}_1 \\ q_1 & q_2 & -\bar{q}_1 \end{pmatrix} \\ \dots \begin{pmatrix} \bar{K}_1 & k_3 & \bar{K}_2 \\ \bar{q}_1 & q_3 & -\bar{q}_2 \end{pmatrix} \dots \begin{pmatrix} \bar{K}_{N-2} & k_N & k \\ \bar{q}_{N-2} & q_N & -q \end{pmatrix} T^{(k_1)q_1}(I_1) T^{(k_2)q_2}(I_2) \dots T^{(k_N)q_N}(I_1) \quad (2.84)$$

2.B Essential relations of tensor operators

2.B.1 Explicit form of $T^{(k)q}(I)$ operators up to the rank $k=7$

k	q	$T^{(k)q}(I)$
0	0	$C(0)I$
1	0	$C(1)iI_z$
1	± 1	$\mp \frac{C(1)i}{\sqrt{2}} I_{\pm}$
2	0	$\frac{C(2)}{\sqrt{6}} (I^2 - 3I_z^2)$
2	± 1	$\pm \frac{C(2)}{2} [I_z, I_{\pm}]_{\pm}$
2	± 2	$-\frac{C(2)}{2} I_{\pm}^2$
3	0	$\frac{C(3)i}{\sqrt{10}} (3I^2 - 5I_z^2 - 1)I_z$
3	± 1	$\pm \frac{C(3)i}{4} \sqrt{\frac{3}{10}} [(I^2 - 5I_z + 1/2), I_{\pm}]_{\pm}$

Continued on next page

Table 2.9 – Continued from previous page

k	q	$T^{(k)q}(I)$
3	± 2	$-C(3)i\sqrt{\frac{3}{4}}I_{\pm}I_zI_{\pm}$
3	± 3	$\pm \frac{C(3)i}{2\sqrt{2}}I_{\pm}^3$
4	0	$\frac{C(4)}{2\sqrt{70}}[(35I_z^4 - 30I_z^2I_z^2 + 25I_z^2 + 3I^4 - 6I^2)]$
4	± 1	$\mp \frac{C(4)}{2\sqrt{14}}[(7I_z^3 - 3I^2I_z - I_z), I_{\pm}]_+$
4	± 2	$\frac{C(4)}{4\sqrt{7}}[(7I_z^2 - I^2 - 5), I_{\pm}^2]_+$
4	± 3	$\mp \frac{C(4)}{2\sqrt{2}}[I_z, I_{\pm}^3]_+$
4	± 4	$\frac{C(4)}{4}I_{\pm}^4$
5	0	$\frac{C(5)i}{6}\sqrt{\frac{1}{14}}[63I_z^5 + 35I_z^3(3 - 2I^2) + I_z(12 - 50I^2 + 15I^4)]$
5	± 1	$\mp \frac{C(5)i}{4}\sqrt{\frac{5}{21}}I_{\pm}[21I_z^4 \pm 42I_z^3 + 7I_z^2(9 - 2I^2) \pm 14I_z(3 - I^2) - 8I^2 + I^4 + 12]$
5	± 2	$\frac{C(5)i}{2}\sqrt{\frac{5}{3}}I_{\pm}^2[3I_z^3 \pm 9I_z^2 + I_z(12 - I^2) \pm (6 - I^2)]$
5	± 3	$\mp \frac{C(5)i}{12}\sqrt{\frac{5}{2}}I_{\pm}^3[9I_z^2 \pm 27I_z + 24 - I^2]$
5	± 4	$C(5)i\sqrt{\frac{5}{16}}I_{\pm}^4[I_z \pm 2]$
5	± 5	$\mp \frac{C(5)i}{4\sqrt{2}}I_{\pm}^5$
6	0	$-\frac{C(6)}{4}\sqrt{\frac{1}{231}}[231I_z^6 + 105I_z^4(7 - I^2) + 21I_z^2(14 - 25I^2 + I^4) + 5(-12I^2 + 8I^4 - I^8)]$
6	± 1	$\pm \frac{C(6)}{4}\sqrt{\frac{1}{22}}I_{\pm}[66I_z^5 \pm 165I_z^4 + 60I_z^3(6 - I^2) \pm 15I_z^2(25 - 6I^2) + 2I_z(117 - 55I^2 + 5I^4) \pm (12 - 40I^2 + I^4)]$
6	± 2	$-\frac{C(6)}{8}\sqrt{\frac{5}{11}}I_{\pm}^2[33I_z^4 \pm 132I_z^3 + 3I_z^2(91 - 6I^2) \pm 6I_z(47 - 6I^2) - 26I^2 + I^4 + 120]$
6	± 3	$\pm \frac{C(6)}{8}\sqrt{\frac{5}{11}}I_{\pm}^3[22I_z^3 \pm 90I_z^2 + 179I_z - 6I^2I_z \mp 9I^2 \pm 120]$
6	± 4	$-\frac{C(6)}{4}\sqrt{\frac{3}{22}}I_{\pm}^4[11I_z^2 \pm 44I_z + 50 - I^2]$
6	± 5	$\pm C(6)\sqrt{\frac{3}{64}}I_{\pm}^5[2I_z \pm 5]$
6	± 6	$-\frac{C(6)}{8}I_{\pm}^6$
7	0	$-\frac{C(7)i}{4}\sqrt{\frac{1}{429}}[429I_z^7 + 231I_z^5(10 - 3I^2) + 21I_z^3(101 - 105I^2 + 15I^4) + I_z(180 - 882I^2 + 385I^4 - 35I^8)]$
7	± 1	$\pm \frac{C(7)i}{8}\sqrt{\frac{7}{858}}I_{\pm}[429I_z^6 \pm 1287I_z^5 + 165I_z^4(23 - 3I^2) \pm 495I_z^3(11 - 2I^2) + 3I_z^2(1832 - 645I^2 + 45I^4) \pm 9I_z(332 - 160I^2 + 15I^4) + 5(144 - 108I^2 + 200I^4 - I^8)]$

Continued on next page

Table 2.9 – Continued from previous page

k	q	$T^{(k)q}(I)$
7	± 2	$-\frac{C(7)i}{8}\sqrt{\frac{7}{143}}I_{\pm}^2[143I_z^5 \pm 715I_z^4 + 55I_z^3(37 - 2I^2) \pm 55I_z^2(59 - 6I^2) + I_z(2862 - 490I^2 + 15I^4) \pm 15(72 - 18I^2 + I^4)]$
7	± 3	$\pm\frac{C(7)i}{8}\sqrt{\frac{7}{286}}I_{\pm}^3[143I_z^4 \pm 858I_z^3 + 11I_z^2(215 - 6I^2) \pm 66I_z(49 - 3I^2) + 3(600 - 62I^2 + I^4)]$
7	± 4	$-\frac{C(7)i}{4}\sqrt{\frac{7}{26}}I_{\pm}^4[13I_z^3 \pm 78I_z^2 + 179I_z - 3I^2I_z \pm 6(25 - I^2)]$
7	± 5	$\pm\frac{C(7)i}{8}\sqrt{\frac{7}{26}}I_{\pm}^5[13I_z^2 \pm 65I_z + 90 - I^2]$
7	± 6	$-C(7)i\sqrt{\frac{7}{8}}I_{\pm}^6[I_z \pm 3]$
7	± 7	$\pm\frac{C(7)i}{8\sqrt{2}}I_{\pm}^7$

Table 2.9: Explicit form of $T^{(k)q}(I)$ operators up to the rank $k=7$

2.B.2 General relation of $T^{(k)q}(I)$ operator with product operators

$$T^{(k)\pm k}(I) = C(k)\left(T^{(1)\pm 1}(I)\right)^k \quad (2.85a)$$

$$T^{(k)q\pm 1}(I) = \frac{1}{\sqrt{(k\pm q+1)(k\mp q)}} \left[I_{\pm}, T^{(k)q}(I) \right] \quad (2.85b)$$

$$T^{(k)q}(I) = \left(\frac{-i}{\sqrt{2}}\right)^k \left[\frac{(k+q)!}{(2k)!(k-q)!}\right]^{1/2} C(I) \underbrace{[I_-, \dots, [I_-, (I_+)^k], \dots]}_{k-q} \quad (2.85c)$$

$$T^{(k)-q}(I) = \left(\frac{i}{\sqrt{2}}\right)^k \left[\frac{(k+q)!}{(2k)!(k-q)!}\right]^{1/2} C(I) \underbrace{[I_+, \dots, [I_+, (I_-)^k], \dots]}_{k-q} \quad (2.85d)$$

2.B.3 Explicit form of $T^{(k)q}(\bar{I})$ operators in multiple spin basis (Essential two spin tensor operators)

$$T^{(0)0}(0..1_j 0..1_l 0..) = \underbrace{\left(\prod_{\substack{s=1 \\ s \neq j,l}}^N \sqrt{\frac{1}{(2I_s+1)}} \sqrt{\frac{3}{I_j(I_j+1)(2I_j+1)}} \sqrt{\frac{3}{I_l(I_l+1)(2I_l+1)}} \right)}_{C(0..1_j 0..1_l 0..)} \frac{1}{\sqrt{3}} I_j \cdot I_l \quad (2.86a)$$

$$T^{(1)0}(0..1_j 0..1_k 0..) = C(0..1_j 0..1_k 0..) \cdot \frac{1}{2\sqrt{2}} [I_j^+ I_k^- - I_j^- I_k^+] \quad (2.86b)$$

$$T^{(2)0}(0..1_j 0..1_k 0..) = C(0..1_j 0..1_k 0..) \cdot \frac{-1}{\sqrt{6}} [3I_{jz} I_{kz} - I_j \cdot I_k] \quad (2.86c)$$

$$T^{(1)\pm 1}(0..1_j 0..1_k 0..) = C(0..1_j 0..1_k 0..) \cdot \frac{1}{2} [I_j^\pm I_{kz} - I_{jz} I_k^\pm] \quad (2.86d)$$

$$T^{(2)\pm 1}(0..1_j 0..1_k 0..) = C(0..1_j 0..1_k 0..) \cdot \pm \frac{1}{2} [I_j^\pm I_{kz} + I_{jz} I_k^\pm] \quad (2.86e)$$

$$T^{(2)\pm 2}(0..1_j 0..1_k 0..) = C(0..1_j 0..1_k 0..) \cdot \frac{-1}{2} I_j^\pm I_k^\pm \quad (2.86f)$$

2.B.4 Relation with level shift operators 79–81

$$|IM\rangle \langle IM'| = (-1)^{I-M} \sum_{k=0}^{2I} \sum_{q=k}^{-k} \sqrt{2k+1} (-i)^k \begin{pmatrix} I & k & I \\ -M & q & M' \end{pmatrix} T^{(k)q}(I) \quad (2.87a)$$

$$T^{(k)q}(I) = \sqrt{2k+1} (i)^k \sum_{M,M'} (-1)^{I-M} \begin{pmatrix} I & k & I \\ -M & q & M' \end{pmatrix} |IM\rangle \langle IM'| \quad (2.87b)$$

These follow from Wigner-Eckart theorem and reduced matrix element 23,38,44,63,65,82–84 given below

$$\langle I || T^{(k)q} || I' \rangle = \sqrt{2k+1} (i)^k \delta_{II'} \quad (2.88)$$

2.B.5 Relation with unnormalized or non-unit tensors 36,51,64

$$T_N^{(k)q}{}_{(K_1 K_2 \dots K_{N-2})} (k_1 k_2 \dots k_N) = (i)^{(k_1+k_2+\dots+k_N)} C(k_1 k_2 \dots k_N) T_{(K_1 K_2 \dots K_{N-2})}^{(k)q} (k_1 k_2 \dots k_N) \quad (2.89)$$

2.B.6 Commutator relation between tensor operators ^{35,37} $T^{(k)q}(\bar{I})$'s

Single spin:

$$\begin{aligned} \left[T^{(k)q}(I), T^{(k')q'}(I) \right] &= \sum_{k'', q''} \varphi(kk'k'') (-1)^{2I} (i)^{k+k'+k''} \sqrt{(2k+1)(2k'+1)(2k''+1)} \\ &\quad \times (-1)^{k-k'+k''} \begin{Bmatrix} k'' & k & k' \\ I & I & I \end{Bmatrix} (-1)^{k''-q''} \begin{pmatrix} k & k' & k'' \\ q & q' & -q'' \end{pmatrix} T^{(k'')q''}(I) \end{aligned} \quad (2.90)$$

with $\varphi(kk'k'') = [1 - (-1)^{k+k'+k''}]$

Multiple spin:

$$\begin{aligned} \left[T_{\{K\}}^{(k)q}(k_1 k_2 \dots k_N), T_{\{K'\}}^{(k')q'}(k'_1 k'_2 \dots k'_N) \right] &= \sum_{\substack{\text{all } k''_{1 \rightarrow N}, q'', \\ K''_{1 \rightarrow N-2}, k''}} \varphi_{j=1 \rightarrow N}(k_j k'_j k''_j) (-1)^{2(I_1+I_2+\dots+I_N)} \\ &\quad \times (i)^{k_1+k_2+\dots+k_N} (i)^{k'_1+k'_2+\dots+k'_N} (i)^{k''_1+k''_2+\dots+k''_N} \sqrt{(2k+1)(2k'+1)(2k''+1)} \\ &\quad \times \sqrt{\prod_{l=1}^{N-2} (2K_l+1)(2K'_l+1)(2K''_l+1) \prod_{j=1}^N (2k_j+1)(2k'_j+1)(2k''_j+1)} \\ &\quad \times (-1)^{k-k'+k''} \begin{Bmatrix} k''_1 & k_1 & k'_1 \\ I_1 & I_1 & I_1 \end{Bmatrix} \begin{Bmatrix} k''_2 & k_2 & k'_2 \\ I_2 & I_2 & I_2 \end{Bmatrix} \dots \begin{Bmatrix} k''_N & k_N & k'_N \\ I_N & I_N & I_N \end{Bmatrix} \\ &\quad \times \begin{Bmatrix} k_1 & k_2 & K_1 \\ k'_1 & k'_2 & K'_1 \\ k''_1 & k''_2 & K''_1 \end{Bmatrix} \begin{Bmatrix} K_1 & k_3 & K_2 \\ K'_1 & k'_3 & K'_2 \\ K''_1 & k''_3 & K''_2 \end{Bmatrix} \dots \begin{Bmatrix} K_{N-2} & k_N & k \\ K'_{N-2} & k'_N & k' \\ K''_{N-2} & k''_N & k'' \end{Bmatrix} \\ &\quad \times (-1)^{k''-q''} \begin{pmatrix} k & k' & k'' \\ q & q' & -q'' \end{pmatrix} T_{\{K''\}}^{(k'')q''}(k''_1 k''_2 \dots k''_N) \end{aligned} \quad (2.91)$$

with $\varphi_{j=1 \rightarrow N}(k_j k'_j k''_j) = [1 - (-1)^{\sum_{j=1}^N k_j+k'_j+k''_j}]$

2.C Transformation properties

In the Euclidean space, transformation from one coordinate axes to another is described through three angles, commonly referred as Euler angles (α, β, γ) . ^{23,38,43,44,51,62,63,82,83} This transformation is accomplished through either the so called passive rotation (shown in Fig. 2.5) or through active rotation (shown in Fig. 2.7).

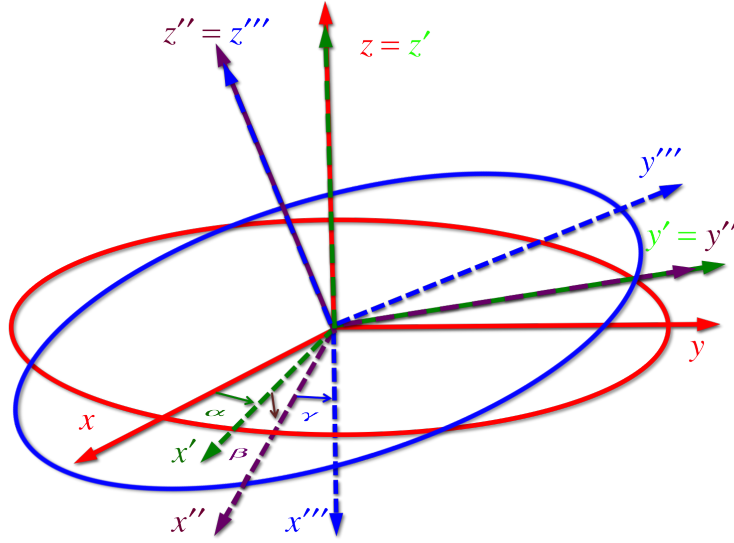


Figure 2.4: Euler angles: A passive rotation by α ($0 \leq \alpha \leq 2\pi$) about z-axis called vertical axis, a passive rotation by β ($0 \leq \beta \leq \pi$) about y' -axis called line of nodes and a passive rotation by γ ($0 \leq \gamma \leq 2\pi$) about z'' -axis called figure axis.

The rotation operator corresponding to passive rotation of coordinate axes frame (for rotation shown in Fig. 2.4) is represented by,

$$\begin{aligned} D(\alpha\beta\gamma) &= e^{-i\gamma I_{z''}} e^{-i\beta I_{y'}} e^{-i\alpha I_z} \\ &= e^{-i\alpha I_z} e^{-i\beta I_{y'}} e^{-i\gamma I_z} \end{aligned} \quad (2.92)$$

For the positive rotation of the coordinate axes system, the relative rotation of vector is negative. Hence the rotation operator corresponding to rotation of any tensor depicted in Fig. 2.4 is represented by

$$\begin{aligned} D(-\alpha - \beta - \gamma) &= e^{i\gamma I_{z''}} e^{i\beta I_{y'}} e^{i\alpha I_z} \\ &= e^{i\alpha I_z} e^{i\beta I_{y'}} e^{i\gamma I_z} \end{aligned} \quad (2.93)$$

Rotation Direction	Passive		Active
	Axes	tensor	tensor
Positive	$D(\alpha\beta\gamma)$	$D(-\alpha - \beta - \gamma)$	$D^{-1}(-\alpha - \beta - \gamma) = D(\gamma\beta\alpha)$
Negative	$D(-\alpha - \beta - \gamma)$	$D(\alpha\beta\gamma)$	$D^{-1}(\alpha\beta\gamma) = D(-\gamma - \beta - \alpha)$

Table 2.10: The rotation operators corresponding to passive and active rotations.

2.C.1 Passive rotation

In the passive rotation, rotation of the coordinate axes frame is accomplished through instantaneous axis, while tensor (or body) is passively fixed in coordinate system.

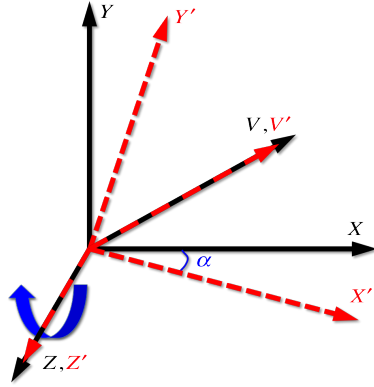


Figure 2.5: A passive rotation of coordinate axes by $-\alpha$ or rotation of vector by α about z-axis.

Positive rotation: By definition, a positive rotation is based on the simple convention, on rotation right handed screw move to wards positive direction of the axis (away from the origin). In quantum theory of angular momentum, this is referred to as anti-clock wise rotation. In this rotation we follow right hand rule which is shown in Fig. 2.6. The

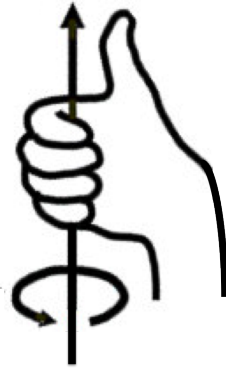


Figure 2.6: Right hand rule: The right thumb denotes the axis of rotation, the remaining curled fingers depicts the direction of the rotation of tensor.

rotation operator corresponding to positive rotation of the vector (Fig. 2.5) is defined by,

$$D(\alpha\beta\gamma) = e^{-i\alpha I_z} e^{-i\beta I_y} e^{-i\gamma I_z} \quad (2.94)$$

The corresponding transformation of the covariant tensor is given by,

$$D(\alpha\beta\gamma) T^{(k)q} D^{-1}(\alpha\beta\gamma) = \sum_{q'=k}^{-k} D_{q'q}^{(k)}(\alpha\beta\gamma) T^{(k)q'} \quad (2.95)$$

In a similar vein, the transformation of contravariant tensor is given by,

$$D(\alpha\beta\gamma)T_q^{(k)}D^{-1}(\alpha\beta\gamma) = \sum_{q'=k}^{-k} D_{q'q}^{(k)}(-\alpha\beta-\gamma)T_{q'}^{(k)} \quad (2.96)$$

where $D_{q'q}^{(k)}(\alpha\beta\gamma)$ ³⁸ are the elements of Wigner D-matrix or Wigner rotation matrix $D^{(k)}(\alpha\beta\gamma)$ called Wigner functions.

$$\begin{aligned} D_{q'q}^{(k)}(\alpha\beta\gamma) &= \langle kq' | D(\alpha\beta\gamma) | kq \rangle \\ &= \langle kq' | e^{-i\alpha I_z} e^{-i\beta I_y} e^{-i\gamma I_z} | kq \rangle \\ &= e^{-iq'\alpha} e^{-iq'\gamma} \langle kq' | e^{-i\beta I_y} | kq \rangle \\ &= e^{-iq'\alpha} e^{-iq'\gamma} d_{q'q}^{(k)}(\beta) \end{aligned} \quad (2.97)$$

with $d_{q'q}^{(k)}(\beta)$ ³⁸ is the element of reduced Wigner rotation matrix $d^{(k)}(\beta)$ called Wigner formula. Some useful relations of Wigner functions and Wigner formulae are given below,

$$\begin{aligned} [D_{q'q}^{(k)}(\alpha\beta\gamma)]^\dagger &= D_{qq'}^{(k)}(-\gamma-\beta-\alpha) & d_{q'q}^{(k)}(\beta) &= (-1)^{q'-q} d_{qq'}^{(k)}(\beta) \\ &= (-1)^{q'-q} D_{-q'-q}^{(k)}(\alpha\beta\gamma) & &= (-1)^{q'-q} d_{q'q}^{(k)}(-\beta) \\ & & &= (-1)^{q'-q} d_{-q'-q}^{(k)}(\beta) \end{aligned} \quad (2.98)$$

2.C.2 Active rotation

Rotation of the tensor or body using space fixed axis system is called active or space fixed rotation. In this rotation, body or tensor is actively rotated along coordinate axis, hence in the literature it is defined as vector rotation.

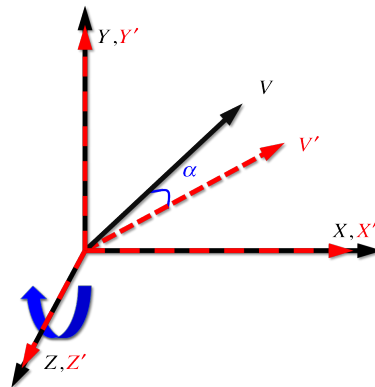


Figure 2.7: An active rotation of a vector with negative rotation by $-\alpha$ about z-axis

Negative rotation: By definition, a negative rotation is based on simple convention, on rotation right handed screw move to wards negative direction of axis (towards the origin).

In quantum theory of angular momentum, this is referred to as clock wise rotation. In this rotation we follow left hand rule which is shown in Fig. 2.8.

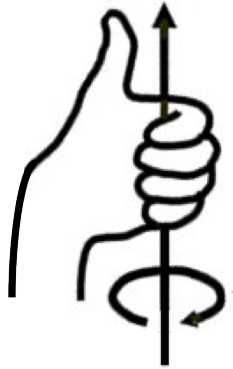


Figure 2.8: Left hand rule: The left thumb denotes the axis of rotation, the remaining curled fingers depicts the direction of the rotation of tensor.

The rotation operator corresponding to negative rotation of vector (Fig. 2.7) is defined by,

$$D^{-1}(\alpha\beta\gamma) = e^{i\gamma I_z} e^{i\beta I_y} e^{i\alpha I_z} \quad (2.99)$$

The corresponding transformation of the covariant tensor given by,

$$D^{-1}(\alpha\beta\gamma)T^{(k)q}D(\alpha\beta\gamma) = \sum_{q'=k}^{-k} D_{qq'}^{(k)}(-\alpha\beta - \gamma)T^{(k)q'} \quad (2.100)$$

In a similar vein, the transformation of contravariant tensor is given by,

$$D^{-1}(\alpha\beta\gamma)T_q^{(k)}D(\alpha\beta\gamma) = \sum_{q'=k}^{-k} D_{qq'}^{(k)}(\alpha\beta\gamma)T_{q'}^{(k)} \quad (2.101)$$

Based on Eqs. (2.95) and (2.100) the transformation of covariant tensors components is described by passive rotation of vector with positive rotation. In a similar vein, (from Eqs. (2.96) and (2.101)) the transformation of contravariant tensors components is described by active rotation of vector with negative rotation.

2.D Floquet theory

In the Floquet formalism,⁶⁶ a periodic time-dependent Hamiltonian, represented in a finite dimensional basis set, is transformed into a time independent Hamiltonian (usually referred as Floquet Hamiltonian) represented in an infinite dimensional basis set via Fourier series expansion.⁶⁶ Vega et al. introduced the Floquet operators^{85,86} for studying the time evolution during MAS in the Floquet-state space. Subsequently, the Floquet approach was formulated into a Fourier state representation by Levante et al.⁸⁷ and to an integral representation by Filip et al.⁸⁸ We can write the state function of the system

with periodic time-dependancy as given below,

$$|\psi(t)\rangle = \sum_{n=-\infty}^{\infty} \sum_{j=1}^l c_{jn}(t) e^{in\omega t} |\varphi_{jn}\rangle \quad (2.102)$$

and the Hamiltonian of the system as:

$$H(t) = \sum_{m=-\infty}^{\infty} H_m e^{im\omega t} \quad (2.103)$$

Now the time-dependent Schrödinger equation given by

$$i\hbar \frac{d|\psi(t)\rangle}{dt} = H(t) |\psi(t)\rangle \quad (2.104)$$

$$\sum_{n_1=-\infty}^{\infty} \sum_{j=1}^l \left(i\hbar \frac{dc_{jn_1}(t)}{dt} e^{in_1\omega t} |\varphi_{jn_1}\rangle - c_{jn_1}(t) (n_1\hbar\omega) e^{in_1\omega t} |\varphi_{jn_1}\rangle \right) = \sum_{m=-\infty}^{\infty} H_m e^{im\omega t} \sum_{n=-\infty}^{\infty} \sum_{s=1}^l c_{sn}(t) e^{in\omega t} |\varphi_{sn}\rangle \quad (2.105)$$

multiplying left side with $\langle \varphi_{jn_1} |$ and equating like powers on both sides for the condition $n_1 = m + n$ or $m = n_1 - n$ we get,

$$\begin{aligned} & \sum_{n_1=-\infty}^{\infty} \left[i\hbar \frac{dc_{jn_1}(t)}{dt} - c_{jn_1}(t) (n_1\hbar\omega) = \langle \varphi_{jn_1} | \sum_{n=-\infty}^{\infty} \sum_{s=1}^l H_{n_1-n} c_{sn}(t) |\varphi_{sn}\rangle \right] \\ \Rightarrow & \sum_{n_1=-\infty}^{\infty} \left\{ i\hbar \frac{dc_{jn_1}(t)}{dt} = \sum_{n=-\infty}^{\infty} \sum_{s=1}^l \underbrace{[\langle \varphi_{jn_1} | H_{n_1-n} |\varphi_{sn}\rangle + n\hbar\omega \delta_{js} \delta_{n_1 n}]}_{H_F} c_{sn}(t) \right\} \end{aligned} \quad (2.106)$$

Now from the above Eq. (2.106) we can write the time independent Floquet Hamiltonian as:

$$\begin{aligned} H_F &= \underbrace{H_{n_1-n}}_{\text{Floquet off-diagonal operator}} + \hbar\omega \underbrace{\sum_{n=-\infty}^{\infty} \sum_{j=1}^l n |\varphi_{jn}\rangle \langle \varphi_{jn}|}_{\text{Floquet diagonal operator}} \\ &= H_m + \hbar\omega I_F \end{aligned} \quad (2.107)$$

Now the time-dependent Schrödinger equation in Floquet basis given by,

$$i\hbar \frac{d|\psi_F(t)\rangle}{dt} = H_F |\psi_F(t)\rangle \quad (2.108)$$

where $|\psi_F(t)\rangle$ represents the Floquet state, defined by,

$$|\psi_F(t)\rangle = \sum_{n=-\infty}^{\infty} \sum_{j=1}^l c_{jn}(t) |\varphi_{jn}\rangle \quad (2.109)$$

The Floquet basis states are constructed as the direct product of spin states $|\varphi_j\rangle$ and Fourier states $|n\rangle$ as given below,

$$|\varphi_{jn}\rangle = |n\rangle \otimes |\varphi_j\rangle \quad (2.110)$$

The off-diagonal contributions in the Floquet Hamiltonian (i.e $H_m = F_m \otimes H$) are represented through Fourier operator F_m ,

$$F_m = \sum_{n=-\infty}^{\infty} |n+m\rangle \langle n| \quad (2.111)$$

The diagonal contributions in the Floquet Hamiltonian (i.e $I_F = F_I \otimes I$) are represented through the I_z equivalent of Fourier diagonal operator F_I ,

$$F_I = \sum_{n=-\infty}^{\infty} n |n\rangle \langle n| \quad (2.112)$$

The following commutators relations between the operators is employed.

$$\begin{aligned} [I_F, I_{x,m}] &= [F_I, F_m]I_x = mF_mI_x = mI_{x,m} \\ [I_{x,m_1}, I_{y,m_2}] &= F_{m_1+m_2}[I_x, I_y] = i\hbar I_{z,m_1+m_2} \end{aligned} \quad (2.113)$$

Similarly the commutator relations of Floquet tensor operators given by,

$$\begin{aligned} [I_F, T_m^{(k)q}] &= [F_I, F_m]T_m^{(k)q} = mF_mT_m^{(k)q} = mT_m^{(k)q} \\ [T_{m_1}^{(k_1)q_1}, T_{m_2}^{(k_2)q_2}] &= F_{m_1+m_2}[T^{(k_1)q_1}, T^{(k_2)q_2}] = cT_{m_1+m_2}^{(k_3)q_3} \end{aligned} \quad (2.114)$$

2.E Normalization factors corresponding to different detection operators in NMR theory

Detection Pulse	I_j^-	$T^{(1)-1}(0..1_j..0)$	I_j^+	$T^{(1)1}(0..1_j..0)$	I_{jz}	$T^{(1)0}(0..1_j..0)$
X	$-iC(0..1_j..0)^2$	$-\sqrt{2}C(0..1_j..0)$	$iC(0..1_j..0)^2$	$-\sqrt{2}C(0..1_j..0)$	$C(0..1_j..0)^2$	$-iC(0..1_j..0)$
Y	$C(0..1_j..0)^2$	$-i\sqrt{2}C(0..1_j..0)$	$C(0..1_j..0)^2$	$i\sqrt{2}C(0..1_j..0)$	$C(0..1_j..0)^2$	$-iC(0..1_j..0)$

Table 2.11: The normalization factors corresponding to different detection operators for typical single X, Y-Pulses.

References

- [1] E. M. Purcell, H. C. Torrey and R. V. Pound, *Phys. Rev.*, 1946, **69**, 37.
- [2] F. Bloch, W. W. Hansen and M. Packard, *Phys. Rev.*, 1946, **69**, 127.
- [3] F. Bloch, *Phys. Rev.*, 1946, **70**, 460.
- [4] F. Bloch, W. W. Hansen and M. Packard, *Phys. Rev.*, 1946, **70**, 474.
- [5] C. P. Slichter, *Principles of magnetic resonance*, Springer Springer Science & Business Media, 2013.
- [6] A. Abragam, *The principles of nuclear magnetism*, Oxford university press, 1961.
- [7] M. H. Levitt, *Spin dynamics: basics of nuclear magnetic resonance*, John Wiley & Sons, 2001.
- [8] M. Mehring, *Principles of high resolution NMR in solids*, Springer Springer Science & Business Media, 2012.
- [9] U. Haeberlen, *High Resolution NMR in Solids Selective Averaging: Supplement 1 Advances in Magnetic Resonance*, Elsevier, 2012, vol. 1.
- [10] M. Mehring, in *Internal Spin Interactions and Rotations in Solids*, John Wiley & Sons, Ltd, 2007.
- [11] E. L. Hahn, *Phys. Rev.*, 1950, **80**, 580.
- [12] S. R. Hartmann and E. L. Hahn, *Phys. Rev.*, 1962, **128**, 2042.
- [13] B. C. Gerstein and C. R. Dybowski, *Transient Techniques in NMR of Solids*, Academic Press, Orlando, 1985.
- [14] P. P. Man, in *Quadrupolar Interactions*, John Wiley & Sons, Ltd, 2007.
- [15] A. Jerschow, *Prog. Nucl. Magn. Reson. Spectrosc.*, 2005, **46**, 63.
- [16] C. J. Gorter, *Physica*, 1936, **3**, 503.
- [17] C. J. Gorter, *Physica*, 1936, **3**, 995.
- [18] I. I. Rabi, *Phys. Rev.*, 1937, **51**, 652.
- [19] I. I. Rabi, J. R. Zacharias, S. Millman and P. Kusch, *Phys. Rev.*, 1938, **53**, 318.
- [20] I. I. Rabi, S. Millman, P. Kusch and J. R. Zacharias, *Phys. Rev.*, 1939, **55**, 526.
- [21] P. A. M. Dirac, *The principles of quantum mechanics*, Oxford university press, 1981.

- [22] A. Messiah, *Quantum Mechanics. I.*, 1958.
- [23] E. Wigner, *Group theory: and its application to the quantum mechanics of atomic spectra*, Elsevier, 2012, vol. 5.
- [24] M. Tinkham, *Group theory and quantum mechanics*, Courier Corporation, 2003.
- [25] R. P. Feynman and A. R. Hibbs, *Quantum mechanics and path integrals*, McGraw-Hill New York, 1965, vol. 2.
- [26] E. U. Condon and G. H. Shortley, *The theory of atomic spectra*, Cambridge University Press, 1951.
- [27] J. Keeler, *Understanding NMR spectroscopy*, John Wiley & Sons, 2011.
- [28] P. Zeeman, *The London, Edinburgh, and Dublin Philosophical Magazine and Journal of Science*, 1897, **44**, 55.
- [29] C. N. Banwell and H. Primas, *Mol. Phys.*, 1963, **6**, 225.
- [30] P.-K. Wang and C. P. Slichter, *Bull. Magn. Reson.*, 1986, **8**, 3.
- [31] R. Ramesh and M. S. Krishnan, *J. Chem. Phys.*, 2001, **114**, 5967.
- [32] M. M. Maricq and J. S. Waugh, *J. Chem. Phys.*, 1979, **70**, 3300.
- [33] E. Vinogradov, P. K. Madhu and S. Vega, *J. Chem. Phys.*, 2001, **115**, 8983.
- [34] O. W. Sørensen, G. W. Eich, M. H. Levitt, G. Bodenhausen and R. R. Ernst, *Prog. Nucl. Magn. Reson. Spectrosc.*, 1984, **16**, 163.
- [35] B. C. Sanctuary and T. K. Halstead, in *Multipole NMR*, ed. S. W. Warren, Academic Press, 1990, vol. 15, p. 79.
- [36] G. J. Bowden and W. D. Hutchison, *J. Magn. Reson.*, 1986, **67**, 403.
- [37] B. C. Sanctuary, *J. Chem. Phys.*, 1976, **64**, 4352.
- [38] D. A. Varshalovich, A. N. Moskalev and V. K. Khersonskii, *Quantum theory of angular momentum*, World Scientific, 1988.
- [39] G. J. Bowden, J. Khachan and J. P. D. Martin, *J. Magn. Reson.*, 1989, **83**, 79.
- [40] G. J. Bowden, W. D. Hutchison and J. Khachan, *J. Magn. Reson.*, 1986, **67**, 415.
- [41] H. A. Buckmaster and R. Chatterjee, *Phys. Status Solidi (b)*, 1998, **209**, 433.
- [42] H. A. Buckmaster, R. Chatterjee and Y. H. Shing, *Phys. Status Solidi (a)*, 1972, **13**, 9.
- [43] B. L. Silver, *Irreducible tensor methods: an introduction for chemists*, Academic Press, 2013, vol. 36.
- [44] A. R. Edmonds, *Angular momentum in quantum mechanics*, Princeton University Press, 1996.
- [45] A. Ramamoorthy and P. T. Narasimhan, *Pramana*, 1991, **36**, 399.
- [46] A. Ramamoorthy and P. T. Narasimhan, *Mol. Phys.*, 1991, **73**, 207.

- [47] A. K. Dubey, A. Ramamoorthy and P. Raghunathan, *Chem. Phys. Lett.*, 1990, **168**, 401.
- [48] T. T. Nakashima, K. J. Harris and R. E. Wasylshen, *J. Magn. Reson.*, 2010, **202**, 162.
- [49] L. Pandey, S. Towta and D. G. Hughes, *J. Chem. Phys.*, 1986, **85**, 6923.
- [50] L. Pandey, M. Kotecha and D. G. Hughes, *Solid State Nucl. Magn. Reson.*, 2000, **16**, 261.
- [51] M. Mehring and V. A. Weberruss, *Object-oriented magnetic resonance: classes and objects, calculations and computations*, Elsevier, 2012.
- [52] R. V. Pound, *Phys. Rev.*, 1950, **79**, 685.
- [53] A. J. Vega, in *Quadrupolar Nuclei in Solids*, John Wiley & Sons, Ltd, 2007.
- [54] M. H. Cohen, F. Reif, F. Seitz and D. Turnbull, *Solid state physics*, 1957, p. 38.
- [55] R. E. Wasylshen, S. E. Ashbrook and S. Wimperis, *NMR of Quadrupolar Nuclei in Solid Materials*, John Wiley & Sons, 2012.
- [56] M. G. Colombo, B. H. Meier and R. R. Ernst, *Chem. Phys. Lett.*, 1988, **146**, 189.
- [57] E. R. Andrew, A. Bradbury and R. G. Eades, *Nature*, 1958, **182**, 1659.
- [58] I. J. Lowe, *Phys. Rev. Lett.*, 1959, **2**, 285.
- [59] J. Zhou, H. Gao and B. C. Sanctuary, *J. Magn. Reson., Ser. A*, 1993, **101**, 119.
- [60] K. Blum, *Density matrix theory and applications*, Springer Springer Science & Business Media, 2012, vol. 64.
- [61] B. C. Sanctuary and M. S. Krishnan, *J. Magn. Reson.*, 1986, **69**, 210.
- [62] A. P. Yutsis, V. Vanagas and I. B. Levinson, 1962.
- [63] M. E. Rose, *Elementary Theory of Angular Momentum*, 1957.
- [64] L. J. Mueller, *Concepts Magn. Reson. Part A*, 2011, **38A**, 221.
- [65] U. Fano and G. Racah, *Irreducible tensorial sets*, Academic Press, New York, 1959, vol. 1.
- [66] J. H. Shirley, *Phys. Rev.*, 1965, **138**, B979.
- [67] J. H. Van Vleck, *Phys. Rev.*, 1929, **33**, 467.
- [68] E. C. Kemble, *The Fundamental Principles of Quantum Physics*, 1958.
- [69] D. Papousek and M. R. Aliev, *Molecular vibrational-rotational spectra*, 1982.
- [70] M. Born, W. Heisenberg and P. Jordan, *Z. Phys.*, 1926, **35**, 557.
- [71] L. H. Thomas, *J. Chem. Phys.*, 1942, **10**, 538.
- [72] M. R. Aliev, J. K. G. Watson and K. N. Rao, *Molecular spectroscopy: modern research*, Academic, New York, 1985, vol. III.

- [73] R. Ramachandran and R. G. Griffin, *J. Chem. Phys.*, 2005, **122**, 164502.
- [74] J. A. R. Coope, R. F. Snider and F. R. McCourt, *J. Chem. Phys.*, 1965, **43**, 2269.
- [75] J. A. R. Coope and R. F. Snider, *J. Math. Phys.*, 1970, **11**, 1003.
- [76] J. A. R. Coope, *J. Math. Phys.*, 1970, **11**, 1591.
- [77] J. A. R. Coope and R. F. Snider, *J. Chem. Phys.*, 1972, **56**, 2049.
- [78] F. M. Chen, H. Moraal and R. F. Snider, *J. Chem. Phys.*, 1972, **57**, 542.
- [79] B. C. Sanctuary, *Mol. Phys.*, 1983, **48**, 1155.
- [80] S. Vega and A. Pines, *J. Chem. Phys.*, 1977, **66**, 5624.
- [81] A. Wokaun and R. R. Ernst, *J. Chem. Phys.*, 1977, **67**, 1752.
- [82] R. N. Zare, *Angular momentum: understanding spatial aspects in chemistry and physics*, Wiley-Interscience, 2013.
- [83] D. M. Brink and G. R. Satchler, *Angular momentum*, Oxford University Press, 1993.
- [84] W. J. Thompson, *Angular momentum*, John Wiley & Sons, 2008.
- [85] A. Schmidt and S. Vega, *J. Chem. Phys.*, 1992, **96**, 2655.
- [86] G. J. Boender, S. Vega and H. d. Groot, *Mol. Phys.*, 1998, **95**, 921.
- [87] T. O. Levante, M. Baldus, B. H. Meier and R. R. Ernst, *Mol. Phys.*, 1995, **86**, 1195.
- [88] D. E. D. C. Filip, X. Filip and S. Hafner, *Mol. Phys.*, 1997, **92**, 757.

Chapter 3

Concept of effective Hamiltonians for Single Quantum (SQ) transitions in multi-level systems

3.1 Background

Theoretical description of radio frequency (RF) pulses on quadrupolar spins is unique and challenging due to the presence of (a) quadrupolar interaction (b) multiple levels in the system.¹⁻⁶ Since quadrupolar nuclei constitute more than 70% of the elements in the periodic table, they are often employed as molecular probes to investigate the local environments in inorganic compounds and clusters.^{5,7-10} Consequently, suites of experimental techniques¹¹⁻¹⁵ centered on the manipulation of the quadrupolar interactions have emerged in the last two decades for investigating the structure of inorganic compounds.^{6,7,9} In all these experiments, the local environment is primarily characterized through the quadrupolar coupling constant and asymmetry parameter and is experimentally obtained through the quantification of the line-shapes and intensity measurements in a single crystal or a polycrystalline sample.^{4,10,14-18} In contrast to spin $I = 1/2$ systems, analytic description of the evolution of the density operator in multiple-pulse experiments has always remained elusive while dealing with quadrupolar systems.

To this end, several theoretical approaches based on fictitious spin operators^{1,19-22} and spherical tensor operator²³⁻³⁴ formalisms have been proposed in the past.^{10,13} In particular, the fictitious spin operator formalism²² has been employed extensively for describing selective excitations in wide range of systems.^{20,21,35-40} Although, these approaches have enhanced our understanding of the spin dynamics involving quadrupolar spin systems, they often remain semi-analytical and have limited utility in describing multiple-pulse experiments involving coupled spin systems that involve quadrupolar nuclei. Addition-

ally, the factors governing the optimal excitation of a particular transition in a multi-level system are less tangible with increasing spin magnitude.

As an alternative, a solution in the form of effective Hamiltonians^{41–44} is proposed for understanding the excitation process in quadrupolar systems. Employing the spherical tensor operator formalism,¹² effective RF Hamiltonians are derived by transforming into the quadrupolar interaction frame. Although, the application of the spherical tensor formalism for describing pulses in quadrupolar systems in the hard-pulse limit is known,^{24–27} the description of pulses in the soft-pulse regime is of practical relevance due to larger magnitude of the quadrupolar coupling constants in comparison to existing RF amplitudes. To this end, a more general treatment in terms of effective RF Hamiltonians is proposed for studying the effect of RF pulses on quadrupolar systems. The proposed effective RF Hamiltonian in the quadrupolar interaction frame encodes the various transition frequencies and is suitable for describing transitions (both selective and non-selective) in a multi-level system. The validity of the secular approximation is thoroughly examined and effective RF Hamiltonians for selective and non-selective excitations are derived from first principles. Additionally, the differences in the excitation conditions in single crystals and polycrystalline sample are investigated and optimum excitation conditions are derived. Depending on the relative magnitudes of the RF amplitude and the quadrupolar coupling constant, optimum conditions required for the excitation of a particular transition are derived from analytic expressions. In particular, the interplay between selectivity/non-selectivity of transitions in multi-level systems is explained in terms of the secular approximation employed in the derivation of effective Hamiltonians. Employing effective RF Hamiltonians, analytic expressions for the density operator are derived along with suitable expressions for the time-domain signal. In terms of the analytical expressions for the density operator, optimum flip angles and duration of pulses are derived.

3.2 Methodology

In this section, the general methodology employed for understanding the effects of RF pulses is outlined. To begin with, the Hamiltonian for an isolated quadrupolar spin system is represented by,

$$H = H_Z + H_Q + H_{RF} \quad (3.1)$$

with H_Z denoting the Zeeman interaction, H_Q the quadrupolar interaction and H_{RF} the interaction of the oscillating RF field with the spin system.

$$H_Z = \hbar\omega_0 I_z \quad (3.2a)$$

$$H_Q = \hbar \sum_{q=-2}^2 G^{(2)q} T^{(2)q} \quad (3.2b)$$

$$H_{RF} = 2\hbar\omega_1 \cos\omega t I_x \quad (3.2c)$$

In the above equation, ω_0 denotes the Larmor frequency, ω the carrier frequency and ω_1 the RF amplitude. The spatial part of the quadrupolar interaction is represented by $G^{(2)q}$, ('q' denotes the coherence order). When the magnitude of the Zeeman interaction exceeds the quadrupolar interaction, to first-order, the quadrupolar interaction is truncated and represented through $T^{(2)0}$ ($G^{(2)0}$ coefficient) operator. Unlike in the spin $I=1/2$ case, the magnitude of the quadrupolar interaction often exceeds other internal spin interactions in a given system. Consequently, analytic description of the density operator during radio-frequency pulses entails the presence of the quadrupolar Hamiltonian. To address these issues, a general description in the form of effective RF Hamiltonians are proposed to describe the effect of RF pulses on quadrupolar spin systems. Specifically, selective and non-selective excitations in quadrupolar systems are described in terms of effective RF Hamiltonians. To provide a pedagogical description of the underlying spin dynamics, we outline the three important stages employed in the analytic calculations.

Stage-I:

In the calculations involving first order quadrupolar interactions, the initial step involves the transformation of the spin Hamiltonian (Eq. (3.1)) into the quadrupolar interaction frame.

$$\tilde{H}(t) = e^{\frac{i}{\hbar}H_Q t} H e^{-\frac{i}{\hbar}H_Q t} \quad (3.3)$$

In equation Eq. (3.3), H_Q denotes only the first-order quadrupolar interaction represented by

$$H_Q = \hbar \underbrace{\frac{1}{C(2)} \cdot \frac{\omega_Q(\alpha, \beta, \gamma)}{\sqrt{6}}}_{G^{(2)0}} \cdot T^{(2)0} \quad (3.4)$$

The term $\omega_Q(\alpha, \beta, \gamma) = \frac{-3\pi C_Q}{I(2I-1)} \left(\frac{3\cos^2\beta-1}{2} + \frac{\eta}{2} \sin^2\beta \cos 2\alpha \right)$ represents the quadrupolar splitting parameter, $C_Q = \frac{e^2 q Q}{h}$ the quadrupolar coupling constant and $C(2) = \sqrt{\frac{30}{(2I+1)I(I+1)(2I+3)(2I-1)}}$. The angle (α, β, γ) denotes the Euler angles required for the transformation from the PAS to LAS.

In the quadrupolar interaction frame, the Zeeman Hamiltonian remains invariant (i.e. $\tilde{H}_Z = H_Z$), while the RF Hamiltonian (see below) acquires multipole character due to the mixing of single-quantum (SQ) coherences corresponding to different ranks.

$$\tilde{H}_{RF}(t) = e^{\frac{i}{\hbar}H_Q t} H_{RF}(t) e^{-\frac{i}{\hbar}H_Q t} \quad (3.5)$$

Depending on the spin magnitude I , the form of the RF Hamiltonian differs and a closed form solution in terms of spherical tensor operators is proposed in the quadrupolar inter-

action frame.

Stage-II:

The next stage in the calculation involves the transformation into the Zeeman interaction frame,

$$\tilde{\tilde{H}}_{RF}(t) = e^{\frac{i}{\hbar}H_z t} \tilde{H}_{RF}(t) e^{-\frac{i}{\hbar}H_z t} \quad (3.6)$$

Employing the secular approximation, the SQ transitions in a given spin system are identified in terms of effective Hamiltonians. Depending on the magnitude of the RF amplitude relative to the quadrupolar coupling constant, the effective RF Hamiltonian reduces to an ‘ I_x ’ operator in the hard pulse regime (non-selective excitation), while in the soft-pulse limit (selective excitation) the Hamiltonian comprises of SQ operators ‘ $T^{(k)\pm 1}$ ’ with $k = 1, 2, \dots, 2I$).

Stage-III:

Employing the appropriate effective RF Hamiltonians, the time-evolution of the system during selective and non-selective excitation is studied from the quantum-Liouville equation.

$$i\hbar \frac{d\tilde{\rho}(t)}{dt} = [\tilde{\tilde{H}}_{RF}, \tilde{\rho}(t)] \quad (3.7)$$

When the Hamiltonian is time-independent, the solution is expressed by,

$$\tilde{\rho}(t) = e^{-\frac{i}{\hbar}\tilde{\tilde{H}}_{RF}t} \tilde{\rho}(0) e^{\frac{i}{\hbar}\tilde{\tilde{H}}_{RF}t} \quad (3.8)$$

with $\rho(0)$ depicting the initial density operator ($\rho(0) \propto I_z$). Employing the above solution, the density operator after a pulse of duration ‘ t_p ’, is calculated.

$$\tilde{\rho}(t_p) = e^{-\frac{i}{\hbar}\tilde{\tilde{H}}_{RF}t_p} \tilde{\rho}(0) e^{\frac{i}{\hbar}\tilde{\tilde{H}}_{RF}t_p} \quad (3.9)$$

Subsequently, employing the appropriate detection operator, the time-domain signal is evaluated using the standard expression given below,

$$\langle \hat{O}(t) \rangle = Tr [\tilde{\rho}(t_p) \tilde{\tilde{O}}(t)] \quad (3.10)$$

In the above equation, $\tilde{\tilde{O}}(t)$ denotes the detection operator in the quadrupolar interaction frame i.e. $\tilde{\tilde{O}}(t) = \exp(\frac{i}{\hbar}H_Q t) \hat{O} \exp(-\frac{i}{\hbar}H_Q t)$. A detailed description of the underlying spin dynamics along with analytic expressions for the time-domain signal is presented in the following sections.

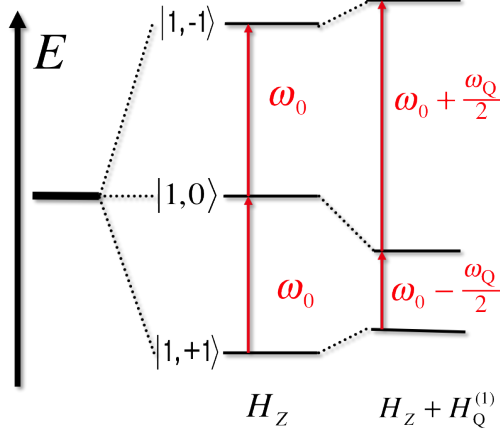


Figure 3.1: Energy level diagram for spin $I=1$ system in the presence of first-order quadrupolar interactions.

3.3 Theory and Discussion

3.3.1 Effective Hamiltonians for $I=1$

3.3.1.1 Static (Single-crystal)

The first order quadrupolar Hamiltonian for a single crystal is represented by,

$$H_Q = \hbar G^{(2)0} \cdot T^{(2)0} \quad (3.11)$$

Following the description in the previous section, the RF Hamiltonian in the quadrupolar interaction frame for an isolated spin $I=1$ system is derived and represented by,

$$\tilde{H}_{RF}(t) = 2\hbar\omega_1 \cos \omega t \left[iT^{(1)1}(a) \cos \sqrt{\frac{3}{2}}G^{(2)0}t - iT^{(2)1}(s) \sin \sqrt{\frac{3}{2}}G^{(2)0}t \right] \quad (3.12)$$

where the suffices (s) and (a) refer to the symmetric and antisymmetric²⁶ combinations^I respectively. Employing Eq. (3.6), the above Hamiltonian is transformed into the Zeeman interaction frame. To elucidate the resonance conditions, the Hamiltonian in the Zeeman interaction frame is re-expressed as a sum of SQ transitions (see Fig. 3.1),

$$\tilde{\tilde{H}}_{RF}(t) = \tilde{\tilde{H}}_{RF,A}(t) + \tilde{\tilde{H}}_{RF,B}(t) \quad (3.13)$$

The Hamiltonians $\tilde{\tilde{H}}_{RF,A}(t)$, $\tilde{\tilde{H}}_{RF,B}(t)$ depict the transitions associated with the excitation

^ISymmetric $T^{(k)q}(s) = T^{(k)q} + T^{(k)-q}$
 Antisymmetric $T^{(k)q}(a) = T^{(k)q} - T^{(k)-q}$

frequencies $\omega = \omega_0 - \sqrt{\frac{3}{2}}G^{(2)0}$ and $\omega = \omega_0 + \sqrt{\frac{3}{2}}G^{(2)0}$ respectively (see Fig. 3.1),

$$\begin{aligned}\tilde{\tilde{H}}_{RF,A}(t) &= \frac{\hbar\omega_1}{2}(iT^{(1)1} + T^{(2)1})e^{-i[\omega - (\omega_0 - \sqrt{\frac{3}{2}}G^{(2)0})]t} - \frac{\hbar\omega_1}{2}(iT^{(1)-1} + T^{(2)-1})e^{+i[\omega - (\omega_0 - \sqrt{\frac{3}{2}}G^{(2)0})]t} \\ \tilde{\tilde{H}}_{RF,B}(t) &= \frac{\hbar\omega_1}{2}(iT^{(1)1} - T^{(2)1})e^{-i[\omega - (\omega_0 + \sqrt{\frac{3}{2}}G^{(2)0})]t} - \frac{\hbar\omega_1}{2}(iT^{(1)-1} - T^{(2)-1})e^{+i[\omega - (\omega_0 + \sqrt{\frac{3}{2}}G^{(2)0})]t}\end{aligned}\quad (3.14)$$

Depending on the choice of the excitation frequency ($\omega_0 \mp \sqrt{\frac{3}{2}}G^{(2)0}$), the above time-dependent Hamiltonian Eq. (3.14) reduces to much simpler time-independent effective Hamiltonian as represented below,

$$\begin{aligned}\tilde{\tilde{H}}_{RF,A} &= \frac{\hbar\omega_1}{2}[iT^{(1)1}(a) + T^{(2)1}(a)] \\ \tilde{\tilde{H}}_{RF,B} &= \frac{\hbar\omega_1}{2}[iT^{(1)1}(a) - T^{(2)1}(a)]\end{aligned}\quad (3.15)$$

In general, the excitation of a transition between any two-levels in a multi-level system depends on (a) the magnitude of the internal interactions (such as dipolar, quadrupolar etc) (b) the amplitude of the RF source. When the amplitude of the employed RF field exceeds the magnitude of the internal spin interactions (inclusive of the quadrupolar interaction), all SQ transitions in a given spin system are excited simultaneously. However, when the magnitude of the quadrupolar interaction exceeds the amplitude of the RF modulation, only selective excitations are possible. Although, these two conditions conform to the two extremes and are well understood, the excitation in the intermediate regime requires a more thorough understanding. To this end, we intend to present an analytic description in terms of effective RF Hamiltonians to elucidate the optimum conditions required for excitations in all the three regimes. The approach presented herein is extended to spins of higher magnitude and forms the preface for the sections that follow.

Case-I: ($\omega_Q \ll \omega_1$)

When the amplitude of the RF field exceeds the internal interactions (inclusive of quadrupolar interaction), all the SQ transitions are excited in the system. For a spin $I=1$, both the transitions ($\omega = \omega_0 \mp \sqrt{\frac{3}{2}}G^{(2)0}$) depicted in Fig. 3.1 are excited simultaneously, resulting in an effective Hamiltonian that comprises of contributions from both $\tilde{\tilde{H}}_{RF,A}(t)$ and $\tilde{\tilde{H}}_{RF,B}(t)$ as depicted in Eq. (3.13). The excitation in this limit is termed non-selective and is described by the effective RF Hamiltonian given below,

$$\begin{aligned}\tilde{\tilde{H}}_{RF,eff} &= \tilde{\tilde{H}}_{RF,A} + \tilde{\tilde{H}}_{RF,B} \\ &= \hbar\omega_1 iT^{(1)1}(a) = \hbar\omega_1 I_x\end{aligned}\quad (3.16)$$

Since, $[T^{(2)0}, \rho(0)] = 0$, the thermal equilibrium density operator ($\rho(0)$) remains invariant in both the quadrupolar and Zeeman interaction frames, i.e. $\tilde{\rho}(0) = \rho(0)$. Subsequently, the density operator after a non-selective (hard) pulse reduces to the familiar form,

$$\tilde{\rho}(t_p)_{Non-selective} = I_z \cos \omega_1 t_p - I_y \sin \omega_1 t_p \quad (3.17)$$

Employing Eq. (3.10), the detection operator in the effective interaction frame is evaluated and represented below,

$$\tilde{T}^{(1)1}(t) = \frac{1}{2} \left(T^{(1)1} + iT^{(2)1} \right) e^{i(\omega_0 + \sqrt{\frac{3}{2}}G^{(2)0})t} + \frac{1}{2} \left(T^{(1)1} - iT^{(2)1} \right) e^{i(\omega_0 - \sqrt{\frac{3}{2}}G^{(2)0})t} \quad (3.18)$$

As depicted in Eq. (3.17), the maximum signal in the transverse plane is obtained when $\omega_1 t_p = \frac{\pi}{2}$. Employing Eq. (3.10), the optimized time-domain signal is evaluated. Since the effective RF Hamiltonian in the non-selective regime includes $\tilde{H}_{RF,A}$ and $\tilde{H}_{RF,B}$ (see Eq. (3.16)), the time-domain signal comprises of both the frequencies as represented below,

$$\begin{aligned} \langle T^{(1)1}(t) \rangle &= \sqrt{2}C(1) \cdot \text{Tr} \left[\tilde{\rho}(t_p) \tilde{T}^{(1)1}(t) \right] \\ &= \sqrt{2}C(1) \cdot \frac{1}{2} \left[e^{i(\omega_0 + \sqrt{\frac{3}{2}}G^{(2)0})t} + e^{i(\omega_0 - \sqrt{\frac{3}{2}}G^{(2)0})t} \right] \end{aligned} \quad (3.19)$$

where the constant $C(1) = \sqrt{\frac{3}{(2I+1)I(I+1)}}$ is derived from Table 2.6 (Section 2.A, Chapter 2). In contrast to pure selective excitation (see Eq. (3.22)), the signal intensity is higher in the case of non-selective excitation and is in accord with experiments.

Case-II: ($\omega_Q \gg \omega_1$)

When the magnitude of the quadrupolar interaction exceeds the amplitude of the RF field (i.e. $\omega_Q \gg \omega_1$), the effective RF Hamiltonian (see Eq. (3.13)) corresponding to the excited transition (excitation frequency $\omega = \omega_0 - \sqrt{\frac{3}{2}}G^{(2)0}$), reduces to

$$\tilde{H}_{RF,eff} = \tilde{H}_{RF,A} \quad (3.20)$$

In this limit, the time-dependent high frequency term $\tilde{H}_{RF,B}(t)$ is neglected under secular approximation. Subsequently, the density operator after the selective pulse (corresponding to the excitation frequency $\omega = \omega_0 - \sqrt{\frac{3}{2}}G^{(2)0}$), is represented by,

$$\tilde{\rho}(t_p)_{Selective} = I_z - \frac{1}{2\sqrt{2}} [T^{(1)1}(s) - iT^{(2)1}(s)] \sin \sqrt{2}\omega_1 t_p - \frac{1}{2} \left(\frac{1}{\sqrt{2}} iT^{(1)0} + \sqrt{\frac{3}{2}} T^{(2)0} \right) (\cos \sqrt{2}\omega_1 t_p - 1) \quad (3.21)$$

As depicted in Eq. (3.21), the maximum signal in the transverse plane is obtained when

$\omega_1 t_p = \frac{\pi}{2\sqrt{2}}$. Employing Eq. (3.10) and Eq. (3.18), the optimized time-domain signal is evaluated and represented by,

$$\langle T^{(1)1}(t) \rangle = \sqrt{2}C(1) \cdot \frac{1}{2\sqrt{2}} e^{i(\omega_0 - \sqrt{\frac{3}{2}}G^{(2)0})t} \quad (3.22)$$

When the excitation frequency chosen corresponds to $\omega = \omega_0 - \sqrt{\frac{3}{2}}G^{(2)0}$, $\tilde{H}_{RF,A}$ in Eq. (3.13) is time-independent while $\tilde{H}_{RF,B}(t)$ is time-dependent and oscillates with a frequency that is proportional to the quadrupolar coupling constant. In such cases, the suitability of invoking the secular approximation in analytic treatments, depend on the relative magnitudes of the quadrupolar coupling constant and the RF amplitude and might lead to erroneous results if the time-dependent terms due to $\tilde{H}_{RF,B}(t)$ are neglected.

To address this issue, an effective RF Hamiltonian corresponding to the selected transition (excitation frequency $\omega = \omega_0 - \sqrt{\frac{3}{2}}G^{(2)0}$) inclusive of the time-dependent term is derived and represented by,

$$\tilde{H}_{RF,eff}(t) = \tilde{H}_{RF,A} + \frac{\hbar\omega_1}{2i\sqrt{6}G^{(2)0}} \left[(iT^{(1)1} - T^{(2)1})(e^{i\sqrt{6}G^{(2)0}t} - 1) + (iT^{(1)-1} - T^{(2)-1})(e^{-i\sqrt{6}G^{(2)0}t} - 1) \right] \quad (3.23)$$

Since, the complete effective RF Hamiltonian comprises of both $\tilde{H}_{RF,A}(t)$ and $\tilde{H}_{RF,B}(t)$, the optimum flip-angles that were deduced (see Eq. (3.21)) are inadequate for improving the selectivity of a particular transition. To alleviate this problem, an additional constraint in the form of the duration of the pulse (t_p) is proposed as a solution to improve the selectivity of the excited transition. As depicted in Eq. (3.23), when the duration of the pulse is adjusted to the quadrupolar coupling constant (i.e. $t_p = 2n\pi/2\sqrt{\frac{3}{2}}G^{(2)0}$), the selectivity of the excited transition could in principle be improved. Hence, for improved selectivity and maximum signal intensity, a unique set of (ω_1, t_p) that simultaneously satisfies Eqs. (3.21) and (3.23) (i.e. $\omega_1 t_p = \frac{\pi}{2\sqrt{2}}$ and $t_p = 2\pi/2\sqrt{\frac{3}{2}}G^{(2)0}$) is required. The above optimum conditions are equally valid for $\omega = \omega_0 + \sqrt{\frac{3}{2}}G^{(2)0}$.

To verify the validity of the analytical predictions, simulations depicting the FT-spectrum of a single crystal are presented in Fig. 3.2 (A1). In these simulations, the amplitude of the RF field was deliberately chosen higher (than the quadrupolar coupling constant) to depict the possible single-quantum transitions in a given system. Alternatively, when the magnitude of the quadrupolar coupling constant exceeds the RF amplitude, only selective excitations are possible. This is illustrated in Fig. 3.2 (A2) through simulations involving selective excitation in a single crystal. To illustrate the validity of the derived analytic expressions, the intensities associated with a particular transition depicted in Fig. 3.2 (A2), have been normalized with respect to their corresponding intensities in the case of non-selective excitations. As depicted, the intensities in the case of selective excitation are lower in contrast to the intensities in non-selective excitations. The preliminary sim-

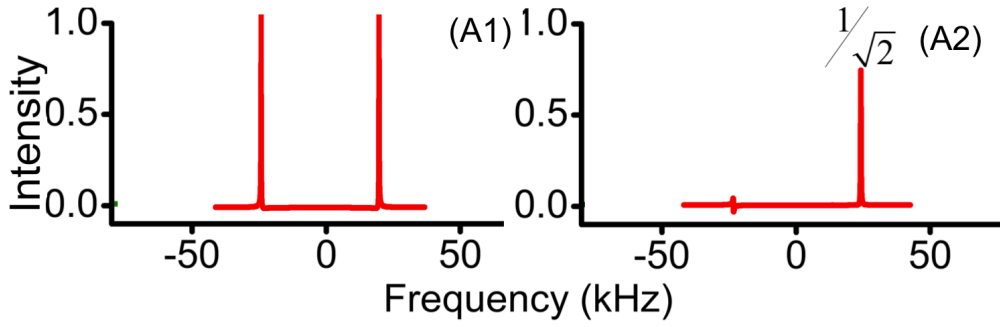


Figure 3.2: Simulations depicting the FT-spectrum of ${}^6\text{Li}$ ($I = 1$) system corresponding to non-selective and selective excitation in a single crystal. The following parameters were employed in the simulations: $C_Q = 30$ kHz and in panel (A1) $\frac{\pi}{2}$ -pulse with RF amplitude $\nu_1 = 150$ kHz, duration $t_p = 1.67 \mu\text{s}$ and excitation frequency $\nu = \nu_0$, in panel (A2) $\frac{\pi}{2\sqrt{2}}$ -pulse with RF amplitude $\nu_1 = 3.98$ kHz, duration $t_p = 44.44 \mu\text{s}$ and excitation frequency 22.5 kHz (i.e $\nu = \nu_0 + \frac{\nu_Q}{2}$).

ulations depicted in Fig. 3.2 (A1) and (A2) yield results that are in excellent agreement with the analytic theory.

To further substantiate the analytic theory, the FT spectrum of a polycrystalline powder sample was simulated. Since the quadrupolar coupling constants in majority of the systems are larger than the RF amplitudes, the objective of our investigation was to derive optimum conditions required for improving (a) the selectivity (b) the signal intensity of the excited transition in a powder sample. In a typical static powder sample, the inherent spatial anisotropy due to restricted mobility results in a wide distribution of quadrupolar coupling constants. As illustrated in Eq. (3.4), the anisotropy in the $G^{(2)0}$ coefficient is described using the spatial variables (α, β) . However, the statistical weight associated with a given set of orientations (α, β) in a polycrystalline sample is different. In particular, the statistical weight for a given value of ‘ β ’ varies with maxima centered at ‘ $\beta = \frac{\pi}{2}$ ’. Consequently, for axially symmetric systems ($\eta = 0$), the excitation frequency depicted by $\omega = \omega_0 \mp \frac{\omega_Q}{2}$ in Fig. 3.1 is modified to $\omega = \omega_0 \pm \frac{\omega_Q}{4}$. To illustrate this aspect, simulations with excitation frequencies corresponding to $\omega = \omega_0 + \frac{\omega_Q}{4}$ in Fig. 3.3 (A1), $\omega = \omega_0 + \frac{\omega_Q}{2}$ in Fig. 3.3 (A2) are presented. As depicted, enhanced signal intensity (see Fig. 3.3 (A1)) is obtained only with the modified resonance condition corresponding to $\omega = \omega_0 + \frac{\omega_Q}{4}$. Interestingly, this orientation dependence is unobserved in the case of the single crystal spectrum shown in Fig. 3.2 (A2).

To further improve the efficiency of the selected transition, a series of numerical simulations with varying flip-angles (implemented by varying the RF amplitude for a given pulse duration) were performed in our studies. As depicted in Fig. 3.4 (see figure (B2)), maximum signal intensity for the selected transition is obtained for a unique flip-angle ($\omega_1 t_p = \theta = \frac{\pi}{2\sqrt{2}}$) (different from the standard $\omega_1 t_p = \theta = \frac{\pi}{2}$) and is in agreement with Eq. (3.21). In contrast to Fig. 3.3 ($\omega_1 t_p = \theta = \frac{\pi}{2}$), the signal intensity in Fig. 3.4 is higher

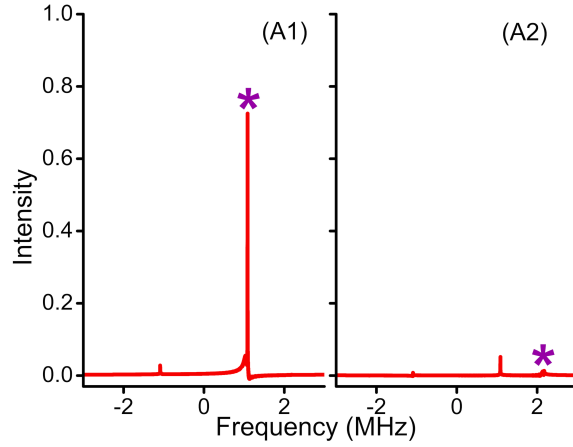


Figure 3.3: Simulations depicting the selective excitation using a $\frac{\pi}{2}$ -pulse ($\nu_1 = 20$ kHz, $t_p = 12.5$ μ s) in a powder sample corresponding to $I=1$ system. The following parameters were employed in the simulations: $I=1$, ${}^6\text{Li}$, $C_Q = 2.9$ MHz, $\nu_Q = 4.35$ MHz, $\eta = 0$. In a typical powder sample, the spectral width for $I=1$ system ranges from $\frac{\nu_Q}{2}$ to $-\frac{\nu_Q}{2}$, however due to higher statistical weight, the maxima is attained at $\pm\frac{\nu_Q}{4}$. The above plots depict the role of the excitation frequency in a powdered sample. The ‘*’ in panel (A1) $\nu_0 + \frac{\nu_Q}{4}$ ($\frac{\nu_Q}{4} = 1.0875$ MHz) and in panel (A2) $\nu_0 + \frac{\nu_Q}{2}$ ($\frac{\nu_Q}{2} = 2.175$ MHz) denotes the frequency of excitation.

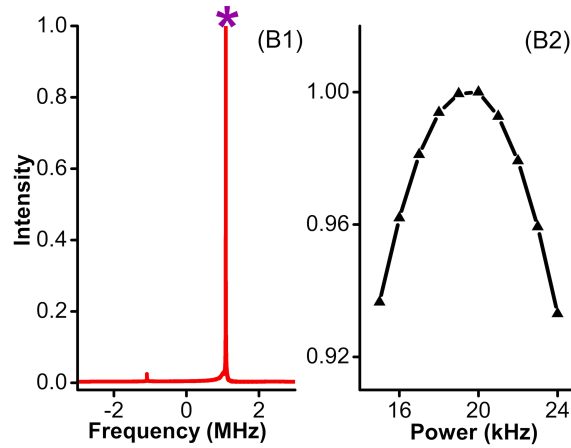


Figure 3.4: Simulations depicting the role of the flip angle in the selective excitation in a powder sample corresponding to $I=1$ system. The quadrupolar parameters are identical to Fig. 3.3 and the frequency of excitation is $\nu_0 + \frac{\nu_Q}{4}$ ($\frac{\nu_Q}{4} = 1.0875$ MHz). The spectrum depicted in panel (B1) corresponds to the flip angle $\frac{\pi}{2\sqrt{2}}$ ($\nu_1 = 20$ kHz, $t_p = 8.84$ μ s). In panel (B2), the intensity is measured as a function of the RF amplitude (ν_1) for $t_p = 8.84$ μ s. As depicted, the maximum intensity is obtained when $\omega_1 t_p = \frac{\pi}{2\sqrt{2}}$ and is in accord with the theoretical predictions.

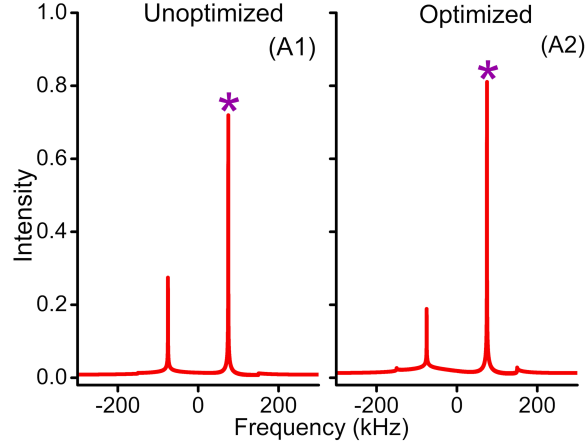


Figure 3.5: Simulations depicting the selective excitation ($\nu = \nu_0 + \frac{\nu_Q}{4}(\frac{\nu_Q}{4} = 75 \text{ kHz})$) in $I=1$ system corresponding to $C_Q = 200 \text{ kHz}$, $\nu_Q = 300 \text{ kHz}$, $\eta=0$. As depicted in the figure (see A1), the excitation is no longer selective in spite of the optimized flip angles and excitation frequency. As described in the theoretical section, the additional peak results from the non-secular time-dependent terms in the effective Hamiltonian. The following parameters were employed in the simulations: in panel (A1) $\nu_1 = 17.68 \text{ kHz}$, $t_p = 10 \mu\text{s}$ and in panel (A2) $\nu_1 = 26.52 \text{ kHz}$, $t_p = 6.67 \mu\text{s}$. As depicted, maximum selectivity is achieved in panel (A2) in spite of employing higher power. Hence, lowering the RF amplitude may not only be the solution for selective excitation.

with the optimum flip angle. Hence, in the pure soft-pulse regime, sets of (ω_1, t_p) could satisfy the condition for the optimum flip angle derived in Eq. (3.21).

From an experimental perspective, the more interesting case arises when the quadrupolar coupling constants are weaker and comparable to existing RF amplitudes. In such cases, the excitations are no longer selective and additional constraints other than the optimized flip-angle are required for improving both the selectivity and efficiency of the selected transition. As described in the previous section, the effective RF Hamiltonian in the intermediate regime is no longer selective and additional constraint is deduced by the manipulation of the time-dependent terms proportional to $\frac{1}{\omega_Q t_p} (e^{i\omega_Q t_p} - 1)$ in the effective Hamiltonian. Following the description in the previous section, the selectivity in such cases is obtained when the duration of the pulse ‘ t_p ’ is adjusted to compensate the time-dependent term in the effective Hamiltonian i.e. $t_p = \frac{2\pi}{\omega_Q}$. In combination with the optimized ‘ t_p ’ and the flip-angle ($\omega_1 t_p = \theta = \frac{\pi}{2\sqrt{2}}$), the selectivity associated with a particular transition is improved. Hence, in the intermediate regime (when the non-secular terms become relevant), maximum selectivity and signal intensity is obtained for a unique set of (ω_1, t_p) . This analytic insight is substantiated through simulations (see Fig. 3.5) depicting a comparison between the selective excitation using the standard and the optimized approach. As depicted, the selectivity and the relative signal intensity in $I=1$ system is enhanced (see panel (A2), in Fig. 3.5) when the duration of the pulse is chosen in accord with Eq. (3.23). To further substantiate this aspect, a comparison is made between simulations employing different pulse widths in Fig. 3.6. Since the intensity of the undesired peaks is proportional to $\frac{1}{\omega_Q t_p}$, increasing ‘ t_p ’ to ‘ $2t_p$ ’ reduces the intensity

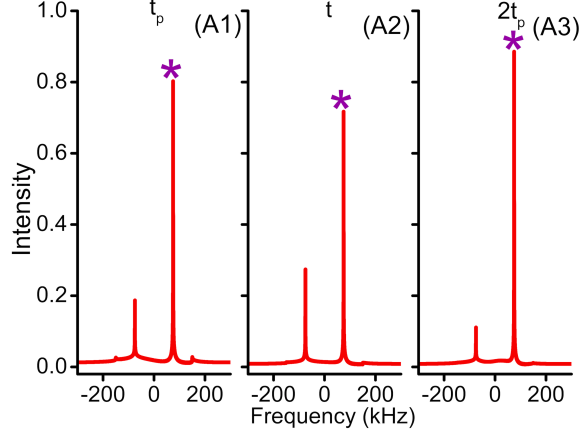


Figure 3.6: Simulations depicting the role of t_p on the efficiency of excitation. The excitation frequency and quadrupolar parameters are identical to Fig. 3.6. The following parameters were employed in the simulations: in panel (A1) $\nu_1 = 26.52$ kHz, $t_p = 6.67$ μ s, in panel (A2) $\nu_1 = 17.68$ kHz, $t_p = 10$ μ s and in panel (A3) $\nu_1 = 13.26$ kHz, $t_p = 13.33$ μ s. The ' t_p ' employed in panel (A3) is twice that of the one employed in panel (A1) and seems to yield both maximum selectivity and signal intensity.

of the undesired peaks to half as depicted in Fig. 3.6 (see panel (A3)).

3.3.1.2 Magic Angle Spinning (Powder-sample)

The Hamiltonian for an isolated quadrupolar spin system under MAS is represented by,

$$H = H_Z + H_{RF} + \hbar \sum_{\substack{m=-2 \\ m \neq 0}}^2 G_m^{(2)0} e^{im\omega_r t} T^{(2)0} \quad (3.24)$$

In Eq. (3.24), $G_m^{(2)0}$ denotes the spatial anisotropy associated with the quadrupolar interaction (also see Table 2.4) and is represented below,

$$G_{Q,m}^{(2)0} = C^Q \sum_{q_2, q_3=-2}^2 R_{Q,P}^{(2)q_3} D_{q_3 q_2}^{(2)}(\Omega_{PM}) D_{q_2 m}^{(2)}(\Omega_{MR}) d_{m0}^{(2)}(\beta_{RL}) \quad (3.25)$$

In the case of selective excitation (corresponding to excitation frequency $\omega = \omega_0 - \sqrt{\frac{3}{2}}G^{(2)0}$), the Hamiltonian after transforming to Zeeman and quadrupolar interaction (see Eq. (3.13)) frame is represented by,

$$\tilde{H} = \hbar \sum_{\substack{m=-2 \\ m \neq 0}}^2 G_m^{(2)0} e^{im\omega_r t} T^{(2)0} - \hbar G^{(2)0} T^{(2)0} + \tilde{H}_{RF,A} \quad (3.26)$$

In contrast to the static case, the Hamiltonian in the rotating frame under MAS is time dependent and periodic. To present a general framework, Floquet theory⁴⁵ was employed in our study. In the Floquet formalism,^{42,46,47} the time-dependent Hamiltonian described in a finite dimensional basis set is transformed into a time-independent Hamiltonian via Fourier series expansion. The proposed Hamiltonian (commonly referred to as Floquet Hamiltonian) is described in an infinite dimensional vector space through an operator basis constructed from the direct product between the spin and the Fourier operators. Employing the irreducible Floquet tensor operators,^{23,48,49} the Floquet Hamiltonian depicting first-order quadrupolar interaction is represented by,

$$H_F = \hbar\omega_r I_F + \hbar \sum_{\substack{m=-2 \\ m \neq 0}}^2 G_m^{(2)0} T_m^{(2)0} - \hbar G^{(2)0} T_0^{(2)0} + \frac{\omega_1}{2} [iT_0^{(1)1}(a) + T_0^{(2)1}(a)] \quad (3.27)$$

In the rotating frame, the RF Hamiltonian is diagonal in the Fourier dimension. To compensate the off-diagonality introduced by the quadrupolar interaction, the Floquet Hamiltonian is transformed by a unitary transformation as illustrated below.

$$\tilde{H}_F = e^{iS_1} H_F e^{-iS_1} \quad (3.28)$$

To facilitate this procedure, the Floquet Hamiltonian H_F is expressed as a sum of two terms.

$$H_F = H_0 + H_1$$

$$H_0 = \hbar\omega_r I_F - \hbar G^{(2)0} T_0^{(2)0} \quad (3.29)$$

$$H_1 = \underbrace{\frac{\omega_1}{2} [iT_0^{(1)1}(a) + T_0^{(2)1}(a)]}_{H_{1,diagonal}} + \hbar \underbrace{\sum_{\substack{m=-2 \\ m \neq 0}}^2 G_m^{(2)0} T_m^{(2)0}}_{H_{1,off-diagonal}} \quad (3.30)$$

The diagonal part of the H_1 comprises of RF Hamiltonian, while the anisotropic part of quadrupolar interaction is classified into $H_{1,off-diagonal}$. The transformation function S_1 , is chosen to compensate the off-diagonality in H_1 (i.e $H_{1,off-diagonal}$)

$$S_1 = -i \sum_{\substack{m=-2 \\ m \neq 0}}^2 \frac{G_m^{(2)0}}{\hbar\omega_r} T_m^{(2)0} \quad (3.31)$$

$$\begin{aligned}
H_1^{(1)} &= H_1 + i[S_1, H_0] \\
&= H_{1,diagonal} + H_{1,off-diagonal} + i[S_1, H_0]
\end{aligned} \tag{3.32}$$

$$H_1^{(1)} = H_{1,diagonal} \quad (\text{or in other words } H_{1,off-diagonal} = -i[S_1, H_0]) \tag{3.33}$$

Employing the BCH expansion, the higher-order corrections to the effective Hamiltonians are evaluated.

$$\begin{aligned}
H_2^{(1)} &= i[S_1, H_{1,diagonal}] \\
H_3^{(1)} &= \frac{-1}{2}[S_1, [S_1, H_{1,diagonal}]] \\
&\vdots \\
&\vdots
\end{aligned}$$

In the Floquet frame work, the effective Floquet Hamiltonian describing a selective pulse is represented by,

$$\begin{aligned}
H_F &= \hbar\omega_r I_F - \hbar G^{(2)0} T_0^{(2)0} \\
&+ \frac{\omega_1}{2} \left[\begin{aligned} &(iT_0^{(1)1} + T_0^{(2)1}) - \sqrt{\frac{3}{2}} \sum_{\substack{m=-2 \\ m \neq 0}}^2 \frac{G_m^{(2)0}}{m\omega_r} (iT_m^{(1)1} + T_m^{(2)1}) + \frac{1}{2!} \left(\frac{3}{2}\right) \sum_{\substack{m_1, m_2=-2 \\ m_1, m_2 \neq 0}}^2 \frac{G_{m_1}^{(2)0} G_{m_2}^{(2)0}}{m_1 m_2 \omega_r^2} (iT_{m_1+m_2}^{(1)1} + T_{m_1+m_2}^{(2)1}) - \dots \\ &-(iT_0^{(1)-1} + T_0^{(2)-1}) - \sqrt{\frac{3}{2}} \sum_{\substack{m=-2 \\ m \neq 0}}^2 \frac{G_m^{(2)0}}{m\omega_r} (iT_m^{(1)-1} + T_m^{(2)-1}) - \frac{1}{2!} \left(\frac{3}{2}\right) \sum_{\substack{m_1, m_2=-2 \\ m_1, m_2 \neq 0}}^2 \frac{G_{m_1}^{(2)0} G_{m_2}^{(2)0}}{m_1 m_2 \omega_r^2} (iT_{m_1+m_2}^{(1)-1} + T_{m_1+m_2}^{(2)-1}).. \end{aligned} \right]
\end{aligned} \tag{3.34}$$

Under special condition (i.e. $n\omega_r = \sqrt{\frac{3}{2}}G^{(2)0}$), the effective Hamiltonian reduces to a much simpler form.

$$\tilde{H}_{F,n} = \frac{\hbar\omega_1}{2} [a_n (iT_{-n}^{(1)1} + T_{-n}^{(2)1}) - b_n (iT_n^{(1)-1} + T_n^{(2)-1})] \tag{3.35}$$

and for m^{th} side band as

$$\tilde{H}_{F,n+m} = \hbar\omega_r I_F + \frac{\hbar\omega_1}{2} [a_{n+m} (iT_{-n+m}^{(1)1} + T_{-n+m}^{(2)1}) - b_{n+m} (iT_{n+m}^{(1)-1} + T_{n+m}^{(2)-1})] \tag{3.36}$$

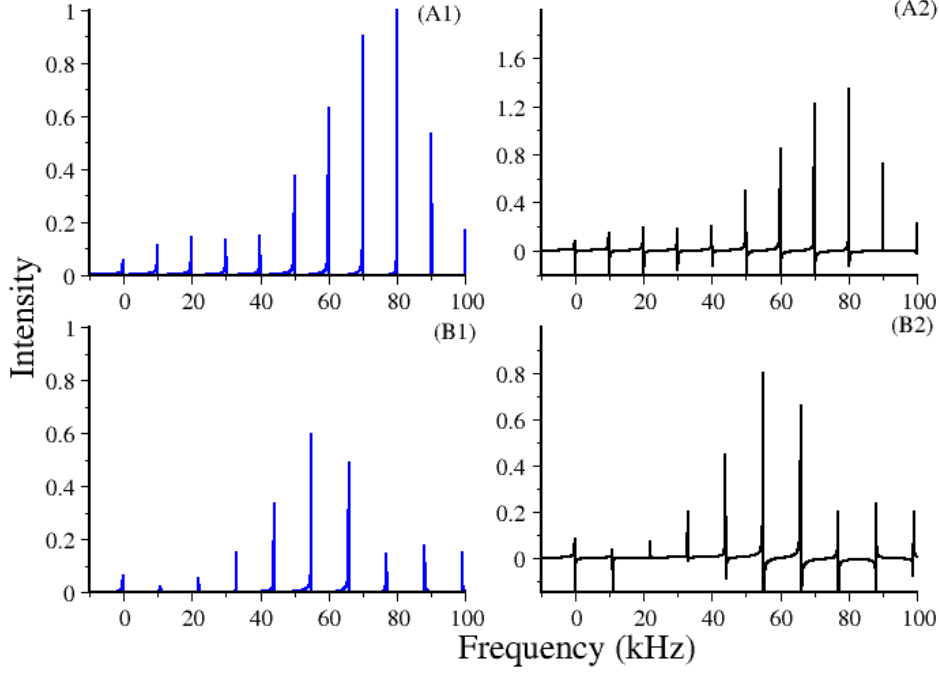


Figure 3.7: Simulations depicting the role of spinning frequency on the excitation efficiency of SQ transitions in spin $I = 1$, (excitation frequency, $\nu = \nu_0 + \frac{\nu_Q}{4}$ or $\nu = \nu_0 + 90$ kHz). The following parameters were employed in the simulations: in panels (A1, A2) $\nu_r = 10$ kHz and in panels (B1, B2) $\nu_r = 11$ kHz. The remaining parameters $C_Q = 240$ kHz ($\nu_Q = 360$ kHz), excitation frequency $\nu = 90$ kHz, $\nu_1 = 31.79$ kHz, $t_p = 5.56 \mu\text{s}$ were held constant in all the simulation. The analytic simulations depicted in panels (A1), (B1) are based on the effective Hamiltonian, while the simulations in panel (A2), (B2) are from Simpson.⁵⁰

where the constants a_n , b_n (for $m=0$) and a_{n+m} , b_{n+m} are given by following equations

$$a_{n+m} = \left[-\sqrt{\frac{3}{2}} \sum_{\substack{m_1=-2 \\ m_1=-n+m \\ m_1 \neq 0}}^2 \frac{G_{m_1}^{(2)0}}{m_1 \omega_r} + \frac{3}{2!2} \sum_{\substack{m_1, m_2=-2 \\ m_1+m_2=-n+m \\ m_1, m_2 \neq 0}}^2 \frac{G_{m_1}^{(2)0} G_{m_2}^{(2)0}}{m_1 m_2 \omega_r^2} - \dots \right] \quad (3.37)$$

$$b_{n+m} = \left[\sqrt{\frac{3}{2}} \sum_{\substack{m_1=-2 \\ m_1=n+m \\ m_1 \neq 0}}^2 \frac{G_{m_1}^{(2)0}}{m_1 \omega_r} + \frac{3}{2!2} \sum_{\substack{m_1, m_2=-2 \\ m_1+m_2=n+m \\ m_1, m_2 \neq 0}}^2 \frac{G_{m_1}^{(2)0} G_{m_2}^{(2)0}}{m_1 m_2 \omega_r^2} \dots \right] \quad (3.38)$$

Subsequently, the density operator after the selective pulse (corresponding to the excita-

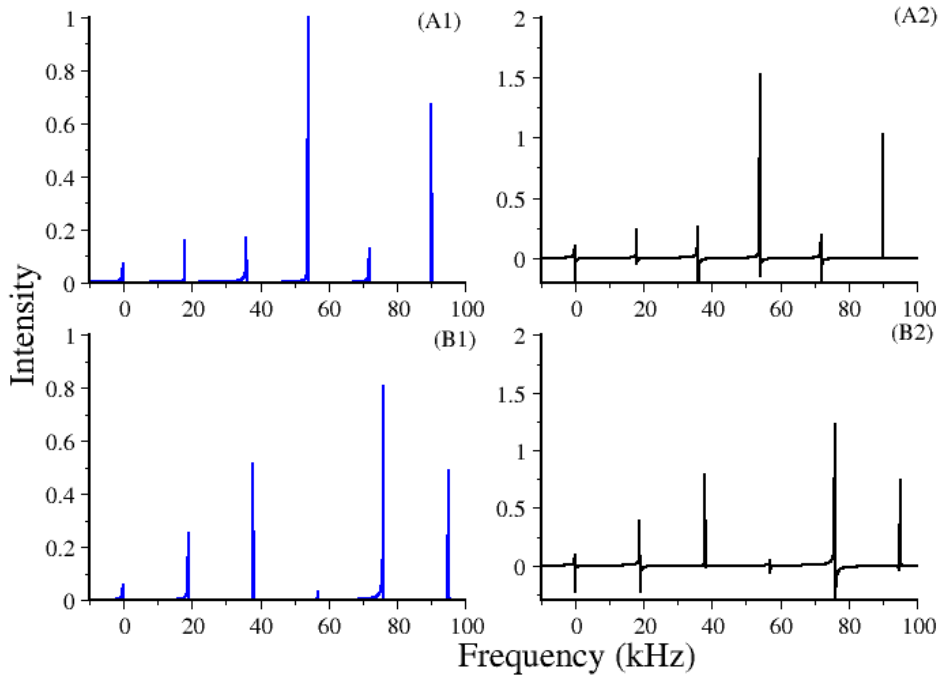


Figure 3.8: Simulations depicting the role of spinning frequency on the excitation efficiency of SQ transitions in spin $I = 1$, (excitation frequency, $\nu = \nu_0 + \frac{\nu_Q}{4}$ or $\nu = \nu_0 + 90$ kHz). The following parameters were employed in the simulations: in panels (A1, A2) $\nu_r = 18$ kHz and in panels (B1, B2) $\nu_r = 19$ kHz. The remaining parameters $C_Q = 240$ kHz ($\nu_Q = 360$ kHz), excitation frequency $\nu = 90$ kHz, $\nu_1 = 31.79$ kHz, $t_p = 5.56$ μ s were held constant in all the simulation. The analytic simulations depicted in panels (A1), (B1) are based on the effective Hamiltonian, while the simulations in panel (A2), (B2) are from Simpson.⁵⁰

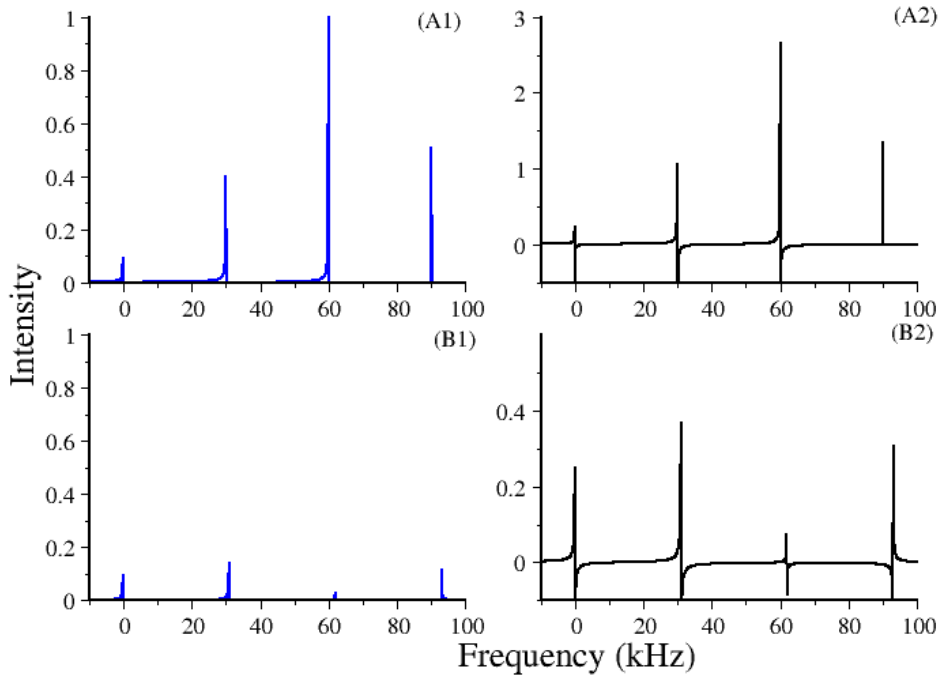


Figure 3.9: Simulations depicting the role of spinning frequency on the excitation efficiency of SQ transitions in spin $I = 1$, (excitation frequency, $\nu = \nu_0 + \frac{\nu_Q}{4}$ or $\nu = \nu_0 + 90$ kHz). The following parameters were employed in the simulations: in panels (A1, A2) $\nu_r = 30$ kHz and in panels (B1, B2) $\nu_r = 31$ kHz. The remaining parameters $C_Q = 240$ kHz ($\nu_Q = 360$ kHz), excitation frequency $\nu = 90$ kHz, $\nu_1 = 31.79$ kHz, $t_p = 5.56 \mu\text{s}$ were held constant in all the simulation. The analytic simulations depicted in panels (A1), (B1) are based on the effective Hamiltonian, while the simulations in panel (A2), (B2) are from Simpson.⁵⁰

tion frequency $\omega = \omega_0 - \sqrt{\frac{3}{2}}G^{(2)0}$, is derived and represented below,

$$\begin{aligned} \tilde{\rho}(t_p)_n = & I_z - \frac{1}{2\sqrt{2a_n b_n}} [a_n(T_{-n}^{(1)1} - iT_{-n}^{(2)1}) + b_n(T_n^{(1)-1} - iT_n^{(2)-1})] \sin(\sqrt{2a_n b_n} \omega_1 t) \\ & - \frac{1}{2\sqrt{2a_n b_n}} (iT_0^{(1)0} + \sqrt{3}T_0^{(2)0}) [\cos(\sqrt{2a_n b_n} \omega_1 t_p) - 1] \end{aligned} \quad (3.39)$$

$$\begin{aligned} \tilde{\rho}(t_p)_{n+m} = & I_z - \frac{1}{2\sqrt{2a_{n+m} b_{n-m}}} [a_{n+m}(T_{-n+m}^{(1)1} - iT_{-n+m}^{(2)1}) + b_{n+m}(T_{n+m}^{(1)-1} - iT_{n+m}^{(2)-1})] \sin(\sqrt{2a_{n+m} b_{n-m}} \omega_1 t) \\ & - \frac{1}{2\sqrt{2a_{n+m} b_{n-m}}} (iT_0^{(1)0} + \sqrt{3}T_0^{(2)0}) [\cos(\sqrt{2a_{n+m} b_{n-m}} \omega_1 t_p) - 1] \end{aligned} \quad (3.40)$$

Accordingly, the detection operator corresponding to the excitation frequency ($\omega_0 - \sqrt{\frac{3}{2}}G^{(2)0}$) in the effective interaction frame is derived and represented below,

$$\begin{aligned} \tilde{T}_A^{(1)1}(t) = & \frac{1}{2} [(T_0^{(1)1} - iT_0^{(2)1}) e^{i(\omega_0)t} + \sqrt{\frac{3}{2}} \sum_{\substack{m=-2 \\ m \neq 0}}^2 \frac{G_m^{(2)0}}{m\omega_r} (T_m^{(1)1} - iT_m^{(2)1}) e^{i(\omega_0+m\omega_r)t} \\ & + \frac{1}{2!} \sqrt{\frac{3}{2}} \sum_{\substack{m_1, m_2=-2 \\ m_1, m_2 \neq 0}}^2 \frac{G_{m_1}^{(2)0} G_{m_2}^{(2)0}}{m_1 m_2 \omega_r^2} (T_{m_1+m_2}^{(1)1} - iT_{m_1+m_2}^{(2)1}) e^{i[\omega_0+(m_1+m_2)\omega_r]t} + \dots] \end{aligned} \quad (3.41)$$

Employing Eq. (3.10), the optimized time-domain signal is evaluated.

$$\langle T^{(1)1}(t) \rangle = \sqrt{2}C(1) \cdot \frac{\sqrt{a_n b_n}}{2\sqrt{2}} \sin(\sqrt{2a_n b_n} \omega_1 t) e^{it(\omega_0 - \sqrt{\frac{3}{2}}G^{(2)0})} \quad (3.42)$$

$$\langle T_m^{(1)1}(t) \rangle = \sqrt{2}C(1) \cdot \frac{\sqrt{a_{n+m} b_{n-m}}}{2\sqrt{2}} \sin(\sqrt{2a_{n+m} b_{n-m}} \omega_1 t) e^{it(\omega_0 - \sqrt{\frac{3}{2}}G^{(2)0} + m\omega_r)} \quad (3.43)$$

In Figs. 3.7 to 3.9, the role of spinning frequency on the selective excitation profile in MAS experiment is depicted. When an integral multiple of the spinning frequency is matched to the quadrupolar off-set frequency ($\frac{\nu_Q}{4}$), the efficiency of excitation increases. The results are in accord with the predictions emerging from the analytic theory.

3.3.2 Effective Hamiltonians for $I=3/2$

3.3.2.1 Static (Single-crystal)

To illustrate the spin dynamics involving half-integral quadrupolar spins, spin $I=3/2$ is employed as a case study in this section. Following the procedure outlined in the previous sections, the RF Hamiltonian in the quadrupolar interaction frame is derived

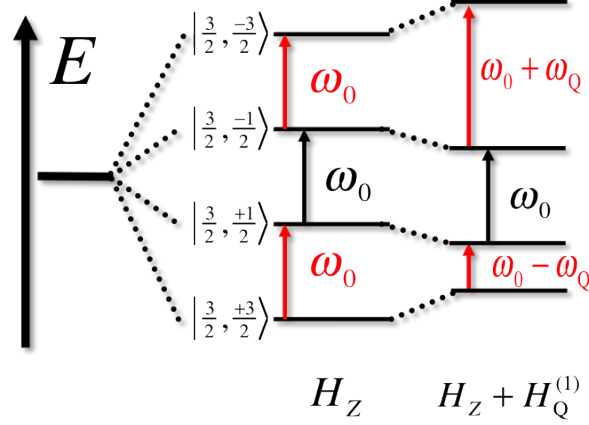


Figure 3.10: Energy level diagram for spin $I=3/2$ system in the presence of first-order quadrupolar interactions.

and represented by,

$$\tilde{H}_{RF}(t) = 2\hbar\omega_1 \cos \omega t \left[\begin{aligned} & iT^{(1)1}(a) \left(\frac{2}{\sqrt{10}} + \frac{3}{\sqrt{10}} \cos G^{(2)0}t \right) - \sqrt{\frac{3}{2}} iT^{(2)1}(s) (\sin G^{(2)0}t) \\ & + \sqrt{\frac{3}{5}} iT^{(3)1}(a) (1 - \cos G^{(2)0}t) \end{aligned} \right] \quad (3.44)$$

In contrast to integral spins, the RF Hamiltonians involving half-integral spins in the quadrupolar-Zeeman interaction frame comprises of the central and satellite transitions as illustrated below,

$$\tilde{H}_{RF}(t) = \tilde{H}_{RF}^{CT}(t) + \tilde{H}_{RF}^{ST}(t) \quad (3.45)$$

As depicted in Fig. 3.10, the RF Hamiltonians associated with the central transition (involving states $|\frac{1}{2}\rangle \rightarrow |-\frac{1}{2}\rangle$) is represented by,

$$\tilde{H}_{RF}^{CT}(t) = \hbar\omega_1 \left[\left(\sqrt{\frac{2}{5}} iT^{(1)1} + \sqrt{\frac{3}{5}} iT^{(3)1} \right) e^{-i(\omega-\omega_0)t} - \left(\sqrt{\frac{2}{5}} iT^{(1)-1} + \sqrt{\frac{3}{5}} iT^{(3)-1} \right) e^{i(\omega-\omega_0)t} \right] \quad (3.46)$$

The satellite transitions associated with the states $|\frac{3}{2}\rangle \rightarrow |\frac{1}{2}\rangle$, $|-\frac{1}{2}\rangle \rightarrow |-\frac{3}{2}\rangle$ are expressed as a set of Hamiltonians given below,

$$\tilde{H}_{RF}^{ST}(t) = \tilde{H}_{RF,1A}^{ST}(t) + \tilde{H}_{RF,1B}^{ST}(t) \quad (3.47)$$

$$\tilde{H}_{RF,1A}^{ST}(t) = \frac{\hbar\omega_1}{2} \left[\begin{array}{l} (\frac{3}{\sqrt{10}}iT^{(1)1} + \sqrt{\frac{3}{2}}iT^{(2)1} - \sqrt{\frac{3}{5}}iT^{(3)1})e^{-it[\omega - (\omega_0 - G^{(2)0})]} \\ -(\frac{3}{\sqrt{10}}iT^{(1)-1} + \sqrt{\frac{3}{2}}iT^{(2)-1} - \sqrt{\frac{3}{5}}iT^{(3)-1})e^{it[\omega - (\omega_0 - G^{(2)0})]} \end{array} \right] \quad (3.48)$$

$$\tilde{H}_{RF,1B}^{ST}(t) = \frac{\hbar\omega_1}{2} \left[\begin{array}{l} (\frac{3}{\sqrt{10}}iT^{(1)1} - \sqrt{\frac{3}{2}}iT^{(2)1} - \sqrt{\frac{3}{5}}iT^{(3)1})e^{-it[\omega - (\omega_0 + G^{(2)0})]} \\ -(\frac{3}{\sqrt{10}}iT^{(1)-1} - \sqrt{\frac{3}{2}}iT^{(2)-1} - \sqrt{\frac{3}{5}}iT^{(3)-1})e^{it[\omega - (\omega_0 + G^{(2)0})]} \end{array} \right] \quad (3.49)$$

The effective RF Hamiltonian describing non-selective excitation is derived by adding Eqs. (3.46) and (3.47) and reduces to the familiar form obtained earlier.

$$\tilde{H}_{RF,Non-selective} = \hbar\omega_1\sqrt{\frac{5}{2}}iT^{(1)1}(a) = \hbar\omega_1I_x \quad (3.50)$$

The transformed detection operator is represented by,

$$\begin{aligned} \tilde{T}^{(1)1}(t) = & (\frac{2}{5}T^{(1)1} + \frac{\sqrt{6}}{5}T^{(3)1})e^{it(\omega_0)} + \frac{1}{2}(\frac{3}{5}T^{(1)1} - \frac{\sqrt{6}}{5}T^{(3)1} + \sqrt{\frac{3}{5}}iT^{(2)1})e^{it(\omega_0 - G^{(2)0})} \\ & + \frac{1}{2}(\frac{3}{5}T^{(1)1} - \frac{\sqrt{6}}{5}T^{(3)1} - \sqrt{\frac{3}{5}}iT^{(2)1})e^{it(\omega_0 + G^{(2)0})} \end{aligned} \quad (3.51)$$

Employing the detection operator (see Eq. (3.51)), the time-domain signal in the case of non-selective excitation is evaluated and represented below,

$$\langle T^{(1)1}(t) \rangle = \sqrt{2}C(1) \cdot \frac{1}{\sqrt{10}} [2e^{it(\omega_0)} + \frac{3}{2}(e^{it(\omega_0 - G^{(2)0})} + e^{it(\omega_0 + G^{(2)0})})] \quad (3.52)$$

In the pure soft-pulse regime ($\omega_Q \gg \omega_1$), selective excitation of either the central or the satellite transition is possible. For e.g, in the selective excitation of the central transition ($\omega = \omega_0$), the effective RF Hamiltonian under secular approximation reduces to,

$$\tilde{H}_{RF}^{CT} = \hbar\omega_1[\sqrt{\frac{2}{5}}iT^{(1)1}(a) + \sqrt{\frac{3}{5}}iT^{(3)1}(a)] \quad (3.53)$$

Subsequently, the density operator after the selective excitation of the central transition reduces to,

$$\tilde{\rho}(t_p)_{CT,S} = I_z - \frac{1}{2}[\sqrt{\frac{2}{5}}T^{(1)1}(s) + \sqrt{\frac{3}{5}}T^{(3)1}(s)] \sin 2\omega_1 t_p - \frac{1}{2}(\sqrt{\frac{1}{5}}iT^{(1)0} + \sqrt{\frac{9}{5}}iT^{(3)0})[\cos 2\omega_1 t_p - 1] \quad (3.54)$$

Based on the above equation, maximum signal in the transverse plane is obtained when

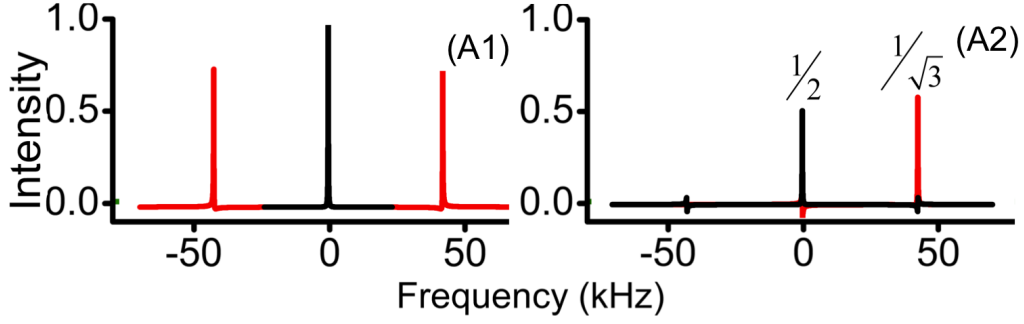


Figure 3.11: Simulations depicting the FT-spectrum of ${}^7\text{Li}$ ($I = 3/2$) system corresponding to non-selective and selective excitation in a single crystal. The following parameters were employed in the simulations: $C_Q = 85$ kHz and in (A1) $\frac{\pi}{2}$ -pulse with RF amplitude $\nu_1 = 150$ kHz, duration $t_p = 1.67$ μs and excitation frequency $\nu = \nu_0$, in (A2) CT $\frac{\pi}{4}$ -pulse with RF amplitude $\nu_1 = 5.31$ kHz, duration $t_p = 23.53$ μs and excitation frequency $\nu = \nu_0$ and ST $\frac{\pi}{2\sqrt{3}}$ -pulse with RF amplitude $\nu_1 = 6.13$ kHz, duration $t_p = 23.53$ μs and excitation frequency 42.5 kHz (i.e. $\nu = \nu_0 + \nu_Q$).

$\omega_1 t_p = \frac{\pi}{4}$, as represented below,

$$\langle T^{(1)1}(t) \rangle = \sqrt{2}C(1) \cdot \frac{1}{2} \sqrt{\frac{2}{5}} e^{i\omega_0 t} \quad (3.55)$$

In a similar vein, the effective RF Hamiltonian corresponding to the selective excitation of one of the satellite transitions (say $\omega = \omega_0 - G^{(2)0}$), is represented by,

$$\tilde{H}_{RF}^{ST} = \frac{\hbar\omega_1}{2} \left[-\frac{3}{\sqrt{10}} iT^{(1)1}(a) + \sqrt{\frac{3}{2}} T^{(2)1}(s) - \sqrt{\frac{3}{5}} iT^{(3)1}(a) \right] \quad (3.56)$$

The corresponding density operator and time-domain signal is evaluated and represented below.

$$\begin{aligned} \tilde{\rho}(t_p)_{ST,S} = & I_z - \frac{1}{\sqrt{5}} \left(\frac{1}{2} iT^{(1)0} + \frac{\sqrt{5}}{2} T^{(2)0} - iT^{(3)0} \right) \left[\cos \sqrt{3}\omega_1 t_p - 1 \right] \\ & - \frac{1}{2\sqrt{3}} \left[\frac{3}{\sqrt{10}} T^{(1)1}(s) - \sqrt{\frac{3}{2}} iT^{(2)1}(s) - \sqrt{\frac{3}{5}} T^{(3)1}(s) \right] \sin \sqrt{3}\omega_1 t_p \end{aligned} \quad (3.57)$$

$$\langle T^{(1)1}(t) \rangle = \sqrt{2}C(1) \cdot \frac{1}{2} \sqrt{\frac{3}{10}} e^{it(\omega_0 - G^{(2)0})} \quad (3.58)$$

In contrast to the central transition, maximum signal intensity in the case of the satellite transition (see Eq. (38)) results when $\omega_1 t_p = \frac{\pi}{2\sqrt{3}}$. Additionally, the effective RF Hamiltonian describing the selective excitation of the central transition comprises of only odd rank SQ operators (see Eq. (3.53)).

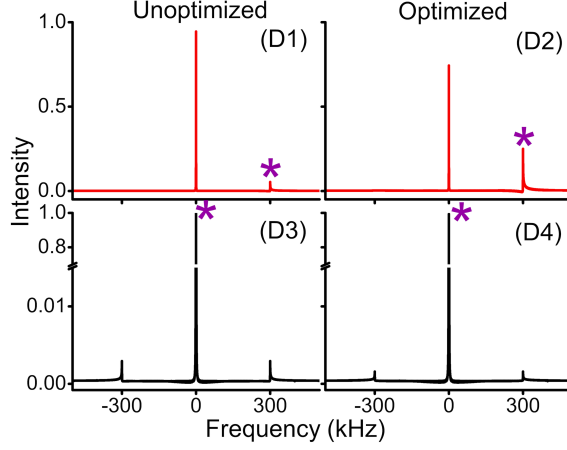


Figure 3.12: Simulations depicting selective excitations ($\nu = \nu_0 + \frac{\nu_Q}{2}$ ($\frac{\nu_Q}{2} = 300$ kHz) in figures D1, D2) and ($\nu = \nu_0$ in figures D3, D4) in I=3/2, system corresponding to $C_Q = 1.2$ MHz, $\nu_Q = 600$ kHz, $\eta = 0$. Since, the difference between adjacent peaks is $\frac{\nu_Q}{2}$, the duration of the pulse $2t_p = 2\left(\frac{\nu_Q}{2}\right)^{-1} = 6.67$ μ s. The optimum flip angles for the satellite transition $\frac{\pi}{2\sqrt{3}}$ (D1, D2) and central transition $\frac{\pi}{4}$ (D3, D4) were employed in the simulations. The following parameters were employed in the simulations: (D1) $\nu_1 = 17.3$ kHz, $t_p = 8.33$ μ s; (D2) $\nu_1 = 21.65$ kHz, $t_p = 6.67$ μ s; (D3) $\nu_1 = 15$ kHz, $t_p = 8.33$ μ s and (D4) $\nu_1 = 18.75$ kHz, $t_p = 6.67$ μ s.

As described in earlier Section 3.3.1.1, the selectivity in the excitation of the central and satellite transitions could further be improved when the duration of the pulse ‘ t_p ’ is adjusted to compensate the undesired terms in the effective Hamiltonian i.e. $t_p = \frac{2n\pi}{G^{(2)0}}$. In combination with the optimum flip-angles based on Eqs. (3.54) and (3.57), the efficiency and selectivity of the excited central ($\omega_1 t_p = \frac{\pi}{4}$) and satellite transitions ($\omega_1 t_p = \frac{\pi}{2\sqrt{3}}$) could further be improved. In Fig. 3.12, simulations depicting the selective excitation in I=3/2 system is presented. As described earlier, the spin I=3/2 system comprises of a central (see figures D3, D4) and a set of satellite transitions (figures D1, D2). The flip angles employed are in accord with those tabulated in Table 3.1.

3.3.2.2 Magic Angle Spinning (Powder-sample)

The Hamiltonian for an isolated quadrupolar spin system under MAS is represented by,

$$H = H_Z + H_{RF} + \hbar \sum_{\substack{m=-2 \\ m \neq 0}}^2 G_m^{(2)0} e^{im\omega_r t} T^{(2)0} \quad (3.59)$$

In the case of selective excitation ($\omega_Q \gg \omega_1$), the Hamiltonian after transforming to Zeeman and quadrupolar interaction (see Eq. (3.13)) ($\omega = \omega_0 - G^{(2)0}$) frame is represented by,

$$\tilde{H} = \hbar \sum_{\substack{m=-2 \\ m \neq 0}}^2 G_m^{(2)0} e^{im\omega_r t} T^{(2)0} - \hbar G^{(2)0} T^{(2)0} + \tilde{H}_{RF,A}^{ST} \quad (3.60)$$

Following the description in the previous section, the Floquet Hamiltonian is derived and represented below,

$$H_F = \hbar\omega_r I_F + \hbar \sum_{\substack{m=-2 \\ m \neq 0}}^2 G_m^{(2)0} T_m^{(2)0} - \hbar G^{(2)0} T_0^{(2)0} + \tilde{H}_{RF,A}^{ST} \quad (3.61)$$

To compensate the off-diagonality due to quadrupolar interaction, the Floquet Hamiltonian is transformed using the transformation function S_1 ($S_1 = -i \sum_{\substack{m=-2 \\ m \neq 0}}^2 \frac{G_m^{(2)0}}{m\omega_r} T_m^{(2)0}$). When an integral multiple of the spinning frequency matches to the quadrupolar frequency, the Floquet Hamiltonian reduces to much simpler form.

$$\tilde{H}_{F,n} = \frac{\hbar\omega_1}{2} [a_n (\frac{3}{\sqrt{10}} iT_{-n}^{(1)1} + \sqrt{\frac{3}{2}} iT_{-n}^{(2)1} - \sqrt{\frac{3}{5}} iT_{-n}^{(3)1}) - b_n (\frac{3}{\sqrt{10}} iT_n^{(1)-1} + \sqrt{\frac{3}{2}} iT_n^{(2)-1} - \sqrt{\frac{3}{5}} iT_n^{(3)-1})] \quad (3.62)$$

and for m^{th} side band as

$$\tilde{H}_{F,n+m} = \hbar\omega_r I_F + \frac{\hbar\omega_1}{2} \begin{bmatrix} a_{n+m} (\frac{3}{\sqrt{10}} iT_{-n+m}^{(1)1} + \sqrt{\frac{3}{2}} iT_{-n+m}^{(2)1} - \sqrt{\frac{3}{5}} iT_{-n+m}^{(3)1}) \\ -b_{n+m} (\frac{3}{\sqrt{10}} iT_{n+m}^{(1)-1} + \sqrt{\frac{3}{2}} iT_{n+m}^{(2)-1} - \sqrt{\frac{3}{5}} iT_{n+m}^{(3)-1}) \end{bmatrix} \quad (3.63)$$

where the constants a_n , b_n (for $m=0$) and a_{n+m} , b_{n+m} given by following equations

$$a_{n+m} = \left[- \sum_{\substack{m_1=-2 \\ m_1=-n+m \\ m_1 \neq 0}}^2 \frac{G_{m_1}^{(2)0}}{m_1\omega_r} + \frac{1}{2!} \sum_{\substack{m_1, m_2=-2 \\ m_1+m_2=-n+m \\ m_1, m_2 \neq 0}}^2 \frac{G_{m_1}^{(2)0} G_{m_2}^{(2)0}}{m_1 m_2 \omega_r^2} - \dots \right] \quad (3.64)$$

$$b_{m+n} = \left[\sum_{\substack{m_1=-2 \\ m_1=n+m \\ m_1 \neq 0}}^2 \frac{G_{m_1}^{(2)0}}{m_1\omega_r} + \frac{1}{2!} \sum_{\substack{m_1, m_2=-2 \\ m_1+m_2=n+m \\ m_1, m_2 \neq 0}}^2 \frac{G_{m_1}^{(2)0} G_{m_2}^{(2)0}}{m_1 m_2 \omega_r^2} \dots \right] \quad (3.65)$$

Subsequently, the density operator after the selective pulse (corresponding to the excita-

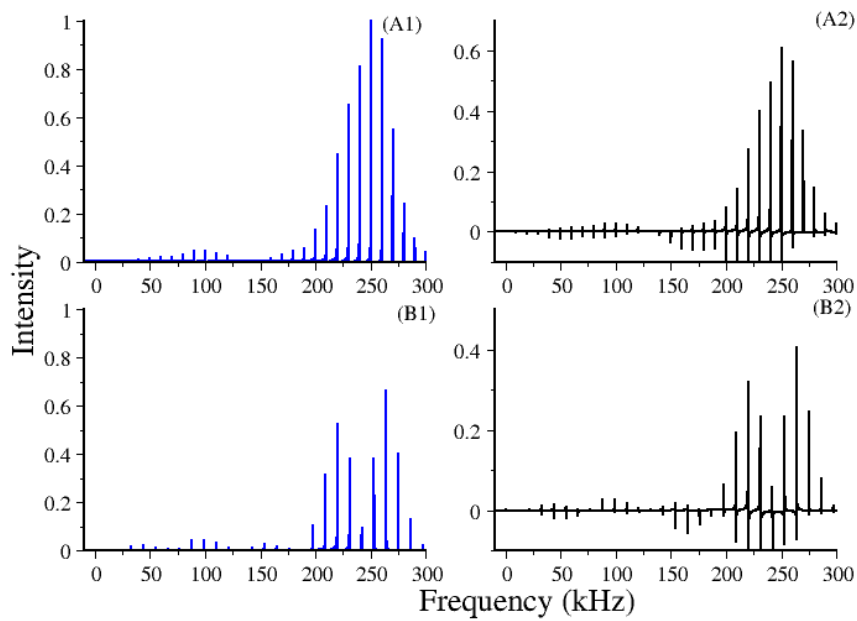


Figure 3.13: Simulations depicting the role of spinning frequency on the excitation efficiency of SQ transitions in spin $I = 3/2$, (excitation frequency, $v = v_0 + \frac{v_Q}{2}$ or $v = v_0 + 270$ kHz). The following parameters were employed in the simulations: in panels (A1, A2) $v_r = 10$ kHz and in panels (B1, B2) $v_r = 11$ kHz. The remaining parameters $C_Q = 1.08$ MHz ($v_Q = 540$ kHz), excitation frequency $v = 270$ kHz, $v_1 = 19.5$ kHz, $t_p = 7.4$ μ s were held constant in all the simulation. The analytic simulations depicted in panels (A1), (B1) are based on the effective Hamiltonian, while the simulations in panel (A2), (B2) are from Simpson.⁵⁰

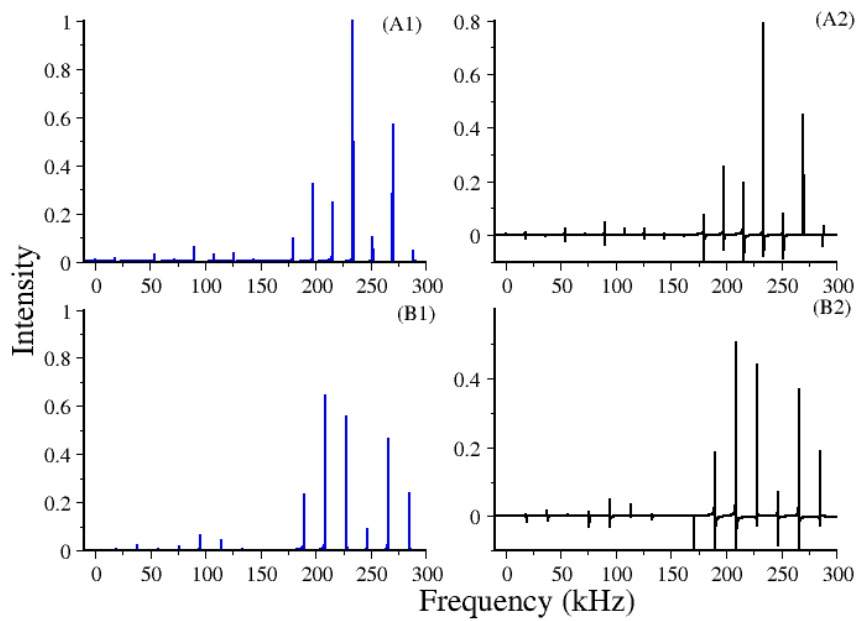


Figure 3.14: Simulations depicting the role of spinning frequency on the excitation efficiency of SQ transitions in spin $I = 3/2$, (excitation frequency, $v = v_0 + \frac{v_Q}{2}$ or $v = v_0 + 270$ kHz). The following parameters were employed in the simulations: in panels (A1, A2) $v_r = 18$ kHz and in panels (B1, B2) $v_r = 19$ kHz. The remaining parameters $C_Q = 1.08$ MHz ($v_Q = 540$ kHz), excitation frequency $v = 270$ kHz, $v_1 = 19.5$ kHz, $t_p = 7.4$ μ s were held constant in all the simulation. The analytic simulations depicted in panels (A1), (B1) are based on the effective Hamiltonian, while the simulations in panel (A2), (B2) are from Simpson.⁵⁰

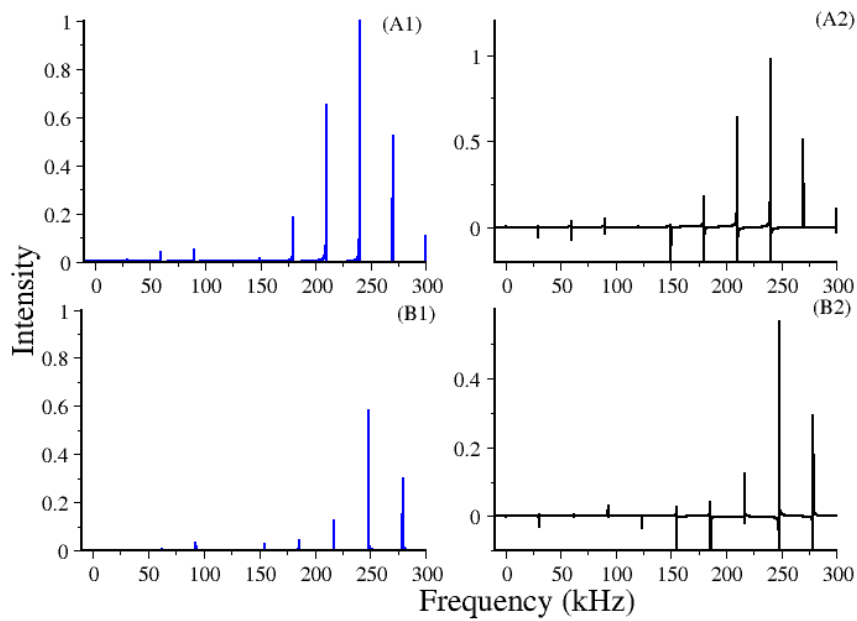


Figure 3.15: Simulations depicting the role of spinning frequency on the excitation efficiency of SQ transitions in spin $I = 3/2$, (excitation frequency, $v = v_0 + \frac{v_Q}{2}$ or $v = v_0 + 270$ kHz). The following parameters were employed in the simulations: in panels (A1, A2) $v_r = 30$ kHz and in panels (B1, B2) $v_r = 31$ kHz. The remaining parameters $C_Q = 1.08$ MHz ($v_Q = 540$ kHz), excitation frequency $v = 270$ kHz, $v_1 = 19.5$ kHz, $t_p = 7.4$ μ s were held constant in all the simulation. The analytic simulations depicted in panels (A1), (B1) are based on the effective Hamiltonian, while the simulations in panel (A2), (B2) are from Simpson.⁵⁰

tion frequency $\omega = \omega_0 - G^{(2)0}$, is evaluated.

$$\begin{aligned} \tilde{\rho}(t_p)_n &= I_z - \frac{1}{\sqrt{5a_n b_n}} \left(\frac{1}{2} i T_0^{(1)0} + \frac{\sqrt{5}}{2} T_0^{(2)0} - i T_0^{(3)0} \right) (\cos \sqrt{3a_n b_n} \omega_1 t_p - 1) \\ &\quad - \frac{1}{2\sqrt{3a_n b_n}} \left[\begin{array}{l} a_n \left(\frac{3}{\sqrt{10}} T_{-n}^{(1)1} - \sqrt{\frac{3}{2}} i T_{-n}^{(2)1} - \sqrt{\frac{3}{5}} T_{-n}^{(3)1} \right) \\ - b_n \left(\frac{3}{\sqrt{10}} T_n^{(1)-1} - \sqrt{\frac{3}{2}} i T_n^{(2)-1} - \sqrt{\frac{3}{5}} T_n^{(3)-1} \right) \end{array} \right] \sin(\sqrt{3a_n b_n} \omega_1 t) \end{aligned} \quad (3.66)$$

$$\begin{aligned} \tilde{\rho}(t_p)_{n+m} &= I_z - \frac{1}{\sqrt{5a_{n+m} b_{n-m}}} \left(\frac{1}{2} i T_0^{(1)0} + \frac{\sqrt{5}}{2} T_0^{(2)0} - i T_0^{(3)0} \right) (\cos \sqrt{3a_{n+m} b_{n-m}} \omega_1 t_p - 1) \\ &\quad - \frac{1}{2\sqrt{3a_{n+m} b_{n-m}}} \left[\begin{array}{l} a_{n+m} \left(\frac{3}{\sqrt{10}} T_{-n+m}^{(1)1} - \sqrt{\frac{3}{2}} i T_{-n+m}^{(2)1} - \sqrt{\frac{3}{5}} T_{-n+m}^{(3)1} \right) \\ - b_{n+m} \left(\frac{3}{\sqrt{10}} T_{n+m}^{(1)-1} - \sqrt{\frac{3}{2}} i T_{n+m}^{(2)-1} - \sqrt{\frac{3}{5}} T_{n+m}^{(3)-1} \right) \end{array} \right] \sin(\sqrt{3a_{n+m} b_{n-m}} \omega_1 t) \end{aligned} \quad (3.67)$$

Accordingly, the detection operator corresponding to excitation $(\omega_0 - G^{(2)0})$ in the effective interaction frame is evaluated and represented below,

$$\begin{aligned} \tilde{T}_A^{(1)1}(t) &= \frac{1}{2} \left[\left(\frac{3}{5} T_0^{(1)1} - \sqrt{\frac{3}{5}} i T_0^{(2)1} - \frac{\sqrt{6}}{5} T_0^{(3)1} \right) e^{i(\omega_0)t} \right. \\ &\quad + \sqrt{\frac{3}{2}} \sum_{\substack{m=-2 \\ m \neq 0}}^2 \frac{G_m^{(2)0}}{m\omega_r} \left(\frac{3}{5} T_m^{(1)1} - \sqrt{\frac{3}{5}} i T_m^{(2)1} - \frac{\sqrt{6}}{5} T_m^{(3)1} \right) e^{i(\omega_0+m\omega_r)t} \\ &\quad + \frac{1}{2!} \sqrt{\frac{3}{2}} \sum_{\substack{m_1, m_2=-2 \\ m_1, m_2 \neq 0}}^2 \frac{G_{m_1}^{(2)0} G_{m_2}^{(2)0}}{m_1 m_2 \omega_r^2} \left(\frac{3}{5} T_{m_1+m_2}^{(1)1} - \sqrt{\frac{3}{5}} i T_{m_1+m_2}^{(2)1} - \frac{\sqrt{6}}{5} T_{m_1+m_2}^{(3)1} \right) e^{i[\omega_0+(m_1+m_2)\omega_r]t} \\ &\quad \left. + \dots \right] \end{aligned} \quad (3.68)$$

Employing Eq. (3.10), the optimized time-domain signal is evaluated.

$$\langle T^{(1)1}(t) \rangle = \sqrt{2} C(1) \cdot \frac{1}{2} \sqrt{\frac{3a_n b_n}{10}} \sin(\sqrt{3a_n b_n} \omega_1 t) e^{it(\omega_0 - G^{(2)0})} \quad (3.69)$$

$$\langle T_m^{(1)1}(t) \rangle = \sqrt{2} C(1) \cdot \frac{1}{2} \sqrt{\frac{3a_{n+m} b_{n-m}}{10}} \sin(\sqrt{3a_{n+m} b_{n-m}} \omega_1 t) e^{it(\omega_0 - G^{(2)0} + m\omega_r)} \quad (3.70)$$

The simulations depicted in Figs. 3.14, 3.15 and 3.17 substantiate the analytic theory. Hence, the choice of the spinning frequency play an important role in the excitation of satellite transition in half-integer quadrupolar spins.

3.3.3 Effective Hamiltonians for $I=5/2$

3.3.3.1 Static (Single-crystal)

As depicted in Fig. 3.16, the spin $I=5/2$ system, comprises of a central and two sets of satellite transitions (denoted by 1 and 2). In the effective RF Hamiltonian framework,

the SQ transitions are represented by,

$$\tilde{H}_{RF}(t) = \tilde{H}_{RF}^{CT}(t) + \tilde{H}_{RF,1}^{ST}(t) + \tilde{H}_{RF,2}^{ST}(t) \quad (3.71)$$

The central transition is depicted by,

$$\tilde{H}_{RF}^{CT}(t) = \frac{\hbar\omega_1}{2} \begin{bmatrix} \left(\frac{9}{\sqrt{35}}iT^{(1)1} + \frac{6}{\sqrt{15}}iT^{(3)1} + 6\sqrt{\frac{5}{42}}iT^{(5)1} \right) e^{-it(\omega-\omega_0)} \\ \left[-\left(\frac{9}{\sqrt{35}}iT^{(1)-1} + \frac{6}{\sqrt{15}}iT^{(3)-1} + 6\sqrt{\frac{5}{42}}iT^{(5)-1} \right) e^{it(\omega-\omega_0)} \right] \end{bmatrix} \quad (3.72)$$

while, the two sets of satellite transitions (with $C_1 = \frac{1}{2}\sqrt{\frac{3}{7}}$) are represented by,

$$\tilde{H}_{RF,1}^{ST}(t) = \tilde{H}_{RF,1A}^{ST}(t) + \tilde{H}_{RF,1B}^{ST}(t) \quad (3.73)$$

$$\tilde{H}_{RF,1A}^{ST}(t) = \frac{\hbar\omega_1}{2} \begin{bmatrix} \left(\frac{8}{\sqrt{35}}iT^{(1)1} + \frac{2}{\sqrt{15}}iT^{(3)1} - 4\sqrt{\frac{5}{42}}iT^{(5)1} + 4\sqrt{\frac{1}{14}}T^{(2)1} + 2\sqrt{\frac{5}{7}}T^{(4)1} \right) e^{-it[\omega-(\omega_0-C_1G^{(2)0})]} \\ \left(\frac{8}{\sqrt{35}}iT^{(1)-1} + \frac{2}{\sqrt{15}}iT^{(3)-1} - 4\sqrt{\frac{5}{42}}iT^{(5)-1} + 4\sqrt{\frac{1}{14}}T^{(2)-1} + 2\sqrt{\frac{5}{7}}T^{(4)-1} \right) e^{it[\omega-(\omega_0-C_1G^{(2)0})]} \end{bmatrix} \quad (3.74)$$

$$\tilde{H}_{RF,1B}^{ST}(t) = \frac{\hbar\omega_1}{2} \begin{bmatrix} \left(\frac{8}{\sqrt{35}}iT^{(1)1} + \frac{2}{\sqrt{15}}iT^{(3)1} - 4\sqrt{\frac{5}{42}}iT^{(5)1} - 4\sqrt{\frac{1}{14}}T^{(2)1} - 2\sqrt{\frac{5}{7}}T^{(4)1} \right) e^{-it[\omega-(\omega_0+C_1G^{(2)0})]} \\ \left(\frac{8}{\sqrt{35}}iT^{(1)-1} + \frac{2}{\sqrt{15}}iT^{(3)-1} - 4\sqrt{\frac{5}{42}}iT^{(5)-1} - 4\sqrt{\frac{1}{14}}T^{(2)-1} - 2\sqrt{\frac{5}{7}}T^{(4)-1} \right) e^{it[\omega-(\omega_0+C_1G^{(2)0})]} \end{bmatrix} \quad (3.75)$$

$$\tilde{H}_{RF,2}^{ST}(t) = \tilde{H}_{RF,2A}^{ST}(t) + \tilde{H}_{RF,2B}^{ST}(t) \quad (3.76)$$

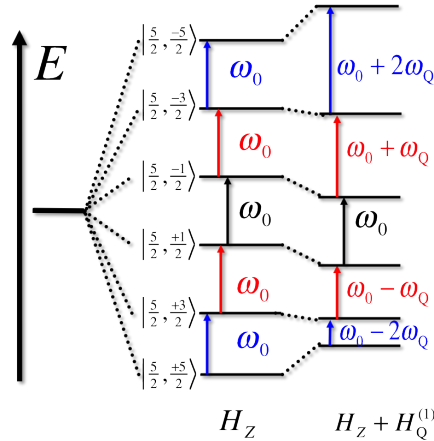


Figure 3.16: Energy level diagram for spin $I=5/2$ system in the presence of first-order quadrupolar interactions.

$$\tilde{H}_{RF,2A}^{ST}(t) = \frac{\hbar\omega_1}{2} \left[\begin{array}{l} \left(\frac{8}{\sqrt{35}}iT^{(1)1} - \frac{2}{\sqrt{15}}iT^{(3)1} + 4\sqrt{\frac{5}{42}}iT^{(5)1} + 4\sqrt{\frac{1}{14}}T^{(2)1} - 2\sqrt{\frac{5}{7}}T^{(4)1} \right) e^{-it[\omega - (\omega_0 - 2C_1G^{(2)0})]} \\ \left(-\frac{8}{\sqrt{35}}iT^{(1)-1} - \frac{2}{\sqrt{15}}iT^{(3)-1} + 4\sqrt{\frac{5}{42}}iT^{(5)-1} + 4\sqrt{\frac{1}{14}}T^{(2)-1} - 2\sqrt{\frac{5}{7}}T^{(4)-1} \right) e^{it[\omega - (\omega_0 - 2C_1G^{(2)0})]} \end{array} \right] \quad (3.77)$$

$$\tilde{H}_{RF,2B}^{ST}(t) = \frac{\hbar\omega_1}{2} \left[\begin{array}{l} \left(\frac{8}{\sqrt{35}}iT^{(1)1} - \frac{2}{\sqrt{15}}iT^{(3)1} + 4\sqrt{\frac{5}{42}}iT^{(5)1} - 4\sqrt{\frac{1}{14}}T^{(2)1} + 2\sqrt{\frac{5}{7}}T^{(4)1} \right) e^{-it[\omega - (\omega_0 + 2C_1G^{(2)0})]} \\ \left(-\frac{8}{\sqrt{35}}iT^{(1)-1} - \frac{2}{\sqrt{15}}iT^{(3)-1} + 4\sqrt{\frac{5}{42}}iT^{(5)-1} - 4\sqrt{\frac{1}{14}}T^{(2)-1} + 2\sqrt{\frac{5}{7}}T^{(4)-1} \right) e^{it[\omega - (\omega_0 + 2C_1G^{(2)0})]} \end{array} \right] \quad (3.78)$$

The effective RF Hamiltonian describing non-selective excitation is derived by adding Eqs. (3.71) and (3.72) and reduces to the familiar form obtained earlier.

$$\tilde{H}_{RF,Non-selective} = \hbar\omega_1\sqrt{\frac{35}{4}}iT^{(1)1}(a) = \hbar\omega_1I_x \quad (3.79)$$

The detection operator in the effective RF interaction frame is derived and represented by,

$$\begin{aligned} \tilde{T}^{(1)1}(t) &= \left(\frac{9}{35}T^{(1)1} + \frac{6}{5}\frac{1}{\sqrt{21}}T^{(3)1} + \frac{1}{7}\sqrt{6}T^{(5)1} \right) e^{it(\omega_0)} \\ &+ \frac{1}{2} \left(\frac{16}{35}T^{(1)1} + \frac{4}{5}\frac{1}{\sqrt{21}}T^{(3)1} - \frac{4}{7}\sqrt{\frac{2}{3}}T^{(5)1} - \frac{4}{7}\sqrt{\frac{2}{5}}iT^{(2)1} - \frac{4}{7}iT^{(4)1} \right) e^{it(\omega_0 - C_1G^{(2)0})} \\ &+ \frac{1}{2} \left(\frac{16}{35}T^{(1)1} + \frac{4}{5}\frac{1}{\sqrt{21}}T^{(3)1} - \frac{4}{7}\sqrt{\frac{2}{3}}T^{(5)1} + \frac{4}{7}\sqrt{\frac{2}{5}}iT^{(2)1} + \frac{4}{7}iT^{(4)1} \right) e^{it(\omega_0 + C_1G^{(2)0})} \\ &+ \frac{1}{2} \left(\frac{2}{7}T^{(1)1} - \frac{2}{\sqrt{21}}T^{(3)1} + \frac{1}{7}\sqrt{\frac{2}{3}}T^{(5)1} - \frac{\sqrt{10}}{7}iT^{(2)1} + \frac{1}{7}iT^{(4)1} \right) e^{it(\omega_0 - 2C_1G^{(2)0})} \\ &+ \frac{1}{2} \left(\frac{2}{7}T^{(1)1} - \frac{2}{\sqrt{21}}T^{(3)1} + \frac{1}{7}\sqrt{\frac{2}{3}}T^{(5)1} + \frac{\sqrt{10}}{7}iT^{(2)1} - \frac{1}{7}iT^{(4)1} \right) e^{it(\omega_0 + 2C_1G^{(2)0})} \end{aligned} \quad (3.80)$$

Employing the detection operator (see Eq. (3.80)), the time-domain signal in the case of non-selective excitation is evaluated and represented below,

$$\langle \tilde{T}^{(1)1}(t) \rangle = \sqrt{2}C(1) \cdot \frac{1}{2\sqrt{35}} [9e^{it(\omega_0)} + 8(e^{it(\omega_0 - C_1G^{(2)0})} + e^{it(\omega_0 + C_1G^{(2)0})}) + 5(e^{it(\omega_0 - 2C_1G^{(2)0})} + e^{it(\omega_0 + 2C_1G^{(2)0})})] \quad (3.81)$$

In the pure soft-pulse regime ($\omega_Q \gg \omega_1$), selective excitation of either the central or the satellite transition is possible. The effective RF Hamiltonian under secular approximation

for selective excitation of the central transition ($\omega = \omega_0$) reduces to,

$$\tilde{H}_{RF}^{CT}(t) = \frac{\hbar\omega_1}{2} \left[\frac{9}{\sqrt{35}} iT^{(1)1}(a) + \frac{6}{\sqrt{15}} iT^{(3)1}(a) + 6\sqrt{\frac{5}{42}} iT^{(5)1}(a) \right] \quad (3.82)$$

Subsequently, the density operator after the selective excitation of the central transition reduces to,

$$\begin{aligned} \tilde{\rho}(t_p) = I_z - \frac{1}{2} & \left(\sqrt{\frac{2}{35}} iT^{(1)0} + \sqrt{\frac{16}{45}} iT^{(3)0} + \frac{10}{3\sqrt{7}} iT^{(5)0} \right) [\cos(3\omega_1 t) - 1] \\ & - \frac{1}{6} \left[\frac{9}{\sqrt{35}} T^{(1)1}(s) + \frac{6}{\sqrt{15}} T^{(3)1}(s) + 6\sqrt{\frac{5}{42}} T^{(5)1}(s) \right] \sin(3\omega_1 t) \end{aligned} \quad (3.83)$$

Based on the above equation, maximum signal in the transverse plane is obtained when $\omega_1 t_p = \frac{\pi}{6}$, as represented below,

$$\langle \tilde{T}^{(1)-1}(t) \rangle = \sqrt{2}C(1) \cdot \frac{3}{2\sqrt{35}} e^{it(\omega_0)} \quad (3.84)$$

In a similar vein, the effective RF Hamiltonian corresponding to the selective excitation of one of the satellite transitions (say $\omega = \omega_0 - C_1 G^{(2)0}$), is represented by,

$$\tilde{H}_{RF,1A}^{ST}(t) = \frac{\hbar\omega_1}{2} \left[\frac{8}{\sqrt{35}} iT^{(1)1}(s) + \frac{2}{\sqrt{15}} iT^{(3)1}(s) - 4\sqrt{\frac{5}{42}} iT^{(5)1}(s) + 4\sqrt{\frac{1}{14}} T^{(2)1}(s) + 2\sqrt{\frac{5}{7}} T^{(4)1}(s) \right] \quad (3.85)$$

The density operator after the selective pulse and the time-domain signal is calculated using the standard procedure.

$$\begin{aligned} \tilde{\rho}(t_p) = I_z - \frac{1}{2} & \left(\sqrt{\frac{2}{35}} iT^{(1)0} + \sqrt{\frac{3}{28}} T^{(2)0} + \sqrt{\frac{1}{20}} iT^{(3)0} + \sqrt{\frac{25}{28}} T^{(4)0} - \sqrt{\frac{25}{28}} iT^{(5)0} \right) [\cos(\sqrt{8}\omega_1 t) - 1] \\ & - \frac{1}{2\sqrt{8}} \left[\frac{8}{\sqrt{35}} T^{(1)1}(s) + \frac{2}{\sqrt{15}} T^{(3)1}(s) - 2\sqrt{\frac{10}{21}} T^{(5)1}(s) - 2\sqrt{\frac{2}{7}} iT^{(2)1}(s) - 2\sqrt{\frac{5}{7}} iT^{(4)1}(s) \right] \sin(\sqrt{8}\omega_1 t) \end{aligned} \quad (3.86)$$

$$\langle \tilde{T}^{(1)1}(t) \rangle = \sqrt{2}C(1) \cdot \sqrt{\frac{2}{35}} e^{it(\omega_0 - C_1 G^{(2)0})} \quad (3.87)$$

The effective RF Hamiltonian corresponding to the selective excitation of one of the satellite transitions (say $\omega = \omega_0 - 2C_1 G^{(2)0}$), is represented by,

$$\tilde{H}_{RF,2A}^{ST}(t) = \frac{\hbar\omega_1}{2} \left[\frac{8}{\sqrt{35}} iT^{(1)1}(s) - \frac{2}{\sqrt{15}} iT^{(3)1}(s) + 4\sqrt{\frac{5}{42}} iT^{(5)1}(s) + 4\sqrt{\frac{1}{14}} T^{(2)1}(s) - 2\sqrt{\frac{5}{7}} T^{(4)1}(s) \right] \quad (3.88)$$

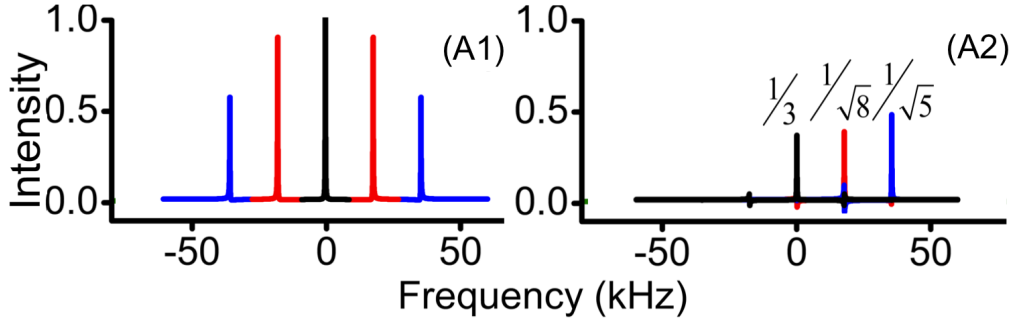


Figure 3.17: Simulations depicting the FT-spectrum of ^{27}Al ($I = 5/2$) system corresponding to non-selective and selective excitation in a single crystal. The following parameters were employed in the simulations: $C_Q = 118$ kHz and in (A1) $\frac{\pi}{2}$ -pulse with RF amplitude $\nu_1 = 150$ kHz, duration $t_p = 1.67 \mu\text{s}$ and excitation frequency $\nu = \nu_0$, in (A2) CT $\frac{\pi}{6}$ -pulse with RF amplitude $\nu_1 = 1.48$ kHz, duration $t_p = 56.5 \mu\text{s}$ and excitation frequency $\nu = \nu_0$, ST1 $\frac{\pi}{2\sqrt{8}}$ -pulse with RF amplitude $\nu_1 = 1.56$ kHz, duration $t_p = 56.5 \mu\text{s}$ and excitation frequency 17.7 kHz (i.e. $\nu = \nu_0 + \nu_Q$ and ST2 $\frac{\pi}{2\sqrt{5}}$ -pulse with RF amplitude $\nu_1 = 1.98$ kHz, duration $t_p = 56.5 \mu\text{s}$ and excitation frequency 35.4 kHz (i.e. $\nu = \nu_0 + 2\nu_Q$).

The corresponding density operator and time-domain signal is evaluated and represented below.

$$\begin{aligned} \tilde{\rho}(t_p) = & I_z - \frac{1}{2} \left(\sqrt{\frac{2}{35}} iT^{(1)0} + \sqrt{\frac{3}{7}} T^{(2)0} - \sqrt{\frac{4}{5}} iT^{(3)0} - \sqrt{\frac{4}{7}} T^{(4)0} + \sqrt{\frac{1}{7}} iT^{(5)0} \right) \left[\cos(\sqrt{5}\omega_1 t) - 1 \right] \\ & - \frac{1}{2\sqrt{5}} \left[\sqrt{\frac{5}{7}} T^{(1)1}(s) - \sqrt{\frac{5}{3}} T^{(3)1}(s) + \sqrt{\frac{5}{42}} T^{(5)1}(s) - \sqrt{\frac{25}{14}} iT^{(2)1}(s) + \sqrt{\frac{5}{7}} iT^{(4)1}(s) \right] \sin(\sqrt{5}\omega_1 t) \end{aligned} \quad (3.89)$$

$$\langle \tilde{T}^{(1)1} \rangle = \sqrt{2}C(1) \cdot \frac{1}{2} \sqrt{\frac{5}{35}} e^{it(\omega_0 - 2C_1 G^{(2)0})} \quad (3.90)$$

Analogous to the spin $I=3/2$ description, the optimum time-period for selective excitation of central and satellite transitions are identical (i.e. $t_p = \frac{2\pi}{C_1 G^{(2)0}}$) with optimum flip-angles $\omega_1 t_p = \frac{\pi}{6}$, $\omega_1 t_p = \frac{\pi}{2\sqrt{8}}$ and $\omega_1 t_p = \frac{\pi}{2\sqrt{5}}$ respectively. The simulation depicted in Fig. 3.17, illustrate the selective and non-selective transitions and those depicted in Fig. 3.18, substantiate analytic theory.

3.3.3.2 Magic Angle Spinning (Powder-sample)

In the case of selective excitation ($\omega = \omega_0 - C_1 G^{(2)0}$), the MAS Hamiltonian after transforming to Zeeman and quadrupolar interaction (see Eq. (3.13)) frame is represented by,

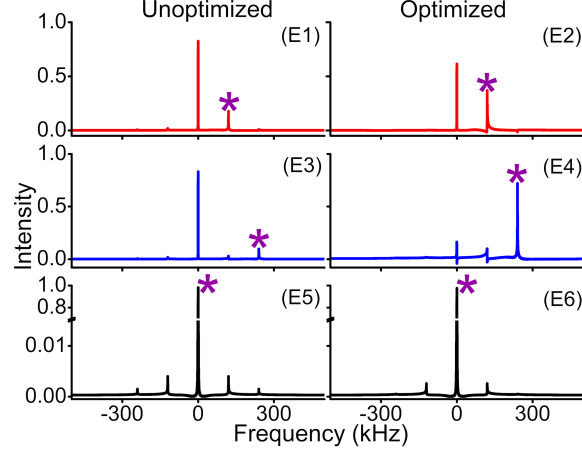


Figure 3.18: Simulations depicting selective excitations ($\nu = \nu_0 + \frac{\nu_Q}{2}$ ($\frac{\nu_Q}{2} = 120$ kHz) in figures E1, E2), ($\nu = \nu_0 + \nu_Q$ ($\nu_Q = 240$ kHz) in figures E3, E4 and $\nu = \nu_0$ in E5, E6) in $I=5/2$, system corresponding to $C_Q = 1.6$ MHz, $\nu_Q = 240$ kHz, $\eta = 0$. Since, the difference between adjacent peaks is $\frac{\nu_Q}{2}$, the duration of the pulse $2t_p = 2(\frac{\nu_Q}{2})^{-1} = 16.67 \mu s$. Based on Table 3.1, the optimum flip angles $\frac{\pi}{2\sqrt{8}}$ (E1, E2), $\frac{\pi}{2\sqrt{5}}$ (E3, E4) for the satellite and $\frac{\pi}{6}$ (E5, E6) for the central transition were employed. The following parameters were employed in the simulations: (E1) $\nu_1 = 4.9$ kHz, $t_p = 18 \mu s$; (E2) $\nu_1 = 5.3$ kHz, $t_p = 16.67 \mu s$; (E3) $\nu_1 = 6.21$ kHz, $t_p = 18 \mu s$; (E4) $\nu_1 = 6.71$ kHz, $t_p = 16.67 \mu s$; (E5) $\nu_1 = 4.63$ kHz, $t_p = 18 \mu s$ and (E6) $\nu_1 = 5$ kHz, $t_p = 16.67 \mu s$.

$$\tilde{H} = \hbar \sum_{\substack{m=-2 \\ m \neq 0}}^2 G_m^{(2)0} e^{im\omega_r t} T^{(2)0} - \hbar G^{(2)0} T^{(2)0} + \tilde{H}_{RF,1A}^{ST} \quad (3.91)$$

Following the description presented in the previous section, the effective Hamiltonian (under $n\omega_r = C_1 G^{(2)0}$) is represented by,

$$\begin{aligned} \tilde{H}_{F,n} = & \frac{\hbar\omega_1}{2} [a_n (\frac{8}{\sqrt{35}} iT_{-n}^{(1)1} + \frac{2}{\sqrt{15}} iT_{-n}^{(3)1} - 4\sqrt{\frac{5}{42}} iT_{-n}^{(5)1} + 4\sqrt{\frac{1}{14}} T_{-n}^{(2)1} + 2\sqrt{\frac{5}{7}} T_{-n}^{(4)1}) \\ & - b_n (\frac{8}{\sqrt{35}} iT_n^{(1)-1} + \frac{2}{\sqrt{15}} iT_n^{(3)-1} - 4\sqrt{\frac{5}{42}} iT_n^{(5)-1} + 4\sqrt{\frac{1}{14}} T_n^{(2)-1} + 2\sqrt{\frac{5}{7}} T_n^{(4)-1})] \end{aligned} \quad (3.92)$$

$$\begin{aligned} \tilde{H}_{F,n+m} = & \hbar\omega_r I_F + \frac{\hbar\omega_1}{2} [a_{n+m} (\frac{8}{\sqrt{35}} iT_{-n+m}^{(1)1} + \frac{2}{\sqrt{15}} iT_{-n+m}^{(3)1} - 4\sqrt{\frac{5}{42}} iT_{-n+m}^{(5)1} + 4\sqrt{\frac{1}{14}} T_{-n+m}^{(2)1} + 2\sqrt{\frac{5}{7}} T_{-n+m}^{(4)1}) \\ & - b_{n+m} (\frac{8}{\sqrt{35}} iT_{n+m}^{(1)-1} + \frac{2}{\sqrt{15}} iT_{n+m}^{(3)-1} - 4\sqrt{\frac{5}{42}} iT_{n+m}^{(5)-1} + 4\sqrt{\frac{1}{14}} T_{n+m}^{(2)-1} + 2\sqrt{\frac{5}{7}} T_{n+m}^{(4)-1})] \end{aligned} \quad (3.93)$$

where the constants a_n , b_n (for $m=0$) and a_{n+m} , b_{n+m} given by following equations

$$a_{n+m} = [-c_1 \sum_{\substack{m_1=-2 \\ m_1=-n+m \\ m_1 \neq 0}}^2 \frac{G_{m_1}^{(2)0}}{m_1 \omega_r} + \frac{c_1^2}{2!} \sum_{\substack{m_1, m_2=-2 \\ m_1+m_2=-n+m \\ m_1, m_2 \neq 0}}^2 \frac{G_{m_1}^{(2)0} G_{m_2}^{(2)0}}{m_1 m_2 \omega_r^2} - \dots] \quad (3.94)$$

$$b_{n+m} = [c_1 \sum_{\substack{m_1=-2 \\ m_1=n+m \\ m_1 \neq 0}}^2 \frac{G_{m_1}^{(2)0}}{m_1 \omega_r} + \frac{c_1^2}{2!} \sum_{\substack{m_1, m_2=-2 \\ m_1+m_2=n+m \\ m_1, m_2 \neq 0}}^2 \frac{G_{m_1}^{(2)0} G_{m_2}^{(2)0}}{m_1 m_2 \omega_r^2} \dots] \quad (3.95)$$

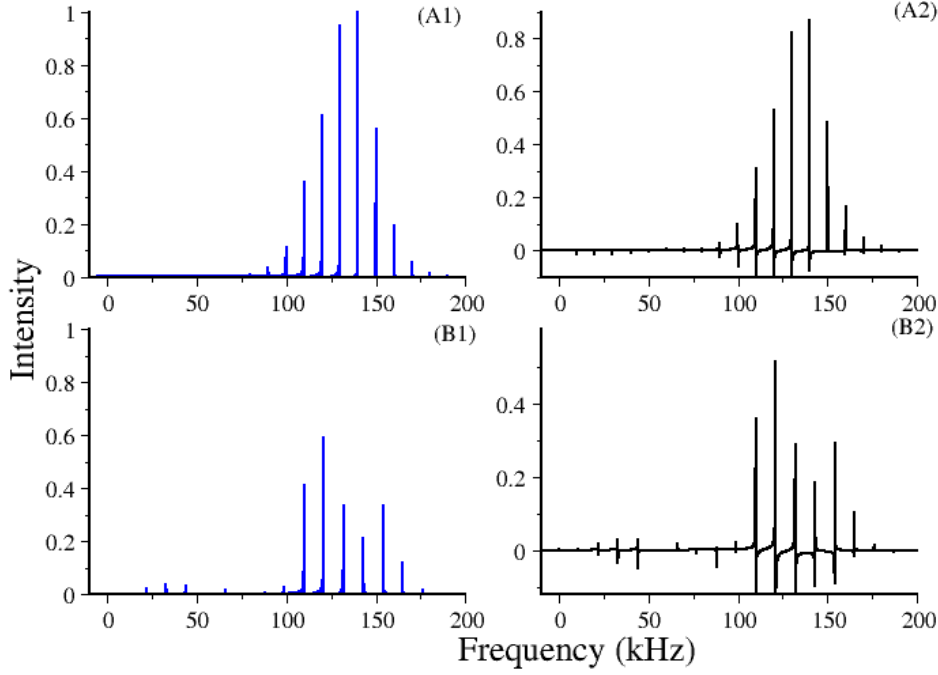


Figure 3.19: Simulations depicting the role of spinning frequency on the excitation efficiency of SQ transitions in spin $I = 5/2$, (excitation frequency, $\nu = \nu_0 + \frac{\nu_Q}{2}$ or $\nu = \nu_0 + 150$ kHz). The following parameters were employed in the simulations: in panels (A1, A2) $\nu_r = 10$ kHz and in panels (B1, B2) $\nu_r = 11$ kHz. The remaining parameters $C_Q = 2.0$ MHz ($\nu_Q = 300$ kHz), excitation frequency $\nu = 150$ kHz, $\nu_1 = 13.33$ kHz, $t_p = 6.63$ μ s held constant. The analytic simulations depicted in panels (A1), (B1) are based on the effective Hamiltonian, while the simulations in panel (A2), (B2) are from Simpson.⁵⁰

Subsequently, the density operator after the selective pulse (corresponding to the excitation frequency $\omega = \omega_0 - C_1 G^{(2)0}$), is represented by,

$$\begin{aligned} \tilde{\rho}(t_p)_n = & I_z - \frac{1}{2\sqrt{a_n b_n}} \left(\sqrt{\frac{2}{35}} i T_0^{(1)0} - \sqrt{\frac{3}{7}} T_0^{(2)0} + \sqrt{\frac{4}{5}} i T_0^{(3)0} + \sqrt{\frac{4}{7}} T_0^{(4)0} - \sqrt{\frac{1}{7}} i T_0^{(5)0} \right) [\cos(\sqrt{8a_n b_n} \omega_1 t_p) - 1] \\ & - \frac{\sin(\sqrt{8a_n b_n} \omega_1 t)}{2\sqrt{8a_n b_n}} \left[\begin{aligned} & a_n \left(\frac{8}{\sqrt{35}} T_{-n}^{(1)1} + \frac{2}{\sqrt{15}} T_{-n}^{(3)1} - 4\sqrt{\frac{5}{42}} T_{-n}^{(5)1} - 4\sqrt{\frac{1}{14}} i T_{-n}^{(2)1} - 2\sqrt{\frac{5}{7}} i T_{-n}^{(4)1} \right) \\ & + b_n \left(\frac{8}{\sqrt{35}} T_n^{(1)-1} + \frac{2}{\sqrt{15}} T_n^{(3)-1} - 4\sqrt{\frac{5}{42}} T_n^{(5)-1} - 4\sqrt{\frac{1}{14}} i T_n^{(2)-1} - 2\sqrt{\frac{5}{7}} i T_n^{(4)-1} \right) \end{aligned} \right] \end{aligned} \quad (3.96)$$

$$\begin{aligned} \tilde{\rho}(t_p)_{n+m} = & I_z - \frac{1}{2\sqrt{a_{n+m} b_{n-m}}} \left(\sqrt{\frac{2}{35}} i T_0^{(1)0} - \sqrt{\frac{3}{7}} T_0^{(2)0} + \sqrt{\frac{4}{5}} i T_0^{(3)0} + \sqrt{\frac{4}{7}} T_0^{(4)0} - \sqrt{\frac{1}{7}} i T_0^{(5)0} \right) [\cos(\sqrt{8a_{n+m} b_{n-m}} \omega_1 t_p) - 1] \\ & - \frac{\sin(\sqrt{8a_{n+m} b_{n-m}} \omega_1 t)}{2\sqrt{8a_{n+m} b_{n-m}}} \left[\begin{aligned} & a_{n+m} \left(\frac{8}{\sqrt{35}} T_{-n+m}^{(1)1} + \frac{2}{\sqrt{15}} T_{-n+m}^{(3)1} - 4\sqrt{\frac{5}{42}} T_{-n+m}^{(5)1} - 4\sqrt{\frac{1}{14}} i T_{-n+m}^{(2)1} - 2\sqrt{\frac{5}{7}} i T_{-n+m}^{(4)1} \right) \\ & + b_{n+m} \left(\frac{8}{\sqrt{35}} T_{n+m}^{(1)-1} + \frac{2}{\sqrt{15}} T_{n+m}^{(3)-1} - 4\sqrt{\frac{5}{42}} T_{n+m}^{(5)-1} - 4\sqrt{\frac{1}{14}} i T_{n+m}^{(2)-1} - 2\sqrt{\frac{5}{7}} i T_{n+m}^{(4)-1} \right) \end{aligned} \right] \end{aligned} \quad (3.97)$$

Accordingly, the detection operator corresponding to excitation frequency $\omega = \omega_0 -$

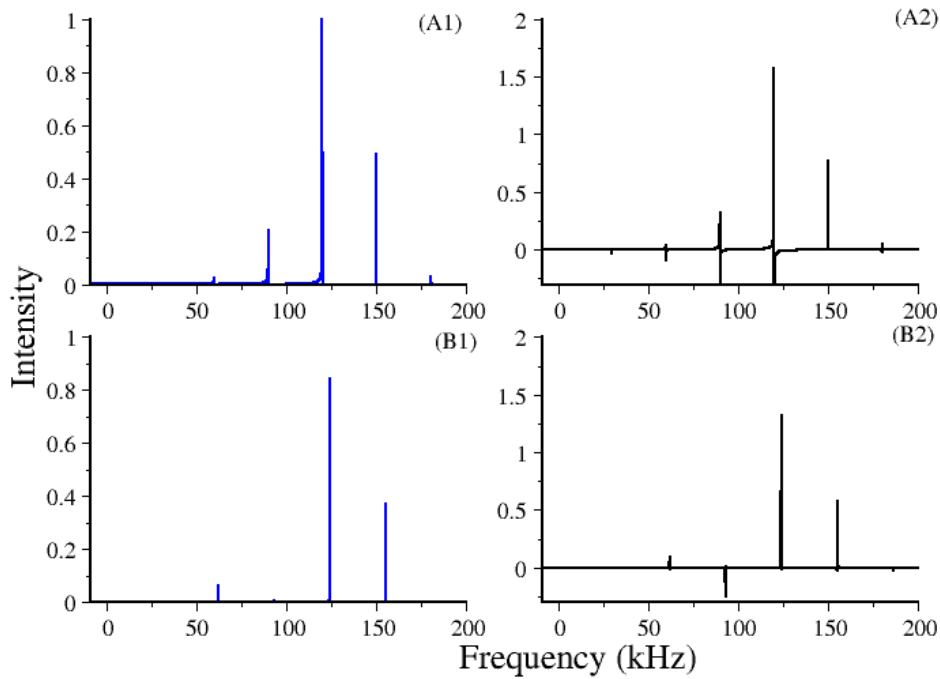


Figure 3.20: Simulations depicting the role of spinning frequency on the excitation efficiency of SQ transitions in spin $I = 5/2$, (excitation frequency, $\nu = \nu_0 + \frac{\nu_Q}{2}$ or $\nu = \nu_0 + 150$ kHz). The following parameters were employed in the simulations: in panels (A1, A2) $\nu_r = 30$ kHz and in panels (B1, B2) $\nu_r = 31$ kHz. The remaining parameters $C_Q = 2.0$ MHz ($\nu_Q = 300$ kHz), excitation frequency $\nu = 150$ kHz, $\nu_1 = 13.33$ kHz, $t_p = 6.63$ μ s held constant. The analytic simulations depicted in panels (A1), (B1) are based on the effective Hamiltonian, while the simulations in panel (A2), (B2) are from Simpson.⁵⁰

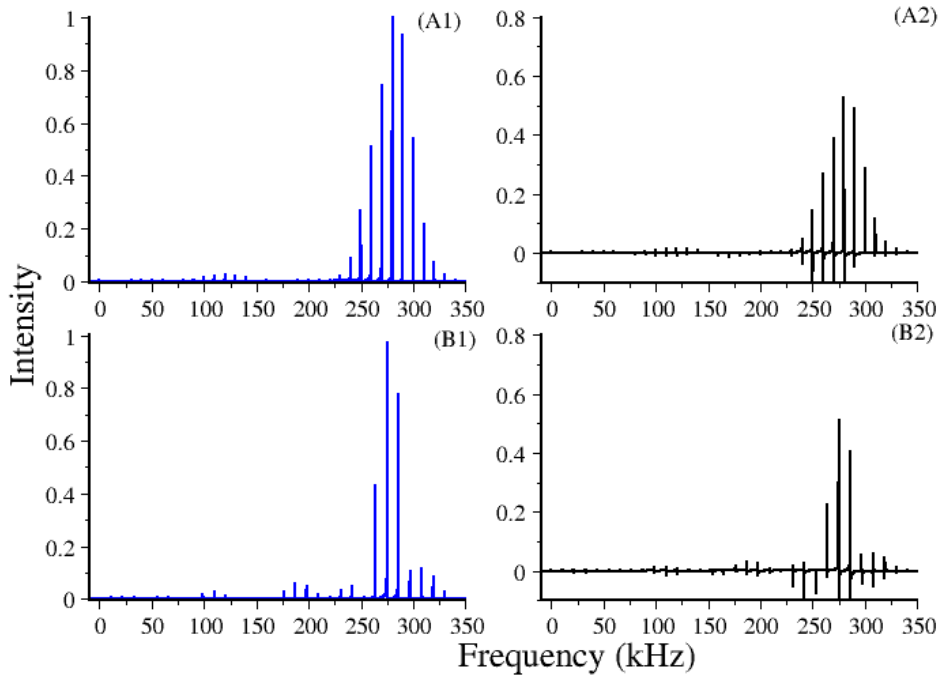


Figure 3.21: Simulations depicting the role of spinning frequency on the excitation efficiency of SQ transitions in spin $I = 5/2$, (excitation frequency, $\nu = \nu_0 + \frac{\nu_Q}{2}$ or $\nu = \nu_0 + 300$ kHz). The following parameters were employed in the simulations: in panels (A1, A2) $\nu_r = 10$ kHz and in panels (B1, B2) $\nu_r = 11$ kHz. The remaining parameters $C_Q = 2.0$ MHz ($\nu_Q = 300$ kHz), excitation frequency $\nu = 300$ kHz, $\nu_1 = 13.33$ kHz, $t_p = 8.39$ μ s held constant. The analytic simulations depicted in panels (A1), (B1) are based on the effective Hamiltonian, while the simulations in panel (A2), (B2) are from Simpson.⁵⁰

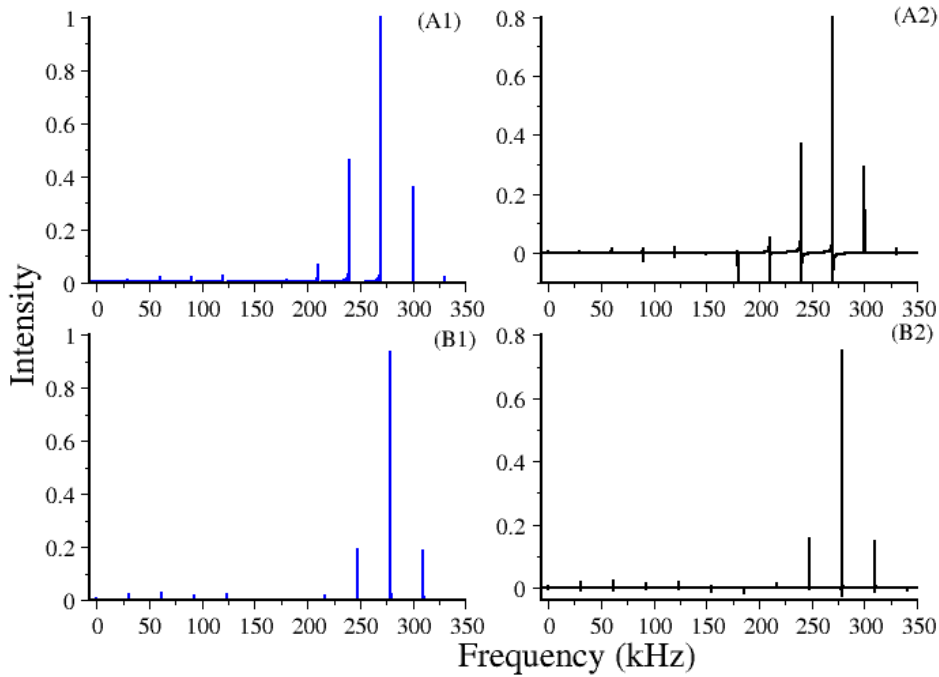


Figure 3.22: Simulations depicting the role of spinning frequency on the excitation efficiency of SQ transitions in spin $I = 5/2$, (excitation frequency, $\nu = \nu_0 + \frac{\nu_Q}{2}$ or $\nu = \nu_0 + 300$ kHz). The following parameters were employed in the simulations: in panels (A1, A2) $\nu_r = 30$ kHz and in panels (B1, B2) $\nu_r = 31$ kHz. The remaining parameters $C_Q = 2.0$ MHz ($\nu_Q = 300$ kHz), excitation frequency $\nu = 300$ kHz, $\nu_1 = 13.33$ kHz, $t_p = 8.39$ μ s held constant. The analytic simulations depicted in panels (A1), (B1) are based on the effective Hamiltonian, while the simulations in panel (A2), (B2) are from Simpson.⁵⁰

$C_1 G^{(2)0}$ in the effective interaction frame is evaluated and represented below,

$$\begin{aligned}
\tilde{T}_{1A}^{(1)1}(t) &= \left(\frac{8}{35} T_0^{(1)1} + \frac{2}{5\sqrt{21}} T_0^{(3)1} - \frac{2}{7} \sqrt{\frac{2}{3}} T_0^{(5)1} - \frac{2}{7} \sqrt{\frac{2}{5}} i T_0^{(2)1} - \frac{2}{7} i T_0^{(4)1} \right) e^{i(\omega_0)t} \\
&+ \sqrt{\frac{3}{2}} \sum_{\substack{m=-2 \\ m \neq 0}}^2 \frac{G_m^{(2)0}}{m\omega_r} \left(\frac{8}{35} T_m^{(1)1} + \frac{2}{5\sqrt{21}} T_m^{(3)1} - \frac{2}{7} \sqrt{\frac{2}{3}} T_m^{(5)1} - \frac{2}{7} \sqrt{\frac{2}{5}} i T_m^{(2)1} - \frac{2}{7} i T_m^{(4)1} \right) e^{i(\omega_0+m\omega_r)t} \\
&+ \frac{1}{2!} \sqrt{\frac{3}{2}} \sum_{\substack{m_1, m_2 = -2 \\ m_1, m_2 \neq 0}}^2 \frac{G_{m_1}^{(2)0} G_{m_2}^{(2)0}}{m_1 m_2 \omega_r^2} \left[\begin{aligned} &\frac{8}{35} T_{m_1+m_2}^{(1)1} + \frac{2}{5\sqrt{21}} T_{m_1+m_2}^{(3)1} - \frac{2}{7} \sqrt{\frac{2}{3}} T_{m_1+m_2}^{(5)1} \\ &- \frac{2}{7} \sqrt{\frac{2}{5}} i T_{m_1+m_2}^{(2)1} - \frac{2}{7} i T_{m_1+m_2}^{(4)1} \end{aligned} \right] e^{i[\omega_0+(m_1+m_2)\omega_r]t} + \dots
\end{aligned} \tag{3.98}$$

Employing Eq. (3.10), the optimized time-domain signal is evaluated.

$$\langle T^{(1)1}(t) \rangle = \sqrt{2} C(1) \cdot \frac{\sqrt{2a_n b_n}}{\sqrt{35}} \sin(\sqrt{8a_n b_n} \omega_1 t) e^{it(\omega_0 - C_1 G^{(2)0})} \tag{3.99}$$

$$\langle T_m^{(1)1}(t) \rangle = \sqrt{2} C(1) \cdot \frac{\sqrt{2a_{n+m} b_{n-m}}}{\sqrt{35}} \sin(\sqrt{8a_{n+m} b_{n-m}} \omega_1 t) e^{it(\omega_0 - C_1 G^{(2)0} + m\omega_r)} \tag{3.100}$$

In a similar vein, the optimized time-domain signal corresponding to the selective excitation of one of the satellite transitions (say $\omega = \omega_0 - 2C_1 G^{(2)0}$), is represented by,

$$\langle T^{(1)1}(t) \rangle = \sqrt{2} C(1) \cdot \frac{\sqrt{5c_n d_n}}{2\sqrt{35}} \sin(\sqrt{5c_n d_n} \omega_1 t) e^{it(\omega_0 - 2C_1 G^{(2)0})} \tag{3.101}$$

$$\langle T^{(1)1}(t) \rangle = \sqrt{2} C(1) \cdot \frac{\sqrt{5c_{n+m} d_{n-m}}}{2\sqrt{35}} \sin(\sqrt{5c_{n+m} d_{n-m}} \omega_1 t) e^{it(\omega_0 - 2C_1 G^{(2)0} + m\omega_r)} \tag{3.102}$$

where the constants c_n, d_n (for $m=0$) c_{n+m}, d_{n+m} given by following equations

$$c_{n+m} = \left[-2c_1 \sum_{\substack{m_1=-2 \\ m_1=-n+m \\ m_1 \neq 0}}^2 \frac{G_{m_1}^{(2)0}}{m_1 \omega_r} + \frac{4c_1^2}{2!} \sum_{\substack{m_1, m_2 = -2 \\ m_1+m_2 = -n+m \\ m_1, m_2 \neq 0}}^2 \frac{G_{m_1}^{(2)0} G_{m_2}^{(2)0}}{m_1 m_2 \omega_r^2} - \dots \right] \tag{3.103}$$

$$d_{n+m} = \left[2c_1 \sum_{\substack{m_1=-2 \\ m_1=n+m \\ m_1 \neq 0}}^2 \frac{G_{m_1}^{(2)0}}{m_1 \omega_r} + \frac{4c_1^2}{2!} \sum_{\substack{m_1, m_2 = -2 \\ m_1+m_2 = n+m \\ m_1, m_2 \neq 0}}^2 \frac{G_{m_1}^{(2)0} G_{m_2}^{(2)0}}{m_1 m_2 \omega_r^2} \dots \right] \tag{3.104}$$

The simulations depicted in Figs. 3.19 to 3.22 substantiate the analytic theory presented in this section. In accord with our description for spin $I = 3/2$, the excitation efficiency of satellite transitions depend on the choice of the spinning frequency.

3.4 Conclusions and Perspectives

In summary, a unified description of the spin dynamics involving irreducible spatial and spin tensor operators is presented for describing the effect of RF pulses in quadrupolar spin

systems. The concept of effective RF Hamiltonians introduced for describing transitions in a multi-level system provides important constraints for improving both the selectivity and efficiency of the excited transitions. The validity of the secular approximation commonly employed in analytic treatments is thoroughly investigated and is well explained and substantiated through extensive numerical simulations. In contrast to existing descriptions in the literature, both selective and non-selective excitations are described in terms of effective Hamiltonians based on spherical tensor operator formalism.

From the above derivations presented in this chapter, it is clear that the excitation efficiency of a particular transition say $|I, m\rangle \rightarrow |I, m - 1\rangle$, depends on parameters that are inherently related to the quadrupolar-coupling constant and the amplitude of the RF irradiation. In the case of non-selective excitation (hard-pulse regime) the optimum flip angle is always $\frac{\pi}{2}$ ($\omega_1 t_p = \frac{\pi}{2}$) and the intensity associated with a particular transition say $|I, m\rangle \rightarrow |I, m - 1\rangle$ is summarized by,

$$\mathbf{I}_{Non-selective} (|I, m\rangle \rightarrow |I, m - 1\rangle) = \frac{[(I + m)(I - m + 1)]}{\sum_{m_I=-I}^I [(I + m_I)(I - m_I + 1)]} \quad (3.105)$$

Interestingly, the optimum flip-angle in the case of selective excitation depends on the states involved and are depicted below along with the expression for the intensity.

$$\theta_{|I,m\rangle \rightarrow |I,m-1\rangle} = \frac{\pi}{2\sqrt{(I + m)(I - m + 1)}} \quad (3.106)$$

$$\mathbf{I}_{Selective} (|I, m\rangle \rightarrow |I, m - 1\rangle) = \frac{\sqrt{(I + m)(I - m + 1)}}{\sum_{m_I=-I}^I [(I + m_I)(I - m_I + 1)]} \quad (3.107)$$

We believe that the analytic approach presented in this chapter could be extended for studying multiple-pulse experiments and understanding phase cycling in quadrupolar systems. In particular, the effective RF Hamiltonians in the soft-pulse regime could be employed to construct phase-alternated schemes to minimize distortions in the powder spectrum. In experiments involving excitation of multi-quantum coherences, the effective RF Hamiltonians provide insights into the choice of a particular sequence. For e.g. in the hard pulse regime, the density operator after a single pulse results in the creation of only single-quantum coherences (of rank 1). Hence, evolution under the quadrupolar Hamiltonian is a prerequisite for the creation of multi-quantum coherences in the three-pulse schemes. Alternatively, in the case of selective pulse excitation, the density operator after a single pulse creates single-quantum coherences corresponding to different ranks. In such cases, an additional pulse creates multi-quantum coherence without evolution under

Spin	Transitions	Intensity	Flip-angle
I	$ m\rangle \leftrightarrow m-1\rangle$	\mathbf{I}	θ
1	$ \pm 1\rangle \leftrightarrow 0\rangle$	$\frac{1}{2\sqrt{2}} \left(\frac{1}{2}\right)$	$\frac{\pi}{2\sqrt{2}}$
$\frac{3}{2}$	$ \frac{1}{2}\rangle \leftrightarrow -\frac{1}{2}\rangle$	$\frac{1}{2} \left(\frac{2}{5}\right)$	$\frac{\pi}{4}$
	$ \frac{\pm 3}{2}\rangle \leftrightarrow \frac{\pm 1}{2}\rangle$	$\frac{\sqrt{3}}{10} \left(\frac{3}{10}\right)$	$\frac{\pi}{2\sqrt{3}}$
$\frac{5}{2}$	$ \frac{1}{2}\rangle \leftrightarrow -\frac{1}{2}\rangle$	$\frac{\sqrt{9}}{35} \left(\frac{9}{35}\right)$	$\frac{\pi}{6}$
	$ \frac{\pm 5}{2}\rangle \leftrightarrow \frac{\pm 3}{2}\rangle$	$\frac{\sqrt{5}}{35} \left(\frac{5}{35}\right)$	$\frac{\pi}{2\sqrt{5}}$
	$ \frac{\pm 3}{2}\rangle \leftrightarrow \frac{\pm 1}{2}\rangle$	$\frac{\sqrt{8}}{35} \left(\frac{8}{35}\right)$	$\frac{\pi}{2\sqrt{8}}$

Table 3.1: Summary of intensities and flip angles for selective excitations in integral and half-integral quadrupolar systems. The intensities depicted in the brackets correspond to non-selective excitation (see Eqs. (3.105) and (3.107)).

quadrupolar Hamiltonian. The formalism presented here provides a framework for understanding these experimental observations in a tangible manner. A formal description of the evolution of the density operator in multi-quantum experiments along with optimum conditions for excitation would be described in the following chapter.

References

- [1] A. Abragam, *The principles of nuclear magnetism*, Oxford university press, 1961.
- [2] C. P. Slichter, *Principles of magnetic resonance*, Springer Springer Science & Business Media, 2013.
- [3] M. Mehring, *Principles of high resolution NMR in solids*, Springer Springer Science & Business Media, 2012.
- [4] D. Freude, *Encyclopedia of Analytical Chemistry.*, 2000.
- [5] P. P. Man, *Encyclopedia of Analytical Chemistry.*, 2000.
- [6] R. E. Wasylshen, S. E. Ashbrook and S. Wimperis, *NMR of Quadrupolar Nuclei in Solid Materials*, John Wiley & Sons, 2012.
- [7] J. J. Fitzgerald, *Solid-state NMR spectroscopy of inorganic materials*, American Chemical Society, 1999.
- [8] E. Oldfield and R. J. Kirkpatrick, *Science*, 1985, **227**, 1537.
- [9] K. J. D. MacKenzie and M. E. Smith, *Multinuclear solid-state nuclear magnetic resonance of inorganic materials*, Elsevier, 2002, vol. 6.
- [10] A. Jerschow, *Prog. Nucl. Magn. Reson. Spectrosc.*, 2005, **46**, 63.
- [11] L. Frydman and J. S. Harwood, *J. Am. Chem. Soc.*, 1995, **117**, 5367.
- [12] A. Medek, J. S. Harwood and L. Frydman, *J. Am. Chem. Soc.*, 1995, **117**, 12779.
- [13] L. Frydman, in *Multiple-Quantum Magic-Angle Spinning Experiments on Half-Integer Nuclei: Fundamentals*, John Wiley & Sons, Ltd, 2007.
- [14] A. J. Vega, in *Quadrupolar Nuclei in Solids*, John Wiley & Sons, Ltd, 2007.
- [15] S. E. Ashbrook and S. Wimperis, *Prog. Nucl. Magn. Reson. Spectrosc.*, 2004, **45**, 53.
- [16] S. E. Ashbrook and S. Wimperis, *J. Am. Chem. Soc.*, 2002, **124**, 11602.
- [17] S. E. Ashbrook and S. Wimperis, *J. Magn. Reson.*, 2002, **156**, 269.
- [18] M. E. Smith and E. R. H. van Eck, *Prog. Nucl. Magn. Reson. Spectrosc.*, 1999, **34**, 159.
- [19] S. Vega and A. Pines, *J. Chem. Phys.*, 1977, **66**, 5624.
- [20] A. Wokaun and R. R. Ernst, *J. Chem. Phys.*, 1977, **67**, 1752.

- [21] S. Vega and Y. Naor, *J. Chem. Phys.*, 1981, **75**, 75.
- [22] S. Vega, *J. Chem. Phys.*, 1978, **68**, 5518.
- [23] B. C. Sanctuary, *J. Chem. Phys.*, 1976, **64**, 4352.
- [24] B. C. Sanctuary and T. K. Halstead, in *Multipole NMR*, ed. S. W. Warren, Academic Press, 1990, vol. 15, p. 79.
- [25] G. J. Bowden, J. Khachan and J. P. D. Martin, *J. Magn. Reson.*, 1989, **83**, 79.
- [26] G. J. Bowden and W. D. Hutchison, *J. Magn. Reson.*, 1986, **67**, 403.
- [27] G. J. Bowden, W. D. Hutchison and J. Khachan, *J. Magn. Reson.*, 1986, **67**, 415.
- [28] H. A. Buckmaster and R. Chatterjee, *Phys. Status Solidi (b)*, 1998, **209**, 433.
- [29] H. A. Buckmaster, R. Chatterjee and Y. H. Shing, *Phys. Status Solidi (a)*, 1972, **13**, 9.
- [30] B. L. Silver, *Irreducible tensor methods: an introduction for chemists*, Academic Press, 2013, vol. 36.
- [31] A. R. Edmonds, *Angular momentum in quantum mechanics*, Princeton University Press, 1996.
- [32] A. Ramamoorthy and P. T. Narasimhan, *Pramana*, 1991, **36**, 399.
- [33] A. Ramamoorthy and P. T. Narasimhan, *Mol. Phys.*, 1991, **73**, 207.
- [34] A. K. Dubey, A. Ramamoorthy and P. Raghunathan, *Chem. Phys. Lett.*, 1990, **168**, 401.
- [35] P. P. Man, *Chem. Phys. Lett.*, 1990, **168**, 227.
- [36] P. P. Man, *Mol. Phys.*, 1992, **76**, 1119.
- [37] P. P. Man, J. Klinowski, A. Trokiner, H. Zanni and P. Papon, *Chem. Phys. Lett.*, 1988, **151**, 143.
- [38] P. P. Man, *J. Magn. Reson., Ser. A*, 1995, **114**, 59.
- [39] P. P. Man, *Mol. Phys.*, 1993, **78**, 307.
- [40] P. P. Man and P. Tougne, *Mol. Phys.*, 1994, **83**, 997.
- [41] D. Papousek and M. R. Aliev, *Molecular vibrational-rotational spectra*, 1982.
- [42] R. Ramesh and M. S. Krishnan, *J. Chem. Phys.*, 2001, **114**, 5967.
- [43] M. K. Pandey and M. S. Krishnan, *J. Chem. Phys.*, 2010, **133**, 174121.
- [44] J. K. G. Watson, *Mol. Phys.*, 2005, **103**, 3283.
- [45] J. H. Shirley, *Phys. Rev.*, 1965, **138**, B979.
- [46] A. Schmidt and S. Vega, *J. Chem. Phys.*, 1992, **96**, 2655.
- [47] G. Goobes, G. J. Boender and S. Vega, *J. Magn. Reson.*, 2000, **146**, 204.
- [48] R. Ramachandran and R. G. Griffin, *J. Chem. Phys.*, 2005, **122**, 164502.
- [49] R. Ramachandran, V. S. Bajaj and R. G. Griffin, *J. Chem. Phys.*, 2005, **122**, 164503.
- [50] M. Bak, J. T. Rasmussen and N. C. Nielsen, *J. Magn. Reson.*, 2000, **147**, 296.

Chapter 4

Theory of Multi-Quantum (MQ) excitation in multi-level systems

4.1 Background

Ever since its inception in 1995, Multi-Quantum^{1,2} (MQ) NMR spectroscopy (due to Frydman and Harwood) of quadrupolar nuclei ($I > 1/2$) has held the centre stage in the structural characterization of inorganic solids owing to the simplicity of its implementation.³⁻⁵ With the combined efforts of several researchers,^{4,6-17} interesting new innovations¹⁸⁻²⁷ to the original scheme have emerged in recent past, resulting in exciting applications of this methodology in studying inorganic clusters comprising of nuclei possessing higher spin quantum numbers. Although, recent advancements in the form of high field magnets, faster spinning modules, efficient high power probes have enabled in better implementation of experiments, improved understanding of the MQ phenomenon is quintessential for both design and interpretation of MQ experiments/experimental data. In particular, improvement to the signal-to-noise ratio (S/N) in MQ experiments (relies on efficient excitation/re-conversion of MQ coherences) remains a daunting task both from an experimental as well as a theoretical perspective. Depending on the relative magnitudes of the quadrupolar coupling constant and the amplitude of the oscillating radio frequency (RF) field, the mode of excitation/re-conversion of MQ coherences in experiments differ.²⁸

In general, the efficiency of excitation differs and suitability of a particular pulse scheme depends on external parameters such as the frequency of excitation, duration, amplitude, spinning frequency and flip angle of the pulse in addition to the intrinsic quadrupolar coupling constant of a particular system. Hence, a suitable analytic framework inclusive of these experimental parameters is essential for understanding the underlying spin dynamics and for reliable extraction of quadrupolar coupling constant and asymmetry parameters in MQ experiments. Here in this chapter, we confine our discussion to the development

of analytic methods for understanding MQ NMR experiments of quadrupolar nuclei in both single-crystal and MAS cases.

To this end, seminal contributions to understand MQ NMR experiments originated from Vega and co-workers.^{29–31} In particular, the approach of Vega and Naor³¹ has been used extensively for the description of MQ-NMR experiments and its variants. In combination with numerical methods^{14,32,33} and the fictitious spin operator formalism,^{29,34} semi-analytical treatments have also emerged for describing both static and MAS experiments involving quadrupolar nuclei.^{14,32,35,36} As an alternative, spherical tensor based formalisms have also been employed for studying quadrupolar spins in both NQR and NMR spectroscopy.^{37–43} In particular, employing the hard-pulse approximation (a condition that is satisfied in systems with smaller quadrupolar coupling constant), multiple-pulse experiments involving quadrupolar nuclei have been studied using the spherical tensor formalism.^{38,42,43} Although, such approaches have helped our understanding of the basic methodology, they are of limited utility in describing systems with larger quadrupolar coupling constants. To address these concerns, an alternate approach in the form of effective Hamiltonians^{36,44–46} based on spherical tensor formalism was recently proposed to describe selective and non-selective excitations in quadrupolar systems.⁴⁷ Here in this chapter, we demonstrate the utility of this approach in understanding the excitation of MQ-coherences in single-pulse experiments involving quadrupolar nuclei.

In the approach of Vega and Naor,³¹ a diagonalized representation of the Hamiltonian (comprising of the RF and the quadrupolar Hamiltonian) was proposed as a solution to describe the spin dynamics in the soft-pulse regime. Although, such an approach has been demonstrated for studying spin I=1, 3/2 systems,^{48–51} their extensions in higher spin systems are less straightforward. Alternatively, by invoking the concept of “Secular Approximation” (also known as rotating wave approximation),⁵² the nuances of MQ excitation is explained through effective RF Hamiltonians. As a test case, excitation of MQ coherences in spin 1 (DQ coherence), spin 3/2 (TQ coherence) and spin 5/2 (TQ, 5Q coherences) systems are described. In Section 4.2, analytic theory of MQ excitation in multi-pulse experiments is discussed along with simulations followed by a brief summary in Section 4.3.

4.2 Theory and Discussion

To understand the nuances of MQ excitation, we begin our discussion with the Hamiltonian of an isolated quadrupolar spin system,

$$H = \underbrace{\hbar\omega_0 I_z}_{H_z} + \underbrace{\hbar G^{(2)0} T^{(2)0}}_{H_Q} + \underbrace{2\hbar\omega_1 \cos \omega t I_x}_{H_{RF}} \quad (4.1)$$

In the above equation, the external interactions are represented in terms of ‘ ω_0 ’ the Larmor frequency, ‘ ω ’ the carrier frequency of the RF field and ‘ ω_1 ’ the amplitude of the RF field. The quadrupolar interaction (to first-order) is represented by $G^{(2)0}$ and is anisotropic for a polycrystalline sample, represented by,

$$G^{(2)0} = \frac{\sqrt{6}}{C(2)} \cdot \frac{\omega_Q(\alpha, \beta, \gamma)}{6} \quad (4.2)$$

The term $\omega_Q(\alpha, \beta, \gamma) = \frac{-3\pi C_Q}{I(2I-1)} \left(\frac{3\cos^2\beta-1}{2} + \frac{\eta}{2}\sin^2\beta \cos 2\alpha \right)$ represents the quadrupolar splitting parameter, $C_Q = \frac{e^2 q Q}{h}$ the quadrupolar coupling constant and $C(2) = \sqrt{\frac{30}{(2I+1)I(I+1)(2I+3)(2I-1)}}$. The angle (α, β, γ) denotes the Euler angles required for the transformation from the PAS to LAS.

To describe the effects of the RF modulation on the system, the Hamiltonian defined in the laboratory frame (Eq. (4.1)) is transformed into the Zeeman-Quadrupolar (Z-Q) interaction frame, resulting in an effective RF Hamiltonian.⁴⁷

$$\tilde{H}_{RF}(t) = e^{i\omega_0 t I_z} \cdot e^{iG^{(2)0} t T^{(2)0}} H e^{-iG^{(2)0} t T^{(2)0}} \cdot e^{-i\omega_0 t I_z} \quad (4.3)$$

Depending on the relative magnitudes of the quadrupolar coupling constant and the RF amplitude, both selective and non-selective excitations have been described in terms of effective RF Hamiltonians (as described in Chapter 3). In the hard pulse limit ($\omega_1 \gg \omega_Q$), the effective RF Hamiltonian reduces to an I_x (for an x-pulse) operator. Here in this chapter, we focus our discussion to the description of MQ experiments in the intermediate regimes. In the following sections, analytic description in the form of effective RF Hamiltonians are presented for understanding the MQ behavior depicted in Figs. 4.1 to 4.3 (for $I = 1$), Figs. 4.4 to 4.6 (for $I = 3/2$) and Figs. 4.7 to 4.9 (for $I = \frac{5}{2}$).

4.2.1 Description for $I=1$ system

4.2.1.1 Static (Single-crystal)

In the Z-Q interaction frame, the RF Hamiltonian corresponding to the excitation frequency $\omega = \omega_0$ is represented by,

$$\tilde{H}_{RF}(t) = \frac{\hbar\omega_{RF}}{2} \left[\begin{array}{l} (iT^{(1)1} + T^{(2)1})e^{-i\sqrt{\frac{3}{2}}G^{(2)0}t} - (iT^{(1)-1} + T^{(2)-1})e^{i\sqrt{\frac{3}{2}}G^{(2)0}t} \\ + (iT^{(1)1} - T^{(2)1})e^{i\sqrt{\frac{3}{2}}G^{(2)0}t} - (iT^{(1)-1} - T^{(2)-1})e^{-i\sqrt{\frac{3}{2}}G^{(2)0}t} \end{array} \right] \quad (4.4)$$

The above RF Hamiltonian is time-dependent and if neglected under “secular approximation” would result in a trivial result i.e. $\tilde{\rho}(t) = \exp(\frac{-i}{\hbar}\tilde{H}_{RF,eff}t)\tilde{\rho}(0)\exp(\frac{i}{\hbar}\tilde{H}_{RF,eff}t) = \tilde{\rho}(0)$. Hence, to explain the observed DQ coherence from the single-pulse experiment, Eq. (4.4) has to be retained. This inference suggests a possible breakdown of the secular

approximation and is bit counter-intuitive, since the amplitude of the RF pulses employed in panel (B1) of Fig. 4.1 is much smaller than quadrupolar coupling constant C_Q . The discrepancy could however be resolved by invoking ‘time’ as a criterion for deciding the suitability of secular approximation. For e.g., when the time-evolution of a quantum system is monitored for shorter time periods, the effects of high frequency oscillating terms are of lesser consequence and could be neglected in the dynamics. However, for longer durations of observation, the oscillating time-dependent terms may have a profound effect as illustrated by the simulations depicted in Figs. 4.1 to 4.9.

To facilitate analytic description and alleviate the complexity due to time-dependent Hamiltonians (i.e. $\tilde{\rho}(\tau) = \exp\left(\frac{-i}{\hbar} \int_0^\tau \tilde{H}_{RF,eff}(t) dt\right) \tilde{\rho}(0) \exp\left(\frac{i}{\hbar} \int_0^\tau \tilde{H}_{RF,eff}(t) dt\right)$), an alternate approach is presented below. In this approach (instead of transforming into the Z-Q interaction frame), the Hamiltonian described in Eq. (4.1) is transformed into the RF frame of reference (for on-resonance irradiation) defined below,

$$\begin{aligned} \tilde{H} &= \exp(i\omega_0 t I_z) H \exp(-i\omega_0 t I_z) \\ &= \hbar G^{(2)0} T^{(2)0} + \hbar \omega_1 I_x \end{aligned} \quad (4.5)$$

Since $\sqrt{6}G^{(2)0} > \omega_1$, effective Hamiltonians based on the method of contact transformation^{45,46,53–55} are proposed to explain the simulation results. Following this approach, the dominant term due to the quadrupolar interaction is included as the zero order Hamiltonian, while the RF part forms the perturbation.

$$\begin{aligned} \tilde{H} &= H_0 + H_1 \\ H_0 &= \hbar G^{(2)0} T^{(2)0} \\ H_1 &= \hbar \omega_1 \left[iT^{(1)1}(a) \right] \end{aligned} \quad (4.6)$$

Employing a unitary transformation defined by S_1 , the above Hamiltonian Eq. (4.5) is transformed into an effective Hamiltonian H_{eff} , illustrated below,

$$H_{eff} = e^{iS_1} \tilde{H} e^{-iS_1} \quad (4.7)$$

Following the standard procedure, the n^{th} order correction to the zero order Hamiltonian

is expressed in terms of operators⁵³ by expanding Eq. (4.7)

$$\begin{aligned}
H_0^{(1)} &= H_0 = \hbar G^{(2)0} T^{(2)0} \\
H_1^{(1)} &= H_1 + i [S_1, H_0] = 0 \\
H_2^{(1)} &= i [S_1, H_1] - \frac{1}{2} [S_1, [S_1, H_0]] \\
&= \frac{\hbar \omega_1^2}{G^{(2)0}} T^{(2)0} + \frac{\hbar \omega_1^2}{\sqrt{6} G^{(2)0}} T^{(2)2}(s)
\end{aligned} \tag{4.8}$$

In the above equation, the transformation function S_1 (i.e. $S_1 = i \frac{2\omega_1}{\sqrt{6} G^{(2)0}} T^{(2)1}(s)$) is chosen carefully to compensate the off-diagonality due to H_1 . Subsequently, the effective Hamiltonian to second order during a pulse is represented by,

$$H_{eff} = \left(\hbar G^{(2)0} + \frac{\hbar \omega_1^2}{G^{(2)0}} \right) T^{(2)0} + \frac{\hbar \omega_1^2}{\sqrt{6} G^{(2)0}} T^{(2)2}(s) \tag{4.9}$$

To have a consistent description, the initial density operator is re-defined in the frame of the transformation function S_1 , as represented below,

$$\begin{aligned}
\tilde{\rho}(0) &= e^{iS_1} I_z e^{-iS_1} \\
&= I_z \cos b + \sin b T^{(2)1}(a)
\end{aligned} \tag{4.10}$$

where $b = \frac{2\omega_1}{\sqrt{6} G^{(2)0}}$. Since $\omega_Q > \omega_1$, the term proportional to $\sin b$ in Eq. (4.10) tends to zero and the term proportional to $\cos b$ tends to 1 i.e the effect of the transformation function S_1 on the density operator can be neglected. Employing the effective Hamiltonian (Eq. (4.9)) the density operator after a pulse (of duration τ) is evaluated and represented by,

$$\begin{aligned}
\tilde{\rho}(\tau) &= e^{-\frac{i}{\hbar} H_{eff} \tau} \tilde{\rho}(0) e^{\frac{i}{\hbar} H_{eff} \tau} \\
&= I_z \cos \theta_1 + i \sin \theta_1 T^{(2)2}(a) \\
&\simeq \tilde{\rho}(\tau) = e^{-iS_1} \tilde{\rho}(\tau) e^{iS_1}
\end{aligned} \tag{4.11}$$

where $\theta_1 = \frac{2\omega_1^2}{\sqrt{6} G^{(2)0}} \tau$. The time-domain signal corresponding to the DQ coherence in the rotating frame is evaluated employing the standard procedure and is represented by,

$$\begin{aligned}
\langle \tilde{T}^{(2)2} \rangle &= Tr[T^{(2)2} \tilde{\rho}(\tau)] \\
&= -i \sin \theta_1
\end{aligned} \tag{4.12}$$

As depicted in Fig. 4.1 (see panels A1 & A2), the frequency of oscillation (DQ coherence) increases with the amplitude of the RF fields, employed in the excitation process. With increase in quadrupolar coupling constant (panels A1 & B1), the frequency of os-

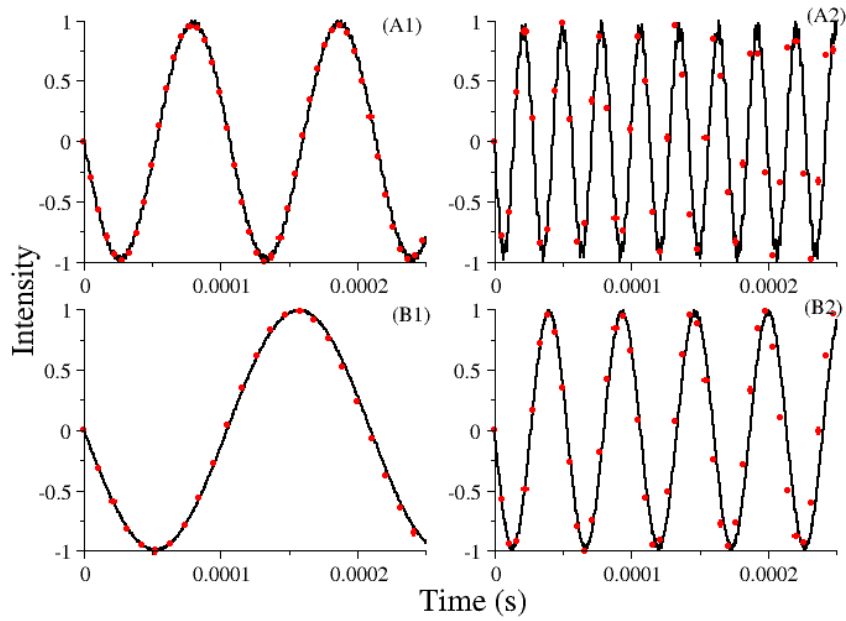


Figure 4.1: Simulations depicting the role of RF amplitude and quadrupolar coupling strength on excitation efficiency of double-quantum (DQ) transitions in single-crystal spin $I = 1$. The following parameters were employed in the simulations: in panel (A1) $C_Q = 0.5$ MHz, $v_1 = 60$ kHz, in panel (A2) $C_Q = 0.5$ MHz, $v_1 = 120$ kHz, in panel (B1) $C_Q = 1.0$ MHz, $v_1 = 60$ kHz and in panel (B2) $C_Q = 1.0$ MHz, $v_1 = 120$ kHz. The remaining parameters spinning frequency $\nu_r = 0$ kHz, $\eta = 0$, excitation frequency $\nu = 0$ kHz were held constant in all the simulation. The analytic simulations depicted red dots are based on the effective Hamiltonian, while the simulations in black solid lines are from Simpson.⁵⁶

cillations decreases. This trends is in accord with the analytic expressions presented in Eq. (4.12).

4.2.1.2 Magic Angle Spinning (Powder-sample)

The Hamiltonian for an isolated quadrupolar spin system under MAS is represented by,

$$H = H_Z + H_{RF} + \hbar \sum_{\substack{m=-2 \\ m \neq 0}}^2 G_m^{(2)0} e^{im\omega_r t} T_m^{(2)0} \quad (4.13)$$

In Eq. (4.13), $G_m^{(2)0}$ denotes the spatial anisotropy associated with the quadrupolar interaction (also see Table 2.4) and is represented below,

$$G_{Q,m}^{(2)0} = C^Q \sum_{q_2, q_3=-2}^2 R_{Q,P}^{(2)q_3} D_{q_3 q_2}^{(2)}(\Omega_{PM}) D_{q_2 m}^{(2)}(\Omega_{MR}) d_{m0}^{(2)}(\beta_{RL}) \quad (4.14)$$

The corresponding Floquet Hamiltonian⁵⁷ in the standard rotating frame is represented by,

$$\tilde{H} = \hbar\omega_r I_F + \hbar \sum_{\substack{m=2 \\ m \neq 0}}^{-2} G_m^{(2)0} T_m^{(2)0} + \hbar\omega_1 I_x \quad (4.15)$$

Unlike the single-crystal, two transformations are necessary in MAS descriptions. To facilitate the contact transformation method, the Hamiltonian is divided into two parts as represented below,

$$H_0 = \hbar \sum_{\substack{m=2 \\ m \neq 0}}^{-2} G_m^{(2)0} T_m^{(2)0} \quad (4.16)$$

$$H_1 = \hbar\omega_r I_F + \hbar\omega_1 I_x \quad (4.17)$$

Following the standard procedure, the higher-order corrections are derived employing the transformation function S_1 (i.e. $S_1 = i \frac{2\omega_1}{\sqrt{6}G_m^{(2)0}} T_m^{(2)1}(s)$), as represented below,

$$\begin{aligned} H_0^{(1)} &= H_0 = \hbar \sum_{\substack{m=2 \\ m \neq 0}}^{-2} G_m^{(2)0} T_m^{(2)0} \\ H_1^{(1)} &= H_1 + i[S_1, H_0] = \hbar\omega_r I_F \\ H_2^{(1)} &= i[S_1, H_1] - \frac{1}{2}[S_1, [S_1, H_0]] \\ &= \sum_{\substack{m=2 \\ m \neq 0}}^{-2} \frac{\hbar\omega_1^2}{G_m^{(2)0}} \left[T_m^{(2)0} + \frac{1}{\sqrt{6}} T_m^{(2)2}(s) \right] - \sum_{\substack{m_1, m_2, m_3=2 \\ m_1+m_2+m_3=0}}^{-2} \frac{\hbar\omega_1^2 G_{m_3}^{(2)0}}{G_{m_1}^{(2)0} G_{m_2}^{(2)0}} \left[T^{(2)0} + \frac{1}{\sqrt{6}} T^{(2)2}(s) \right] \end{aligned} \quad (4.18)$$

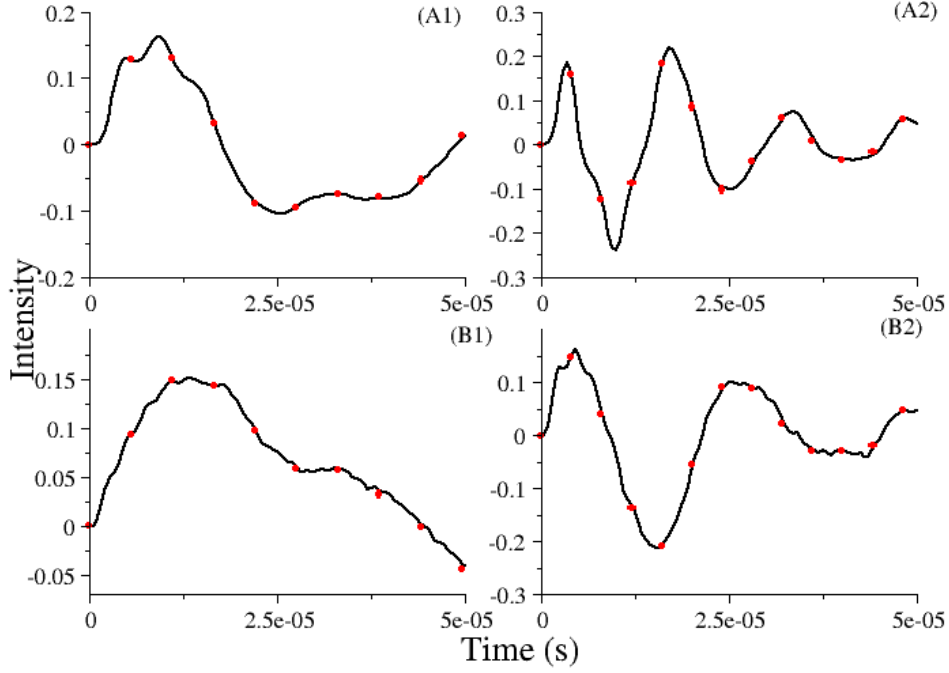


Figure 4.2: Simulations depicting the role of RF amplitude and quadrupolar coupling strength on excitation efficiency of double-quantum (DQ) transitions in spin $I = 1$. The following parameters were employed in the simulations: in panel (A1) $C_Q = 0.5$ MHz, $\nu_1 = 60$ kHz, in panel (A2) $C_Q = 0.5$ MHz, $\nu_1 = 120$ kHz, in panel (B1) $C_Q = 1.0$ MHz, $\nu_1 = 60$ kHz and in panel (B2) $C_Q = 1.0$ MHz, $\nu_1 = 120$ kHz. The remaining parameters spinning frequency $\nu_r = 10$ kHz, $\eta=0$, excitation frequency $\nu = 0$ kHz were held constant in all the simulation. The analytic simulations depicted red dots are based on the effective Hamiltonian, while the simulations in black solid lines are from Simpson.⁵⁶

The effective Hamiltonian after first transformation is divided based on the diagonality in the Fourier basis as in conventional way and is given below,

$$\begin{aligned}
 H_{eff} &= H_0^{(1)} + H_1^{(1)} + H_2^{(1)} \\
 &= H_0 + H_1
 \end{aligned}
 \tag{4.19}$$

where

$$\begin{aligned}
 H_0 &= \hbar\omega_r I_F - \sum_{\substack{m_1, m_2, m_3=2 \\ m_1+m_2+m_3=0}}^{-2} \frac{\hbar\omega_1^2 G_{m_3}^{(2)0}}{G_{m_1}^{(2)0} G_{m_2}^{(2)0}} \left[T^{(2)0} + \frac{1}{\sqrt{6}} T^{(2)2}(s) \right] \\
 H_1 &= \hbar \sum_{\substack{m=2 \\ m \neq 0}}^{-2} G_m^{(2)0} T_m^{(2)0} + \sum_{\substack{m=2 \\ m \neq 0}}^{-2} \frac{\hbar\omega_1^2}{G_m^{(2)0}} \left[T_m^{(2)0} + \frac{1}{\sqrt{6}} T_m^{(2)2}(s) \right]
 \end{aligned}
 \tag{4.20}$$

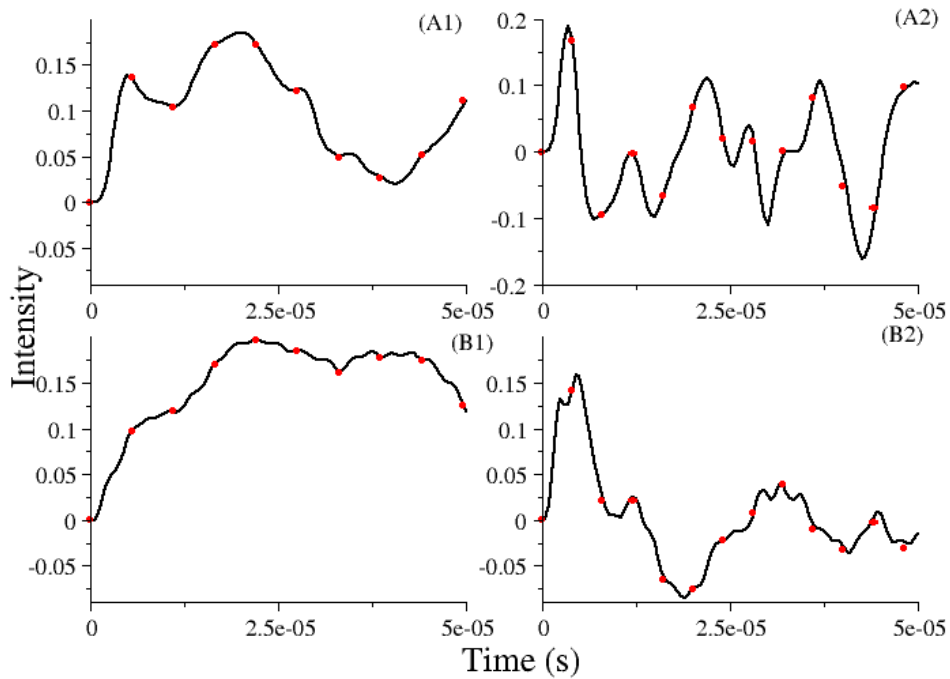


Figure 4.3: Simulations depicting the role of RF amplitude and quadrupolar coupling strength on excitation efficiency of double-quantum (DQ) transitions in spin $I = 1$. The following parameters were employed in the simulations: in panel (A1) $C_Q = 0.5$ MHz, $\nu_1 = 60$ kHz, in panel (A2) $C_Q = 0.5$ MHz, $\nu_1 = 120$ kHz, in panel (B1) $C_Q = 1.0$ MHz, $\nu_1 = 60$ kHz and in panel (B2) $C_Q = 1.0$ MHz, $\nu_1 = 120$ kHz. The remaining parameters spinning frequency $\nu_r = 30$ kHz, $\eta=0$, excitation frequency $\nu = 0$ kHz were held constant in all the simulation. The analytic simulations depicted red dots are based on the effective Hamiltonian, while the simulations in black solid lines are from Simpson.⁵⁶

The corresponding transformation function^{55,58} is represented by,

$$S_2 = - \sum_{\substack{m=2 \\ m \neq 0}}^{-2} \frac{iG_m^{(2)0}}{m\omega_r} T_m^{(2)0} - \sum_{\substack{m=2 \\ m \neq 0}}^{-2} \frac{i\omega_1^2}{G_m^{(2)0} m\omega_r} \left[T_m^{(2)0} + \frac{1}{\sqrt{6}} T_m^{(2)2}(s) \right] \quad (4.21)$$

Employing the above transformation function, the final effective Hamiltonian after two transformations is represented by,

$$H_{eff} = \hbar\omega_r I_F - \sum_{\substack{m_1, m_2, m_3=2 \\ m_1+m_2+m_3=0}}^{-2} \frac{\hbar\omega_1^2 G_{m_3}^{(2)0}}{G_{m_1}^{(2)0} G_{m_2}^{(2)0}} \left[T^{(2)0} + \frac{1}{\sqrt{6}} T^{(2)2}(s) \right] \quad (4.22)$$

To have a consistent description, the initial density operator is re-defined in the frame of the transformation function S_1 and S_2 , as represented below,

$$\begin{aligned} \tilde{\rho}(0) &= e^{iS_2} e^{iS_1} I_z e^{-iS_1} e^{-iS_2} \\ &= I_z \cos c \end{aligned} \quad (4.23)$$

with $c = \sum_{\substack{m=-2 \\ m \neq 0}}^2 \frac{2\omega_1^2}{m\omega_r \sqrt{G_m^{(2)0} G_{-m}^{(2)0}}}$. Employing the effective Hamiltonian (Eq. (4.22)) the density operator after a pulse (of duration τ) is evaluated and represented by,

$$\tilde{\rho}(\tau) = \cos c [I_z \cos \theta_2 + i \sin \theta_2 T^{(2)2}(a)] \quad (4.24)$$

where $\theta_2 = \sum_{\substack{m_1, m_2, m_3=2 \\ m_1+m_2+m_3=0}}^{-2} \frac{2\omega_1^2 G_{m_3}^{(2)0}}{G_{m_1}^{(2)0} G_{m_2}^{(2)0}} \tau$. Subsequently, the density operator after the pulse is transformed back into the standard rotating frame through the reverse transformations as illustrated.

$$\begin{aligned} \tilde{\rho}(\tau)_{DQ} &= e^{-iS_1} e^{-iS_2} \tilde{\rho}(\tau) e^{iS_2} e^{iS_1} \\ &= \cos^2 c [i \sin \theta_2 T^{(2)2}(a)] \end{aligned} \quad (4.25)$$

The time-domain signal corresponding to the DQ coherence in standard rotating frame is evaluated employing standard procedure and is represented by,

$$\begin{aligned} \langle \tilde{T}^{(2)2} \rangle &= Tr [T^{(2)2} \tilde{\rho}(\tau)] \\ &= -i \cos^2 c \sin \theta_2 \end{aligned} \quad (4.26)$$

To substantiate the validity of the analytic theory, excitation of DQ transition in spin $I = 1$ is depicted in Figs. 4.2 and 4.3. In contrast to the result obtained from single-crystal, the excitation efficiency is much lower in MAS experiments involving powder samples. This decrease in the efficiency is due to the presence of $\cos^2 c$ term in Eq. (4.26).

As depicted, the simulations emerging from the effective Hamiltonians are in excellent agreement with those emerging from exact numerical methods.

4.2.2 Description for $I=3/2$ system

4.2.2.1 Static (Single-crystal)

Following the description for the $I = 1$ case, the Hamiltonian for an isolated spin ($I = 3/2$) system is represented as a sum of two terms.

$$\begin{aligned}\tilde{H} &= H_0 + H_1 \\ H_0 &= \hbar G^{(2)0} T^{(2)0} \\ H_1 &= \hbar \omega_1 \sqrt{\frac{5}{2}} i T^{(1)1}(a)\end{aligned}\tag{4.27}$$

Employing the transformation function $S_1 = i\sqrt{\frac{3}{2}} \frac{\omega_1}{G^{(2)0}} T^{(2)1}(s)$, the effective Hamiltonian $H_{eff} = e^{iS_1} H e^{-iS_1}$ is derived. In contrast to spin $I = 1$ system, corrections to third order are essential for the creation of TQ coherence in single-pulse experiments involving spin $I = 3/2$ systems. Neglecting the off-diagonal contributions and retaining terms that commute with H_0 , the effective Hamiltonian is re-written as follows:

$$H_{eff} = \left(\hbar G^{(2)0} + \frac{3\hbar\omega_1^2}{2G^{(2)0}} \right) T^{(2)0} - \frac{3\hbar\omega_1^3}{4(G^{(2)0})^2} i T^{(3)3}(a)\tag{4.28}$$

In a similar vein, the initial density operator (I_z) is transformed as represented below,

$$\tilde{\rho}(0) = I_z + \frac{1}{\sqrt{2}} T^{(2)1}(a) \sin b + \frac{1}{\sqrt{5}} \left(-iT^{(1)0} + 2iT^{(3)0} \right) (\cos b - 1)\tag{4.29}$$

with $b = \sqrt{3} \frac{\omega_1}{G^{(2)0}}$. Employing the effective Hamiltonian (Eq. (4.28)) the density operator after a pulse (of duration τ), is evaluated and represented below.

$$\begin{aligned}\tilde{\rho}(\tau) &= e^{-\frac{i}{\hbar} H_{eff} \tau} \tilde{\rho}(0) e^{\frac{i}{\hbar} H_{eff} \tau} \\ \tilde{\rho}(\tau) &= e^{-iS_1} \tilde{\rho}(\tau) e^{iS_1} = I_z + \frac{3}{2} \sin \theta_1 T^{(3)3}(s) + \frac{3}{2\sqrt{5}} \left(-3iT^{(1)0} + iT^{(3)0} \right) (\cos \theta_1 - 1)\end{aligned}\tag{4.30}$$

where $\theta_1 = \frac{3\omega_1^3 \tau}{2(G^{(2)0})^2}$. Accordingly, the time-domain signal for TQ coherence is evaluated (i.e. $Tr[-T^{(3)3} \tilde{\rho}(\tau)]$)^I and represented by,

$$\langle T^{(3)3} \rangle = -\frac{3}{2} \sin \theta_1\tag{4.31}$$

^IThe negative sign in the detection operator corresponding to odd quantum coherence is arising from the convention we used for RF nutation frequency (i.e $\omega_1 = -\gamma B_1$)

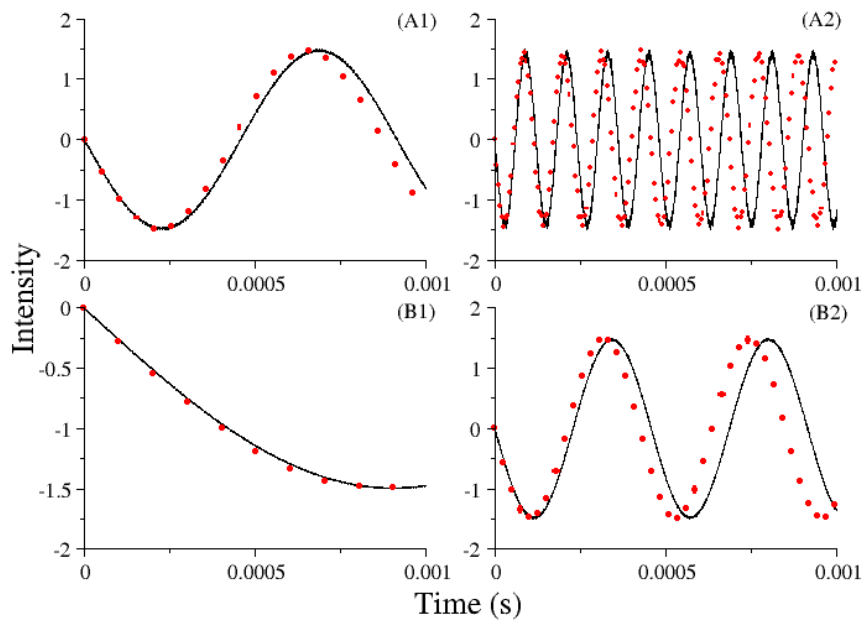


Figure 4.4: Simulations depicting the role of RF amplitude and quadrupolar coupling strength on excitation efficiency of triple-quantum (TQ) transitions in single-crystal spin $I = 3/2$. The following parameters were employed in the simulations: in panel (A1) $C_Q = 1.08$ MHz, $\nu_1 = 60$ kHz, in panel (A2) $C_Q = 1.08$ MHz, $\nu_1 = 120$ kHz, in panel (B1) $C_Q = 2.16$ MHz, $\nu_1 = 60$ kHz and in panel (B2) $C_Q = 2.16$ MHz, $\nu_1 = 120$ kHz. The remaining parameters spinning frequency $\nu_r = 0$ kHz, $\eta=0$, excitation frequency $\nu = 0$ kHz were held constant in all the simulation. The analytic simulations depicted red dots are based on the effective Hamiltonian, while the simulations in black solid lines are from Simpson.⁵⁶

The simulations presented in Fig. 4.4 shows similar trends exhibited for spin $I = 1$ system and are in good agreement with exact numerical methods.

4.2.2.2 Magic Angle Spinning (Powder-sample)

Following the description for spin $I = 1$ system, the initial Hamiltonian (Eq. (4.13)) is transformed using the unitary transformation function $S_1 = i\sqrt{\frac{3}{2}}\frac{\omega_1}{G_m^{(2)0}}T_m^{(2)1}(s)$ and is divided as represented below,

$$H_{eff} = H_0 + H_1 \quad (4.32)$$

where

$$\begin{aligned} H_0 &= \hbar\omega_r I_F - \sum_{\substack{m_1, m_2=2 \\ m_1+m_2=0}}^{-2} \frac{3\hbar\omega_1^3}{4G_{m_1}^{(2)0}G_{m_2}^{(2)0}} iT^{(3)3}(a) \\ H_1 &= \hbar \sum_{\substack{m=2 \\ m \neq 0}}^{-2} G_m^{(2)0} T_m^{(2)0} - \sum_{\substack{m_1, m_2=2 \\ m_1+m_2 \neq 0}}^{-2} \frac{3\hbar\omega_1^3}{4G_{m_1}^{(2)0}G_{m_2}^{(2)0}} iT_{m_1+m_2}^{(3)3}(a) \end{aligned} \quad (4.33)$$

The corresponding transformation function is represented by,

$$S_2 = - \sum_{\substack{m=2 \\ m \neq 0}}^{-2} \frac{iG_m^{(2)0}}{m\omega_r} T_m^{(2)0} - \sum_{\substack{m_1, m_2=2 \\ m_1+m_2 \neq 0}}^{-2} \frac{3\hbar\omega_1^3}{4(m_1+m_2)\omega_r G_{m_1}^{(2)0}G_{m_2}^{(2)0}} T_{m_1+m_2}^{(3)3}(a) \quad (4.34)$$

Subsequently, the final effective Hamiltonian after two transformations is derived and represented by,

$$H_{eff} = \hbar\omega_r I_F - \sum_{\substack{m_1, m_2=2 \\ m_1+m_2=0}}^{-2} \frac{3\hbar\omega_1^3}{4G_{m_1}^{(2)0}G_{m_2}^{(2)0}} iT^{(3)3}(a) \quad (4.35)$$

The initial density operator is re-defined in the frame of the transformation function S_1 and S_2 , as represented below,

$$\begin{aligned} \tilde{\tilde{\rho}}(0) &= e^{iS_2} e^{iS_1} I_z e^{-iS_1} e^{-iS_2} \\ &= \frac{9 \cos c}{10} I_z \end{aligned} \quad (4.36)$$

where $c = \sum_{\substack{m_1, m_2=2 \\ m_1+m_2 \neq 0}}^{-2} \frac{3\omega_1^3}{2(m_1+m_2)\omega_r \sqrt{G_{m_1}^{(2)0}G_{m_2}^{(2)0}G_{-m_1}^{(2)0}G_{-m_2}^{(2)0}}}$. Employing the effective Hamiltonian

Eq. (4.35), the density operator after a pulse (of duration τ) is evaluated and represented by,

$$\tilde{\tilde{\rho}}(\tau) = \frac{9 \cos c}{10} \left[I_z + \frac{3}{2} \sin \theta_2 T^{(3)3}(s) + \frac{3}{2\sqrt{5}} \left(-3iT^{(1)0} + iT^{(3)0} \right) (\cos \theta_2 - 1) \right] \quad (4.37)$$

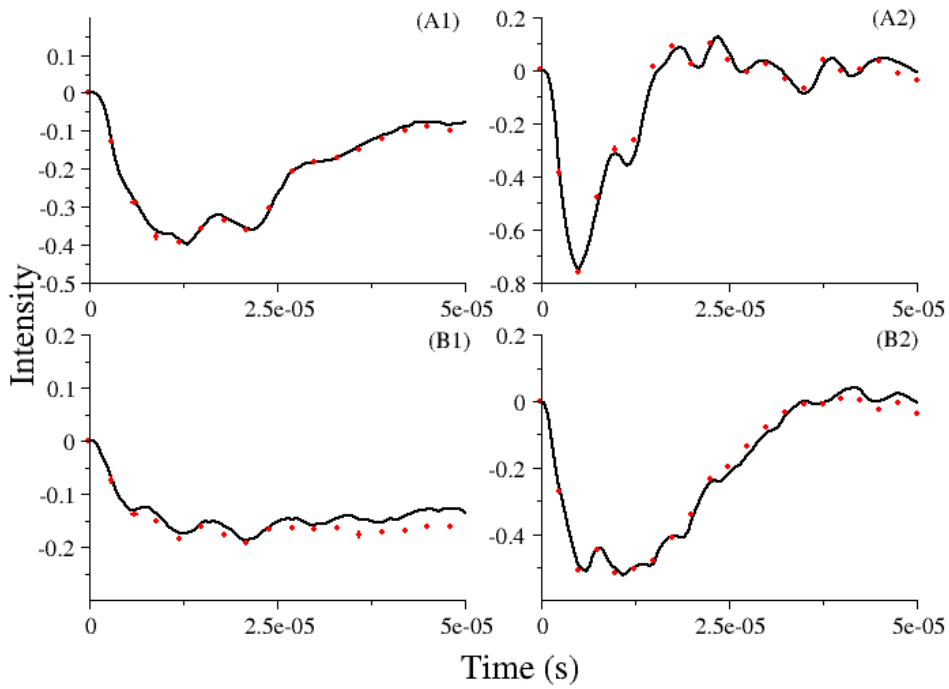


Figure 4.5: Simulations depicting the role of RF amplitude and quadrupolar coupling strength on excitation efficiency of triple-quantum (TQ) transitions in spin $I = 3/2$. The following parameters were employed in the simulations: in panel (A1) $C_Q = 1.08$ MHz, $\nu_1 = 60$ kHz, in panel (A2) $C_Q = 1.08$ MHz, $\nu_1 = 120$ kHz, in panel (B1) $C_Q = 2.16$ MHz, $\nu_1 = 60$ kHz and in panel (B2) $C_Q = 2.16$ MHz, $\nu_1 = 120$ kHz. The remaining parameters spinning frequency $\nu_r = 10$ kHz, $\eta=0$, excitation frequency $\nu = 0$ kHz were held constant in all the simulation. The analytic simulations depicted red dots are based on the effective Hamiltonian, while the simulations in black solid lines are from Simpson.⁵⁶

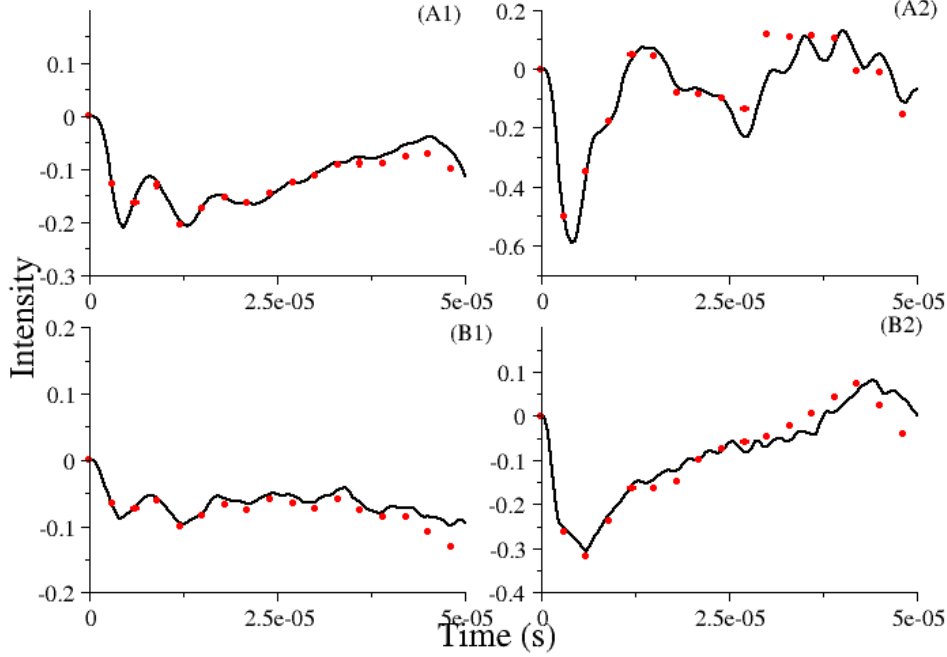


Figure 4.6: Simulations depicting the role of RF amplitude and quadrupolar coupling strength on excitation efficiency of triple-quantum (TQ) transitions in spin $I = 3/2$. The following parameters were employed in the simulations: in panel (A1) $C_Q = 1.08$ MHz, $v_1 = 60$ kHz, in panel (A2) $C_Q = 1.08$ MHz, $v_1 = 120$ kHz, in panel (B1) $C_Q = 2.16$ MHz, $v_1 = 60$ kHz and in panel (B2) $C_Q = 2.16$ MHz, $v_1 = 120$ kHz. The remaining parameters spinning frequency $v_r = 30$ kHz, $\eta=0$, excitation frequency $v = 0$ kHz were held constant in all the simulation. The analytic simulations depicted red dots are based on the effective Hamiltonian, while the simulations in black solid lines are from Simpson.⁵⁶

where $\theta_2 = \sum_{\substack{m_1, m_2=2 \\ m_1+m_2=0}}^{-2} \frac{3\omega_1^3}{2G_{m_1}^{(2)0}G_{m_2}^{(2)0}} \tau$. To have a consistent description, the density operator after the pulse is transformed back into the standard rotating frame through the reverse transformations as illustrated.

$$\begin{aligned} \tilde{\rho}(\tau)_{TQ} &= e^{-iS_1} e^{-iS_2} \tilde{\tilde{\rho}}(\tau) e^{iS_2} e^{iS_1} \\ &= \frac{27 \cos^2 c}{20} \sin \theta_2 T^{(3)3}(s) \end{aligned} \quad (4.38)$$

The time-domain signal corresponding to TQ in standard rotating frame is evaluated employing standard procedure and is represented by,

$$\begin{aligned} \langle \tilde{T}^{(3)3} \rangle &= Tr[-T^{(3)3} \tilde{\rho}(\tau)] \\ &= \frac{-27 \cos^2 c}{20} \left(\frac{3}{2} \sin \theta_2\right) \end{aligned} \quad (4.39)$$

The simulations depicted in Figs. 4.5 and 4.6, substantiate the analytic predictions emerging from the effective Hamiltonian.

4.2.3 Description for $I=5/2$ system

4.2.3.1 Static (Single-crystal)

$$\begin{aligned}
\tilde{H} &= H_0 + H_1 \\
H_0 &= \hbar G^{(2)0} T^{(2)0} \\
H_1 &= \hbar \omega_1 \sqrt{\frac{35}{4}} i T^{(1)1}(a)
\end{aligned} \tag{4.40}$$

Following the description presented in the previous Sections 4.2.1.1 and 4.2.2.1, the effective Hamiltonian for spin $I = 5/2$ system is derived by employing the transformation function $S_1 = \frac{13\omega_1}{\sqrt{6}G^{(2)0}} iT^{(2)1}(a) + \frac{\sqrt{15}\omega_1}{G^{(2)0}} iT^{(4)1}(a)$. Employing the higher-order corrections, the effective Hamiltonian depicting the TQ & 5Q excitation in spin $I = 5/2$ is derived.

$$H_{eff,TQ} = \left(\hbar G^{(2)0} + \frac{13\hbar\omega_1^2}{2G^{(2)0}} \right) T^{(2)0} - \frac{49\hbar\omega_1^3}{2(G^{(2)0})^2} iT^{(3)3}(a) \tag{4.41}$$

$$H_{eff,5Q} = \left(\hbar G^{(2)0} + \frac{13\hbar\omega_1^2}{2G^{(2)0}} - \frac{1477\hbar\omega_1^4}{24(G^{(2)0})^3} \right) T^{(2)0} + \left(\frac{15\hbar\omega_1^2}{\sqrt{3}G^{(2)0}} - \frac{595\hbar\omega_1^4}{2\sqrt{3}(G^{(2)0})^3} \right) T^{(4)0} + \frac{245\hbar\omega_1^5}{12(G^{(2)0})^4} iT^{(5)5}(a) \tag{4.42}$$

Employing the effective Hamiltonians Eqs. (4.41) and (4.42), the density operators corresponding to TQ and 5Q after a pulse (of duration τ), is evaluated and represented below.

$$\tilde{\rho}(\tau) = e^{-\frac{i}{\hbar} H_{eff} \tau} \tilde{\rho}(0) e^{\frac{i}{\hbar} H_{eff} \tau} \tag{4.43}$$

$$\tilde{\rho}(\tau)_{TQ} = I_z + \sqrt{\frac{5}{2}} \left(T^{(3)3}(s) \right) \sin \theta_1 + \frac{1}{2\sqrt{5}} \left(-18\sqrt{\frac{2}{7}} iT^{(1)0} + iT^{(3)0} \right) (\cos \theta_1 - 1) \tag{4.44}$$

$$\tilde{\rho}(\tau)_{5Q} = I_z - \frac{5}{2} \left(T^{(5)5}(s) \right) \sin \theta_2 + 5\sqrt{5} \left(-\sqrt{\frac{1}{14}} iT^{(1)0} + \frac{1}{6} iT^{(3)0} \right) (\cos \theta_2 - 1) \tag{4.45}$$

where $\theta_1 = \frac{49\sqrt{\frac{5}{2}}\omega_1^3}{3(G^{(2)0})^2} \tau$ and $\theta_2 = \frac{245\omega_1^5}{6(G^{(2)0})^4} \tau$. Accordingly, the optimized time-domain signal corresponding to TQ and 5Q coherence is evaluated and represented by,

$$\begin{aligned}
\langle \tilde{T}^{(3)3} \rangle &= Tr[-T^{(3)3} \tilde{\rho}(\tau)] \\
&= -\sqrt{\frac{5}{2}} \sin \theta_1
\end{aligned} \tag{4.46}$$

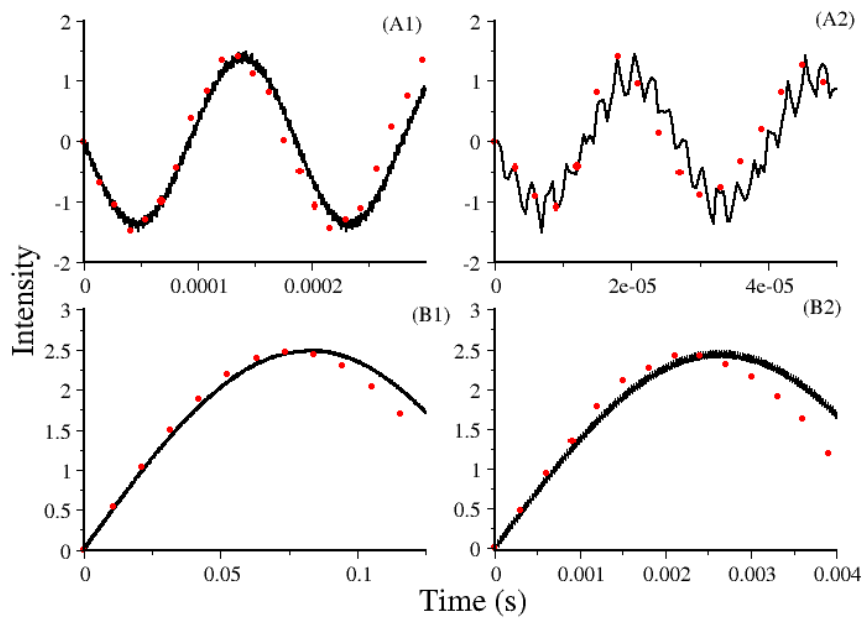


Figure 4.7: Simulations depicting the role of RF amplitude on excitation efficiency of triple-quantum (TQ) transition in panels (A1 & A2) and five-quantum (5Q) transition in panels (B1 & B2) in single-crystal spin $I = 5/2$. The following parameters were employed in the simulations: in panel (A1 & B1) $\nu_1 = 60$ kHz and in panel (A2 & B2) $\nu_1 = 120$ kHz. The remaining parameters $C_Q = 3.2$ MHz spinning frequency $\nu_r = 0$ kHz, $\eta=0$, excitation frequency $\nu = 0$ kHz were held constant in all the simulation. The analytic simulations depicted red dots are based on the effective Hamiltonian, while the simulations in black solid lines are from Simpson.⁵⁶

$$\begin{aligned}
\langle \tilde{T}^{(5)5} \rangle &= Tr[-T^{(5)5} \tilde{\rho}(\tau)] \\
&= \frac{5}{2} \sin \theta_2
\end{aligned} \tag{4.47}$$

The simulations presented in Fig. 4.7 shows similar trends exhibited for spin $I = 1$ and $I = 3/2$ system and are in good agreement with exact numerical methods.

4.2.3.2 Magic Angle Spinning (Powder-sample)

Following the description presented in the previous section, the initial Hamiltonian is transformed using the unitary transformation function $S_1 = \frac{13\omega_1}{\sqrt{6}G^{(2)0}} iT_m^{(2)1}(a) + \frac{\sqrt{15}\omega_1}{G^{(2)0}} iT_m^{(4)1}(a)$.

Five-quantum (5Q):

The transformed Hamiltonian corresponding to 5Q is divided as represented below to facilitate the second contact transformation.

$$H_{eff} = H_0 + H_1 \tag{4.48}$$

where

$$\begin{aligned}
H_0 &= \hbar\omega_r I_F + \sum_{\substack{m_1, m_2, m_3, m_4=2 \\ m_1+m_2+m_3+m_4=0}}^{-2} \frac{245\hbar\omega_1^5}{12G_{m_1}^{(2)0} G_{m_2}^{(2)0} G_{m_3}^{(2)0} G_{m_4}^{(2)0}} iT^{(5)5}(a) \\
H_1 &= \hbar \sum_{\substack{m=2 \\ m \neq 0}}^{-2} G_m^{(2)0} T_m^{(2)0} + \sum_{\substack{m_1, m_2, m_3, m_4=2 \\ m_1+m_2+m_3+m_4 \neq 0}}^{-2} \frac{245\hbar\omega_1^5}{12G_{m_1}^{(2)0} G_{m_2}^{(2)0} G_{m_3}^{(2)0} G_{m_4}^{(2)0}} iT_{m_1+m_2+m_3+m_4}^{(5)5}(a)
\end{aligned} \tag{4.49}$$

The corresponding transformation function is represented by,

$$S_2 = -\sum_{\substack{m=2 \\ m \neq 0}}^{-2} \frac{iG_m^{(2)0}}{m\omega_r} T_m^{(2)0} - \sum_{\substack{m_1, m_2, m_3, m_4=2 \\ m_1+m_2+m_3+m_4 \neq 0}}^{-2} \frac{245\hbar\omega_1^5}{12(m_1+m_2+m_3+m_4)\omega_r G_{m_1}^{(2)0} G_{m_2}^{(2)0} G_{m_3}^{(2)0} G_{m_4}^{(2)0}} T_{m_1+m_2+m_3+m_4}^{(5)5}(a) \tag{4.50}$$

The final effective Hamiltonian after two transformations is represented by,

$$H_{eff} = \hbar\omega_r I_F - \sum_{\substack{m_1, m_2, m_3, m_4=2 \\ m_1+m_2+m_3+m_4=0}}^{-2} \frac{245\hbar\omega_1^5}{12G_{m_1}^{(2)0} G_{m_2}^{(2)0} G_{m_3}^{(2)0} G_{m_4}^{(2)0}} iT^{(5)5}(a) \tag{4.51}$$

The initial density operator is re-defined in the frame of the transformation function S_1 and S_2 , as represented below,

$$\begin{aligned}
\tilde{\rho}(0) &= e^{iS_2} e^{iS_1} I_z e^{-iS_1} e^{-iS_2} \\
&= \frac{5}{7} I_z \cos c
\end{aligned} \tag{4.52}$$

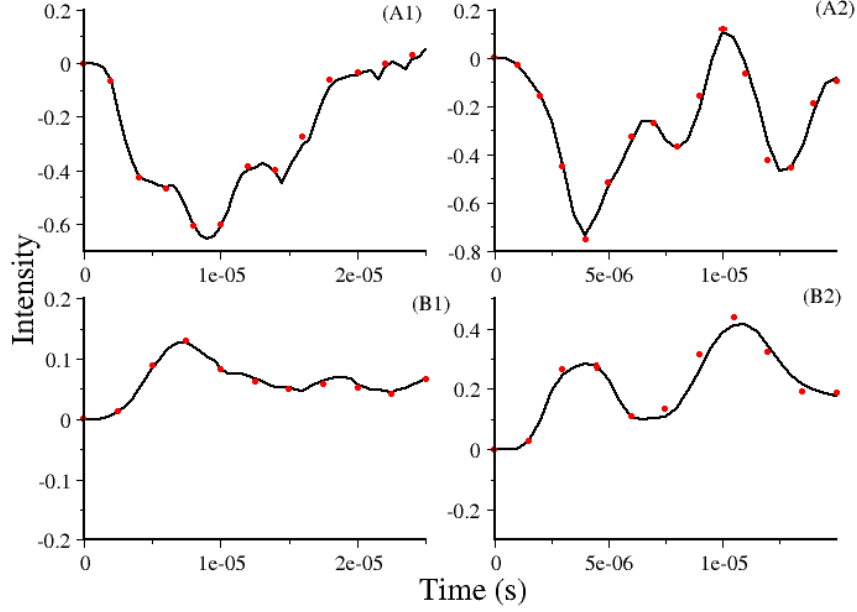


Figure 4.8: Simulations depicting the role of RF amplitude on excitation efficiency of triple-quantum (TQ) transition in panels (A1 & A2) and five-quantum (5Q) transition in panels (B1 & B2) in spin $I = 5/2$. The following parameters were employed in the simulations: in panel (A1 & B1) $\nu_1 = 60$ kHz and in panel (A2 & B2) $\nu_1 = 120$ kHz. The remaining parameters $C_Q = 3.2$ MHz spinning frequency $\nu_r = 10$ kHz, $\eta=0$, excitation frequency $\nu = 0$ kHz were held constant in all the simulation. The analytic simulations depicted red dots are based on the effective Hamiltonian, while the simulations in black solid lines are from Simpson.⁵⁶

where $c = \sum_{\substack{m_1, m_2, m_3, m_4=2 \\ m_1+m_2+m_3+m_4 \neq 0}}^{-2} \frac{245\hbar\omega_1^5}{6(m_1+m_2+m_3+m_4)\omega_r \sqrt{G_{m_1}^{(2)0} G_{m_2}^{(2)0} G_{m_3}^{(2)0} G_{m_4}^{(2)0} G_{-m_1}^{(2)0} G_{-m_2}^{(2)0} G_{-m_3}^{(2)0} G_{-m_4}^{(2)0}}}$. Employing the effective Hamiltonian Eq. (4.51), the density operator after a pulse (of duration τ) is evaluated and represented by,

$$\tilde{\tilde{\rho}}(\tau) = e^{-\frac{i}{\hbar}H_{eff}} \tilde{\tilde{\rho}}(0) e^{\frac{i}{\hbar}H_{eff}} \quad (4.53)$$

$$\begin{aligned} \tilde{\rho}(\tau)_{5Q} &= e^{-iS_1} e^{-iS_2} \tilde{\tilde{\rho}}(\tau) e^{iS_2} e^{iS_1} \\ &= \frac{5}{7} \cos c \left[\frac{-5}{2} T^{(5)5}(s) \sin \theta_3 \right] \end{aligned} \quad (4.54)$$

where $\theta_3 = \sum_{\substack{m_1, m_2, m_3, m_4=2 \\ m_1+m_2+m_3+m_4 \neq 0}}^{-2} \frac{245\hbar\omega_1^5}{6(m_1+m_2+m_3+m_4)\omega_r G_{m_1}^{(2)0} G_{m_2}^{(2)0} G_{m_3}^{(2)0} G_{m_4}^{(2)0}} \tau$. Accordingly, The time-domain signal corresponding to 5Q is evaluated.

$$\begin{aligned} \langle \tilde{T}^{(5)5} \rangle &= Tr[-T^{(5)5} \tilde{\rho}(\tau)] \\ &= \frac{5}{7} \cos^2 c \left(\frac{5}{2} \sin \theta_3 \right) \end{aligned} \quad (4.55)$$

Triple-quantum (TQ):

In a similar vein, The transformed Hamiltonian corresponding to TQ is represented by,

$$H_{eff} = H_0 + H_1 \quad (4.56)$$

where

$$\begin{aligned} H_0 &= \hbar\omega_r I_F - \sum_{\substack{m_1, m_2=2 \\ m_1+m_2=0}}^{-2} \frac{49\hbar\omega_1^3}{2G_{m_1}^{(2)0} G_{m_2}^{(2)0}} iT^{(3)3}(a) \\ H_1 &= \hbar \sum_{\substack{m=2 \\ m \neq 0}}^{-2} G_m^{(2)0} T_m^{(2)0} - \sum_{\substack{m_1, m_2=2 \\ m_1+m_2 \neq 0}}^{-2} \frac{49\hbar\omega_1^3}{2G_{m_1}^{(2)0} G_{m_2}^{(2)0}} iT_{m_1+m_2}^{(3)3}(a) \end{aligned} \quad (4.57)$$

The corresponding transformation function is given by,

$$S_2 = - \sum_{\substack{m=2 \\ m \neq 0}}^{-2} \frac{iG_m^{(2)0} T_m^{(2)0}}{m\omega_r} - \sum_{\substack{m_1, m_2=2 \\ m_1+m_2 \neq 0}}^{-2} \frac{49\hbar\omega_1^3}{2(m_1+m_2)\omega_r G_{m_1}^{(2)0} G_{m_2}^{(2)0}} T_{m_1+m_2}^{(3)3}(a) \quad (4.58)$$

Employing the two transformation functions, the final effective Hamiltonian after two transformations is represented by,

$$H_{eff} = \hbar\omega_r I_F - \sum_{\substack{m_1, m_2=2 \\ m_1+m_2=0}}^{-2} \frac{49\hbar\omega_1^3}{2G_{m_1}^{(2)0} G_{m_2}^{(2)0}} iT^{(3)3}(a) \quad (4.59)$$

The initial density operator is re-defined in the frame of the transformation function S_1 and S_2 , as represented below,

$$\begin{aligned} \tilde{\rho}(0) &= e^{iS_2} e^{iS_1} I_z e^{-iS_1} e^{-iS_2} \\ &= \frac{9}{35} (\cos 4d + 2 \cos \sqrt{10}d) I_z \end{aligned} \quad (4.60)$$

with $d = \sum_{\substack{m_1, m_2=2 \\ m_1+m_2 \neq 0}}^{-2} \frac{49\omega_1^3}{6(m_1+m_2)\omega_r \sqrt{G_{m_1}^{(2)0} G_{m_2}^{(2)0} G_{-m_1}^{(2)0} G_{-m_2}^{(2)0}}}$. Employing the effective Hamiltonian

Eq. (4.59), the density operator after a pulse (of duration τ) is evaluated and represented by,

$$\begin{aligned} \tilde{\rho}(\tau)_{TQ} &= e^{-iS_1} e^{-iS_2} \tilde{\rho}(0) e^{iS_2} e^{iS_1} \\ &= \frac{9}{35} (\cos^2 4d + 2 \cos^2 \sqrt{10}d) \sqrt{\frac{5}{2}} \sin \theta_4 T^{(3)3}(s) \end{aligned} \quad (4.61)$$

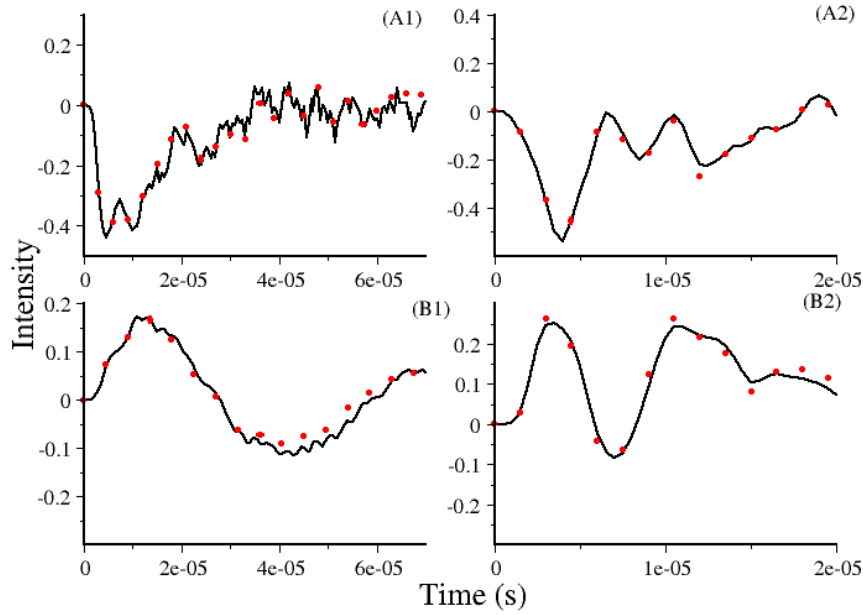


Figure 4.9: Simulations depicting the role of RF amplitude on excitation efficiency of triple-quantum (TQ) transition in panels (A1 & A2) and five-quantum (5Q) transition in panels (B1 & B2) in spin $I = 5/2$. The following parameters were employed in the simulations: in panel (A1 & B1) $\nu_1 = 60$ kHz and in panel (A2 & B2) $\nu_1 = 120$ kHz. The remaining parameters $C_Q = 3.2$ MHz spinning frequency $\nu_r = 30$ kHz, $\eta=0$, excitation frequency $\nu = 0$ kHz were held constant in all the simulation. The analytic simulations depicted red dots are based on the effective Hamiltonian, while the simulations in black solid lines are from Simpson.⁵⁶

with $\theta_4 = \sum_{\substack{m_1, m_2=2 \\ m_1+m_2=0}}^{-2} \frac{49\sqrt{\frac{5}{2}}\omega_1^3}{3G_{m_1}^{(2)0}G_{m_2}^{(2)0}}\tau$. Accordingly, The time-domain signal corresponding to TQ is evaluated.

$$\begin{aligned} \langle \tilde{T}^{(3)3} \rangle &= Tr[-T^{(3)3}\tilde{\rho}(\tau)] \\ &= \frac{1}{35}(4 \cos^2 4c + 10 \cos^2 \sqrt{10}c)(-\sqrt{\frac{5}{2}} \sin \theta_4) \end{aligned} \quad (4.62)$$

The simulations presented in Figs. 4.8 and 4.9 illustrate the role of RF amplitudes and quadrupolar coupling constants in the excitation profile. In general the efficiency of MQ excitations increases with the amplitude of the RF field employed in MQMAS experiments. By constant, the efficiency of excitation is inversely proportional to the quadrupolar coupling constant. This trend is exhibited in all the spin systems described in this chapter and is in agreement with the numerical simulations.

4.3 Conclusions and Perspectives

In summary, the concept of effective RF Hamiltonians presents an attractive approach for understanding the phenomenon of multi-quantum (MQ) excitation in quadrupolar nuclei. Employing effective RF Hamiltonians, the mechanism of MQ excitation is investigated. In the original two-pulse scheme (incorporated from solution NMR), evolution under the quadrupolar Hamiltonian between pulses was essential for the creation of MQ coherence. However, this requirement is crucial only to systems with smaller quadrupolar coupling constants. Since the magnitude of the quadrupolar coupling constant exceeds the RF amplitude in majority of the systems, the original two-pulse MQ excitation scheme was subsequently refined to a single-pulse experiment. From a theoretical perspective, this refinement of the experimental scheme could be explained by invoking the concept of effective Hamiltonians introduced in this chapter. For example, when $\omega_1 > \omega_Q$ (hard-pulse limit), the effective RF Hamiltonian in the Z-Q interaction frame reduces to an (for an X-pulse) I_x operator. Consequently, the density operator after the initial pulse comprises of only SQ coherences (of rank 1). To create SQ coherences of higher ranks ($k > 1$), evolution under quadrupolar Hamiltonian is mandatory. Introduction of a second pulse is essential to convert the higher rank SQ coherences ($k > 1$) into MQ coherences. Hence, evolution under the quadrupolar Hamiltonian is a prerequisite for creating MQ coherences in two-pulse experiments. Interestingly, the above description is invalid when the magnitude of the quadrupolar coupling constant exceeds the RF amplitude.

By contrast, excitation of MQ coherences in single-pulse experiments (see Figs. 4.1 to 4.9) relies on the time-dependent terms in the effective Hamiltonian, suggesting a possible breakdown of the secular approximation. This inference of ours is bit counter-intuitive. Hence, the suitability of secular approximation in MQ NMR experiments depends on the duration of the pulses employed in the study. When the duration of the pulses is longer, the time-dependent oscillating terms have an important role in the excitation of MQ coherences. Consequently, the excitation period is often longer in single pulse experiments. The analytic theory presented in this chapter could be employed to develop models for quantify the MQMAS experiments.

References

- [1] L. Frydman and J. S. Harwood, *J. Am. Chem. Soc.*, 1995, **117**, 5367.
- [2] A. Medek, J. S. Harwood and L. Frydman, *J. Am. Chem. Soc.*, 1995, **117**, 12779.
- [3] A. Samoson and E. Lippmaa, *Phys. Rev. B*, 1983, **28**, 6567.
- [4] J. H. D. Freude, in *Quadrupolar Effects in Solid State Magnetic Resonance*, Springer, Berlin, 1993.
- [5] L. Frydman, in *Multiple-Quantum Magic-Angle Spinning Experiments on Half-Integer Nuclei: Fundamentals*, John Wiley & Sons, Ltd, 2007.
- [6] J. P. Amoureux, *Solid State Nucl. Magn. Reson.*, 1993, **2**, 83.
- [7] J. P. Amoureux and C. Fernandez, *Solid State Nucl. Magn. Reson.*, 1998, **10**, 211.
- [8] S. E. Ashbrook and S. Wimperis, *Prog. NMR spectrosc.*, 2004, **45**, 53.
- [9] S. E. Ashbrook, J. McManus, M. J. Thrippleton and S. Wimperis, *Prog. in Nuc. Mag. Reson.*, 2009, **55**, 160.
- [10] C. Fernandez and J. P. Amoureux, *Solid State Nuc. Mag. Reson.*, 1996, **5**, 315.
- [11] A. Goldbourt and P. K. Madhu, *Monatshefte fur Chemie*, 2012, **133**, 1497.
- [12] A. Goldbourt, P. K. Madhu, S. Kababya and S. Vega, *Solid State Nuc. Mag. Reson.*, 2000, **18**, 1.
- [13] P. J. Grandinetti, in *Dynamic Angle Spinning*, John Wiley & Sons, Ltd, 2007.
- [14] A. Jerschow, *Prog. NMR spectrosc.*, 2005, **46**, 63.
- [15] P. P. Man, in *Quadrupolar Interactions*, John Wiley & Sons, Ltd, 2007.
- [16] P. P. Man, *Encyclopaedia of Analytical Chemistry*, 2000, 12224.
- [17] A. J. Vega, in *Quadrupolar Nuclei in Solids*, John Wiley & Sons, Ltd, 2007.
- [18] G. Wu, D. Rovnyak and R. G. Griffin, *J. Am. Chem. Soc.*, 1996, **118**, 9326.
- [19] G. Wu, D. Rovnyank, B. Sun and R. G. Griffin, *Chem Phys Lett*, 1995, **249**, 210.
- [20] A. Goldbourt, P. K. Madhu and S. Vega, *Chem. Phys. Lett*, 2000, **320**, 448.
- [21] T. Vosegaard, F. H. Larsen, H. J. Jakobsen, P. D. Ellis and N. C. Nielsen, *J. Am. Chem. Soc.*, 1997, **119**, 9055.

- [22] Z. Gan, *J. Am. Chem. Soc.*, 2000, **122**, 3242.
- [23] C. Fernandez, L. Delevoye, J. P. Amoureux, D. P. Lang and M. Pruski, *J. Am. Chem. Soc.*, 1997, **119**, 6858.
- [24] S. P. Brown and S. Wimpersi, *J. Magn. Reson.*, 1997, **128**, 42.
- [25] D. Iuga, H. Schafer, R. Verhagen and A. P. M. Kentgens, *J. Magn. Reson.*, 2000, **147**, 192.
- [26] S. E. Ashbrook and S. Wimperis, *J. Am. Chem. Soc.*, 2002, **124**, 11602.
- [27] B. Hu, J. P. Amoureux, J. Trebosc and S. Hafner, *J. Magn. Reson.*, 2008, **192**, 8.
- [28] D. Srivastava, R. Venkata SubbaRao and R. Ramachandran, *PCCP*, 2013, **15**, 6699.
- [29] S. Vega, *J. Chem. Phys.*, 1978, **68**, 5518.
- [30] S. Vega, T. W. Shattuck and A. Pines, *Phys. Rev. A*, 1980, **22**, 638.
- [31] S. Vega and Y. J. Naor, *J. Chem. Phys.*, 1981, **75**, 75.
- [32] N. C. Nielsen, H. Bildsoe and H. J. Jakobsen, *Chem Phys Lett*, 1992, **191**, 205.
- [33] T. Charpentier, C. Fermon and J. Virlet, *J. Magn. Reson.*, 1998, **132**, 181.
- [34] A. Wokaun and R. R. Ernst, *J. Chem. Phys.*, 1977, **67**, 1752.
- [35] L. Marinelli, A. Medek and L. Frydman, *J. Magn. Reson.*, 1998, **132**, 88.
- [36] A. K. Khitrin, J. Xu and A. Ramamoorthy, *J. Chem. Phys.*, 2012, **136**, 214504.
- [37] B. C. Sanctuary, *J. Chem. Phys.*, 1976, **64**, 4352.
- [38] B. C. Sanctuary and T. K. Halstead, *Adv. Magn. Opt. Reson.*, 1990, **15**, 79.
- [39] R. Reddy and P. T. Narasimhan, *Mol. Phys.*, 1991, **72**, 509.
- [40] A. Ramamoorthy and P. T. Narasimhan, *Mol. Phys.*, 1991, **73**, 207.
- [41] A. Ramamoorthy and P. T. Narasimhan, *Pramana-J. Phys.*, 1991, **36**, 399.
- [42] G. J. Bowden and W. D. Hutchison, *J. Magn. Reson.*, 1986, **67**, 403.
- [43] G. J. Bowden, W. D. Hutchinson and J. Khachan, *J. Magn. Reson.*, 1986, **67**, 415.
- [44] B. C. Sanctuary, *Phys. Rev. A*, 1979, **20**, 1169.
- [45] M. R. Aliev and V. T. Aleksanyan, *Optika Spectroscopia*, 1968, **24**, 520.
- [46] M. R. Aliev and V. T. Aleksanyan, *Optika Spectroscopia*, 1968, **24**, 695.
- [47] R. Venkata SubbaRao, D. Srivastava and R. Ramachandran, *PCCP*, 2013, **15**, 2081.
- [48] P. P. Man, *Chem. Phys. Lett*, 1990, **168**, 227.
- [49] P. P. Man, *Mol. Phys.*, 1990, **69**, 337.

- [50] P. P. Man, *Mol. Phys.*, 1992, **76**, 1119.
- [51] P. P. Man, *J. Chem. Phys.*, 1992, **89**, 335.
- [52] P. F. Bernath, *Spectra of atoms and molecules*, Oxford University Press, New York, 2005.
- [53] D. Papousek and M. R. Aliev, *Molecular vibrational-rotational spectra*, 1982.
- [54] J. H. V. Vleck, *Phys. Rev.*, 1929, **33**, 467.
- [55] R. Ramesh and M. S. Krishnan, *J. Chem. Phys.*, 2001, **114**, 5967.
- [56] M. Bak, J. T. Rasmussen and N. C. Nielsen, *J. Magn. Reson.*, 2000, **147**, 296.
- [57] J. H. Shirley, *Phys. Rev. B*, 1965, **4**, 979.
- [58] E. Vinogradov, P. Madhu and S. Vega, *J. Chem. Phys.*, 2001, **115**, 8983–9000.

Chapter 5

Conclusions and Perspectives

The utility of NMR spectroscopy as a tool for characterizing molecular structure depends on the accuracy of the constraints estimated through experiments. To facilitate this process, a formal understanding of the nuclear spin interactions at the atomic level is quintessential in the interpretation of experimental data as well as in the design of new experiments (that includes improvements to existing experimental schemes). In particular, the description of NMR experiments in the solid-state has always remained a challenging task both from an experimental and theoretical perspective. To this end, we believe that the present thesis makes a modest attempt to address some of the pertinent issues of relevance to both experimentalist and theoreticians in the field of magnetic resonance. As a preliminary step, a unified description of the nuclear spin interactions in terms of irreducible spatial and spin tensor operators is presented in this thesis with important derivations. In contrast to spin $1/2$ nuclei, the spherical tensor formalism is of extreme importance in the study of quadrupolar nuclei. Although, several excellent treatise on spherical tensor formalism do exist in the literature, a consistent description along with appropriate conventions has always remained a mystery. The phase factors and normalization constants employed in the construction of the tensor operators are examined thoroughly and are derived systematically for facilitating their extension in the description of NMR experiments that involve both spin $1/2$ and quadrupolar nuclei.

In the second half of the thesis, the concept of effective RF Hamiltonians is introduced to describe the spectroscopically allowed transitions in quadrupolar nuclei. In contrast to their spin $1/2$ counterparts, analytic description of the transitions in quadrupolar nuclei is fraught with difficulty owing to the presence of (a) multiple levels (b) quadrupolar interactions. Employing the spherical tensor operator formalism, effective RF Hamiltonians are proposed for describing both selective and non-selective transitions in quadrupolar nuclei. Depending on the magnitude of the quadrupolar coupling constant, important constraints for improving both the selectivity and efficiency of the excited transitions are

derived employing the density matrix formalism. The validity of the secular approximation commonly employed in analytical treatments is thoroughly investigated in all regimes and is well explained and substantiated through extensive numerical and analytic simulations. In contrast to existing descriptions in the literature, both selective and non-selective excitations are described in terms of effective Hamiltonians based on the spherical tensor operator formalism. In combination with Floquet theory, the effective RF Hamiltonian approach presented in this thesis is extended for describing MAS (magic angle spinning) experiments in solid-state NMR. Below, we summarize the three major highlights of this thesis.

5.1 Concept of effective RF Hamiltonians

To verify the authenticity of the normalised spherical tensor operators presented in this thesis, transitions in quadrupolar nuclei (spin $I=1, 3/2$ and $5/2$) were investigated in static systems. Employing the concept of effective Hamiltonians, an analytic framework based on the density operator formalism is presented for elucidating the optimum conditions for exciting transitions in quadrupolar nuclei. Depending on the spin-quantum number and the participating levels, optimum flip angles are derived along with appropriate excitation frequency (see Fig. 5.1). Although, the application of the spherical tensor formalism for describing pulses in quadrupolar systems in the hard-pulse limit is known, the description of pulses in the soft-pulse regime is of practical relevance. To this end, a more general treatment in terms of effective RF Hamiltonians for studying the effect of RF pulses on quadrupolar systems is presented. The proposed effective RF Hamiltonian in the quadrupolar interaction frame encodes the various transition frequencies and is suitable for describing transitions (both selective and non-selective) in a multi-level system. The validity of the secular approximation is thoroughly examined and effective RF Hamiltonians for selective and non-selective excitations are derived from first principles. Additionally, the differences in the excitation conditions in single crystals and polycrystalline sample are investigated and optimum excitation conditions are derived. Depending on the relative magnitudes of the RF amplitude and the quadrupolar coupling constant, the optimum conditions required for the excitation of a particular transition are derived from analytical expressions. In particular, the interplay between selectivity/non-selectivity of transitions in multi-level systems is explained in terms of the secular approximation employed in the derivation of effective Hamiltonians. Employing the effective RF Hamiltonians, analytical expressions for the density operator are derived along with suitable expressions for the time-domain signal. Based on the analytical expressions for the density operator, optimum flip angles and durations of pulses are derived for both integral and half-integral systems. The simulations presented in Figs. 5.1 and 5.2 are representative of the conditions that are required for optimizing transitions in a multi-level system.

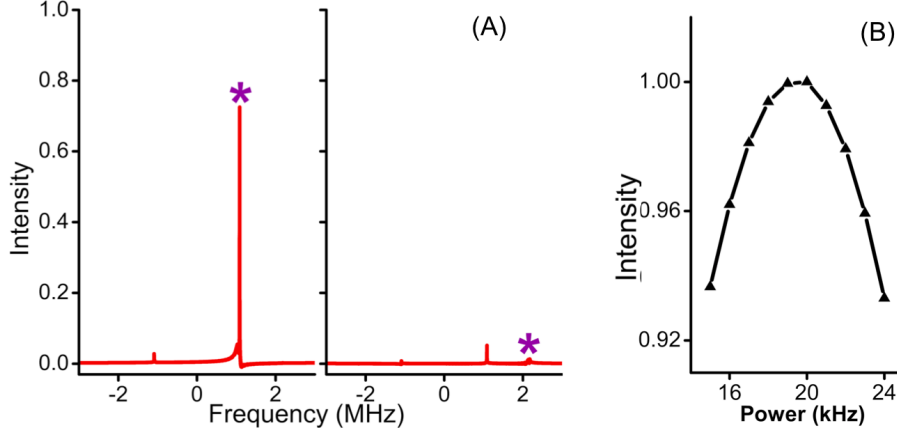


Figure 5.1: Simulations depicting in panel (A) the role of excitation frequency using a $\frac{\pi}{2}$ -pulse ($\nu_1 = 20$ kHz, $t_p = 12.5$ μ s) and in panel (B) the role of the flip angle in the selective excitation of a powder sample corresponding to $I=1$ system. The following parameters were employed in the simulations: ($I=1$, ${}^6\text{Li}$, $C_Q = 2.9$ MHz, $\nu_Q = 4.35$ MHz, $\eta = 0$). In a typical powder sample, the spectral width for $I=1$ system ranges from $\frac{\nu_Q}{2}$ to $-\frac{\nu_Q}{2}$, however due to higher statistical weight, the maxima is attained at $\pm\frac{\nu_Q}{4}$ ($\frac{\nu_Q}{4} = 1.0875$ MHz) as depicted in panel (A). In panel (B), the intensity is measured as a function of the RF amplitude (ν_1) for $t_p = 8.84$ μ s and the frequency of excitation $\nu_0 + \frac{\nu_Q}{4}$ ($\frac{\nu_Q}{4} = 1.0875$ MHz). As depicted, the maximum intensity is obtained when $\omega_1 t_p = \frac{\pi}{2\sqrt{2}}$ and is in accord with the theoretical predictions.

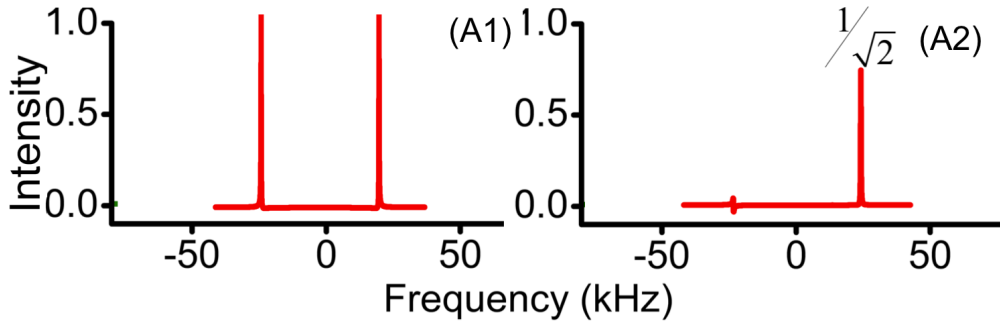


Figure 5.2: Simulations depicting the FT-spectrum of ${}^6\text{Li}$ ($I = 1$) system corresponding to non-selective and selective excitation in a single crystal. The following parameters were employed in the simulations: $C_Q = 30$ kHz, $\eta=0$ and in panel (A1) $\frac{\pi}{2}$ -pulse with RF amplitude $\nu_1 = 150$ kHz, duration $t_p = 1.67$ μ s and excitation frequency $\nu = \nu_0$, in panel (A2) $\frac{\pi}{2\sqrt{2}}$ -pulse with RF amplitude $\nu_1 = 3.98$ kHz, duration $t_p = 44.44$ μ s and excitation frequency 22.5 kHz (i.e $\nu = \nu_0 + \frac{\nu_Q}{2}$).

5.2 Excitation of satellite transitions in MAS experiments

Integrating Floquet theory and the method of contact transformation, effective Floquet Hamiltonians are proposed for describing MAS experiments. To begin with, excitation of single-quantum transitions in quadrupolar systems under MAS conditions is investigated. In the case of integral quadrupolar spin systems, the excitation frequency of SQ transitions

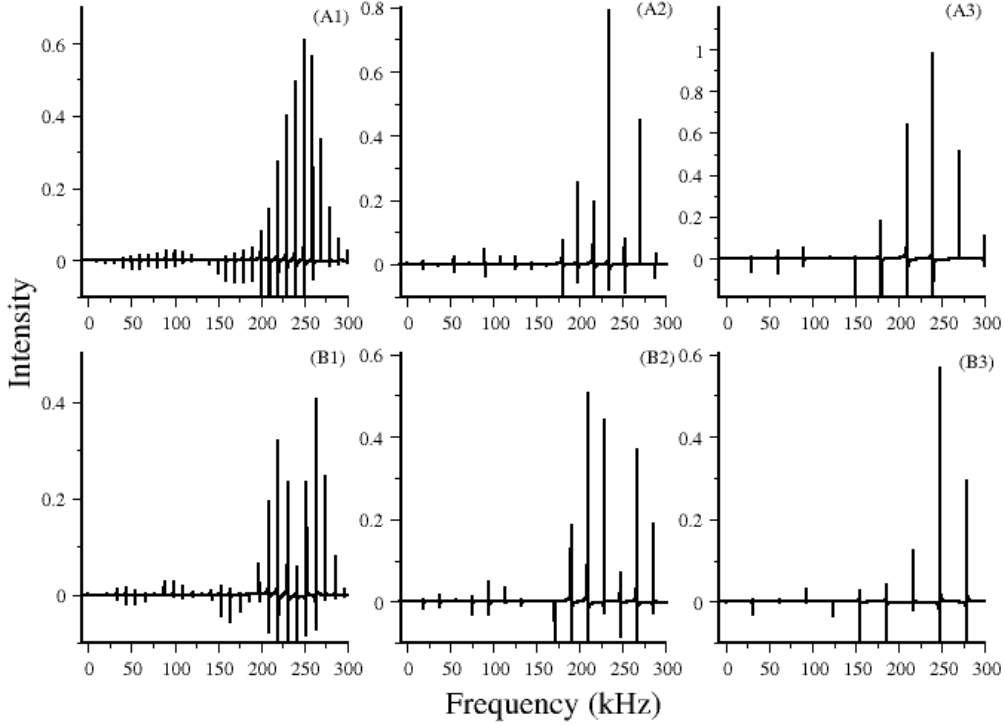


Figure 5.3: Numerical simulations depicting the role of spinning frequency on the excitation efficiency of SQ transitions in spin $I = 3/2$, (excitation frequency, $\nu = \nu_0 + \frac{\nu_Q}{2}$ or $\nu = \nu_0 + 270$ kHz). The following spinning frequency was employed in the simulations: in panel (A1) $\nu_r = 10$ kHz, in panel (B1) $\nu_r = 11$ kHz, in panel (A2) $\nu_r = 18$ kHz, in panel (B2) $\nu_r = 19$ kHz, in panel (A3) $\nu_r = 30$ kHz and in panel (B3) $\nu_r = 31$ kHz. The remaining parameters $C_Q = 1.08$ MHz ($\nu_Q = 540$ kHz), $\eta=0$, excitation frequency $\nu = 270$ kHz, $\nu_1 = 19.5$ kHz, $t_p = 7.4 \mu\text{s}$ were held constant in all the simulation.

has a profound dependence on the first-order quadrupolar interactions. By contrast, the central transitions in half-integral quadrupolar spins are independent of first-order quadrupolar interactions. In a typical powder sample, precise matching of the excitation frequency is hindered due to the anisotropic nature of the quadrupolar interaction. Our objective in this study was to design alternate strategies for improving the excitation of SQ transitions in both integral and half-integral quadrupolar systems. To this end, the simulations depicted in Fig. 5.3 illustrate an interesting trend. When the off-set frequency (proportional to quadrupolar frequency) is matched to an integral multiples of the sample spinning frequency ($n\omega_r = \omega_Q$), enhanced excitation efficiency of the satellite transitions is observed both in the integral and half-integral quadrupolar spin systems. This observation of ours was deduced based on the effective Hamiltonians and is well corroborated through both analytic and numerical simulations (see Fig. 5.3). A detailed description of this resonance phenomenon is discussed in the thesis.

5.3 Excitation of MQ transitions in MAS experiments

To extend the utility of the effective Hamiltonian approach, excitation of MQ transition in quadrupolar systems was investigated under MAS conditions. In contrast to other existing descriptions, the effective RF Hamiltonian approach, presents an attractive framework for understanding the phenomenon of multi-quantum (MQ) transitions in quadrupolar nuclei. In the original two-pulse scheme (incorporated from solution NMR), evolution under the quadrupolar Hamiltonian between pulses was essential for the creation of MQ coherence. However, this requirement is crucial only to systems with smaller quadrupolar coupling constants. Since the magnitude of the quadrupolar coupling constant exceeds the RF amplitude in majority of the systems, the original two-pulse MQ excitation scheme was subsequently refined to a single-pulse experiment. From a theoretical perspective, this refinement of the experimental scheme could be explained by invoking the concept of effective Hamiltonians introduced in this thesis. For example, when $\omega_1 > \omega_Q$ (hard-pulse limit), the effective RF Hamiltonian in the Z-Q interaction frame reduces to an (for an X pulse) I_x operator. Consequently, the density operator after the initial pulse comprises of only SQ coherences (of rank 1). Hence, evolution under quadrupolar Hamiltonian is required to create SQ coherences of higher ranks ($k > 1$). Introduction of a second pulse is essential to convert the higher rank SQ coherences ($k > 1$) into MQ coherences. Hence, evolution under the quadrupolar Hamiltonian is a prerequisite for creating MQ coherences in two-pulse experiments. Interestingly, the above description is invalid when the magnitude of the quadrupolar coupling constant exceeds the RF amplitude. When $\omega_Q \gg \omega_1$, the form of the effective RF Hamiltonian differs and is sequence specific. The subsequent action of pulses, facilitates the creation of MQ coherences without the requirement for evolution under the quadrupolar Hamiltonian. Since the pulses employed are of shorter duration, the time-dependent terms in the effective Hamiltonian are neglected in these experiments under secular approximation. By contrast, excitation of MQ coherences in single-pulse experiments relies on the time-dependent terms in the effective Hamiltonian. Hence, the suitability of secular approximation in MQ NMR experiments depends on the duration of the pulses employed in the study. When the duration of the pulses is longer, the time-dependent oscillating terms have an important role in the excitation of MQ coherences. The predictions emerging from the analytic theory are well corroborated with simulations emerging from exact numerical methods (see Fig. 5.4).

We believe that the theoretical framework presented in this thesis would provide the necessary impetus for the development of sophisticated multiple pulse experiments involving quadrupolar nuclei.

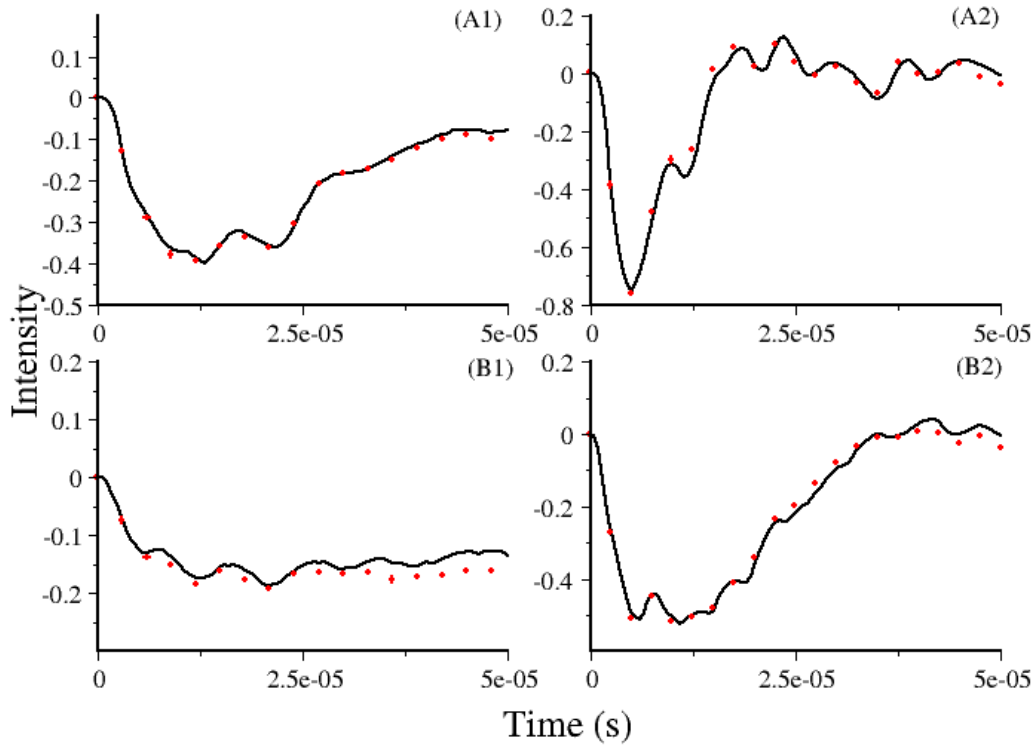


Figure 5.4: Simulations depicting the role of RF amplitude and quadrupolar coupling strength on excitation efficiency of triple-quantum (TQ) transitions in spin $I = 3/2$. The following parameters were employed in the simulations: in panel (A1) $C_Q = 1.08$ MHz, $v_1 = 60$ kHz, in panel (A2) $C_Q = 1.08$ MHz, $v_1 = 120$ kHz, in panel (B1) $C_Q = 2.16$ MHz, $v_1 = 60$ kHz and in panel (B2) $C_Q = 2.16$ MHz, $v_1 = 120$ kHz. The remaining parameters spinning frequency $v_r = 10$ kHz, $\eta=0$, excitation frequency $v = 0$ kHz were held constant in all the simulation. The analytic simulations depicted red dots are based on the effective Hamiltonian, while the simulations in black solid lines are from Simpson.

Research Publications

1. *Concept of effective Hamiltonians for transitions in multi-level systems*; **Venkata SubbaRao, R.**; Srivastava, D.; Ramachandran, R. *PCCP* **2013**, *15*, 2081.
2. *Understanding multi-quantum NMR through secular approximation*, Srivastava, D.; **Venkata SubbaRao, R.**; Ramachandran, R. *PCCP* **2013**, *15*, 6699.

Doctoral Committee

Research Supervisor (Convener)

Dr. R. Ramachandran

Department of Chemical Sciences, IISER Mohali

Members

Prof. K. S. Viswanathan

Department of Chemical Sciences, IISER Mohali

Dr. P. Balanarayan

Department of Chemical Sciences, IISER Mohali

Curriculum Vitae

Name : Venkata SubbaRao R

Date of Birth : July 10, 1985

Educational Qualifications

Bachelor of Science (B.Sc.) 2005

University : Acharya Nagarjuna University, Guntur, Andhrapradesh, India

Specialization : (Maths, Physics & Chemistry)

Master of Science (M.Sc.) 2007

University : Andhra University, Vishakhapattanam, Andhrapradesh, India

Specialization : Organic Chemistry

Doctor of Philosophy (Ph.D.) 2016

Institution : Indian Institute of Science Education and Research (IISER) Mohali,
Mohali, Punjab, India

Specialization : Physical Chemistry (Solid-State NMR)